UNIVERSITÉ DE NEUCHÂTEL

Numerical Optimization of Dirichlet-Laplace Eigenvalues on Domains in Surfaces

Thèse

présentée à la Faculté des sciences
pour obtenir le grade de docteur ès sciences par

Régis Straubhaar

soutenue avec succès le 31 mai 2013
et acceptée sur proposition du jury

Prof. Olivier Besson	co-directeur de thèse, rapporteur
Prof. Bruno Colbois	co-directeur de thèse, rapporteur
Prof. Pedro Freitas	rapporteur (Université de Lisbonne)
Prof. Alexandre Girouard	rapporteur (Université Laval)

Institut de mathématiques, Université de Neuchâtel,
Rue Emile–Argand 11, CH–2000 Neuchâtel

UNIVERSITÉ DE NEUCHÂTEL

Faculté des sciences
Secrétariat-décanat de Faculté
Rue Emile-Argand 11
2000 Neuchâtel - Suisse
Tél: + 41 (0)32 718 2100
E-mail: secretariat.sciences@unine.ch

IMPRIMATUR POUR THESE DE DOCTORAT

La Faculté des sciences de l'Université de Neuchâtel autorise l'impression de la présente thèse soutenue par

Monsieur Régis STRAUBHAAR

Titre:

"Numerical Optimization of Dirichlet-Laplace Eigenvalues on Domains in Surfaces"

sur le rapport des membres du jury:

- Prof. Bruno Colbois, Université de Neuchâtel, co-directeur de thèse
- Prof. Olivier Besson, Université de Neuchâtel, co-directeur de thèse
- Prof. Pedro Freitas, Université de Lisbonne, Portugal
- Prof. Alexandre Girouard, Université Laval, Québec

Neuchâtel, le 20 juin 2013

Le Doyen, Prof. P. Kropf

Abstract

The spectrum of the Dirichlet-Laplace operator defined on a bounded domain in a smooth and complete surface consists in a strictly positive sequence, increasing to infinity. The aim of this thesis is to approximate numerically the first eigenvalues of this operator using a finite element based method, then to address the following optimization problem: what is the domain which minimizes the k-th eigenvalue among all domains of a given area, and what is this eigenvalue equal to? This latter has its roots in the Faber-Krahn and Krahn-Szegő theorems, which answer the question for the first and the second eigenvalue of a domain in the Euclidean space. For higher eigenvalues and other underlying surfaces like the sphere and hyperbolic space, shape optimization has been performed to provide domains which are candidates to be solutions. This gives rise to some observations about the comparison of eigenvalues of domains in various surfaces. The problem of locating a circular obstacle inside a ball to maximize the first eigenvalues is also addressed in this document.

Keywords: Spectral geometry; Dirichlet-Laplace operator; Eigenvalues; Numerical approximations; Shape optimization; Finite Element Method; Uzawa Algorithm.

Résumé

Le spectre de l'opérateur de Laplace-Dirichlet défini sur un domaine borné d'une surface lisse et complète est une suite strictement positive, croissante, tendant vers l'infini. Le but de cette thèse est d'approcher les premières valeurs propres de cet opérateur de manière numérique à l'aide d'une méthode d'éléments finis, puis de considérer le problème d'optimisation suivant : quel est le domaine qui minimise la k-ème valeur propre parmi tous les domaines d'aire donnée, et que vaut cette valeur propre ? Ce dernier trouve son origine dans les théorèmes de Faber-Krahn et Krahn-Szegő, qui règlent le cas de la première et de la deuxième valeur propre d'un domaine de l'espace euclidien. Des méthodes en optimisation de forme ont été élaborées pour proposer des domaines candidats à être solution pour des valeurs propres plus élevées ainsi que pour d'autres surfaces sous-jacentes comme la sphère et l'espace hyperbolique. Cela a donné lieu à des observations sur la comparaison de valeurs propres associées à des domaines sur différentes surfaces. Le problème du placement d'un obstacle circulaire à l'intérieur d'une boule afin de maximiser les premières valeurs propres est aussi abordé dans cette thèse.

Mots clés : Géométrie spectrale ; Opérateur de Dirichlet-Laplace ; Valeurs propres ; Approximations numériques ; Optimisation de forme ; Méthode des éléments finis ; Algorithme d'Uzawa.

Remerciements

Ce travail a été en partie financé par la subvention n° 20-137696/1 du Fonds National Suisse de la recherche scientifique (FNS).

En premier lieu, mes remerciements les plus chaleureux vont à mes directeurs de thèse, Olivier Besson et Bruno Colbois. Il ne m'est pas possible d'énumérer vos nombreuses qualités dont j'ai bénéficié pendant ces quatre ans, aussi n'en soulignerai-je qu'une, dont tout doctorant n'a pas la chance de pouvoir profiter. Je n'aurais sans doute pas eu l'opportunité de rencontrer autant de chercheurs sans tes nombreuses relations, Bruno. Cela m'a permis d'élargir mes connaissances et de remettre avantageusement en question mon travail. Et lorsque le doute s'insinuait trop vivement, la porte du bureau d'en face, celui d'Olivier, était toujours ouverte. J'ai énormément apprécié ta capacité à transmettre, en plus de tes connaissances indéniables, ta motivation et ta confiance. Chacun à votre manière, vous avez guidé mes premiers pas dans la recherche. Merci pour tout à vous deux.

Mes remerciements vont aussi aux Professeurs Pedro Freitas et Alexandre Girouard pour m'avoir fait le privilège de prendre part à mon jury et pour avoir consacré du temps à lire ma thèse. Vos questions pertinentes, vos suggestions de références bibliographiques et vos commentaires instructifs m'ont permis d'améliorer ce document. De surcroît, malgré le caractère solennel de la soutenance, vous avez su y faire régner un climat décontracté.

Qu'il est agréable d'imaginer et d'écrire ces quelques lignes dont je me suis longtemps refusé à esquisser les mots. Il est temps de remercier mes collègues, qui resteront pour la plupart, j'en suis sûr, mes amis. Et même sans nécessairement avoir élucidé les problèmes que j'ai rencontrés dans mon travail, leur présence m'a été bénéfique.

Celui qui m'a le plus apporté, notamment sur le plan mathématique, est certainement Alex. Tu as toujours pris le temps de m'écouter et de répondre précisément aux questions plus ou moins pertinentes que je me posais. Merci de m'avoir fait profiter de ta vaste expérience. Par ailleurs, l'anglais employé dans cette thèse, s'il n'est de loin pas parfait, aurait été de bien plus mauvaise qualité sans l'aide de mes co-bureaux, Ana et PN, qui se sont pris au jeu de la traduction. Disons que vous avez tous les deux gagné la compétition. Je pense aussi à Fabien qui m'a fourni son code au début de ma thèse.

Merci David d'avoir partagé plus d'une fois un souper, si propice à ces précieuses discussions qui nous ont animés. Ces quatre ans de thèse m'auront également permis d'apprécier tes nombreuses qualités.

Olivier, Kola (et ta petite famille), Greg, Dennis (tu reviens quand tu veux), vous qui m'avez précédé à l'Institut, c'était un plaisir de vous côtoyer et de partager nos impressions sur ce périple que représente une thèse. Quel bonheur de pouvoir vous compter parmi mes amis.

Je ne t'oublie pas Bastien, toi qui a veillé à ne pas me faire manquer ces désormais mythiques pauses au *Saloon*, ni tous leurs protagonistes qui se reconnaîtront. Danke Raphael für deine Freundlichkeit und deinen Humor.

Je tiens également à adresser un mot à Christine, la secrétaire, toujours de bonne humeur et prête à rendre service, ainsi qu'aux étudiants qui, même s'ils ne s'en rendent pas compte, m'ont donné à maintes reprises un ballon d'oxygène fort appréciable. Enfin, je pense à tous ceux avec qui j'ai bu un verre, pris un repas, regardé un match de foot, bref, simplement passé un bon moment.

Finalement, mes remerciements vont à mes parents et à mon frère. Qu'il est bon et rassurant de pouvoir compter sur votre soutien et votre écoute indéfectibles. Votre générosité tout en simplicité est inestimable.

Mumu, tu as vu mon moral osciller durant cette thèse faite de hauts et de bas. Mais tu as toujours su me faire escalader le sommet suivant. Avec toi, je me réjouis de découvrir la suite. J'en suis impatient ! Merci.

La véritable réalité des choses, c'est l'idée qu'on s'en fait.

Gustave Le Bon

Contents

Chapter 1

Introduction

This thesis is mainly concerned with an optimization problem from the field of spectral geometry. The notions involved in its definition are addressed within this framework. However, the approach chosen to deal with this problem comes mostly from numerical analysis. This context made of two different areas of mathematics is present throughout this document. In order to be understandable for people who are less familiar with one of them, some relatively elementary notions from both are recalled. As an illustration, special care is taken to develop explicitly geometric notions as well as to outline the part of the Finite Element Method required for this work.

To get quickly to the heart of the matter in this introduction, some notions are postponed to the next sections where they are properly defined. However when this happens, the corresponding claim is carefully indicated. After setting the framework of the topic with a few motivations, this introduction deals with the issues addressed in this thesis, through theoretical statements, state-of-the-art results and personal contributions.

Context and motivations

Let (M, g) be a smooth, complete Riemannian manifold [1] and let $\Omega_M \subset M$ be a domain, namely a bounded open set in M. Moreover assume that g is smooth. Although this introduction takes place in any dimension, only two-dimensional manifolds are considered in the rest of this thesis. Let Δ_g denote the Laplace operator [2]. The underlying problem is this:

$$(\mathcal{P}) \left\{ \begin{array}{rcll} \text{Find a map } u := u_{\Omega_M} : \Omega_M \to \mathbb{R}, u \not\equiv 0, \text{ and a scalar } \lambda := \lambda_{\Omega_M} \text{ such that} & & & \\ -\Delta_g u & = & \lambda u & \text{in } \Omega_M, \\ u & = & 0 & \text{on } \partial\Omega_M. \end{array} \right.$$

1. The fundamental definition of a Riemannian manifold is not repeated in this document. See [dC76, Definition 5-10.5a] for a definition.

2. See Subsection 2.1.3 and Equation (3.1) for its expression using local coordinates.

The spectral theorem[3] ensures that there exist a strictly positive sequence

$$0 < \lambda_{1,\Omega_M} \leq \lambda_{2,\Omega_M} \leq ... \nearrow +\infty,$$

tending to $+\infty$ and a sequence of functions $(u_{n,\Omega_M})_{n\in\mathbb{N}\setminus\{0\}}$, forming a Hilbert basis of $L^2(\Omega_M)$, such that for all $n \in \mathbb{N}\setminus\{0\}$, $(\lambda_{n,\Omega_M}, u_{n,\Omega_M})$ is a solution of $(\mathcal{P})$. Of course, these *eigenvalues* λ_{n,Ω_M} and *eigenfunctions* $u_{n,\Omega}$ highly depend[4] on the underlying domain Ω_M. In this case, the set of all the eigenvalues forms the *spectrum of the Laplace operator* on Ω_M—it is also called the *spectrum of* Ω_M for convenience—. In this thesis, a numerical study of the spectrum is proposed, from the approximation of eigenvalues of certain domains in various manifolds to the optimization of eigenvalues with respect to the domain.

Two domains which have the same spectrum are called *isospectral*. One of the interesting properties of the spectrum is its invariance under isometries[5], meaning that two isometric domains are isospectral. The converse statement does not hold as proved by J. Milnor who exhibited a pair of 16-dimensional isospectral flat tori which are not isometric [Mil64]. With regard to the particular case of two-dimensional domains, M. Kac asked his famous question "Can one hear the shape of a drum?"[6] [Kac66]. A negative answer in the form of two isospectral planar domains was later given by C. Gordon, D. Webb and S. Wolpert in [GWW92] and followed thereafter by families of isospectral planar domains [BCDS94]. See Figure 1.1. Both rely on qualitative arguments avoiding explicit computations of the spectrum of the domains involved. Actually, the behaviour of the spectrum of a domain subject to small perturbations has been intensively studied, resulting in numerous theorems. The classical references [BGM71], [Bér86] and [Cha84] present a qualitative study in spectral geometry. It shows that the spectrum is a useful tool for *comparing* several domains, which is observed using numerical experiments for two and three-dimensional domains [Reu06]. This observation gave rise to the development of applications for shape recognition.

As M. Kac already knew [Kac66], geometric and topological properties of a smooth and bounded planar domain can be derived from its spectrum. More generally for a domain Ω_M in a manifold of dimension $N \in \mathbb{N}\setminus\{0\}$ with boundary $\partial\Omega_M$ *regular enough*, the asymptotic behaviour of large eigenvalues give information about some of the domain's features. An illustration of this is the famous Weyl asymptotic formula[7],

$$\lambda_{k,\Omega_M}^{N/2} \sim \frac{(2\pi)^N}{\omega_N} \frac{k}{\mathrm{vol}_g(\Omega_M)}, \qquad \text{as } k \to \infty,$$

3. See Theorem 3.1.2.

4. This dependence is also indicated using the notation $\lambda_n(\Omega_M)$.

5. The definition of an isometry implies directly that there exist two charts within the coefficients of the metric of two isometric Riemannian manifolds are equal. Hence, the expressions (3.1) of the Laplace operator in both surfaces are the same.

6. As stated in [CH53, Section V.5], every eigenfrequency f_k of a drum corresponds to $\sqrt{\lambda_{k,\Omega}}$, where $\lambda_{k,\Omega}$ is the k-th eigenvalue associated to the domain Ω representing the drumhead.

7. See [Cha84, Section VII.3] where $\partial\Omega_M$ is supposed to be piecewise smooth.

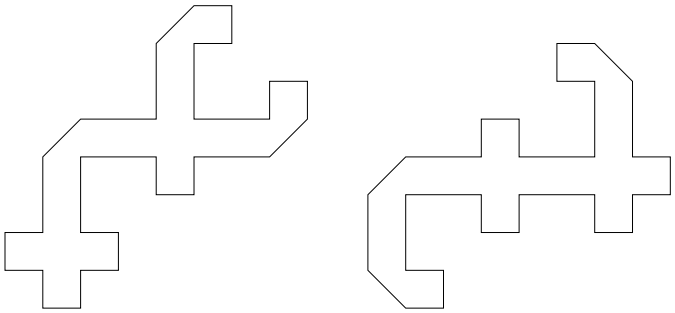

Figure 1.1: The isospectral domains given in [GWW92].

where ω_N denotes the volume of the unit ball of $\mathbb{R}^N$ and vol_g the volume measured using the metric g. Another general formula involving the spectrum and properties of the underlying domain is given in [MS67], namely

$$(4\pi t)^{\frac{N}{2}} \sum_{k\geq 1} \mathrm{e}^{-\lambda_{k,\Omega_M} t} = \mathrm{vol}_g(\Omega_M) + \frac{(4\pi t)^{\frac{1}{2}}}{4} \mathrm{vol}(\partial\Omega_M) + \frac{t}{3} \int_{\Omega_M} K - \frac{t}{6} \int_{\partial\Omega_M} J + o(t^{\frac{3}{2}}),$$

where J is the mean curvature of the boundary $\partial\Omega_M$ and K is the scalar curvature.

Individual eigenvalues can also deliver information. As an illustration, consider the characterization of the eigenvalues given by the Rayleigh quotient and the Min-max theorem [8], namely

$$\lambda_{k,\Omega_M} = \min_{E_k \in \mathcal{V}_k} \max_{v \in E_k \setminus \{0\}} \frac{\displaystyle\int_{\Omega_M} |\boldsymbol{\nabla} \boldsymbol{v}|^2 \, \mathrm{d}V_g}{\displaystyle\int_{\Omega_M} v^2 \, \mathrm{d}V_g},$$

where $\mathcal{V}_k$ denotes the set of all subspaces E_k of $H_0^1(\Omega_M)$ of dimension k. In particular for $k = 1$,

$$\lambda_{1,\Omega_M} = \min_{u \in H_0^1(\Omega_M) \setminus \{0\}} \frac{\displaystyle\int_{\Omega_M} |\boldsymbol{\nabla} \boldsymbol{u}|^2 \, \mathrm{d}V_g}{\displaystyle\int_{\Omega_M} v^2 \, \mathrm{d}V_g}.$$

Together with symmetric decreasing rearrangements of functions [9], it leads to the Faber-Krahn inequality, conjectured by Lord Rayleigh [Ray45].

8. See also Definition 3.3.1 and Theorem 3.3.2.
9. See [Kes06] for symmetrization techniques.

Theorem 1.1.1 (Faber-Krahn inequality, [Fab23], [Kra25]). *Let $\Omega_{\mathbb{R}^N} \subset \mathbb{R}^N$ be a bounded open set of volume $V > 0$ and $\Omega^*_{1,\mathbb{R}^N} \subset \mathbb{R}^N$ be the open ball of same volume. Then,*

$$\lambda_1(\Omega^*_{1,\mathbb{R}^N}) \leq \lambda_1(\Omega_{\mathbb{R}^N}),$$

with equality if and only if $\Omega_{\mathbb{R}^N} = \Omega^*_{1,\mathbb{R}^N}$.

This result also holds in the sphere and in hyperbolic space as mentioned in [Cha84, Section IV.2]. Note it will be recovered numerically for these three surfaces in Section 5.2. About arbitrary Riemannian manifolds, a theorem from [PS09] asserts that in the neighbourhood of each non-degenerated critical point p of the scalar curvature, there exist *small* extremal domains for the first eigenvalue which are *close* to a geodesic ball centred at p. By extremal domains, the authors mean that the derivative of the first eigenvalue—seen as a real valued function of a volume preserving deformation—vanishes. With regard to the second eigenvalue, the analogous result to the Faber-Krahn inequality is the Krahn-Szegő inequality.

Theorem 1.1.2 (Krahn-Szegő inequality, [Kra26] [10]). *Let $\Omega_{\mathbb{R}^N} \subset \mathbb{R}^N$ be a bounded open set of volume $V > 0$ and $\Omega^*_{2,\mathbb{R}^N} \subset \mathbb{R}^N$ be the domain consisting of two disjoint open balls of volume $V/2$. Then,*

$$\lambda_2(\Omega^*_{2,\mathbb{R}^N}) \leq \lambda_2(\Omega_{\mathbb{R}^N}),$$

with equality if and only if $\Omega_{\mathbb{R}^N} = \Omega^*_{2,\mathbb{R}^N}$.

Its proof follows directly from the Faber-Krahn inequality together with the Courant nodal theorem [11] and a rescaling argument. The latter makes use of the invariance under homothety of the functional [12]

$$\Omega \longmapsto \lambda_{k,\mathbb{R}^N}(\Omega)\ \mathrm{vol}(\Omega)^{2/N}, \quad k \in \mathbb{N} \setminus \{0\}, \tag{1.1}$$

defined on regular bounded domains in $\mathbb{R}^N$.

For a volume $V = 1$, the minimal value reached by the ball $\Omega^*_{1,\mathbb{R}^N} \subset \mathbb{R}^N$ is given by

$$\lambda_1(\Omega^*_{1,\mathbb{R}^N}) = \omega_N^{2/N}\, j^2_{N/2-1,1},$$

where $j_{N/2-1,1}$ denotes the first zero of the $N/2-1$ Bessel function $J_{N/2-1}$, whereas

$$\lambda_2(\Omega^*_{2,\mathbb{R}^N}) = 2^{2/N}\, \lambda_1(\Omega^*_{1,\mathbb{R}^N}),$$

see [Cha84, Section IV.2, Remark 4]. The definition of the Bessel functions and their detailed study make explicit the eigenvalues for the ball of $\mathbb{R}^N$. However, except for very

10. G. Pólya attributed the result to G. Szegő in his paper [Pól55], but this inequality was also pusblished independently by I. Hong [Hon54] one year earlier.

11. A *nodal domain* of a function u defined on a domain Ω_M is a connected component of the set $\Omega_M \setminus \overline{\{x \in \Omega_M \mid u(x) = 0\}}$. This theorem asserts that the number of nodal domains of an eigenfunction u_k associated to λ_k is at most k, for all $k \in \mathbb{N}$. See [CH53, Section VI.6].

12. It follows from direct computations.

specific domains such as a rectangle in the plane, getting explicit values is *unfeasible* for general domains. This is a first reason to deal with the spectrum of the Dirichlet-Laplace operator using a numerical approach.

Another argument to consider computational approximations is related to the optimization problem generalizing the Faber-Krahn and Krahn-Szegő inequalities to any eigenvalue λ_k, namely

$$(\mathcal{P}_{opt}) \begin{cases} \text{Find an open set } \Omega^*_{k,M} \subset M \text{ of volume } V > 0, \text{ such that} \\ \qquad \lambda_k(\Omega^*_{k,M}) \leq \lambda_k(\Omega_M), \\ \text{for all open sets } \Omega_M \subset M \text{ of volume } V. \end{cases}$$

Indeed, for any integer $k \geq 3$, no analogous results to the Faber-Krahn or to the Krahn-Szegő inequalities exist. Nevertheless, legitimacy of the problem $(\mathcal{P}_{opt})$ has been enhanced by a recent result by D. Bucur [Buc12] for quasi-open sets—instead of open sets—in $\mathbb{R}^N$, $N \geq 1$, also reached independently by D. Mazzoleni and A. Pratelli [MP13]. This result claims that a solution exists in such a class of domains for any k. Furthermore, it ensures the optimizer to be bounded and to have finite perimeter.

Several numerical experiments have been performed to find a candidate to be the optimizer in $(\mathcal{P}_{opt})$. E. Oudet is a precursor in this field with his work [Oud04]. It is restricted to the domains in $\mathbb{R}^2$ minimizing the first ten eigenvalues. It suggests—as expected by the mathematical community—that the candidate associated to the third and fourth eigenvalues are a disc and two disc of different area respectively. Thereafter, his results were improved by P. R. S. Antunes and P. Freitas in their paper [AF12], where they found a different shape for the candidate associated to the seventh eigenvalue. They also extended the results to the first fifteen eigenvalues, see Figure 1.2, as well as to Neumann and Robin boundary conditions with J.B. Kennedy in [AFK13]. With regard to Neumann-Laplace eigenvalues which form a positive sequence $0 = \mu_0(\Omega_M) < \mu_1(\Omega_M) \leq \mu_2(\Omega_M) \leq ... \nearrow +\infty$, the relevant optimization problem is to maximize the k-th eigenvalue μ_k among all domains of a given volume. The counterpart to Faber-Krahn inequality is the Szegő-Weinberger inequality [Wei56]. It claims, for domains of volume 1, that

$$\mu_1(\Omega) \leq \mu_1(\Omega^{**}_{1,\mathbb{R}^N}) = \omega_N^{2/N}\, p^2_{N/2,1},$$

where $\Omega^{**}_{1,\mathbb{R}^N}$ is a ball of volume 1 in $\mathbb{R}^N$ and $p_{N/2,1}$ denotes the first zero of the derivative of the function $t \mapsto t^{1-N/2}J_{N/2}$. M. S. Ashbaugh and R. D. Benguria extended this inequality to domains contained in a hemisphere of $\mathbb{S}^N$, as well as to smooth domains in $\mathbb{D}^N$ [AB01].

Moreover, a theorem by A. Girouard, N. Nadirashvili, and I. Polterovich [GNP09] is the analogous result to the Krahn-Szegő inequality in dimension 2. It asserts, for simply connected planar domains of volume 1, that

$$\mu_2(\Omega) < 2\mu_1(\Omega^{**}_{1,\mathbb{R}^N})\,\mathrm{vol}(\Omega^{**}_{1,\mathbb{R}^N}),$$

with equality attained in the limit by a family of domains degenerating to a disjoint union of two identical disks.

Figure 1.2: Planar domains minimizing the fifth (left) up to the fifteenth (right) eigenvalue among domains of a given volume from [AF12].

Issues addressed in this thesis and ensuing results

The two main topics of this thesis are the numerical approximation of eigenvalues of the Laplace operator on domains in surfaces, and their numerical optimization with respect to the domain. The numerical method used to perform approximation of eigenvalues is based on the Finite Element Method. To take into consideration the curvature of a general manifold, the computations take place in the open set of a chart. Contrary to *classical* surface discretization which interpolates a surface in $\mathbb{R}^3$—see [JU08]—, the advantage is that surfaces which are non-embeddable in $\mathbb{R}^3$, such as hyperbolic space, can be considered. The metric contribution is then introduced into the components of the matrices involved in the approximated problem. Indeed, the eigenvalues appearing in a finite linear system are used to approximate the desired eigenvalues of the Laplace operator. For this purpose, a Lanczos method is performed. The surfaces chosen for numerical approximations of eigenvalues are $\mathbb{R}^2$, the sphere $\mathbb{S}^2$, hyperbolic space through the Poincaré disc model $\mathbb{D}^2$ and a family of surfaces with non-constant curvature.

The optimization problem $(\mathcal{P}_{opt})$ is addressed numerically by minimizing the first fifteen eigenvalues for a domain in $\mathbb{R}^2$ to recover the results in [AF12]. Then, the analogous optimization problem in the sphere $\mathbb{S}^2$ and in the Poincaré disc model $\mathbb{D}^2$ are carried out numerically. It leads to Table 1.1 [13] repeated from the main part of this document. Note the value reported for the thirteenth eigenvalue is slightly larger in the sphere than hyperbolic space. Moreover, the optimizers $\Omega^*_{k,\mathbb{D}^2}$, $k = 1, \dots, 15$, in the Poincaré disc are displayed in Figure 1.3.

The *shape optimization* process to deal with $(\mathcal{P}_{opt})$ relies on a descent method algorithm, which takes advantage of the Hadamard Variational Formula (4.6) given subsequently. The volume constraint [14] appearing in $(\mathcal{P}_{opt})$ is handled with a Uzawa Algorithm, which is a new approach. The optimal domain is obtained by finding a saddle point of a Lagrangian $\mathcal{L}$ of the form $\mathcal{L}(\Omega, \mu) = \lambda_k(\Omega) + \mu(\mathrm{vol}(\Omega) - V)$, where the notations are precisely defined in Chapter 4. Up to now, optimization on surfaces different from the plane does not seem to have been studied numerically. As a comparison in $\mathbb{R}^2$, the Finite Element Method is also used in [Oud04] to compute eigenvalues approximation, whereas an algorithm based on the Method of Fundamental Solutions [15] is employed in [AF12].

13. The values displayed in this table are computed with masslumping (the notion of masslumping is recalled in Definition 2.2.9).

14. The invariance under homothety of the functional given by (1.1) allows to bypass this volume constraint for optimization in $\mathbb{R}^2$. Indeed, different values in the volume constraints lead to the same optimal domain in $(\mathcal{P}_{opt})$ up to a rescaling transformation.

15. [BT05] and [FHM67] are classical references on this issue.

Table 1.1: Numerical approximation of $\lambda_k(\Omega^*_{k,M})$, for $\Omega^*_{k,M}$ the optimizer of volume 0.1 in $M = \mathbb{S}^2$, $\mathbb{R}^2$, $\mathbb{D}^2$ for the k-th eigenvalue, $k = 1, \ldots, 15$.

k	$\lambda_k(\Omega^*_{k,\mathbb{S}^2}) \subset \mathbb{S}^2$	$\lambda_k(\Omega^*_{k,\mathbb{R}^2}) \subset \mathbb{R}^2$	$\lambda_k(\Omega^*_{k,\mathbb{D}^2}) \subset \mathbb{D}^2$
1	180.855	181.7	182.639
2	364.356	363.9	364.827
3	460.927	463.0	464.068
4	639.377	647.8	653.612
5	784.251	785.3	789.829
6	888.975	890.5	894.214
7	1063.127	1065.1	1089.251
8	1199.235	1200.1	1207.212
9	1330.355	1340.6	1341.360
10	1439.525	1448.2	1445.205
11	1583.765	1605.5	1632.550
12	1738.957	1743.7	1757.700
13	1890.493	1888.4	1887.360
14	1999.437	2022.2	2026.394
15	2125.772	2111.6	2148.878

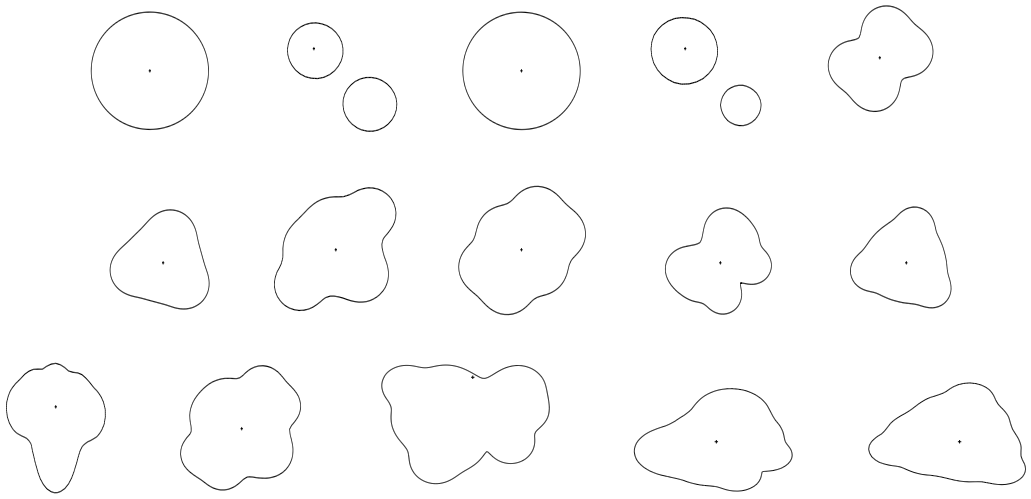

Figure 1.3: Optimizers of volume 0.1 in $\mathbb{D}^2$ for the k-th eigenvalue, $k = 1, \ldots, 15$, left to right, then downwards. The point in the domains denotes the origin of $\mathbb{D}^2$.

Contrary to the former, this is a meshless method, representing computer memory and computational time savings.

Another optimization problem is about the placement of a circular obstacle inside a domain. This issue is discussed in [Hen06, Section 3.5]. In this thesis, the maximization of an eigenvalue of a ball with respect to the location of a circular obstacle inside is addressed numerically. After validation for the first and second eigenvalues in the plane, in the sphere and in the Poincaré disc which are theoretically known[16], investigations are carried out for the third, fourth and fifth eigenvalues in these three surfaces. Note the optimal placement seems to be related to the extremal points of the corresponding eigenfunction defined on the ball without obstacle.

As regard with the numerical optimization of eigenvalues with respect to the domain, this work does not claim to deliver a proof of the optimality of a domain but only approximate candidates to be an optimizer. Indeed, on the one hand the algorithm reaches local—and not global—minima, and on the other hand it is in general *almost unfeasible* to prove theoretically that a domain is in fact a solution. Even for $k = 3$ in $\mathbb{R}^2$, it is not yet proven that the disc is the optimizer, despite numerical confirmations and *agreement*[17] in the mathematical community. Notice that not only can an explicit expression for the boundary of the optimal domain not be guessed for $k \geq 5$, but it is

16. The first and second eigenvalues are maximal when the obstacle is located at the centre of the ball. For λ_1, this result is stated in [Her63] for $\mathbb{R}^2$ and in [AA05] for $\mathbb{S}^2$ and for $\mathbb{D}^2$. It is extended to λ_2 in [ESK08].

17. As stated in Open Problem 8 from [Hen06]. This reference also states that S. A. Wolf and J. B. Keller proved that the disc in $\mathbb{R}^2$ is a local minimizer for λ_3 [WK94]. However, computations together with numerical experiments by A. Berger seem to invalidate that the ball in $\mathbb{R}^3$ minimizes λ_3.

also very likely that no such explicit description is possible. However, some interesting properties can be derived, such as the fact that the candidate obtained numerically to be the domain minimizing the thirteenth eigenvalue in the plane is not symmetric [AF12]. Another curiosity raised by numerical investigations is given by the comparison of the value of the first eigenvalue $\lambda_1(\Omega^*_{1,M})$ associated to the optimal domain $\Omega^*_{1,M}$ in various curved surfaces M. For this numerical experiment, the sphere $\mathbb{S}^2$ whose curvature equals 1, the upper sheet H of a hyperboloid whose curvature lies between 0 and 1, the plane and the Poincaré disc whose curvature equals -1 are addressed. The optimizer is a ball—centred at the point of maximal curvature for H—in each of these surfaces and for a volume of 0.01, the following inequalities hold

$$\lambda_1(\Omega^*_{1,\mathbb{S}^2}) < \lambda_1(\Omega^*_{1,\mathbb{R}^2}) < \lambda_1(\Omega^*_{1,\mathbb{D}^2}) < \lambda_1(\Omega^*_{1,H})$$

and the corresponding values are

$$1816.57 < 1816.80 < 1817.6 < 1819.10.$$

It could have been expected—at least for small volumes—that there is a ranking of such eigenvalues with respect to the curvature. But the eigenvalue resulting from the experiment in the upper sheet of a hyperboloid is not between those coming from the plane and the sphere. It is even higher than the eigenvalue of the ball in the Poincaré disc. A same ranking appears also for the second and for higher eigenvalues. Such kinds of observations were possible thanks to numerical investigations.

Organisation of the thesis

This document is organized in five chapters and three appendices. After this introduction, Chapter 2 presents basic notions and tools from geometry, the Finite Element Method and the Lanczos method to find eigenvalues associated to a finite linear system. The third chapter deals with the underlying problem, that is, the computation of eigenvalues of the Dirichlet-Laplace operator. After its theoretical statement and its numerical approximation, the estimation of the error between an exact eigenvalue and its approximation is performed and also illustrated using numerical examples. It is followed by numerical validations for specific domains such as a ball in $\mathbb{R}^2$ and by experiments in the plane $\mathbb{R}^2$, the sphere $\mathbb{S}^2$, the Poincaré disc $\mathbb{D}^2$ and a manifold with non-constant curvature. The problem of locating an obstacle in a ball to minimize its first eigenvalues is also addressed, as well as a comparison of the first eigenvalues of a ball in $\mathbb{R}^2$, $\mathbb{S}^2$ and $\mathbb{D}^2$. It is based on the prepublication [Str12a]. Then, Chapters 4 and 5 are devoted to the optimization problem ($\mathcal{P}_{opt}$). The former introduces shape optimization required to establish the main formula to deform a domain and also the Uzawa algorithm to extend the problem on domains in manifolds. The latter states the problem theoretically and displays numerical results: some validations to recover optimal candidates already obtained in [AF12] and some investigations in $\mathbb{S}^2$ and $\mathbb{D}^2$, together with some optimizations in a sheet of a hyperboloid. The numerical results presented in Chapter 5

are those in [Str12b]. Finally, the document ends with three appendices: the first one deals with some notions of functional analysis, especially Sobolev spaces which are the suitable framework for the underlying and optimization problems. Appendix B provides a detailed example of the optimization of an eigenvalue with respect to a domain in a manifold—namely $\lambda_7(\Omega_M)$ for Ω_M in the Poincaré disc $\mathbb{D}^2$—, whereas some additional numerical values are displayed in Appendix C.

Chapter 2

Fundamental tools

This chapter is devoted to recall some classical notions and tools about various concepts involved in the following chapters. This thesis takes place between two main fields of mathematics, namely geometry and numerical analysis. To be as accessible as possible, a choice has been made to present some basic notions required from both. Notations very common in mathematics are used in this chapter in order to avoid needless complexity, even if they do not coincide with the usual ones which exist in these particular fields. However, special care has been taken to mention the more frequent notations when it happens.

This chapter is divided into three parts: the first one is about Riemannian geometry and calculus on a manifold. In this part, some classical tools are introduced in the framework of a manifold and the expression of the volume element, of the gradient of a function and of the Laplace operator are explicitly established in local coordinates using a chart (U, α). Precisely, performing the computations using a chart is a specificity of our approach and it is particularly helpful for the numerical implementation of our method. The second section is a short introduction to the Finite Element Method, restricted to the aspects and results that are useful in the sequel. It leads to consider approximation of functional spaces by discretized spaces, and to approach the computation of integrals using quadrature rules. The notion of *masslumping* is also addressed. Finally, the last section is concerned with the Lanczos method, used to solve finite dimensional eigenproblems. In each part, some classical references about these topics are given.

Throughout this chapter, $N \in \mathbb{N} \setminus \{0\}$ stands for the dimension of the ambient space.

2.1 About differential geometry and calculus on manifolds

In this section, M denotes a differentiable manifold of dimension N. Assume that M is smooth, that is, M is of class $\mathcal{C}^\infty$, although less regularity would be sufficient. Moreover, (M, g) denotes a Riemannian manifold of dimension N.

2.1.1 Differential forms, volume element and integration on a manifold

This subsection begins with the definition of several notions and tools useful to introduce operators and integration on a manifold, and with some of them properties. The reference book they are derived from is [Boo75], especially its chapter V. Refer to it for the proofs of the results presented below as well as for some complements intentionally skipped here. With regard to the development of the notion of integration over a manifold, see [dC94, Chapter 4]. Thereafter, a more technical part is dedicated to the expression of the volume element in local coordinates.

In this subsection, V denotes a vector space over $\mathbb{R}$ of dimension N and V^* its dual space. Although only dimension $N = 2$ is needed for our purpose, this topics is exposed in any dimension, because it does not add any extra difficulties.

Definition 2.1.1 (Derived from [Boo75, Definition V-5.1]). A *tensor* ϕ on V is a multilinear map

$$\phi : \underbrace{V \times \cdots \times V}_{r \text{ times}} \times \underbrace{V^* \times \cdots \times V^*}_{s \text{ times}} \longrightarrow \mathbb{R},$$

where $r \in \mathbb{N}$ denotes the *covariant order* of ϕ and $s \in \mathbb{N}$ its *contravariant order*.

Notation 2.1.2. From now on, $r \in \mathbb{N}$ and $s \in \mathbb{N}$ always stand for non-negative integer. The set of all tensors of covariant order r and contravariant order s is denoted by $\mathcal{T}^r_s(V)$. It is a vector space over $\mathbb{R}$ of dimension N^{r+s}, see [Boo75, Theorem 5.2] for a proof. In the following, only covariant tensors are used, that is $s = 0$, and the set of all covariant tensors of order r is denoted by $\mathcal{T}^r(V)$ instead of $\mathcal{T}^r_0(V)$. Set $\mathcal{T}^0(V) = \mathbb{R}$ by convention.

Notation 2.1.3. Throughout this document, vectors and vector fields are denoted using bold font. Moreover, the transpose of a matrix A is denoted by A^T and the transpose of the inverse A^{-1} of a matrix A by A^{-T}.

Definition 2.1.4 ([Boo75, Definition V-5.3]). A $\mathcal{C}^\infty(M)$*-covariant tensor field of order* $r \in \mathbb{N}$ on a manifold M is a function $\phi : M \to \cup_{p \in M} \mathcal{T}^r(T_pM)$, $p \mapsto \phi_p$, such that for all $C^\infty(M)$-vector fields $\boldsymbol{X_1}, \ldots, \boldsymbol{X_r}$, the map

$$\begin{aligned} \phi(X_1, \ldots, X_r) : M &\to \mathbb{R} \\ p &\mapsto \phi_p(\boldsymbol{X_1}(p), \ldots, \boldsymbol{X_r}(p)), \end{aligned}$$

is a $\mathcal{C}^\infty(M)$-function.

The set of all $\mathcal{C}^\infty(M)$-covariant tensor fields of order r on M is denoted by $\mathcal{T}^r(M)$. Set $\mathcal{T}^0(M) = \mathcal{C}^\infty(M)$ by convention.

Definition 2.1.5 ([Boo75, Definitions V-5.4 and V-6.12]). A covariant tensor $\phi \in \mathcal{T}^r(V)$, of order $r \in \mathbb{N}$ is *symmetric*, respectively *alternating*, if for each $\boldsymbol{v_1}, \ldots, \boldsymbol{v_r} \in V$,

$$\phi(\boldsymbol{v_1}, \ldots, \boldsymbol{v_i}, \ldots, \boldsymbol{v_j}, \ldots, \boldsymbol{v_r}) = \phi(\boldsymbol{v_1}, \ldots, \boldsymbol{v_j}, \ldots, \boldsymbol{v_i}, \ldots, \boldsymbol{v_r}), \quad \forall\, 1 \leq i, j \leq r,$$

respectively

$$\phi(\boldsymbol{v_1},\ldots,\boldsymbol{v_i},\ldots,\boldsymbol{v_j},\ldots,\boldsymbol{v_r}) = -\phi(\boldsymbol{v_1},\ldots,\boldsymbol{v_j},\ldots,\boldsymbol{v_i},\ldots,\boldsymbol{v_r}), \quad \forall\, 1 \leq i,j \leq r.$$

By extension, a tensor field is *symmetric*, respectively *alternating*, if it has this property at each point. Moreover, an alternating covariant tensor field of order r on a manifold M is called an *exterior differential form of degree* r, or simply a *r-form*.

Remark 2.1.1. The set of all symmetric tensors, respectively alternating tensors, forms a subspace of $\mathcal{T}^r(V)$, denoted by $\Sigma^r(V)$, respectively $\Lambda^r(V)$. Moreover, $\Sigma^r(V) \cap \Lambda^r(V) = \{0\}$. The same remark holds for a manifold M instead of V, with the notations $\Sigma^r(M)$, respectively $\Lambda^r(M)$.

Remark 2.1.2. Let $\{\boldsymbol{e_1},\ldots,\boldsymbol{e_N}\}$ be a basis of V and $\phi \neq 0$ be a alternating covariant tensor of order $r = N$ on V. Then, a direct computation involving the multilinearity of ϕ gives, for all $\boldsymbol{v_1},\ldots,\boldsymbol{v_N} \in V$, with $\boldsymbol{v_i} = \sum_{j=1}^{N} C_{i,j}\boldsymbol{e_j}$, $i = 1,\ldots N$,

$$\phi(\boldsymbol{v_1},\ldots,\boldsymbol{v_N}) = \det C\ \phi(\boldsymbol{e_1},\ldots,\boldsymbol{e_N}),$$

where C is the matrix with component $C_{i,j}$ on the i-th row and j-th column.

Definition - Proposition 2.1.6 ([Boo75, Definition V-6.1 and Theorem V-6.2]). Let $\phi \in \mathcal{T}^r(V)$ and $\psi \in \mathcal{T}^s(V)$ be two covariant tensors. The *product* of ϕ and ψ, denoted $\phi \otimes \psi$ is a tensor of order $r+s$ defined by

$$\phi \otimes \psi(\boldsymbol{v_1},\ldots,\boldsymbol{v_r},\boldsymbol{v_{r+1}}\ldots,\boldsymbol{v_{r+s}}) = \phi(\boldsymbol{v_1},\ldots,\boldsymbol{v_r})\boldsymbol{\psi(v_{r+1}},\ldots,\boldsymbol{v_{r+s}}),$$

for all $\boldsymbol{v_1},\ldots,\boldsymbol{v_{r+s}} \in V$. The product defines a mapping $(\phi,\psi) \mapsto \phi \otimes \psi$ of $\mathcal{T}^r(V) \times \mathcal{T}^s(V) \to \mathcal{T}^{r+s}(V)$ which is bilinear and associative.

By extension, the *product* of two covariant tensor fields on a manifold M is defined at each point $p \in M$, using the previous definition on the vector space T_pM:

Definition - Proposition 2.1.7 ([Boo75, Theorem V-6.3]). Let $\phi \in \mathcal{T}^r(M)$, and $\psi \in \mathcal{T}^s(M)$ be two covariant tensor fields over a manifold M. The *product* of ϕ and ψ, denoted $\phi \otimes \psi$, is a covariant tensor field of order $r+s$ on M defined by

$$\phi \otimes \psi(p) = \phi_p \otimes \psi_p, \quad \forall p \in M.$$

The product defines an application $\mathcal{T}^r(M) \times \mathcal{T}^s(M) \to \mathcal{T}^{r+s}(M)$, $(\phi,\psi) \mapsto \phi \otimes \psi$, which is bilinear and associative.

Remark 2.1.3. The tensor product of alternating tensors on V is not, in general, an alternating tensor on V. It leads to introduce another notion of product, which verifies this property.

Definition 2.1.8 ([Boo75, Definition V-6.5 and Lemma V-6.6]). The mapping $\wedge : \Lambda^r(V) \times \Lambda^s(V) \to \Lambda^{r+s}(V)$, $(\phi, \psi) \mapsto \phi \wedge \psi$, defined by

$$\phi \wedge \psi(\boldsymbol{v_1}, \ldots, \boldsymbol{v_{r+s}}) = \frac{1}{r!s!} \sum_{\sigma \in \mathfrak{S}(r+s)} \operatorname{sgn}(\sigma) \phi \otimes \psi(\boldsymbol{v_{\sigma(1)}}, \ldots, \boldsymbol{v_{\sigma(r+s)}})$$

for all $\boldsymbol{v_1}, \ldots, \boldsymbol{v_{r+s}} \in V$, where $\mathfrak{S}(N)$ denotes the set of all permutations of $\{1, \ldots, N\}$ and $\operatorname{sgn}(\sigma)$ denotes the signature of σ, is called *exterior product* or *wedge product* of ϕ and ψ. This product is bilinear and associative.

Remark 2.1.4 ([Boo75, Corollary V-6.7]). It is a straightforward calculation to see that if $\phi_i \in \Lambda^{r_i}(V)$, $r_i \in \mathbb{N}$, $i = 1, \ldots, k$, then for all $\boldsymbol{v_1}, \ldots, \boldsymbol{v_{r_1+\cdots+r_k}} \in V$

$$\begin{aligned} &\phi_1 \wedge \cdots \wedge \phi_k(\boldsymbol{v_1}, \ldots, \boldsymbol{v_{r_1+\cdots+r_k}}) \\ &\quad = \frac{1}{r_1! \ldots r_k!} \sum_{\sigma \in \mathfrak{S}(r_1+\cdots+r_k)} \operatorname{sgn}(\sigma) \phi_1 \otimes \cdots \otimes \phi_k(\boldsymbol{v_{\sigma(1)}}, \ldots, \boldsymbol{v_{\sigma(r_1+\cdots+r_k)}}). \end{aligned}$$

Definition 2.1.9 ([Boo75, Definition V-7.5]). A manifold M is *orientable* if it is possible to define a $\mathcal{C}^\infty(M)$-N-form ϕ on M which is not zero at any point. In this case, M is said to be *oriented* by ϕ.

Theorem 2.1.10 ([Boo75, Theorem V-7.7]). *Let (M, g) be an orientable Riemannian manifold. Corresponding to an orientation of M there is a uniquely determined N-form Φ which gives the orientation and which has the value $+1$ on every oriented orthonormal frame.*

Definition 2.1.11. The N-form Φ of the previous theorem is called *volume element* and is denoted [1] by $\mathrm{d}V_g$.

Notation 2.1.12. Let $\mathcal{T}(V) = \oplus_{i=0}^{\infty} \mathcal{T}^r(V)$ and $\Lambda(V) = \oplus_{i=0}^{\infty} \Lambda^r(V)$. These two direct sums are actually associative algebra, see [Boo75, Corollary V-6.8]. Moreover it holds that $\Lambda(V) = \oplus_{i=0}^{N} \Lambda^r(V)$, see [Boo75, Theorem V-6.10].

Theorem 2.1.13 ([Boo75, Definition V-6.11]). *Let V and W be two finite dimensional vector spaces and $F_* : W \to V$ be a linear mapping. Then, the mapping $F^* : \mathcal{T}(V) \to \mathcal{T}(W)$ defined by, $F^*(\phi)(\boldsymbol{w}) = \phi(F_*(\boldsymbol{w}))$ for all $\phi \in \mathcal{T}(V)$ and $\boldsymbol{w} \in W$, takes $\Lambda(V)$ into $\Lambda(W)$ and is a homomorphism of these (exterior) algebras.*

In particular, if α denotes the map of a chart (U, α) in a neighbourhood of a point $p \in M$, the derivative $T.\alpha^{-1} : \mathbb{R}^N \to \cup_{q \in U} T_q M$ of α^{-1} is a linear mapping. Thus it can be employed to *transport* the volume element from M to $\mathbb{R}^N$ using $T.\alpha^{-1*}$.

The required tools are now at our disposal to give the expression of the volume element in local coordinates. This expression is intensively used in the sequel and especially in the numerical implementation. That is the reason why the following development is made

1. This notation comes from its use in measure theory, as it appears later.

explicitly, although it is a particular case of Remark 2.1.2. Let (M, g) be a Riemannian manifold oriented by the volume element $\mathrm{d}V_g$, and let (α, U) be a chart of M in the neighbourhood of a point $p \in M$. Let $\{\boldsymbol{E_1}(p), \ldots, \boldsymbol{E_N}(p)\}_{p\in U}$ denote [2] the basis of T_pM such that

$$T_p\alpha\, \boldsymbol{E_i}(p) = \boldsymbol{\partial x_i}|_{\alpha(p)}, \quad \forall i = 1, \ldots, N, \tag{2.1}$$

where $\{\boldsymbol{\partial x_i}\}_{i=1}^N$ denotes the usual *local coordinates* [3]. However, there is no particular reason for $\{\boldsymbol{E_1}(p), \ldots, \boldsymbol{E_N}(p)\}_{p\in U}$ to be orthonormal with respect to the Riemannian metric $g(p)$, so in general $\mathrm{d}V_g(\boldsymbol{E_1}(p), \ldots, \boldsymbol{E_N}(p)) \neq 1$. Thus, we consider an orthonormal (with respect to $g(p)$) basis $\{\boldsymbol{F_1}(p), \ldots, \boldsymbol{F_N}(p)\}_{p\in U}$ of T_pM, that is $g(p)(\boldsymbol{F_i}(p), \boldsymbol{F_j}(p)) = \delta_{ij}$. So, it allows us to express the vectors $\boldsymbol{E_i}(p)$, $i = 1, \ldots, N$, using the basis $\{\boldsymbol{F_k}(p)\}_{k=1}^N$:

$$\boldsymbol{E_i}(p) = \sum_{k=1}^{N} A_{i,k}(p)\boldsymbol{F_k}(p), \quad A_{i,k} \in \mathbb{R},\ 1 \leq i, k \leq N,$$

or equivalently,

$$\underbrace{\begin{pmatrix} | & & | \\ E_1(p) & \cdots & E_N(p) \\ | & & | \end{pmatrix}}_{=:\, E(p)} = \underbrace{\begin{pmatrix} A_{1,1}(p) & \cdots & A_{1,N}(p) \\ \vdots & \ddots & \vdots \\ A_{N,1}(p) & \cdots & A_{N,N}(p) \end{pmatrix}}_{=:\, A(p)} \underbrace{\begin{pmatrix} - & F_1(p) & - \\ & \vdots & \\ - & F_N(p) & - \end{pmatrix}}_{=:\, F(p)}.$$

At each point $p \in M$, the metric g can be represented by a matrix $G(\alpha(p))$ using the local coordinates, that is

$$G_{i,j}(\alpha(p)) = g(p)(\boldsymbol{E_i}(p), \boldsymbol{E_j}(p)), \quad 1 \leq i, j \leq N. \tag{2.2}$$

Then,

$$\begin{aligned} G_{i,j}(\alpha(p)) &= g(p)\left(\sum_{k=1}^{N} A_{i,k}(p)\boldsymbol{F_k}(p), \sum_{k=1}^{N} A_{j,k}(p)\boldsymbol{F_k}(p)\right) \\ &= \sum_{k=1}^{N} A_{i,k}(p)A_{j,k}(p) = (A(p)A^T(p))_{i,j}. \end{aligned} \tag{2.3}$$

2. Although α does not appear in the notation of $\boldsymbol{E_i(p)}$, $i = 1, \ldots, N$, these vectors actually depend on the chart.

3. Actually, the local coordinates do not depend on the point $\alpha(p)$ where they are estimated. They are sometimes denoted by $\left\{\frac{\boldsymbol{\partial}}{\boldsymbol{\partial x_i}}\right\}_{i=1}^N$.

Besides,

$$\begin{aligned}
\mathrm{d}V_g(\boldsymbol{E_1}(p),\dots,\boldsymbol{E_N}(p)) &= \mathrm{d}V_g\left(\sum_{k_1=1}^{N} A_{1,k_1}(p)\boldsymbol{F_{k_1}}(p),\dots,\sum_{k_N=1}^{N} A_{N,k_N}(p)\boldsymbol{F_{k_N}}(p)\right)\\
&= \sum_{k_1,\dots,k_N=1}^{N} A_{1,k_1}(p)\cdots A_{N,k_N}(p)\mathrm{d}V_g(\boldsymbol{F_{k_1}}(p),\dots,\boldsymbol{F_{k_N}}(p))\\
&\overset{\sigma(i):=k_i}{=} \sum_{\sigma\in\mathfrak{S}(N)} \mathrm{sgn}(\sigma)A_{1,\sigma(1)}(p)\cdots A_{N,\sigma(N)}(p)\\
&= \det A(p) \;=\; \sqrt{\det G(\alpha(p))}, \qquad (2.4)
\end{aligned}$$

where the last equality comes from equality (2.3).

There is still a manipulation remaining, consisting in expressing the volume element in $\alpha(U)\subset\mathbb{R}^N$, where U is the open set of the chart. Since $p\mapsto T_{\alpha(p)}\alpha^{-1*}\mathrm{d}V_g$ is an N-form[4] on $\mathbb{R}^N$ by Theorem 2.1.13, it can be written at a point $p\in\alpha(U)$ as

$$T_{\alpha(p)}\alpha^{-1*}\mathrm{d}V_g = f(p)\,\mathrm{d}x_1(p)\wedge\cdots\wedge\mathrm{d}x_N(p), \qquad (2.5)$$

where $f:\alpha(U)\to\mathbb{R}$ is a $\mathbb{C}^\infty(\alpha(U))$-function to be determined and $\{\mathrm{d}x_j\}_{j=1}^N$ is the dual basis of $\{\boldsymbol{\partial x_k}\}_{k=1}^N$, that is, $\mathrm{d}x_j\left(\boldsymbol{\partial x_k}\right)=\delta_{j,k}$, where δ_{jk} denotes the Kronecker symbol. First, notice that, for $p\in U$,

$$\begin{aligned}
T_{\alpha(p)}\alpha^{-1*}\mathrm{d}V_g\left(\boldsymbol{\partial x_1},\dots,\boldsymbol{\partial x_N}\right) &:= \mathrm{d}V_g\left(T_{\alpha(p)}\alpha^{-1}\boldsymbol{\partial x_1},\dots,T_{\alpha(p)}\alpha^{-1}\boldsymbol{\partial x_N}\right)\\
&= \mathrm{d}V_g(\boldsymbol{E_1}(p),\dots,\boldsymbol{E_N}(p))\\
&= \sqrt{\det G(\alpha(p))} \qquad (2.6)
\end{aligned}$$

where the last equality comes from (2.4). Then, for any $\boldsymbol{v_i}=\sum_{k_i=1}^N v_{i,k_i}\boldsymbol{\partial x_{k_i}}\in\mathbb{R}^N$, $i=1,\dots,N$, it holds that

$$\begin{aligned}
&T_{\alpha(p)}\alpha^{-1*}\mathrm{d}V_g(\boldsymbol{v_1},\dots,\boldsymbol{v_n})\\
&= T_{\alpha(p)}\alpha^{-1*}\left(\sum_{k_1=1}^{N} v_{1,k_1}\boldsymbol{\partial x_{k_1}},\dots,\sum_{k_N=1}^{N} v_{N,k_N}\boldsymbol{\partial x_{k_N}}\right)\\
&= \sum_{k_1,\dots,k_N=1}^{N} v_{1,k_1}\cdots v_{N,k_N}T_{\alpha(p)}\alpha^{-1*}\mathrm{d}V_g\left(\boldsymbol{\partial x_{k_1}},\dots,\boldsymbol{\partial x_{k_N}}\right)\\
&= \sum_{\sigma\in\mathfrak{S}(N)} \mathrm{sgn}(\sigma)v_{1,\sigma(1)}\cdots v_{N,\sigma(N)}T_{\alpha(p)}\alpha^{-1*}\mathrm{d}V_g\left(\boldsymbol{\partial x_1},\dots,\boldsymbol{\partial x_N}\right)\\
&\overset{(2.6)}{=} \sqrt{\det G(\alpha(p))}\sum_{\sigma\in\mathfrak{S}(N)} \mathrm{sgn}(\sigma)v_{1,\sigma(1)}\cdots v_{N,\sigma(N)}.
\end{aligned}$$

4. This N-form is called *pullback* of $\mathrm{d}V_g$ by α^{-1}. It is more often denoted by $\alpha^{-1*}\mathrm{d}V_g$.

On the other hand,

$$\begin{aligned}
&\mathrm{d}x_1 \wedge \cdots \wedge \mathrm{d}x_N(\boldsymbol{v_1}, \ldots, \boldsymbol{v_N}) \\
&= \mathrm{d}x_1 \wedge \cdots \wedge \mathrm{d}x_N \left(\sum_{k_1=1}^{N} v_{1,k_1} \boldsymbol{\partial x_{k_1}}, \ldots, \sum_{k_N=1}^{N} v_{N,k_N} \boldsymbol{\partial x_{k_N}} \right) \\
&= \sum_{k_1,\ldots,k_N=1}^{N} v_{1,k_1} \cdots v_{N,k_N}\, \mathrm{d}x_1 \wedge \cdots \wedge \mathrm{d}x_N \left(\boldsymbol{\partial x_{k_1}}, \ldots, \boldsymbol{\partial x_{k_N}} \right) \\
&= \sum_{\sigma \in \mathfrak{S}(N)} \mathrm{sgn}(\sigma) v_{1,\sigma(1)} \cdots v_{N,\sigma(N)} \underbrace{\mathrm{d}x_1 \wedge \cdots \wedge \mathrm{d}x_N \left(\boldsymbol{\partial x_1}, \ldots, \boldsymbol{\partial x_N} \right)}_{=1}.
\end{aligned}$$

Finally, the volume element can be expressed in local coordinates by

$$T_{\alpha(p)} \alpha^{-1*} \mathrm{d}V_g(\boldsymbol{v_1}, \ldots, \boldsymbol{v_n}) = \sqrt{\det G(\alpha(p))}\, \mathrm{d}x_1 \wedge \cdots \wedge \mathrm{d}x_N(\boldsymbol{v_1}, \ldots, \boldsymbol{v_N}), \tag{2.7}$$

for all $\boldsymbol{v_1}, \ldots, \boldsymbol{v_N} \in \mathbb{R}^N$. Hence, $f = \sqrt{\det G}$ in equality (2.5).

Following [dC94, Chapter 4], the notion of integrals over a Riemannian manifold (M, g) can be now addressed. The aim is to compute integrals of a function over $\alpha(U)$, for a given chart (α, U) using the expression of the volume element in local coordinates. Indeed, it will be useful again for the numerical computations involved in the sequel. Before dealing with integrals of a function, let us first define the integral of an N-form over a bounded subset of $\mathbb{R}^N$.

Definition 2.1.14. Let ϕ be an N-form in an open subset $D \subset \mathbb{R}^N$ with compact support K contained in U. If ϕ is written as $\phi = f \mathrm{d}x_1 \wedge \cdots \wedge \mathrm{d}x_N$, for a $\mathcal{C}^\infty(D)$-function f, then the *integral of ϕ over D* is defined by

$$\int_D \phi = \int_K f\, \mathrm{d}x_1 \ldots \mathrm{d}x_N,$$

where $\mathrm{d}x_1 \ldots \mathrm{d}x_N$ denotes the Lebesgue measure on $\mathbb{R}^N$.

The map α of a chart allows to extend this definition to an oriented manifold. To avoid convergence problems, it is convenient—although generally not required—to assume the support of the N-form to be compact. It holds for instance if M is compact. Moreover, make first the assumption that the support of the N-form is contained in an open set of a chart.

Definition 2.1.15. Let (M, g) be an oriented Riemannian manifold [5], ϕ be a N-form on M having compact support in the open set U of a chart (α, U). The *integral of ϕ over M* is defined by

$$\int_M \phi = \int_{\alpha(U)} T.\alpha^{-1*} \phi.$$

5. The metric g does not play any role in this definition.

The orientability of the manifold ensures that this definition does not depend on the choice of the map. The choice of an orientation for M fixes the sign of the integral. Finally, if ϕ has compact support, but not completely inside the open set of a chart, then to integrate ϕ over the entire manifold, a partition of unity $\{\psi_i\}$ compatible with the covering by the open sets of the charts is required. Indeed, it allows to apply the previous definition to each $\psi_i\phi$. The integral of ϕ over M is then the sum of the integrals of the $\psi_i\phi$ over M.

Now, the definition of an integral of a function $f : M \to \mathbb{R}$ over a Riemannian manifold (M, g) follows naturally.

Definition 2.1.16. Let (M, g) be an oriented Riemannian manifold, and let $\mathrm{d}V_g$ be the associated volume element. A function $f : M \to \mathbb{R}$ is *integrable over* M if f has compact support in M. Furthermore, the *integral of* f *over* M is the integral of the N-form[6] $f\mathrm{d}V_g$.

Remark 2.1.5. Assume f to be as in the previous definition. If the support of f is compact and included in the open set U of a chart (α, U), then,

$$\int_M f\mathrm{d}V_g = \int_{\alpha(U)} T.\alpha^{-1*}(f\mathrm{d}V_g) = \int_{\alpha(U)} f \circ \alpha^{-1}\sqrt{\det G}\,\mathrm{d}x_1 \ldots \mathrm{d}x_N,$$

by equation (2.7). This formula will be intensively used for the eigenvalue problem on a Riemannian manifold.

The classical and *expected* properties of the integral defined above are proved in [Boo75, Section VI-2].

2.1.2 Expression of the gradient in local coordinates

This subsection is based on the second chapter of [GHL04].

Definition 2.1.17 ([Cha84, Definition I-1])**.** Let $f : M \to \mathbb{R}$ be a function of class $\mathcal{C}^\infty(M)$. The *gradient* of f, denoted $\boldsymbol{\nabla f}$ is the vector field on M defined by

$$g(p)(\boldsymbol{\nabla f}(p), \boldsymbol{Z}(p)) = \boldsymbol{Z}(f)(p), \quad \forall \boldsymbol{Z} \in \chi(M),\ \forall p \in M,$$

where $\chi(M)$ denotes the vector space of all vector fields of class $\mathcal{C}^\infty(M)$.

Remark 2.1.6. The Riesz representation Theorem (Theorem A.1.3) ensures that the gradient of a function f is well defined.

Proposition 2.1.18. *Let $f, h \in \mathcal{C}^\infty(M)$. Then,*

$$\begin{aligned} \boldsymbol{\nabla}(\boldsymbol{f} + \boldsymbol{h}) &= \boldsymbol{\nabla f} + \boldsymbol{\nabla h}, \\ \boldsymbol{\nabla}(\boldsymbol{fh}) &= f\boldsymbol{\nabla h} + h\boldsymbol{\nabla f}. \end{aligned}$$

6. The N-form $f\mathrm{d}V_g$ has compact support in M.

Remark 2.1.7. Let (α, U) be a chart of M in the neighbourhood of a point $p \in M$. As in the previous subsection with equation (2.2), consider the family of matrices $\{G(\alpha(p))\}_{p\in U}$ representing the metric g at each point $p \in U$ in the usual local coordinates $\{\boldsymbol{\partial x_i}\}_{i=1}^N$. Let us carry out an analogous development as the one that gave the expression of the volume element in local coordinates. The gradient of a function $f \in \mathcal{C}^\infty(M)$ can be expressed at a point $p \in U$ in the basis $\{\boldsymbol{E_i}(p)\}_{i=1}^N$ defined in equation (2.1), that is

$$\boldsymbol{\nabla f}(p) = \sum_{k=1}^{N} \beta_k(p) \boldsymbol{E_k}(p),$$

thus, for all $i = 1, \ldots, N$,

$$g(p)(\boldsymbol{\nabla f}(p), \boldsymbol{E_i}(p)) = \sum_{k=1}^{N} \beta_k(p) G_{k,i}(\alpha(p)).$$

For $p \in U$, the definition of the gradient applied to $\boldsymbol{Z}(p) = \boldsymbol{E_i}(p)$, $i = 1, \ldots, N$, and the definition of $\{\boldsymbol{E_i}(p)\}_{i=1}^N$, yield

$$g(p)(\boldsymbol{\nabla f}(p), \boldsymbol{E_i}(p)) = \boldsymbol{E_i}(f)(p) = T_{\alpha(p)}\alpha^{-1} \boldsymbol{\partial x_i}(f)(p) = \boldsymbol{\partial x_i}(f \circ \alpha^{-1})(\alpha(p)).$$

Hence, for all $i = 1, \ldots, N$,

$$\boldsymbol{\partial x_i}(f \circ \alpha^{-1})(\alpha(p)) = \sum_{k=1}^{N} \beta_k(p) G_{k,i}(\alpha(p)),$$

that is,

$$\boldsymbol{\nabla_{us}(f \circ \alpha^{-1})}(\alpha(p)) = G^T(\alpha(p)) \boldsymbol{\nabla f}(p),$$

where ∇_{us} denotes the usual gradient operator acting on functions defined on an open set of $\mathbb{R}^N$. Finally, the gradient of f in local coordinates is given, for all $p \in U$, by [7]

$$\boldsymbol{\nabla f} = G^{-T} \boldsymbol{\nabla_{us}(f \circ \alpha^{-1})} \circ \alpha,$$

or by

$$\boldsymbol{\nabla f} = G^{-1} \boldsymbol{\nabla_{us}(f \circ \alpha^{-1})} \circ \alpha, \tag{2.8}$$

thanks to the symmetry of G since it represents a metric.

In order to define the divergence and the Laplace operators on a Riemannian manifold (M, g), several tools need to be introduced.

Definition 2.1.19 ([GHL04, Definition 1.52 bis]). Let $U \subset M$ be an open set of M. The *Lie bracket* is the mapping $[\cdot, \cdot] : \chi(U) \times \chi(U) \to \chi(U)$ defined by

$$[\boldsymbol{X}, \boldsymbol{Y}] = \boldsymbol{XY} - \boldsymbol{YX}, \quad \boldsymbol{X}, \boldsymbol{Y} \in \chi(U).$$

7. As mentioned before, G^{-T} denotes the transpose of the inverse of the matrix G.

Remark 2.1.8. The Lie bracket is a $\mathbb{R}$-bilinear, anticommutative mapping, and satisfies the *Jacobi identity*, that is,

$$[\boldsymbol{X},[\boldsymbol{Y},\boldsymbol{Z}]]+[\boldsymbol{Y},[\boldsymbol{Z},\boldsymbol{X}]]+[\boldsymbol{Z},[\boldsymbol{X},\boldsymbol{Y}]]=0. \quad \forall \boldsymbol{X},\boldsymbol{Y},\boldsymbol{Z}\in\chi(U).$$

Definition 2.1.20 ([GHL04, Definitions 2.49 and 2.50]). A *connection* on M is a mapping $\nabla:\chi(M)\times\chi(M)\to\chi(M)$, denoted by $(\boldsymbol{X},\boldsymbol{Y})\mapsto\nabla_{\boldsymbol{X}}\boldsymbol{Y}$, such that for all $\boldsymbol{X},\boldsymbol{Y},\boldsymbol{\xi},\boldsymbol{\zeta}\in\chi(M)$ and for all $f\in\mathcal{C}^\infty(M)$:

(i) $\nabla_{\boldsymbol{\xi}}(f\boldsymbol{X}+\boldsymbol{Y})(p)=\boldsymbol{\xi}(f)(p)\boldsymbol{X}(p)+f(p)\nabla_{\boldsymbol{\xi}}\boldsymbol{X}(p)+\nabla_{\boldsymbol{\xi}}\boldsymbol{Y}(p)$;

(ii) $\nabla_{f\boldsymbol{\xi}+\boldsymbol{\zeta}}(\boldsymbol{X})(p)=f(p)\nabla_{\boldsymbol{\xi}}\boldsymbol{X}(p)+\nabla_{\boldsymbol{\zeta}}\boldsymbol{X}(p)$.

Moreover, $\nabla_{\boldsymbol{X}}\boldsymbol{Y}$ is said to be *torsion-free* if it also satisfies

(iii) $[\boldsymbol{X},\boldsymbol{Y}](p)=(\nabla_{\boldsymbol{X}}\boldsymbol{Y}-\nabla_{\boldsymbol{Y}}\boldsymbol{X})(p)$.

Theorem 2.1.21 ([GHL04, Theorem 2.51]). *Let (M,g) be a Riemannian manifold. Then, there exists a unique torsion-free connection ∇ satisfying for all $\boldsymbol{X},\boldsymbol{Y},\boldsymbol{\xi}\in\chi(M)$,*

$$\boldsymbol{\xi}(g(\boldsymbol{X},\boldsymbol{Y})(p))=g(\nabla_{\boldsymbol{\xi}}\boldsymbol{X}(p),\boldsymbol{Y}(p))+g(\boldsymbol{X}(p),\nabla_{\boldsymbol{\xi}}\boldsymbol{Y}(p)).$$

Definition 2.1.22 ([GHL04, Definition 2.53]). The connection defined in the above theorem is called the *Levi-Civita connection*.

Remark 2.1.9. It can ben shown [8] that the Levi-Civita connection is characterized by

$$\begin{aligned} g(\nabla_{\boldsymbol{X}}\boldsymbol{Y},\boldsymbol{Z}) &= \frac{1}{2}\left(\boldsymbol{X}(g(\boldsymbol{Y},\boldsymbol{Z}))+\boldsymbol{Y}(g(\boldsymbol{Z},\boldsymbol{X}))-\boldsymbol{Z}(g(\boldsymbol{X},\boldsymbol{Y}))\right.\\ &\quad \left.+g(\boldsymbol{Z},[\boldsymbol{X},\boldsymbol{Y}])-g(\boldsymbol{X},[\boldsymbol{Y},\boldsymbol{Z}])+g(\boldsymbol{Y},[\boldsymbol{X},\boldsymbol{Z}])\right). \end{aligned}$$

for all $\boldsymbol{X},\boldsymbol{Y},\boldsymbol{Z}\in\chi(M)$. Henceforth, ∇ denotes the Levi-Civita connection on (M,g).

Definition 2.1.23 ([GHL04, Definition 2.67]). Let $c:I\to M$ be a smooth curve. A *vector field along* c is a curve $X:I\to TM$, such that $X(t)\in T_{c(t)}M$, for any $t\in I$.

The vector space of all vector fields along c is denoted by $\chi_c(M)$.

Definition - Proposition 2.1.24 ([GHL04, Theorem 2.68]). Let $c:I\to M$ be a smooth curve. There exists a unique operator, denoted by $\frac{D}{dt}$ and called *covariant derivative*, defined on the vector space of all vector fields along c, which satisfies to the following conditions:

(i) for all $X\in\chi_c(M)$, $f\in\mathcal{C}^\infty(I)$,

$$\frac{D}{dt}fX(t)=f(t)\frac{D}{dt}X(t)+f'(t)X(t);$$

8. See the proof of [GHL04, Theorem 2.51].

(ii) if there exists a neighbourhood of t_0 in I such that X is the restriction to c of a vector field $\boldsymbol{Y}$ defined on a neighbourhood of $c(t_0)$ in M, then

$$\frac{D}{dt}X(t_0) = \nabla_{c'(t_0)}\boldsymbol{Y}(c(t_0)).$$

Definition 2.1.25 ([GHL04, Definitions 2.71 and 2.77]). Let $c : I \to M$ be a smooth curve. A vector field X along c is said to be *parallel* if $\frac{D}{dt}X(t) \equiv 0$. A curve γ on M is called a *geodesic* if $\gamma'(t)$ is a parallel vector field along γ, that is, if $\frac{D}{dt}\gamma'(t) \equiv 0$.

2.1.3 Divergence and Laplace operators in local coordinates

Now the divergence operator, then the Laplace operator are defined using the notions introduced in the previous subsection, following [Cha84, Chapter I].

Definition 2.1.26 ([Cha84, Definition I.2]). Let $\boldsymbol{X} \in \chi(M)$ be a vector field of class $\mathcal{C}^\infty(M)$. For all $p \in M$, consider the mapping $\psi_p : T_pM \to T_pM$ defined by

$$\boldsymbol{\xi} \mapsto \psi_p(\boldsymbol{\xi}) = \nabla_{\boldsymbol{\xi}}\boldsymbol{X}.$$

The *divergence* of $\boldsymbol{X}$, denoted by $\operatorname{div}\boldsymbol{X}$, is the mapping from M to $\mathbb{R}$ defined by

$$\operatorname{div}\boldsymbol{X}(p) = \text{ trace } (\psi_p),$$

for all $p \in M$.

Remark 2.1.10. With the notations of the previous definition, for all $p \in M$, there exists a bijection $\phi : \mathbb{R}^N \to T_pM$, $\boldsymbol{v} \mapsto \boldsymbol{\phi(v)}$, depending on the chart (α, U) containing p, given by

$$\boldsymbol{\phi(v)}(f) = \boldsymbol{v}(f \circ \alpha^{-1}), \quad \forall f \in \mathcal{C}^k(M), k \geq 1.$$

The trace in Definition 2.1.26 is the trace of the matrix representing[9] the linear mapping $\phi^{-1} \circ \psi_p \circ \phi$.

Proposition 2.1.27. *Let $\boldsymbol{X}, \boldsymbol{Y} \in \chi(M)$ be two vector fields of class $\mathcal{C}^\infty(M)$. Then,*

(i) $\operatorname{div}\boldsymbol{X} \in \mathcal{C}^\infty(M)$;

(ii) $\operatorname{div}(\boldsymbol{X} + \boldsymbol{Y}) = \operatorname{div}\boldsymbol{X} + \operatorname{div}\boldsymbol{Y}$;

(iii) $\operatorname{div}(f\boldsymbol{X}) = f \operatorname{div}\boldsymbol{X} + g(\boldsymbol{\nabla f}, \boldsymbol{X})$, *for all* $f \in \mathcal{C}^\infty(M)$.

Definition 2.1.28 ([Cha84, Definition I.3]). Let $f \in \mathcal{C}^\infty(M)$. The *Laplace operator* of f, or *laplacian* of f, is the function $\Delta f : M \to \mathbb{R}$, defined by

$$\Delta f = \operatorname{div}(\boldsymbol{\nabla f}).$$

Sometimes Δ is denoted by Δ_g to specify the dependency upon g.

9. It makes sense since the trace of a matrix is invariant under change of basis.

Proposition 2.1.29. *Let $f, h \in \mathcal{C}^\infty(M)$. Then,*

(i) $\Delta f \in \mathcal{C}^\infty(M)$;

(ii) $\Delta(f+h) = \Delta f + \Delta h$;

(iii) $\operatorname{div}(h\boldsymbol{\nabla f}) = h\Delta f + g(\boldsymbol{\nabla h}, \boldsymbol{\nabla f})$;

(iv) $\Delta(fh) = h\Delta f + g(\boldsymbol{\nabla f}, \boldsymbol{\nabla h}) + f\Delta h$.

As for the volume element and the gradient, the expression of the divergence operator and of the Laplace operator in the local coordinates $\{\boldsymbol{\partial x_i}\}_{i=1}^N$ will be useful for the main part of the document. For this purpose, consider a chart (α, U) in the neighbourhood of a point $p \in M$ and denote by $G(\alpha(p))$ the matrix representing $g(p)$ in this basis.

If the vector field $\boldsymbol{X} \in \chi(M)$ of class $\mathcal{C}^\infty(M)$ can be written using local coordinates as $\boldsymbol{X} = \sum_{j=1}^N \xi_j \boldsymbol{\partial x_j}$, then

$$\operatorname{div} \boldsymbol{X} = \frac{1}{\sqrt{\det(G)}} \sum_{j=1}^N \boldsymbol{\partial x_j} \left(\xi_j \sqrt{\det(G)} \right).$$

Moreover, if $f \in \mathcal{C}^k(U)$, $k \geq 2$, then

$$\Delta f = \frac{1}{\sqrt{\det(G)}} \sum_{j,k=1}^N \boldsymbol{\partial x_j} \left(G^{j,k} \sqrt{\det(G)} \boldsymbol{\partial x_k} f \right), \tag{2.9}$$

where $G^{j,k}$ denotes the (j,k)-component of the inverse G^{-1} of the matrix G.

To derive properly these expressions, a development [10] involving *Christoffel symbols* has to be carried out. It is built throughout the first section of [Cha84, Chapter I].

2.1.4 Results of calculus on a manifold

The following reminders from [Cha84, Section I.2] are classical results of vector calculus in the framework of a Riemannian manifold.

Theorem 2.1.30 (Divergence Theorem I)**.** *If $\boldsymbol{X} \in \chi(M)$ is a vector field of class $\mathcal{C}^\infty(M)$ with compact support in M, then*

$$\int_M \operatorname{div} \boldsymbol{X} \, \mathrm{d}V_g = 0,$$

where $\mathrm{d}V_g$ denotes the volume element given in Definition 2.1.11.

Assume moreover that M is oriented and has a boundary ∂M with induced $(N-1)$-volume element denoted by $\mathrm{d}\sigma$. The notion of boundary ∂M can be found in [Boo75, Definition VI.4.1], whereas to define $\mathrm{d}\sigma$, the *exterior differentiation* of a differential form is required. For this latter, we refer to [Boo75, Section V.8].

10. It is a similar development as the one derived for the expression of the volume element and of the gradient in local coordinates, but it is more technical.

Theorem 2.1.31 (Divergence Theorem II). *Let $\boldsymbol{X} \in \chi(\overline{M})$ be a vector field of class $\mathcal{C}^\infty(\overline{M})$ with compact support on $\overline{M}$. Then,*

$$\int_M \operatorname{div} \boldsymbol{X} \, \mathrm{d}V_g = \int_{\partial M} g(\boldsymbol{X}, \boldsymbol{n}) \, \mathrm{d}\sigma,$$

where $\boldsymbol{n}$ denotes the outward unit normal (with respect to g) vector field on the boundary ∂M.

Theorem 2.1.32 (Green's formula). *Let $f, h \in \mathcal{C}^\infty(\overline{M})$ be two functions such that $h\boldsymbol{\nabla} \boldsymbol{f}$ has compact support on $\overline{M}$. Then,*

$$\int_M h \Delta f \, \mathrm{d}V_g = \int_{\partial M} h \, g(\boldsymbol{\nabla} \boldsymbol{f}, \boldsymbol{n}) \, \mathrm{d}\sigma - \int_M g(\boldsymbol{\nabla} \, \boldsymbol{f}, \boldsymbol{\nabla} \, \boldsymbol{h}) \, \mathrm{d}V_g,$$

where $\boldsymbol{n}$ denotes the outward unit normal (with respect to g) vector field on the boundary ∂M.

2.2 Some notions about the Finite Element Method

2.2.1 Definitions

This section is mainly from the book [Cia78] and [EG02], but this recall is restricted to the notions useful for the future applications to our problem. The former reference book is classic in this field and covers the topic very broadly. Most of the following definitions are derived from its second chapter. Throughout this section, Ω denotes a domain of $\mathbb{R}^N$, that is a bounded open set of $\mathbb{R}^N$.

Definition 2.2.1. A *mesh* $\mathcal{M}$ of a domain $\Omega \subset \mathbb{R}^N$ is a subdivision in a finite number of subsets K_i, $i = 1, \ldots, I$, such that

(i) $\bar{\Omega} = \bigcup_{i=1}^{I} K_i$;

(ii) Every K_i, $i = 1, \ldots, I$, is closed and has a non-empty interior $\overset{\circ}{K}_i$;

(iii) Every K_i, $i = 1, \ldots, I$, has a Lipschitz boundary ∂K_i;

(iv) $\overset{\circ}{K}_i \cap \overset{\circ}{K}_j = \emptyset$ for all K_i, K_j, $i, j = 1, \ldots, I$, $i \neq j$.

Remark 2.2.1. If the sets K_i, $i = 1, \ldots, I$, consist of N-simplices, then usually an additional condition on $\mathcal{M}$ is required:

(v) For all K_i, K_j, $i, j = 1, \ldots, I$, $i \neq j$, the intersection $K_i \cap K_j$ is either empty, or is a shared vertex, or is a shared face (edge).

Two examples of *forbidden situations* involving subsets K of a mesh are presented in Figure 2.1.

Figure 2.1: The couples of 2-simplices (or triangles) $\{K_i, K_j\}$ and $\{K_{i'}, K_{j'}\}$ does not satisfy the condition (v). Moreover, the couple $\{K_{i'}, K_{j'}\}$ does not verify (iv) neither.

Definition 2.2.2. A *finite element* in $\mathbb{R}^N$ is a triple (K, P, Σ) where:

(i) K is a closed subset of $\mathbb{R}^N$ with a non-empty interior and a Lipschitz boundary;

(ii) P is a space of real-valued functions defined over the set K;

(iii) Σ is a finite set of linearly independent linear forms $\sigma_i : P \to \mathbb{R}$, $i = 1, \ldots, M$.

Moreover, Σ is P-*unisolvent*, that is for all real numbers α_i, $i = 1, \ldots, M$, there exists a unique function $p \in P$ which satisfies

$$\sigma_i(p) = \alpha_i, \quad i = 1, \ldots, M.$$

Remark 2.2.2. The P-unisolvence property implies in particular that there exist functions φ_i^{loc}, $i = 1, \ldots, M$, which satisfy

$$\sigma_j(\varphi_i^{\mathrm{loc}}) = \delta_{ij}, \quad i, j = 1, \ldots, M.$$

Definition 2.2.3. With the previous notations, the functions φ_i^{loc}, $i = 1, \ldots, M$, are called *local shape functions*.

Definition 2.2.4. Let (K, P, Σ) be a finite element in $\mathbb{R}^N$. If there exist M points $s_1, \ldots, s_M \in K$, called *nodes*, such that for all $p \in P$,

$$\sigma_i(p) = p(s_i), \quad i = 1, \ldots, M,$$

then the triple (K, P, Σ) is called a *Lagrange finite element*.

Remark 2.2.3. In this context, the local shape functions φ_i^{loc}, $i = 1, \ldots, M$, satisfy

$$\varphi_i^{\mathrm{loc}}(s_j) = \delta_{ij}, \quad i, j = 1, \ldots, M,$$

where $\delta_{i,j}$ denotes the Kronecker symbol.

A family of examples is given by the Lagrange finite elements of type $\mathcal{P}_k$, $k \in \mathbb{N}$, whose definition is recalled here.

Definition 2.2.5. Let $\mathbb{P}_k$, $k \in \mathbb{N}$, denote the space of all polynomial in N variables with real coefficents and of degree lower or equal to k, that is

$$\mathbb{P}_k := \left\{ p : \mathbb{R}^N \to \mathbb{R} : p(x_1, \dots, x_N) = \sum_{i_1+\cdots+i_N \leq k} \alpha_{i_1,\dots,i_N} x_1^{i_1} \cdots x_N^{i_N},\ \alpha_{i_1,\cdots,i_N} \in \mathbb{R} \right\}.$$

A finite element (K, P, Σ) is called a *Lagrange finite element of type* $\mathcal{P}_k$ in $\mathbb{R}^N$, or simply *finite element of type* $\mathcal{P}_k$, if

- K is a N-simplex;
- $P = \mathbb{P}_k|_K$;
- The set of nodes $\{s_i\}_{i=1}^M$ appearing in Definition 2.2.4 coincides with the set

$$S := \left\{ \left(\frac{i_1}{k} P_1^{\text{loc}}, \dots, \frac{i_{N+1}}{k} P_{N+1}^{\text{loc}} \right),\ 0 \leq i_1, \dots, i_{N+1} \leq k,\ 0 < i_1 + \cdots + i_{N+1} \leq k \right\},$$

  where $P_1^{\text{loc}}, \dots, P_{N+1}^{\text{loc}}$ denote the vertices of K.

Remark 2.2.4. It makes sense to consider Lagrange finite elements of type $\mathcal{P}_k$ since the P-unisolvence property is readily verified[11] for such a finite element. Moreover, for $k, N \in \mathbb{N}$, it holds that

$$M := \#S = \dim \mathbb{P}_k = \binom{N+k}{k}.$$

Usually, finite elements of type $\mathcal{P}_k$ for $k = 1, 2$, are used. See Figure 2.2. An advantage provided by such elements is that if $(\hat{K}, \hat{P}, \hat{\Sigma})$ and (K, P, Σ) are two finite elements of type $\mathcal{P}_k$, then they can be compared in the following way.

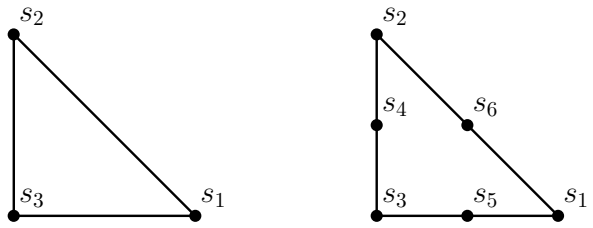

Figure 2.2: Lagrange finite element of type $\mathcal{P}_1$ (left) and of type $\mathcal{P}_2$ (right) in $\mathbb{R}^2$.

Definition 2.2.6. Two Lagrange finite elements $(\hat{K}, \hat{P}, \hat{\Sigma})$ and (K, P, Σ) are called *affine-equivalent* if there exists an invertible affine mapping $F : \mathbb{R}^N \to \mathbb{R}^N$, $F(\hat{x}) = B(\hat{x}) + b$, $B \in \mathbb{M}_N(\mathbb{R})$, $b \in \mathbb{R}^N$, such that

- $K = F(\hat{K})$;
- $P = \{p : K \to \mathbb{R}, p = \hat{p} \circ F^{-1}, \hat{p} \in \hat{P}\}$;
- $s_i = F(\hat{s}_i), i = 1, \dots, M$.

11. See for instance [EG02, Sections 2.2 and 2.3].

See Figure 2.5 for an illustration in a particular case. In the sequel, finite elements of type $\mathcal{P}_1$ are used to approximate the spectrum of the Dirichlet-Laplace operator. The fact that every couple of such elements is affine-equivalent is crucial for the numerical implementation.

2.2.2 The Galerkin method

Let $(V, (\cdot|\cdot))$ be a Hilbert space, $a : V \times V \to \mathbb{R}$ a symmetric, continuous, V-elliptic [12] bilinear form and $l : V \to \mathbb{R}$ a continuous linear form. Consider the following linear abstract variational problem

$$(\mathcal{P}_{abs}) \begin{cases} \text{Find } u \in V \text{ such that} \\ a(u, v) = l(v), \quad \forall v \in V, \end{cases}$$

which admits a unique solution by the Lax-Milgram Theoreom [13]. The *Galerkin method* consists in approximating $(\mathcal{P}_{abs})$ by defining *similar* problems in each element of a family $(V_h)_h$ of finite dimensional subspaces of V:

$$(\mathcal{P}_{abs,h}) \begin{cases} \text{Find } u_h \in V_h \text{ such that} \\ a(u_h, v_h) = l(v_h), \quad \forall v_h \in V_h. \end{cases}$$

Since $V_h \subset V$, there exists a unique solution to $(\mathcal{P}_{abs,h})$ thanks to the same result. The usual way to get $(V_h)_h$ is to create a family of associated meshes $(\mathcal{M}_h)_h$ of Ω. The subscript h stands for the dependence on the geometry of the mesh, more precisely

$$h := \max_{K \in \mathcal{M}_h} h_K = \max_{K \in \mathcal{M}_h} \operatorname{diam}(K),$$

where the (abusive) notation $K \in \mathcal{M}_h$ denotes the fact that K is the geometric set of a finite element (K, Σ, P) of the mesh $\mathcal{M}_h$ (K will denote the geometric subset of a finite element for the remainder of this section and this notation will be used in the sequel). The parameter h is usually called the *diameter* of the mesh $\mathcal{M}_h$. The famous Céa's Lemma [14] indicates that if the following approximation property

$$\lim_{h \to 0} \inf_{v_h \in V_h} \|v - v_h\|_V = 0, \quad \forall v \in V, \tag{2.10}$$

holds, then the approximated solution u_h tends to u for the norm $\|\cdot\|_V$. Indeed, on the first hand, the linearity of l and bilinearity of a imply $a(u - u_h, v_h) = 0$ for all $v_h \in V_h$. On the other hand, if C_{ell} and C_{cont} denote respectively the V-ellipticity constant and the continuity constant [15] of a, then

$$C_{ell} \|u - u_h\|_V^2 \leq a(u - u_h, u - u_h) = a(u - u_h, u - v_h) \leq C_{cont} \|u - u_h\|_V \|u - v_h\|_V .$$

12. The V-ellipticity is recalled in Definition A.1.4.
13. See Theorem A.1.5 in the appendix.
14. See [Cia78, Theorem 2.4.1].
15. It means that $\alpha = C_{ell}$ and $C = C_{cont}$ respectively in Definition A.1.4.

So,

$$\|u - u_h\|_V \leq \frac{C_{cont}}{C_{ell}} \inf_{v_h \in V_h} \|u - v_h\|_V .$$

In order to verify the condition imposed by (2.10), a standard assumption is to ask the family $(\mathcal{M}_h)_h$ to be regular in the following sense:

Definition 2.2.7. A family of meshes $(\mathcal{M}_h)_h$ of Ω is called *regular* if it verifies:

(i) h approaches 0 ;

(ii) There exists a constant $\gamma > 0$ such that

$$\forall h, \forall K \in \mathcal{M}_h, \frac{h_K}{\rho_K} \leq \gamma,$$

where ρ_K denotes the diameter of the largest sphere inscribed in K.

Obviously, the first condition is necessary in order to *approximate* V increasingly better by the family $(\mathcal{M}_h)_h$. However, the condition (ii), which forces elements not to be too *flat*, has to be added to allow global convergence of functions in V_h to functions in V. This fact is stated more precisely in Theorem 2.2.8 for particular choices of V and V_h. See also Figure 2.3

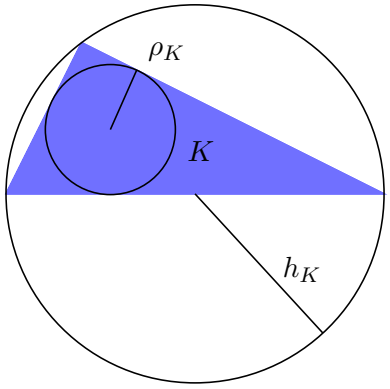

Figure 2.3: A triangle K with diameter h_K and whose the largest circle inscribed in K has a ray of length ρ_K.

In the sequel, the spectrum of the Dirichlet-Laplace operator is approximate within this framework. More precisely, the suitable choice for the space V is the Sobolev space [16] $H_0^1(\Omega)$ over a polygonal domain $\Omega \subset \mathbb{R}^2$. Moreover, a mesh made of finite elements of

16. See Definition-Proposition A.2.11.

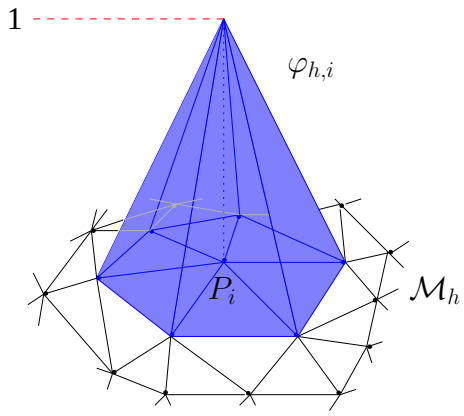

Figure 2.4: Shape function $\varphi_{h,i}$.

type $\mathcal{P}_1$ is used to set

$$V_h = \left\{ v_h \in \mathcal{C}^0\left(\overline{\Omega}\right) \;\middle|\; v_h|_{\partial\Omega} \equiv 0,\ v_h|_K \text{ affine for all triangles } K \text{ of the mesh } \mathcal{M}_h \right\}. \tag{2.11}$$

Let N_h be the number of nodes[17] P_i of all the elements K forming the mesh $\mathcal{M}_h$. For all $i = 1, \ldots, N_h$, let $\varphi_{h,i}$ denote the functions given by

$$\varphi_{h,i} \in V_h, \quad \varphi_{h,i}(P_j) = \delta_{ij}, \quad \forall\, 1 \leq i, j \leq N_h, \tag{2.12}$$

where δ_{ij} is the classical notation for the Kronecker symbol. See Figure 2.4, where a *shape function* $\varphi_{h,i}$ is represented. It is straightforward that $\{\varphi_{h,i}\}_{i=1}^{N_h}$ is a basis of V_h, so every $v_h \in V_h$ can be written as

$$v_h(x) = \sum_{i=1}^{N_h} v_h(P_i)\varphi_{h,i}(x), \quad \forall x \in \Omega. \tag{2.13}$$

Thus, it defines an interpolation operator $\Pi_h : V \to V_h$, $v \to \Pi_h(v) = v_h$. Besides, the local interpolation operator $\Pi_{h,K}$ over K can be defined analogously by

$$\Pi_{h,K}(v) = \sum_{i=1}^{3} v(s_i)\varphi_i^{\text{loc}}, \quad \forall v \in V,$$

where the notations of defintions 2.2.3 and 2.2.4 are used. Then, there exists a constant $C > 0$ such that the following upper bounds[18]

$$\|v - \Pi_{h,K} v\|_{H_0^m(K)} \leq C\, h_K^{2-m} \left(\frac{h_K}{\rho_K}\right)^m \|v\|_{H_0^2(K)}, \quad m = 0, 1, 2,$$

17. By extension, these points are called *nodes of the mesh* $\mathcal{M}_h$.
18. A more general statement of this result can be found in [EG02, Theorem 2.7.2].

holds for all $v \in H^2(K)$, where the Sobolev space $H^2(K)$ and the semi-norm $\|\cdot\|_{H_0^m(K)}$ are both defined in the appendix (see A.2.9 and A.2.17). The ratio h_K/ρ_k appears in this last expression, thus, to extend this local result to the whole domain Ω, the condition (ii) in the definition 2.2.7 of a regular family of meshes is necessary. A classical result for global convergence is [Cia78, Theorem 3.2.1], which can be transcribed here in our context as follows.

Theorem 2.2.8. *Let Ω be a polygonal domain, let V be the space $H_0^1(\Omega)$ and let V_h be defined by (2.11). Consider a regular family $(\mathcal{M}_h)_h$ of meshes consisting of Lagrange finite elements of type $\mathcal{P}_1$, and the interpolation operator Π_h over Ω. Then, there exists a constant C, independant of h, such that for all $v \in H^2 \cap H_0^1(\Omega)$,*

$$\|v - \Pi_h v\|_{H^m(\Omega)} \leq C\, h^{2-m}\, \|v\|_{H_0^2(\Omega)}\,, \quad m = 0, 1,$$

where the norms $\|\cdot\|_{H^m(\Omega)}$ and $\|\cdot\|_{H_0^2(\Omega)}$ are given in Definition A.2.9 and in Proposition A.2.17.

2.2.3 Numerical implementation: quadrature rule and storage

Let us come back to the problems $(\mathcal{P}_{abs})$ and $(\mathcal{P}_{abs,h})$ defined at the beginning of the previous subsection, with the particular choices $V = H_0^1(\Omega)$ and V_h defined by (2.11)—so finite element of type $\mathcal{P}_1$ is appropriate—, with its basis $\{\varphi_{h,i}\}_{i=1}^{N_h}$ given by (2.12). The notation $\boldsymbol{u_h} \in \mathbb{R}^{N_h}$ is abusively used again for the vector whose j-th component $(\boldsymbol{u_h})_j$ is the value of the solution u_h to $(\mathcal{P}_{abs,h})$ at node P_j, $j = 1, \ldots, N_h$, of a mesh $\mathcal{M}_h$ of Ω, that is

$$u_h(x) = \sum_{j=1}^{N_h} (\boldsymbol{u_h})_j\, \varphi_{h,j}(x), \quad \forall x \in \Omega. \tag{2.14}$$

It is sufficient to verify the equality on V_h appearing in $(\mathcal{P}_{abs,h})$ only for each basis functions $\varphi_{h,i}$. Hence, thanks to the bilinearity of a, the problem $(\mathcal{P}_{abs,h})$ can be rewritten as

$$(\mathcal{P}_{abs,h}) \begin{cases} \text{Find } \boldsymbol{u_h} \in \mathbb{R}^{N_h} \text{ such that} \\ \displaystyle\sum_{j=1}^{N_h} a(\varphi_{h,j}, \varphi_{h,i})\, (\boldsymbol{u_h})_j = l(\varphi_{h,i}), \quad \forall i = 1, \ldots, N_h. \end{cases}$$

Finally, denoting by $A \in \mathbb{M}_{N_h}(\mathbb{R})$ the matrix defined by

$$A_{i,j} = a(\varphi_{h,j}, \varphi_{h,i}), \quad i, j = 1, \ldots, N_h,$$

and by $\boldsymbol{b} \in \mathbb{R}^{N_h}$ the vector defined by

$$b_i = l(\varphi_{h,i}), \quad i = 1, \ldots, N_h,$$

the final formulation of problem $(\mathcal{P}_{abs,h})$ is

$$(\mathcal{P}_{abs,h}) \begin{cases} \text{Find } \boldsymbol{u_h} \in \mathbb{R}^{N_h} \text{ such that} \\ A\boldsymbol{u_h} = \boldsymbol{b}. \end{cases}$$

In order to solve this problem, the first task to perform is to build the matrix A and the vector $\boldsymbol{b}$. Frequently, the components $A_{i,j}$ of A consist of integrals involving $\varphi_{h,i}$ and $\varphi_{h,j}$. Moreover, A is symmetric. For example, in Chapter 3, a matrix $M \in \mathbb{M}_{N_h}(\mathbb{R})$ arises, whose components are defined by

$$M_{i,j} = \int_{\Omega} \varphi_{h,j}\varphi_{h,i}, \quad i,j = 1,\ldots,N_h,$$

as mentioned [19] by the equation (3.4). Since the support of the basis function φ_i is reduced [20] to the triangles K such that P_i belongs to K, it follows that

$$M_{i,j} = \sum_{\substack{(K,P,\Sigma)\in\mathcal{M}_h \\ P_i,P_j\in K}} \int_K \varphi_{h,j}\varphi_{h,i}, \quad i,j = 1,\ldots,N_h.$$

Nevertheless, instead of computing each component of M one by one, a more suitable way of proceeding is to add the contribution of each triangle K of $\mathcal{M}_h$ to the components corresponding to the associated nodes of K. It means that for each K, whose vertices are denoted $P_1^{loc}, P_2^{loc}, P_3^{loc}$, a *local matrix* $M_K^{loc} \in \mathbb{M}_3(\mathbb{R})$ is built, such that

$$M_K^{loc}{}_{i,j} = \int_K \varphi_j^{loc}\varphi_i^{loc}, \quad i,j = 1,\ldots,3,$$

where φ_i^{loc} is the basis function taking value 1 at P_i^{loc}, $i = 1,2,3$. The algorithm of construction of a symmetric matrix is given by (I denotes the number of triangles K in the mesh $\mathcal{M}_h$)

Matrix construction abstract algorithm

```
Initialize M ← 0;
for K = 1 to I do
    Compute the 3 by 3 local matrix M_K^loc;
    for i = 1 to 3 do
        Assemble the local matrix into the global matrix by performing:
        for j = i to 3 do
            M[P_i, P_j] ← M[P_i, P_j] + M_K^loc[i, j];
        end j;
    end i;
end K;
```

Algorithm 1.

19. Actually, the equation reported in this remainder corresponds to the particular case where the underlying manifold is an open set of $\mathbb{R}^2$, since the volume element $\mathrm{d}V_g$ appearing in equation (3.4), is here the Lebesgue measure. The general case is not considered in this section for the sake of clarity. See Chapter 3 for details.

20. An important aspect of the Finite Element Method is that the support of the basis functions φ_i is *small*, in order to make the computation of these integrals numerically inexpensive.

Two points deserve to be developed: the numerical computation of the local matrix and the step of assembling and storage of the local matrix into the global matrix—this is discussed later—.

As mentioned before, the Finite Element Method will be applied to our problem with finite elements of type $\mathcal{P}_1$. It is easy to show that every such element (K, P, Σ) is affine equivalent to the element $(\hat{K}, \hat{P}, \hat{\Sigma})$, called *reference element*, defined by

$$\begin{aligned} \hat{K} &:= \{(\hat{x}_1, \hat{x}_2) \in \mathbb{R}^2 : \hat{x}_1, \hat{x}_2 \geq 0, \hat{x}_1 + \hat{x}_2 \leq 1\}; \\ \hat{P} &:= \mathbb{P}_1|_{\hat{K}}; \\ \hat{\Sigma} &:= \{(1,0), (0,1), (0,0)\}, \end{aligned}$$

with associated local shape functions $\hat{\varphi}_i^{\text{loc}}$, $i = 1, 2, 3$, defined for $\hat{x} \in \hat{K}$, by

$$\begin{aligned} \hat{\varphi}_1^{\text{loc}}(\hat{x}_1, \hat{x}_2) &= \hat{x}_1; \\ \hat{\varphi}_2^{\text{loc}}(\hat{x}_1, \hat{x}_2) &= \hat{x}_2; \\ \hat{\varphi}_3^{\text{loc}}(\hat{x}_1, \hat{x}_2) &= 1 - \hat{x}_1 - \hat{x}_2. \end{aligned}$$

Indeed, denoting clockwise by P_1^{loc}, P_2^{loc} and P_3^{loc} the vertices of K—or equivalently, the nodes of Σ—, it is sufficient to take in Definition 2.2.6 the function $F_K := F : \mathbb{R}^2 \to \mathbb{R}^2$, defined by

$$F_K(\hat{x}) = \sum_{i=1}^{3} \hat{\varphi}_i^{\text{loc}}(\hat{x}) P_i^{loc}, \quad \forall \hat{x} \in \hat{K},$$

so that the local shape functions φ_i^{loc} defined on K satisfy $\hat{\varphi}_i^{\text{loc}} = \varphi_i^{\text{loc}} \circ F_K$, $i = 1, 2, 3$, and

$$\det DF_K(\hat{x}) = \left(\boldsymbol{P_1^{loc} - P_3^{loc}} \,\middle|\, \boldsymbol{P_2^{loc} - P_3^{loc}} \right) > 0,$$

since K is a (non flat) triangle and F_k is orientation preserving. So, the Jacobian determinant of F_K does not depend on the point $\hat{x}$ where it is computed. See Figure 2.5. The property of affine-equivalence is extensively used to transport the computation of integrals over K onto $\hat{K}$. Indeed, for an integrable function $\Psi : K \to \mathbb{R}$ defined on K, the change of variables $x = F_K(\hat{x})$ gives

$$\int_K \Psi(x)\, \mathrm{d}x = \det DF_K(\hat{x}) \int_{\hat{K}} \Psi \circ F_K(\hat{x})\, \mathrm{d}\hat{x}.$$

So building the whole matrix M reduces to apply a quadrature rule to approximate integrals only over $\hat{K}$. In the sequel, we employ a quadrature rule of the form[21]

$$\int_{\hat{K}} \Psi \circ F_K(\hat{x})\, \mathrm{d}\hat{x} \simeq \frac{1}{6} \sum_{l=1}^{3} \Psi \circ F_K(\hat{\lambda}_l), \tag{2.15}$$

21. The 1/6 factor comes from the product of a uniform weight 1/3 and the area of $\hat{K}$ equal to 1/2.

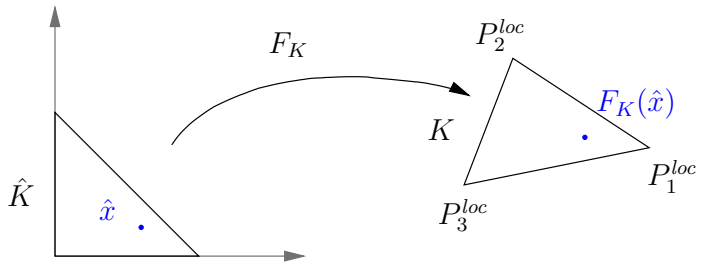

Figure 2.5: The mapping F_k takes the set $\hat{K}$ of the reference element into the set K of an element (K, P, Σ). F_K is the explicit invertible affine mapping in Definition 2.2.6 that makes $(\hat{K}, \hat{P}, \hat{\Sigma})$ and (K, P, Σ) affine-equivalent.

with two different choices of *integration points* $\hat{\lambda}_l$, namely

$$\hat{\lambda}_1 = (1,0),\ \hat{\lambda}_2 = (0,1),\ \hat{\lambda}_3 = (0,0), \tag{2.16}$$

$$\text{and} \quad \hat{\lambda}'_1 = \left(0, \frac{1}{2}\right),\ \hat{\lambda}'_2 = \left(\frac{1}{2}, 0\right),\ \hat{\lambda}'_3 = \left(\frac{1}{2}, \frac{1}{2}\right). \tag{2.17}$$

Remark 2.2.5. The approximation (2.15) with the choice of integration points given by (2.16) is actually an equality if ψ is a polynomial function of degree at most 1, whereas with the choice of integration points given by (2.16), it is exact for all polynomial functions of degree at most 2. See [QSS07, Subsection 9.9.2].

Definition 2.2.9. The approximation (2.15) with the choice of integration points given by (2.16) defines a quadrature rule using *masslumping*. By opposition, the choice of integration points given by (2.17) makes (2.15) a quadrature rule *without masslumping*.

The notion of masslumping is addressed within the framework of eigenvalues optimization in Subsection 3.5.1.

The terminology of the last definition comes from the form taken by the matrix M, called *mass matrix* in elasticity theory: the component $M_{i,j}$, $i, j = 1, \ldots, N_h$, can be computed over the reference element $\hat{K}$ and then approximated using a quadrature rule of the form (2.15), that is

$$\begin{aligned}
M_{i,j} &= \sum_{\substack{(K,P,\Sigma)\in\mathcal{M}_h \\ P_i,P_j\in K}} \int_K \varphi_{h,j}(x)\varphi_{h,i}(x)\mathrm{d}x = \sum_{\substack{(K,P,\Sigma)\in\mathcal{M}_h \\ P_i,P_j\in K}} \int_K \varphi^{\mathrm{loc}}_{\mathrm{loc}_K(j)}(x)\varphi^{\mathrm{loc}}_{\mathrm{loc}K(i)}(x)\mathrm{d}x \\
&= \sum_{\substack{(K,P,\Sigma)\in\mathcal{M}_h \\ P_i,P_j\in K}} \det DF_K \int_{\hat{K}} \hat{\varphi}^{\mathrm{loc}}_{\mathrm{loc}_K(j)}(\hat{x})\hat{\varphi}^{\mathrm{loc}}_{\mathrm{loc}_K(i)}(\hat{x})\mathrm{d}\hat{x} \\
&\simeq \frac{1}{6} \sum_{\substack{(K,P,\Sigma)\in\mathcal{M}_h \\ P_i,P_j\in K}} \det DF_K \sum_{l=1}^{3} \hat{\varphi}^{\mathrm{loc}}_{\mathrm{loc}_K(i)}(\hat{\lambda}_l)\hat{\varphi}^{\mathrm{loc}}_{\mathrm{loc}_K(j)}(\hat{\lambda}_l),
\end{aligned}$$

where $\mathrm{loc}_K(i) \in \{1,2,3\}$ denotes the local numbering in K of the node i, $1 \leq i \leq N_h$. The quadrature rule whose integration points are given by (2.16) leads to $M_{i,j} = \delta_{i,j}$, where $\delta_{i,j}$ denotes the Kronecker symbol, since $\psi = \varphi_{h,j}\varphi_{h,i}$ and $\hat{\varphi}^{\mathrm{loc}}_{\mathrm{loc}_K(i)}(\hat{\lambda}_l) = \delta_{\mathrm{loc}_K(i),l}$. Thus, all non-zero component of the mass matrix M are *lumped* on the diagonal. With the other choice (2.16) of integration points, M is no longer diagonal, but still remains sparse [22] so a *judicious way* of storage must be used. It leads us to the second point we wanted to develop in the algorithm 1.

Assume two points of a triangle K are locally numbered $P^{loc}_{\mathrm{loc}_K(i)}$ and $P^{loc}_{\mathrm{loc}_K(j)}$, and globally numbered P_i and P_j. Adding naively the contribution $M^{loc}_{K\ \mathrm{loc}_K(i),\mathrm{loc}_K(j)}$ of this element to the associated component $M_{i,j}$ of the global matrix would imply to handle a *large* and sparse N_h by N_h matrix M. Instead, a standard storage for the matrix M, known as Compressed Sparse Row (CSR) [23], is used. It consists in storing a sparse m by n matrix A with nz non-zero components, using three vectors: a real vector $\boldsymbol{aa}$ of size nz containing the non-zero values of A, and two integers vectors $\boldsymbol{ia}$ and $\boldsymbol{ja}$ with respective size $m+1$ and nz to determine the location in A of these non-zero elements. Precisely, using square brackets to indicate a component of a vector as it is in a standard computer program, it yields:

- $\boldsymbol{aa}[i]$ is the i-th non-zero value of A listed left-to-right, then top-to-bottom, $i = 1,\ldots,nz$;
- $\boldsymbol{ia}[i]$ is the index in $\boldsymbol{aa}$ of the first non-zero element of row i in A, $i = 1,\ldots,m$, and $\boldsymbol{ia}[m+1] = nz+1$ by convention and for practical reasons. In other words, the non-zero components lying on the i-th row of A are stored in $\boldsymbol{aa}[ia[i]],\ldots,\boldsymbol{aa}$[ia[i+1]-1];
- $\boldsymbol{ja}[i]$ is the index of the column in A of the i-th component of $\boldsymbol{aa}$, $i = 1,\ldots,nz$.

Thus, if $A_{i,j} \neq 0$ is the k-th non-zero element of A, then $\boldsymbol{aa}[k] = A_{i,j}$, $\boldsymbol{ia}[i] \leq k < \boldsymbol{ia}[i+1]$ and $\boldsymbol{ja}[k] = j$.

To compare the amount of memory needed to store the matrix M using or not the CSR method, consider for a moment a mesh $\mathcal{M}_h$ with N_h points inside the underlying domain as a graph $\Gamma = (V,E)$. The *degree* $\deg(v)$ of a vertex $v \in V$ is the number of edges $e \in E$ such that v belongs to e, or equivalently, the number of *neighbours* of v. Denoting by $d := \max_{v\in V} \deg(v)$ the maximal degree of Γ, then at most $2dN_h + (N_h+1) = (2d+1)N_h + 1$ memory locations are needed, compared with ${N_h}^2$ without using CSR. Usually, d is small, so large is the gain.

The assembling of the local matrix M^{loc}_K into the global matrix M has to be carried out with caution, see [Saa03, Section 2.3].

2.3 The Lanczos method

Throughout this section, $A \in \mathbb{M}_N(\mathbb{R})$ denotes a N by N symmetric matrix with real components.

22. No rigorous definition is known to the author. However, in [GMS92], the authors refer to the following informal definition due to J. H. Wilkinson: a sparse matrix is any matrix with enough zeros that it pays to take advantage of them.

23. It is also known as Compressed Row Storage (CRS), see [Saa03, Section 3.4].

2.3.1 Definition and basic properties

Given such a matrix A, the spectral theorem in finite dimensional space reads as follows.

Theorem 2.3.1. *Let $A \in \mathbb{M}_N(\mathbb{R})$, be a symmetric, definite, positive matrix. Then, there exist $0 \leq \lambda_1 \leq \lambda_2 \leq \cdots \leq \lambda_N \in \mathbb{R}_{\geq 0}$, and $\boldsymbol{x_1}, \ldots, \boldsymbol{x_N} \in \mathbb{R}^N$ consisting in a orthonormal basis of $\mathbb{R}^N$, such that*

$$A\boldsymbol{x_k} = \lambda_k \boldsymbol{x_k},$$

for all $k = 1, \ldots, N$.

Notation 2.3.2. Throughout this document, the eigenvalues of A are numbered in ascending order and when confusion can occurs, the associated matrix is precised by indicating $\lambda(A)$ instead of λ, for instance.

Moreover, in this section, $(\cdot|\cdot)$ denotes the usual inner product on $\mathbb{R}^N$, and $\|\cdot\|$ denotes the resulting Euclidean norm.

This theorem states the existence of eigenvalues and eigenvectors, whereas the Lanczos method provides increasingly better estimates of extremal eigenvalues of A through a family of matrices $T_k \in \mathbb{M}_k(\mathbb{R})$. This method is so called[24], after the Hungarian mathematician K. Lánczos, and there exist several variants to it.

The aim is to apply this method to a problem involving a large and sparse matrix A, a case in which it is efficient. It is specially indicated[25] when we are interested in the first or last eigenvalues and eigenvectors of A. To get quickly to the heart of the matter, consult [GVL96, Chapter 9], or to go deeper into this topic, [CW02] provides a detailed outline in various situations depending in particular on the properties of the matrix A. This subsection is based on both references. Finally, [LSY98] is useful for the software implementation.

Let us try to understand where this method comes from. First, recall the notion of Rayleigh quotient and the Min-max Theorem, given in the finite dimensional context.

Definition 2.3.3. The *Rayleigh quotient* is defined for a matrix A and a non-zero vector $x \in \mathbb{R}^N$, by

$$R_A(\boldsymbol{x}) = \frac{(A\boldsymbol{x}|\boldsymbol{x})}{(\boldsymbol{x}|\boldsymbol{x})}.$$

Theorem 2.3.4 (Min-max Theorem, [CW02, Theorem 8.1.2])**.** *With the previous notations and denoting by $\mathcal{S}_i$ the set of all subspace of $\mathbb{R}^N$ of dimension $i \leq N$, it yields*

$$\lambda_i = \min_{V \in \mathcal{S}_i} \max_{\boldsymbol{x} \in V \setminus \{0\}} R_A(\boldsymbol{x}),$$

24. Sometimes reference is made to the *Arnoldi-Lanczos Method*, after the name of the American engineer Walter Edwin Arnoldi, which is a generalization of the Lanczos Method for any matrix.

25. The reasons will be clear when the algorithm will be given

in particular,

$$\begin{aligned}\lambda_1 &= \min_{\boldsymbol{x}\neq 0} R_A(\boldsymbol{x}),\\ \lambda_N &= \max_{\boldsymbol{x}\neq 0} R_A(\boldsymbol{x}).\end{aligned}$$

Assume that an orthonormal basis $\{\boldsymbol{q_i}\}_{1\leq i\leq N}$ of $\mathbb{R}^N$ is at our disposal and denote by Q_k, $1\leq k\leq N$, the N by k matrix whose i-th column is the vector $\boldsymbol{q_i}$. For $1\leq k\leq N$, set

$$\begin{aligned}m_k &:= \lambda_1(Q_k^T A Q_k),\\ M_k &:= \lambda_k(Q_k^T A Q_k).\end{aligned}$$

Using the Min-max Theorem,

$$\begin{aligned}m_k &= \min_{\boldsymbol{x}\neq 0}\frac{(AQ_k\boldsymbol{x}|Q_k\boldsymbol{x})}{(\boldsymbol{x}|\boldsymbol{x})} = \min_{\boldsymbol{x}\neq 0}\frac{(AQ_k\boldsymbol{x}|Q_k\boldsymbol{x})}{(Q_k\boldsymbol{x}|Q_k\boldsymbol{x})} \geq \lambda_1(A),\\ M_k &= \max_{\boldsymbol{x}\neq 0}\frac{(AQ_k\boldsymbol{x}|Q_k\boldsymbol{x})}{(\boldsymbol{x}|\boldsymbol{x})} = \max_{\boldsymbol{x}\neq 0}\frac{(AQ_k\boldsymbol{x}|Q_k\boldsymbol{x})}{(Q_k\boldsymbol{x}|Q_k\boldsymbol{x})} \leq \lambda_N(A),\end{aligned}$$

where the second equalities hold since $\{\boldsymbol{q_i}\}_{1\leq i\leq N}$ is orthonormal. In particular, $m_N = \lambda_1(A)$ and $M_N = \lambda_N(A)$ because A and $Q_N^T A Q_N$ are by definition similar. The Lanczos method consists in choosing iteratively the $\boldsymbol{q_i}$ in order to obtain increasingly better estimates of $\lambda_1(A)$ and $\lambda_N(A)$. Given $\{\boldsymbol{q_i}\}_{1\leq i\leq N}$, for $k<N$, $\boldsymbol{q_{k+1}}$ must be chosen in a *judicious* way. To this end, consider $\boldsymbol{x_k}\in span\{\boldsymbol{q_1},\ldots,\boldsymbol{q_k}\}$ such that $R_A(\boldsymbol{x_k}) = m_k$. Since $\nabla R_A(\boldsymbol{x})$ is pointing into the steepest (positive) direction of the surface given by $\{(\boldsymbol{x}, R_A(\boldsymbol{x})), \boldsymbol{x}\in\mathbb{R}^N\setminus\{\boldsymbol{0}\}\}$ at point $\boldsymbol{x}$, in order to obtain $m_{k+1}<m_k$, $\boldsymbol{q_{k+1}}$ could be chosen such that

$$\nabla R_A(\boldsymbol{x_k})\in span\{\boldsymbol{q_1},\ldots,\boldsymbol{q_{k+1}}\}. \tag{2.18}$$

In a similar way for M_{k+1}, denoting by $\boldsymbol{y_k}\in span\{\boldsymbol{q_1},\ldots,\boldsymbol{q_k}\}$ the vector satisfying $R_A(\boldsymbol{y_k}) = M_k$, the following extra condition on $\boldsymbol{q_{k+1}}$ could be imposed

$$\nabla R_A(\boldsymbol{y_k})\in span\{\boldsymbol{q_1},\ldots,\boldsymbol{q_{k+1}}\}. \tag{2.19}$$

Thanks to the equality

$$\nabla R_A(\boldsymbol{x}) = \frac{2}{(\boldsymbol{x}|\boldsymbol{x})}(A\boldsymbol{x} - R_A(\boldsymbol{x})\boldsymbol{x}),$$

obtained after easy computations, notice that $\nabla R_A(\boldsymbol{x})\in span\{\boldsymbol{x}, A\boldsymbol{x}\}$, thus if

$$span\{\boldsymbol{q_1},\ldots,\boldsymbol{q_k}\} = span\{\boldsymbol{q_1}, A\boldsymbol{q_1},\ldots,A^{k-1}\boldsymbol{q_1}\}, \tag{2.20}$$

and if $\boldsymbol{q_{k+1}}$ satisfies $span\{\boldsymbol{q_1},\ldots,\boldsymbol{q_{k+1}}\} = span\{\boldsymbol{q_1}, A\boldsymbol{q_1},\ldots,A^k\boldsymbol{q_1}\}$, both conditions (2.18) and (2.19) hold simultaneously and it yields $m_{k+1}<m_k$ and $M_{k+1}>M_k$.

Definition 2.3.5. Let $A \in \mathbb{M}_N(\mathbb{R})$ be a matrix and $\boldsymbol{v} \in \mathbb{R}^N$ be any vector. The *k-order Krylov matrix* associated to A and $\boldsymbol{v}$ is the N by k matrix defined by

$$K(A, \boldsymbol{v}, k) = \left[\boldsymbol{v}, A\boldsymbol{v}, A^2\boldsymbol{v}, \ldots, A^{k-1}\boldsymbol{v}\right],$$

for all $k = 1, \ldots, N$, and its range

$$\mathcal{K}(A, \boldsymbol{v}, k) = span\left\{\boldsymbol{v}, A\boldsymbol{v}, A^2\boldsymbol{v}, \ldots, A^{k-1}\boldsymbol{v}\right\},$$

is called *k-order Krylov subspace* associated to A and $\boldsymbol{v}$.

With this terminology, the task to be performed is to find a not too expensive manner to build an orthonormal basis for the Krylov subspaces $\mathcal{K}(A, \boldsymbol{q_1}, k)$. For this purpose, starting from an arbitrary $\boldsymbol{q_1}$ with Euclidean norm equals 1, set $\tilde{\boldsymbol{q_2}} := A\boldsymbol{q_1} - (A\boldsymbol{q_1}|\boldsymbol{q_1})\boldsymbol{q_1}$ in order to have a new vector in the span of $\{\boldsymbol{q_1}, A\boldsymbol{q_1}\}$ orthogonal to $\boldsymbol{q_1}$. If $\tilde{\boldsymbol{q_2}} \neq 0$, set $\boldsymbol{q_2} := \tilde{\boldsymbol{q_2}}/\|\tilde{\boldsymbol{q_2}}\|$. The following vectors are built by orthogonalizing with respect to the last two basis vectors and then normalized, namely, for $k \geq 2$,

$$\begin{aligned} \tilde{\boldsymbol{q}}_{\boldsymbol{k+1}} &= A\boldsymbol{q_k} - (A\boldsymbol{q_k}|\boldsymbol{q_k})\boldsymbol{q_k} - (A\boldsymbol{q_k}|\boldsymbol{q_{k-1}})\boldsymbol{q_{k-1}}, \\ \boldsymbol{q_{k+1}} &= \frac{1}{\|\tilde{\boldsymbol{q}}_{\boldsymbol{k+1}}\|}\tilde{\boldsymbol{q}}_{\boldsymbol{k+1}}. \end{aligned}$$

Then it is sufficient to guarantee the orthonormality of the families $\{\boldsymbol{q_i}\}_{1 \leq i \leq k}$, for all $k = 1, \ldots, N$. Indeed, by induction on k, if $\{\boldsymbol{q_i}\}_{1 \leq i \leq k}$ is orthonormal, then $\boldsymbol{q_{k+1}}$ is orthogonal to $\boldsymbol{q_k}$ and $\boldsymbol{q_{k-1}}$ by construction, and for $1 \leq i \leq k-2$,

$$\begin{aligned} (\boldsymbol{q_{k+1}}|\boldsymbol{q_i}) &= \frac{1}{\|\tilde{\boldsymbol{q}}_{\boldsymbol{k+1}}\|}(A\boldsymbol{q_k} - (A\boldsymbol{q_k}|\boldsymbol{q_k})\boldsymbol{q_k} - (A\boldsymbol{q_k}|\boldsymbol{q_{k-1}})\boldsymbol{q_{k-1}}|\boldsymbol{q_i}) = \frac{1}{\|\tilde{\boldsymbol{q}}_{\boldsymbol{k+1}}\|}(\boldsymbol{q_k}|A\boldsymbol{q_i}) \\ &= \frac{1}{\|\tilde{\boldsymbol{q}}_{\boldsymbol{k+1}}\|}(\boldsymbol{q_k}|\boldsymbol{q_{i+1}}\|\tilde{\boldsymbol{q}}_{\boldsymbol{i+1}}\| + (A\boldsymbol{q_i}|\boldsymbol{q_i})\boldsymbol{q_i} + (A\boldsymbol{q_i}|\boldsymbol{q_{i-1}})\boldsymbol{q_{i-1}}) = 0, \end{aligned}$$

where the second equality comes from the symmetry of A, and the third one from the definition of $\boldsymbol{q_{i+1}}$, from the orthonormality of $\{\boldsymbol{q_i}\}_{1 \leq i \leq k}$ and from the fact that $A\boldsymbol{q_i}$ belongs to $\mathcal{K}(A, \boldsymbol{v}, k)$. Actually, for $i = 1$, $\boldsymbol{q}_0$ should be set to 0 so that the last term in the last inner product makes sense.

If for some $1 \leq k \leq N-1$, $\tilde{\boldsymbol{q}}_{\boldsymbol{k+1}} = 0$, then the process breaks down. But, it means that $\{\boldsymbol{q_1}, \ldots, \boldsymbol{q_k}\}$ spans an invariant subspace of A, or equivalently, that $k = rank(K(A, \boldsymbol{q_1}, N))$. Thus, in order to find each eigenvalue of A it is sufficient to ask $\boldsymbol{q_1}$ to have a non-zero projection on every eigenvector of A. Such a condition holds with probability 1, so no special choice of $\boldsymbol{q_1}$ is needed in practice. More precisely, by noticing in the previous development that $A\boldsymbol{q_k}$ can by written in terms of solely $\boldsymbol{q_{k-1}}$, $\boldsymbol{q_k}$ and $\boldsymbol{q_{k+1}}$, it yields readily, for all $k = 1, \ldots, rank(K(A, \boldsymbol{q_1}, N))$,

$$AQ_k = Q_k T_k + \tilde{\boldsymbol{q}}_{\boldsymbol{k+1}}\boldsymbol{e_k}^T,$$

where $\boldsymbol{e_k} \in \mathbb{R}^k$ is the last canonical basis vector of $\mathbb{R}^k$, and

$$T_k = \begin{pmatrix} \alpha_1 & \beta_1 & 0 & \dots & 0 \\ \beta_1 & \alpha_2 & \ddots & \ddots & \vdots \\ 0 & \ddots & \ddots & \ddots & 0 \\ \vdots & \ddots & \ddots & \ddots & \beta_{k-1} \\ 0 & \dots & 0 & \beta_{k-1} & \alpha_k \end{pmatrix} \in \mathbb{M}_k(\mathbb{R}),$$

where

$$\begin{aligned} \alpha_k &= (A\boldsymbol{q_k}|\boldsymbol{q_k}), \quad k = 1, \dots, N, \\ \beta_k &= (A\boldsymbol{q_{k+1}}|\boldsymbol{q_k}), \quad k = 1, \dots, N-1. \end{aligned}$$

Moreover, the condition (2.20) expressing that $\{\boldsymbol{q_i}\}_{1 \le i \le k}$ is a basis of $\mathcal{K}(A, \boldsymbol{q_1}, k)$ holds, since it clearly holds for $k = 1$ and by induction on $k = 1, \dots, N$, if it is true for $j = 1, \dots, k$, then

$$\boldsymbol{q_{k+1}} = A\boldsymbol{q_k} - \alpha_k \boldsymbol{q_k} - \beta_{k-1}\boldsymbol{q_{k-1}} \in \mathit{span}\{\boldsymbol{q_{k-1}}, \boldsymbol{q_k}, A\boldsymbol{q_k}\} \subset \mathit{span}\{\boldsymbol{q_1}, \dots, A^{k-1}\boldsymbol{q_1}, A^k\boldsymbol{q_k}\}$$

by induction assumption. Finally, since there exist $c_1, \dots, c_k \in \mathbb{R}$ such that $\boldsymbol{q_k} = c_1\boldsymbol{q_1} + \dots + c_k A^{k-1}\boldsymbol{q_1}$, it implies $A\boldsymbol{q_k} \in \mathit{span}\{A\boldsymbol{q_1}, \dots, A^k\boldsymbol{q_1}\}$.

Definition 2.3.6. With the previous notations, the matrix T_k is called *Lanczos matrix of order k*, the vectors $\boldsymbol{q_k}$ are called *Lanczos vectors*. Moreover, an eigenvalue μ of T_k is called a *Ritz value* of A and the vector $\boldsymbol{v} := Q_k\boldsymbol{u}$, where $\boldsymbol{u}$ is the eigenvector of T_k associated to μ, is called a *Ritz vector* of A and by extension, $(\mu, \boldsymbol{v})$ is called a *Ritz pair* of A.

If the process reaches $k = N$, then $AQ_N = Q_N T_N$ and so the Ritz values of A are the eigenvalues of A, and the associated eigenvectors are the Ritz vectors. Thus, the problem is reduced to compute the eigenvalues of a tridiagonal matrix. However, in practice N is large and the process stops for $k \ll N$. The quality of the approximation of the extremal eigenvalues of A by those of T_k is stated in a result by Y. Saad, which reads, adapted in our notations, as follows:

Theorem 2.3.7 ([Saa80, Theorem 2]). *For $m \le N$ such that $\boldsymbol{q_m}$ provided by the Lanczos method is not zero, let $\mu_1 < \dots < \mu_m$ be the eigenvalues of T_m, $\{\boldsymbol{x_k}\}_{1 \le k \le m}$ be an orthonormal family of eigenvectors of A associated to $\lambda_1, \dots, \lambda_m$. Assume that $\boldsymbol{q_1}$ has a non-zero projection on every x_k, $k = 1, \dots, m$. If [26] $\mu_{i-1} < \lambda_i$ for some $i = 1, \dots, m$, then*

$$0 \le \mu_i - \lambda_i \le (\lambda_N - \lambda_i)\left(\frac{K_i}{T_{m-i}(\gamma_i)} \tan \alpha(\boldsymbol{x_i}, \boldsymbol{q_1})\right)^2$$

26. For $i = 1$, there is no additional condition, so set $\mu_0 = -1$.

where

$$K_i = \prod_{j=1}^{i-1} \frac{\lambda_N - \mu_j}{\lambda_i - \mu_j},$$

and where T_{m-i} *denotes the Chebyshev polynomial of the first kind of degree* $m-i$ *given by*

$$T_{m-i}(x) = \frac{1}{2}\left((x+\sqrt{x^2-1})^{m-i} + (x-\sqrt{x^2-1})^{m-i}\right),$$

$\gamma_i = 1 + 2(\lambda_{i+1} - \lambda_i)/(\lambda_N - \lambda_i)$ *and* $\alpha(\boldsymbol{x_i}, \boldsymbol{q_1})$ *denotes the angle between* $\boldsymbol{x_i}$ *and* $\boldsymbol{q_1}$.

This result emphasizes the influence of the initial vector $\boldsymbol{q_1}$ on the approximation through its angle with the first eigenvectors of A, but mainly, it raises the *convergence rate* through the Chebyshev polynomial T_{m-i} in γ_i. The behaviour of T_k, as k tends to ∞, is well known: in our context, if $\sqrt{(\gamma_j - 1)/2}\,(m-j) > 1$, then it holds[27] that

$$T_{m-i}(\gamma_i) \sim \mathrm{e}^{2(m-i)\sqrt{(\gamma_i-1)/2}}.$$

2.3.2 Implementation of the method

As before, let $\boldsymbol{q_1}$ be an initial arbitrary vector of Euclidean norm equals 1. For practical reason, notice that for $k < rank(K(A, \boldsymbol{q_1}, N))$,

$$\|\tilde{\boldsymbol{q}}_{\boldsymbol{k+1}}\|\boldsymbol{q_{k+1}} = \tilde{\boldsymbol{q}}_{\boldsymbol{k+1}} = A\boldsymbol{q_k} - \alpha_k \boldsymbol{q_k} - \beta_{k-1}\boldsymbol{q_{k-1}}, \tag{2.21}$$

and taking the inner product against $\boldsymbol{q_{k+1}}$ implies

$$\|\tilde{\boldsymbol{q}}_{\boldsymbol{k+1}}\| = (A\boldsymbol{q_k}|\boldsymbol{q_{k+1}}) = \beta_k.$$

The Lanczos algorithm can now be expressed as follows:

Lanczos basic Algorithm

$\boldsymbol{q_1}$ given.
Initialize $\beta_0 \leftarrow 1$; $\boldsymbol{q_0} \leftarrow \boldsymbol{0}$; $\tilde{\boldsymbol{q}}_{\boldsymbol{0}} \leftarrow \boldsymbol{q_1}$; $k \leftarrow 0$;
while $\beta_k \neq 0$
  $\boldsymbol{q_{k+1}} \leftarrow \tilde{\boldsymbol{q}}_{\boldsymbol{k}}/\beta_k$; $k \leftarrow k+1$; $\alpha_k \leftarrow (A\boldsymbol{q_k}|\boldsymbol{q_k})$;
  $\tilde{\boldsymbol{q}}_{\boldsymbol{k}} \leftarrow A\boldsymbol{q_k} - \alpha_k\boldsymbol{q_k} - \beta_{k-1}\boldsymbol{q_{k-1}}$;
  $\beta_k \leftarrow \|\tilde{\boldsymbol{q}}_{\boldsymbol{k}}\|$;
end

Algorithm 2.

27. See [Par80, Appendix B]. Here, we recall that m should be large in order to get a *good* approximation of the spectrum of A.

Actually, $\beta_k = 0$ *never* occurs on a computer. To approximate numerically the first k eigenvalues of A, we fix[28] $m > k$ and use the Lanczos algorithm until computing β_m. At this step, m Ritz pairs $(\mu_1, \boldsymbol{v_1}), \ldots, (\mu_m, \boldsymbol{v_m})$ of A are at our disposal as approximations of the corresponding eigenpairs of A. The Ritz values are numbered in ascending order. Noticing that if $T_k \boldsymbol{u} = \mu \boldsymbol{u}$, then the vector $\boldsymbol{v} = Q_k \boldsymbol{u}$ verifies

$$\begin{aligned} \|A\boldsymbol{v} - \mu \boldsymbol{v}\| &= \|AQ_k\boldsymbol{u} - Q_k\mu\boldsymbol{u}\| = \|(AQ_k - Q_kT_k)\boldsymbol{u}\| = \|\tilde{\boldsymbol{q}}_{\boldsymbol{k+1}}\boldsymbol{e_k}^T\boldsymbol{u}\| \\ &= \|\tilde{\boldsymbol{q}}_{\boldsymbol{k+1}}\|\|(\boldsymbol{u})_k| = |\beta_k||(\boldsymbol{u})_k|, \end{aligned}$$

where the last equality comes from (2.21), and where $(\boldsymbol{u})_k$ denotes the k-th component of the vector $\boldsymbol{u}$. The stopping criterion used numerically consists in controlling the quantity $|\beta_k||(\boldsymbol{u_i})_k|$, with $\boldsymbol{v_i} = Q_m \boldsymbol{u_i}$. In general, this criterion is not satisfied (after reaching m the first time). Thus, the process restarts using a *judicious* choice of $\boldsymbol{q_1}$, involving the orthonormal vectors previously computed, until convergence (actually, an implicit shifted QR algorithm is achieved). A detailed description of the exact implementation can be found in [LSY98], which goes beyond the scope of this subsection whose aim was to understand the grounds of this method. Moreover, this way of restarting the process is designed to get good estimates of the associated eigenvectors.

Remark 2.3.1. Besides, rounding errors due to finite precision on a computer induce a loss of orthogonality for the vectors $\boldsymbol{q_k}$. But Paige in [Pai71] noticed that this loss is caused by combination of rounding errors together with convergence for the eigenvalues. There exist modified Lanczos methods carrying out a re-orthogonalization but the counterpart price is a bearable extra memory place and additional computational time. But there too, some variants—as one carrying block computations—exist in order to be more efficient ...

In the sequel, to approximate the spectrum of the Dirichlet-Laplace operator, a linear system has to be solved, which is of the form

$$S\boldsymbol{u} = \lambda M \boldsymbol{u}, \tag{2.22}$$

where $S, M \in \mathbb{M}_N(\mathbb{R})$ are symmetric and positive definite matrices[29], and $(\lambda, \boldsymbol{u}) \in \mathbb{R}_{>0} \times \mathbb{R}^N$ are a sought eigenpair, with λ belonging to the smallest eigenvalues. To transform this system into one appearing in Theorem 2.3.1, we perform the Cholesky decomposition of M into

$$M = L^T L,$$

where $L \in \mathbb{M}_N(\mathbb{R})$ is an upper triangular symmetric matrix. Setting $\boldsymbol{v} := L\boldsymbol{u}$, it yields

$$L^{-T} S L^{-1} \boldsymbol{v} = \lambda \boldsymbol{v},$$

and since $L^{-T}SL^{-1}$ is symmetric, the Lanczos method can be applied. To solve this system avoiding the explicit computation of L^{-1}, we successively

(i) solve the triangular system $L\boldsymbol{w} = \boldsymbol{v}$;

28. In [LSY98, Section A.1.4], they recommend to assign $m = 2k$.
29. From elasticity theory, the matrix S is called *stiffness* matrix.

(ii) compute $\boldsymbol{x} := S\boldsymbol{w}$;

(iii) solve the triangular system $L^T\boldsymbol{y} = \boldsymbol{x}$.

Finally, the eigenvector $\boldsymbol{u}$ in (2.22) can be recoverd by solving the triangular system $L\boldsymbol{u} = \boldsymbol{v}$.

Thus, as shown by the implementation of the algorithm, the user must only provide a routine performing a matrix-vector product to apply the Lanczos method—together with the ARPACK package [30]—in order to solve numerically the system given by (2.22).

30. It is described in [LSY98].

Chapter 3

Computation of eigenvalues of the Dirichlet-Laplacian

This chapter is based on the prepublication [Str12a], which can makes redundancies occur with the previous chapter. The goal of this article is to compute numerically the spectrum of the Dirichlet-Laplace operator on a domain in a surface [1] using a finite element based method. This algorithm is detailed and an estimation of the error made in approximating an eigenvalue is presented and checked on theoretically known examples. Then, the results of computations are exhibited, especially for domain in surfaces different from $\mathbb{R}^2$.

In the present chapter, more details are given about the tools and notions used in [Str12a]. In particular, the existence of solutions is established for the eigenvalue problem consisting in finding a non-zero map $u : \Omega_M \to \mathbb{R}$ and a scalar $\lambda \in \mathbb{R}$, such that $-\Delta_g u = \lambda u$, on the domain Ω_M, with Dirichlet boundary conditions. The variational formulation of the problem is derived into details, followed by a discussion about the equivalence with the initial formulation of the problem, through the regularity of $\partial\Omega_M$. This variational formulation is suitable for the numerical computations based on the approximation of the problem, which is the subject of the second section. Then, the error made in doing this approximation, both for the eigenvalues and the eigenfunctions, is presented in the third and fourth section. Finally, the examples exhibited in the article are repeated. It consists in numerical validations for a ball in $\mathbb{R}^2$ together with some experiments for balls of various volumes in the sphere $\mathbb{S}^2$ and in hyperbolic space. A comparison between the eigenvalues of the Dirichlet-Laplace operator on these balls in these three surfaces is carried out. Perforated balls and a family of surfaces of revolution with various curvatures are other examples presented here.

1. Precise definition of the notions approached in this short introduction are given in details in the first section below.

3.1 Theoretical statement of the problem

Let (M, g) be a smooth, complete Riemannian manifold of dimension 2 and $\Omega_M \subset M$ be a domain, namely a bounded open set in M. First, assume that $\partial\Omega_M$ is *regular enough*[2] and that g is smooth. These assumptions on $\partial\Omega_M$ and g are weakened later. Analogously to Subsection 2.1, a Riemannian metric g being an inner product on each tangent space of the manifold, it can be represented at each point x of M by a matrix $G(\pi(x)) \in \mathbb{M}_2(\mathbb{R})$ using a chart (U, π), where $\Omega_M \subset U \subset M$ and $\pi : U \to \mathbb{R}^2$ is a diffeomorphism onto its range. Denote by x_1, x_2 the local coordinates, and by Δ_g the Laplace operator given for all $f \in \mathcal{C}^\infty(M)$ by

$$\Delta_g f = \frac{1}{\sqrt{\det(G)}} \sum_{j,k=1}^{2} \partial x_j \left(G^{jk} \sqrt{\det(G)} \partial x_k f \right), \tag{3.1}$$

where G^{jk} is the (j,k)-component of the inverse of the matrix G as outlined in Subsection 2.1.3. Consider the following problem

$$(\mathcal{P}) \begin{cases} \text{Find a map } u := u_{\Omega_M} : \Omega_M \to \mathbb{R}, u \not\equiv 0, \text{ and a scalar } \lambda := \lambda_{\Omega_M} \text{ such that} \\ \qquad -\Delta_g u = \lambda u \quad \text{in } \Omega_M, \\ \qquad u = 0 \quad \text{on } \partial\Omega_M. \end{cases}$$

Definition 3.1.1. The map u is called an *eigenfunction* associated to the *eigenvalue* λ. The couple (u, λ) is called an *eigensolution* or an *eigenpair*.

Let $\mathcal{C}_c^\infty(\Omega_M)$ denote the space of $\mathcal{C}^\infty(\Omega_M)$-functions with compact support in Ω_M, $H^k(\Omega_M)$ the Sobolev space of order $k \in \mathbb{N} \setminus \{0\}$, and $H_0^1(\Omega_M)$ the closure in $H^1(\Omega_M)$ of $\mathcal{C}_c^\infty(\Omega_M)$. The space $H^s(\Omega)$, for a domain Ω and a scalar $s \in \mathbb{R}$, briefly appears subsequently in the discussion about the regularity of the solutions to the problem $(\mathcal{P})$. For a complete definition of Sobolev spaces and connected notions, see Subsection A.2 in the appendix.

The spectral theorem is the main tool to prove the existence of eigensolutions. For a proof of this classical result, see for example [Bre11, Theorem 6.11].

Theorem 3.1.2 (spectral theorem)**.** *Let $(E, (\cdot|\cdot))$ be a separable Hilbert space of infinite dimension and T be a positive, self-adjoint and compact operator on E. Then, there exist a sequence $(x_m)_{m\in\mathbb{N}\setminus\{0\}}$ of eigenvectors defining a Hilbert basis of E and a sequence $(\mu_m)_{m\in\mathbb{N}\setminus\{0\}}$ of associated eigenvalues converging to 0, such that $Tx_m = \mu_m x_m$.*

To prove the existence of eigensolutions to the problem $(\mathcal{P})$ let us first consider $f \in L^2(\Omega_M)$ and u a solution to the problem

$$(\mathcal{P}_f) \begin{cases} \text{Find } u \in H^2(\Omega_M), \text{ such that} \\ \quad -\Delta_g u = f \quad \text{in } \Omega_M, \\ \quad u = 0 \quad \text{on } \partial\Omega_M. \end{cases}$$

2. For instance assume that $\partial\Omega_M$ is smooth.

The Green Formula [3] shows that u belongs to $H_0^1(\Omega_M)$ and is solution of the problem

$$(\mathcal{WP}_f)\begin{cases} \text{Find } u \in H_0^1(\Omega_M) \text{ such that} \\ \displaystyle\int_{\Omega_M} g(\boldsymbol{\nabla u}, \boldsymbol{\nabla v})\,\mathrm{d}V_g = \int_{\Omega_M} fv\,\mathrm{d}V_g, \quad \forall v \in H_0^1(\Omega_M), \end{cases}$$

where $\mathrm{d}V_g$ denotes the volume element on M and ∇ the gradient associated to g, as defined in Section 2.1. Using the developments made in that section, the volume element $\mathrm{d}V_g$ can be written in terms of Lebesgue measure using the local coordinates in $\pi(U)$ as $\mathrm{d}V_g = \sqrt{\det G}\,\mathrm{d}x_1\mathrm{d}x_2$, and the gradient of a function $v \in H_0^1(\Omega_M)$ is given by

$$\boldsymbol{\nabla v} = G^{-1}\boldsymbol{\nabla_{us}}(\boldsymbol{v} \circ \boldsymbol{\pi^{-1}}),$$

where $\boldsymbol{\nabla_{us}} = (\partial x_1, \partial x_2)$ denotes the usual gradient in $\mathbb{R}^2$ in the sense of the distributions theory, see Section A.2 in the appendix. The left hand side of the equality in $(\mathcal{WP}_f)$ can be rewritten over $\Omega := \pi(\Omega_M)$ using the bilinear form

$$\begin{aligned} a : H_0^1(\Omega) \times H_0^1(\Omega) &\to \mathbb{R} \\ (u, v) &\mapsto a(u, v) = \int_{\Omega} \boldsymbol{\nabla u}^T G^{-1} \boldsymbol{\nabla v} \sqrt{\det G}, \end{aligned}$$

and the right hand side with the linear form

$$\begin{aligned} l_f : H_0^1(\Omega) &\to \mathbb{R} \\ v &\mapsto l_f(v) = \int_{\Omega} fv\sqrt{\det G}. \end{aligned}$$

In order to apply the Lax-Milgram Theorem [4] in this context, assume the components $G_{i,j}$, $i, j = 1, 2$, of the matrix G to satisfy

(H_1) $G_{i,j}$ is bounded on Ω_M for $i, j = 1, 2$;

(H_2) there exists $C > 0$ such that $\det G \geq C$ on Ω_M.

A sufficient condition for these assumptions to hold is that there exists a compact set K such that $\Omega_M \subset K \subset U$. Indeed, the components $G_{i,j}$, $i, j = 1, 2$, and thus $\det G$ are continuous maps. With these assumptions, the bilinear form a is continuous, $H_0^1(\Omega_M)$-elliptic [5], with constant of ellipticity denoted by C_{ell}. The linear form l_f is continuous, thanks to the Poincaré's inequality [6]. So, the Lax-Milgram Theorem holds: there exists a unique solution $u \in H_0^1(\Omega_M)$ to the problem $(\mathcal{WP}_f)$.

3. See Section A.2 in the appendix.
4. See Theorem A.1.5.
5. See Definition A.1.4.
6. It is recalled in Proposition A.2.16.

It is natural at this point to consider the space $L^2(\Omega)$ endowed with the scalar product $(\cdot|\cdot)_H$ given by

$$(v|w)_H = \int_\Omega v(\mathbf{x})w(\mathbf{x})\sqrt{\det G(\mathbf{x})}\,\mathrm{d}\mathbf{x}, \quad \forall v, w \in L^2(\Omega), \tag{3.2}$$

where $\mathbf{x} = (x_1, x_2)$. The assumptions made on g ensure this space, denoted by H, to be a Hilbert space and the norm $\|\cdot\|_H$ to be equivalent to $\|\cdot\|_{L^2(\Omega)}$. For convenience, C_- and C_+ denotes the two positive constants such that, for all $f \in L^2(\Omega)$,

$$C_-\|f\|_{L^2(\Omega)} \leq \|f\|_H \leq C_+\|f\|_{L^2(\Omega)}. \tag{3.3}$$

Thus, with these notations, the following operator is well defined

$$\begin{aligned} T_D : H &\to H \\ f &\mapsto u, \end{aligned}$$

where u is the solution to the problem $(\mathcal{WP}_f)$. Moreover, T_D satisfies the assumptions of the spectral theorem: first, T_D is positive since for $f \in H$ and u solution of $(\mathcal{WP}_f)$,

$$(T_D f|f)_H = \int_\Omega fu\sqrt{\det G} = l_f(u) = a(u,u) \geq 0,$$

by $H_0^1(\Omega_M)$-ellipticity of a. Actually, T_D is strictly positive since $f \not\equiv 0$ implies $u \not\equiv 0$. Secondly, T_D is self-adjoint since for $f, g \in H$, and $u = T_D f$, $w = T_D g$, the equality in $(\mathcal{WP}_f)$ applied to $v = w$ gives

$$a(u,w) = l_f(w),$$

and in $(\mathcal{WP}_g)$ applied with $v = u$,

$$a(w,u) = l_g(u),$$

thus

$$(f|T_D g)_H = l_f(w) = a(u,w) = l_g(u) = (T_D f|g)_H\,.$$

Finally, to see that T_D is compact, we first show that T_D is bounded in $H_0^1(\Omega)$: let $f \in H$ and $u = T_D f$. The equality in $(\mathcal{WP}_f)$ applied to $v = u$ gives

$$C_{ell}\|u\|^2_{H_0^1(\Omega)} \leq a(u,u) = l_f(u) \leq \|f\|_H\|u\|_H \leq C^2C_+^2\|f\|_{H_0^1(\Omega)}\|u\|_{H_0^1(\Omega)},$$

where $C > 0$ is the constant appearing in the Poincaré's inequality. So

$$\|T_D f\|_{H_0^1(\Omega)} = \|u\|_{H_0^1(\Omega)} \leq \frac{C^2C_+^2}{C_{ell}}\|f\|_{H_0^1(\Omega)}.$$

Since $T_D : H \to H_0^1(\Omega)$ is bounded, $i : H_0^1(\Omega) \hookrightarrow L^2(\Omega)$ is compact by the Rellich's Theorem [7] and since $\|\cdot\|_H$ and $\|\cdot\|_{L^2(\Omega)}$ are equivalent, T_D is compact. The spectral theorem can be applied in that context: there exist a sequence $(u_n)_{n\in\mathbb{N}\setminus\{0\}}$ of eigenvectors defining a Hilbert basis of H and a sequence $(\mu_n)_{m\in\mathbb{N}\setminus\{0\}}$ of positive associated eigenvalues converging to 0, such that $T_D u_n = \mu_n u_n$ for all $n \in \mathbb{N}\setminus\{0\}$.

The equality $T_D u_n = \mu_n u_n$ means that $u = \mu_n u_n$ is a solution to $(\mathcal{WP}_{u_n})$, that is

$$\int_{\Omega_M} g(\boldsymbol{\nabla u}, \boldsymbol{\nabla v})\,\mathrm{d}V_g = \int_{\Omega_M} u_n v\,\mathrm{d}V_g \quad \forall v \in H_0^1(\Omega_M),$$

Using the notations $\lambda_{n,\Omega} := 1/\mu_n$ and $u_{n,\Omega} := u_n$ for all $n \in \mathbb{N}\setminus\{0\}$, this means that there exist a strictly positive sequence

$$0 < \lambda_{1,\Omega} \leq \lambda_{2,\Omega} \leq ... \nearrow +\infty,$$

tending to $+\infty$ and a sequence of functions $(u_{n,\Omega})_{n\in\mathbb{N}\setminus\{0\}}$, forming a Hilbert basis of H, such that for all $n \in \mathbb{N}\setminus\{0\}$, $(\lambda_{n,\Omega}, u_{n,\Omega})$ is solution of the problem

$$(\mathcal{WP}) \begin{cases} \text{Find } u \in H_0^1(\Omega_M), u \not\equiv 0, \text{ and } \lambda \in \mathbb{R} \text{ such that} \\ \displaystyle\int_{\Omega_M} g(\boldsymbol{\nabla u}, \boldsymbol{\nabla v})\,\mathrm{d}V_g = \lambda \int_{\Omega_M} uv\,\mathrm{d}V_g, \quad \forall v \in H_0^1(\Omega_M). \end{cases}$$

Definition 3.1.3. The problem $(\mathcal{WP})$ is a *weak formulation* of the problem $(\mathcal{P})$. A couple (u, λ) solution of $(\mathcal{WP})$ is called a *weak solution* or a *weak eigenpair*. The scalar λ is called a *weak eigenvalue* and the function u a *weak eigenfunction*.

In the sequel, the dependence on the domain is sometimes explicitly indicated by specifying (weak-)eigenvalue of Ω_M or (weak-)eigenfunction of Ω_M and will be denoted by $\lambda_n(\Omega_M)$. On the contrary when no ambiguity is possible, the subscript indicating the domain will be omitted, as in u_n.

Remark 3.1.1. The orthogonality in H is the orthogonality in $L^2(\Omega_M)$ endowed with the measure given by the volume element $\mathrm{d}V_g$.

A natural question which arises now is to know when a weak eigenpair (λ, u) is a solution to the initial problem $(\mathcal{P})$. Actually, it depends on the regularity of the boundary of the domain Ω_M, or equivalently on the boundary of the domain Ω, since π is supposed to be a diffeomorphism. Without going into details, the rest of this subsection is dedicated to a discussion about several cases.

First, if $\partial\Omega_M$ is at least of class $\mathcal{C}^2$, all the previous computations hold (in particular, the Green Formula and the well definition of the spaces used). Moreover, if (λ, u) is a weak solution, then u is solution of $(\mathcal{WP}_{\lambda u})$. And by the Theorem 8.12 in [GT01], u is also in $H^2(\Omega_M) \cap H_0^1(\Omega_M)$. Thus, for all $\varphi \in \mathcal{C}_c^\infty(\Omega_M)$,

$$\int_{\Omega_M} -\Delta_g u\,\varphi\,\mathrm{d}V_g = \lambda \int_{\Omega_M} u\varphi\,\mathrm{d}V_g,$$

7. See Theorem A.2.18 in the appendix.

by the Green Formula. Finally, by definition of $\mathcal{C}_c^\infty(\Omega_M)$, the equality $-\Delta_g u = \lambda u$ holds in Ω and (u, λ) is also an eigensolution.

Remark 3.1.2. As stated in Theorem 8.13 in [GT01], the regularity of the eigenfunction u is *the same* as the regularity of the boundary of the domain. More precisely, if $\partial\Omega_M$ is of class $\mathcal{C}^{k+2}$, then u is of class $\mathcal{C}^{k+2}(\Omega_M)$, for all $k \in \mathbb{N}$. In particular, $\partial\Omega_M$ of class $\mathcal{C}^\infty$ implies u of class $\mathcal{C}^\infty(\Omega_M)$.

If Ω is only supposed to have a polygonal boundary, the Green Formula still holds, so an eigenpair (u, λ) is also a weak eigenpair, as stated in [Gri85, Theorem 1.5.3.1]. The converse is not necessarily true, and depends on the largest angle ω of the polygon described by $\partial\Omega$. In this situation, the condition $u \in H^{1+\pi/\omega}(\Omega)$ holds, see [Gri92, Corollary 2.4.4 and Remark 2.4.6]. In particular, if Ω is a convex polygonal set, a weak eigenpair is also an eigenpair.

Keeping this in mind, we focus in the sequel on the problem $(\mathcal{WP})$ and its solutions to avoid ambiguity.

3.2 Numerical processing of the problem

A finite element method is used to solve numerically the problem $(\mathcal{P})$. The Galerkin method [8] consists in reformulating $(\mathcal{WP})$ as a *similar* problem in a family of finite dimensional functional subspaces $V_h \subset H_0^1(\Omega)$ associated to a family of meshes $\mathcal{M}_h$:

$$(\mathcal{WP}_h) \begin{cases} \text{Find } u_h \in V_h, u_h \not\equiv 0, \text{ and } \lambda_h \in \mathbb{R} \text{ such that} \\ a(u_h, v_h) = \lambda_h (u_h | v_h)_H, \quad \forall v_h \in V_h. \end{cases}$$

Note that because of the regularity of π, $(\mathcal{WP}_h)$ can be expressed in terms of functions directly defined on Ω.

Definition 3.2.1. The problem $(\mathcal{WP}_h)$ is an *approximated problem* of the problem $(\mathcal{WP})$. A couple (u_h, λ_h) solution of $(\mathcal{WP}_h)$ is called an *approximated solution* or an *approximated eigenpair*. The scalar λ_h is called an *approximated eigenvalue* and the function u_h an *approximated eigenfunction*.

Existence of approximated solutions holds thanks to the finite dimension of V_h and the inclusion $V_h \subset H_0^1(\Omega)$: there exist a strictly positive sequence

$$0 < \lambda_{h,1,\Omega} \leq \lambda_{h,2,\Omega} \leq ... \leq \lambda_{h,N_h,\Omega}\,,$$

where $N_h = \dim V_h$ and a sequence of functions $(u_{h,n,\Omega})_{n=1,...,N_h}$, being an orthonormal basis of V_h, such that for all $n = 1, \dots N_h$, $(\lambda_{h,n,\Omega}, u_{h,n,\Omega})$ is solution of the problem $(\mathcal{WP}_h)$. The subscript h stands for the dependence on the geometry of the mesh, more precisely

$$h := \max_{K \in \mathcal{M}_h} h_K = \max_{K \in \mathcal{M}_h} \operatorname{diam}(K),$$

8. See Subsection 2.2.2 for more details.

where K is the geometric element of a finite element (K, Σ, P) of the mesh $\mathcal{M}_h$. Moreover, the family of spaces $(V_h)_h$ is supposed to be associated to a regular family $(\mathcal{M}_h)_h$ of meshes in the sense of Definition 2.2.7. For the computations, a finite element method made of triangles of type $\mathcal{P}_1$ is used, as defined in Definition 2.2.5. It implies, for all h, that

$$V_h = \left\{ v_h \in \mathcal{C}^0\left(\overline{\Omega}\right) \mid {v_h}_{|\partial\Omega} \equiv 0,\ {v_h}_{|K} \text{ affine for all triangles } K \text{ of the mesh } \mathcal{M}_h \right\}.$$

Following the classical process of the finite element method, consider a basis $\{\varphi_{h,i}\}_{i=1}^{N_h}$ of V_h, given by

$$\varphi_{h,i} \in V_h, \quad \varphi_{h,i}(P_j) = \delta_{ij}, \quad \forall\, 1 \leq i, j \leq N_h,$$

where P_i denotes the nodes of $\mathcal{M}_h$ inside Ω and δ_{ij} the Kronecker symbol, $1 \leq i, j \leq N_h$, as recalled in Section 2.2. With these notations, every function $v_h \in V_h$ can be written as

$$v_h(x) = \sum_{i=1}^{N_h} v_h(P_i)\varphi_{h,i}(x), \quad \forall x \in \Omega,$$

and the bilinear form a and the linear form l are completely determined by the values $a(\varphi_{h,j}, \varphi_{h,i})$ and $l(\varphi_{h,i})$ respectively, $1 \leq i, j \leq N_h$. So, introducing the matrices $M \in \mathbb{M}_{N_h}(\mathbb{R})$ and $S \in \mathbb{M}_{N_h}(\mathbb{R})$ given by

$$M_{i,j} = \int_\Omega \varphi_{h,j}\varphi_{h,i}\,\mathrm{d}V_g, \quad \forall 1 \leq i, j \leq N_h, \tag{3.4}$$

$$S_{i,j} = a(\boldsymbol{\nabla\varphi_{h,j}}, \boldsymbol{\nabla\varphi_{h,i}}), \quad \forall 1 \leq i, j \leq N_h, \tag{3.5}$$

the approximated problem can be reformulated as

$$(\mathcal{WP}_h) \begin{cases} \text{Find } \mathbf{u_h} \in \mathbb{R}^{N_h}, \mathbf{u_h} \neq 0 \text{ and } \lambda_h \in \mathbb{R} \text{ such that} \\ S\mathbf{u_h} = \lambda_h M \mathbf{u_h}. \end{cases}$$

By coercivity of a, S is positive definite. This problem is then solved numerically with a Lanczos process from the ARPACK library, as recalled in Section 2.3.

Remark 3.2.1. The integrals appearing in the computation of matrices M and S are approximated using quadrature formula: both without masslumping (nodes of an element coincide with the middle of its edges) and also for M, with masslumping (nodes of an element coincide with the vertices, that makes M to be diagonal). See Subsection 2.2.3.

The approximated problem is used numerically and so, the solutions obtained are *only* approximated eigenpairs. Thus, it is natural to wonder how *close* are the approximated solutions to the exact ones. Of course, it depends on the domain Ω and on the quality of the mesh $\mathcal{M}_h$. It is the main point of the next subsection.

3.3 Estimation of the error $|\lambda_{h,k} - \lambda_k|$

Two results are given in this section: the first one gives a bound on the error $|\lambda_{h,k} - \lambda_k|$ from [RT83, Chapter 6] and [Bof10, Chapters 7 and 8]. This section follows the presentation made in [RT83, Chapter 6], although a slight adaptation of context is necessary to take into consideration the influence of the metric g in the bilinear form a and in the norm $\|\cdot\|_H$. The second result, from [BO87], is more precise in the case of a multiple eigenvalue but more complicated. It is given without proof.

The notations of the previous sections are used again. Besides, assume that the domain Ω has a polygonal boundary to consider only the error made by the approximation of $H_0^1(\Omega)$ by V_h and not the error due to the approximation of Ω itself.

First, let us recall a classical and important result.

Definition 3.3.1. For $v \in H_0^1(\Omega)$, $v \neq 0$, the *Rayleigh quotient* is defined by

$$\mathcal{R}(v) = \frac{a(v,v)}{(v|v)_H} = \frac{\displaystyle\int_\Omega \boldsymbol{\nabla} \boldsymbol{v}^T G^{-1} \boldsymbol{\nabla} \boldsymbol{v} \, \mathrm{d}V_g}{\displaystyle\int_\Omega v^2 \, \mathrm{d}V_g}.$$

Proposition 3.3.2 (Min-max Theorem)**.** *For all $k \in \mathbb{N} \setminus \{0\}$,*

$$\lambda_k = \min_{E_k \in \mathcal{V}_k} \max_{v \in E_k \setminus \{0\}} \mathcal{R}(v),$$

where $\mathcal{V}_k$ denotes the set of all subspaces E_k of $H_0^1(\Omega)$ of dimension k.

Proof. On the first hand, denoting by $M(\lambda_k)$ the subspace spanned by the k first eigenfunctions (if λ_k is not simple, for example $\lambda_{k-i+1} = \cdots = \lambda_k = \cdots = \lambda_{k+j}$, pick any i associated eigenfunctions), and writing $v = \sum_{j=1}^k \alpha_j v_j$ an element of $M(\lambda_k)$,

$$\begin{aligned}
\min_{E_k \in \mathcal{V}_k} \max_{v \in E_k \setminus \{0\}} \mathcal{R}(v) &\leq \max_{v \in M(\lambda_k) \setminus \{0\}} \mathcal{R}(v) \\
&= \max_{(\alpha_1, \ldots, \alpha_k) \neq (0, \ldots, 0)} \frac{\sum_{j=1}^k \alpha_j^2 a(u_j, u_j)}{\sum_{j=1}^k \alpha_j^2} \\
&= \max_{(\alpha_1, \ldots, \alpha_k) \neq (0, \ldots, 0)} \frac{\sum_{j=1}^k \alpha_j^2 \lambda_j}{\sum_{j=1}^k \alpha_j^2} \leq \lambda_k,
\end{aligned}$$

by H-orthonormality of the eigenfunctions. In particular, notice that over $M(\lambda_k)$, the Rayleigh quotient is maximal at u_k and $\mathcal{R}(u_k) = \lambda_k$. On the other hand, for $E_k \in \mathcal{V}_k$, it is always possible, by an orthogonality process, to choose $v^* \in E_k$ such that $(v^*|u_i)_H = 0$ for all $i = 1, \ldots, k-1$. Such a vector can be written $v^* = \sum_{j \geq k} \alpha_j u_j$, so

$$\min_{E_k \in \mathcal{V}_k} \max_{v \in E_k \setminus \{0\}} \mathcal{R}(v) \geq \min_{E_k \in \mathcal{V}_k} \mathcal{R}(v^*) = \frac{\sum_{j \geq k} \alpha_j^2 \lambda_j}{\sum_{j \geq k} \alpha_j^2} \geq \lambda_k.$$

■

This result being valid in a more general framework, it holds of course also for the approximated eigenvalues (with a similar proof), namely for all $k = 1, \ldots, N_h$,

$$\lambda_{h,k} = \min_{E_{h,k} \in \mathcal{V}_{h,k}} \max_{v_h \in E_{h,k} \setminus \{0\}} \mathcal{R}(v_h),$$

where $\mathcal{V}_{h,k}$ denotes the set of all subspaces $E_{h,k}$ of V_h of dimension k. Furthermore, the following inequality holds for all $k = 1, \ldots, N_h$,

$$\lambda_k \leq \lambda_{k,h}\,, \quad 1 \leq k \leq N_h. \tag{3.6}$$

Indeed, since $V_h \subset H_0^1(\Omega)$, all subspace of V_h of dimension k is also a subspace of $H_0^1(\Omega)$ of dimension k, and

$$\lambda_k = \min_{E_k \in \mathcal{V}_k} \max_{v \in E_k \setminus \{0\}} \mathcal{R}(v) \leq \min_{E_k \in \mathcal{V}_{h,k}} \max_{v_h \in E_k \setminus \{0\}} \mathcal{R}(v_h) = \lambda_{h,k},$$

The converse estimation is the main part to establish the error $|\lambda_{h,k} - \lambda_k|$. In that aim, we follow the presentation in [RT83]. Let us introduce $\Pi_h : H_0^1(\Omega) \mapsto V_h$ the elliptic projection operator uniquely determined by

$$a(v - \Pi_h v, v_h) = 0, \quad \forall v_h \in V_h.$$

Both following lemmas do not need to be adapted from [RT83], but they are given with a proof, for the sake of completeness.

Lemma 3.3.3 ([RT83, Lemma 6.4-1]). *Set* $\sigma_{h,k} := \inf_{\substack{v \in M(\lambda_k) \\ \|v\|_H = 1}} \|\Pi_h v\|_H$ *for all integers* $k \geq 1$. *If* $\sigma_{h,k} > 0$, *then for all integer* $1 \leq k \leq N_h$,

$$\lambda_{h,k} \leq \frac{\lambda_k}{\sigma_{h,k}^2}.$$

Proof. Let $M(\lambda_k)$ be the subspace spanned by the k first eigenfunctions. Since $\sigma_{h,k} > 0$, $\dim(\Pi_h M(\lambda_k)) = k$. Choosing $E_{h,k} = \Pi_h M(\lambda_k)$ in the Min-max Theorem yields

$$\lambda_{h,k} \leq \max_{v_h \in \Pi_h M(\lambda_k) \setminus \{0\}} \mathcal{R}(v_h) = \max_{v \in M(\lambda_k), \|v\|_H = 1} \frac{a(\Pi_h v, \Pi_h v)}{\|\Pi_h v\|_H^2} \leq \max_{v \in M(\lambda_k), \|v\|_H = 1} \frac{a(v,v)}{\|\Pi_h v\|_H^2},$$

by homogeneity of $\mathcal{R}$ and by definition of the elliptic projection operator Π_h. Since

$$\lambda_k = \max_{v \in M(\lambda_k)} \mathcal{R}(v),$$

it implies

$$\lambda_{h,k} \leq \max_{v \in M(\lambda_k), \|v\|_H = 1} \frac{a(v,v)}{\|\Pi_h v\|_H^2} \leq \lambda_k \sup_{v \in M(\lambda_k), \|v\|_H = 1} \frac{1}{\|\Pi_h v\|_H^2} = \frac{\lambda_k}{\sigma_{h,k}^2}.$$

■

Lemma 3.3.4 ([RT83, Lemma 6.4-2]). *For all integer $k \geq 1$, there exists a constant $C_1 := C_1(k) > 0$, independent of h, such that for all subspaces V_h of V of dimension $k \leq N_h$,*

$$\sigma_{h,k}^2 \geq 1 - C_1 \sup_{\substack{v \in M(\lambda_k) \\ \|v\|_H = 1}} \|v - \Pi_h v\|_{H_0^1(\Omega)}^2 .$$

In particular, the inequality holds for $C_1 = 2C_{cont}\sqrt{k}\lambda_1^{-1}$, where C_{cont} is the constant of continuity of a.

Remark 3.3.1. For all $u, v \in H_0^1(\Omega)$, it holds that

$$a(u,v) = \int_\Omega \boldsymbol{\nabla u}^T G^{-1} \boldsymbol{\nabla v} \sqrt{\det G} \leq \sup_{x \in \Omega} \sqrt{\det G(x)}\ \|u\|_{H_0^1(\Omega)} \|v\|_{H_0^1(\Omega)} .$$

So, a bound for the continuity constant of a is given by $C_{cont} \leq \sup_{x\in\Omega} \sqrt{\det G(x)}$ which is finite by assumption.

Proof. Let $v \in M(\lambda_k)$, $\|v\|_H = 1$. Let us write v as $v = \sum_{j=1}^k \alpha_j u_j$ with $\sum_{j=1}^k \alpha_j^2 = 1$, by orthonormality. So,

$$1 - \|\Pi_h v\|_H^2 = (v - \Pi_h v | v + \Pi_h v)_H = - \|v - \Pi_h v\|_H^2 + 2\,(v - \Pi_h v | v)_H ,$$

thus,

$$\|\Pi_h v\|_H^2 \geq 1 - 2\,(v - \Pi_h v | v)_H .$$

Besides, since $\lambda_j > 0$ for all $j \in \mathbb{N} \setminus \{0\}$,

$$(v - \Pi_h v | v)_H = \sum_{j=1}^k \alpha_j\,(v - \Pi_h v | u_j)_H = \sum_{j=1}^k \alpha_j \lambda_j^{-1} a(v - \Pi_h v, u_j).$$

The equality $a(v - \Pi_h v, v_h) = 0$ holds in particular for $v_h = \Pi_h u_j$, so,

$$(v - \Pi_h v | v)_H = \sum_{j=1}^k \alpha_j \lambda_j^{-1} a(v - \Pi_h v, u_j - \Pi_h u_j),$$

and by definition of C_{cont}, the Minkowski inequality yields

$$\begin{aligned}
(v - \Pi_h v | v)_H &\leq C_{cont} \|v - \Pi_h v\|_{H_0^1(\Omega)} \sum_{j=1}^k |\alpha_j| \lambda_j^{-1} \|u_j - \Pi_h u_j\|_{H_0^1(\Omega)} \\
&\leq C_{cont} \|v - \Pi_h v\|_{H_0^1(\Omega)} \left(\sum_{j=1}^k \alpha_j^2 \lambda_j^{-2} \right)^{1/2} \left(\sum_{j=1}^k \|u_j - \Pi_h u_j\|_{H_0^1(\Omega)}^2 \right)^{1/2} \\
&\leq C_{cont} \|v - \Pi_h v\|_{H_0^1(\Omega)} \lambda_1^{-1} \sqrt{k} \sup_{\substack{v \in M(\lambda_k) \\ \|v\|_H = 1}} \|v - \Pi_h v\|_{H_0^1(\Omega)} .
\end{aligned}$$

Denoting by $C_1 = 2C_{cont}\sqrt{k}\lambda_1^{-1}$, it holds that

$$\|\Pi_h v\|_H^2 \geq 1 - C_1 \sup_{\substack{v \in M(\lambda_k) \\ \|v\|_H = 1}} \|v - \Pi_h v\|_{H_0^1(\Omega)}^2 .$$

■

The next proposition states that an approximated eigenvalue $\lambda_{h,k}$ converges to the corresponding eigenvalue λ_k. It is the main result we wanted to develop. Furthermore, if the associated eigenfunctions are sufficiently regular, namely at least $H^2(\Omega)$, then it leads to an order of convergence $O(h^2)$ for $|\lambda_{h,k} - \lambda_k|$.

Proposition 3.3.5. *For all integer $1 \leq k \leq N_h$, and for $h > 0$ small enough, there exists a constant $C_2 > 0$ independent of the subspace V_h of dimension k, such that*

$$0 \leq \lambda_{h,k} - \lambda_k \leq C_2 \sup_{\substack{v \in M(\lambda_k) \\ \|v\|_H = 1}} \inf_{v_h \in V_h} \|v - v_h\|_{H_0^1(\Omega)}^2 .$$

In particular, the inequality holds with

$$C_2 = 2C_1 \frac{C_{cont}^2}{C_{ell}^2}\lambda_k = 4\sqrt{k}\frac{C_{cont}^3}{C_{ell}^2}\frac{\lambda_k}{\lambda_1},$$

where C_1 is the constant appearing in Lemma 3.3.4 and C_{cont}, resp. C_{ell}, denotes the constant of continuity of a, resp. of $H_0^1(\Omega)$-ellipticity of a.

Remark 3.3.2. The properties of the mesh and of the elements used, involving piecewise linear functions, ensure [9] that

$$\lim_{h \to 0} \inf_{v_h \in V_h} \|v - v_h\|_{H_0^1(\Omega)} = 0, \quad \forall v \in H_0^1(\Omega).$$

Proof of proposition 3.3.5. For all $v \in H_0^1(\Omega)$,

$$\begin{aligned} C_{ell}\,\|v - \Pi_h v\|_{H_0^1(\Omega)}^2 &\leq a(v - \Pi_h v, v - \Pi_h v) \\ &= a(v - \Pi_h v, v - v_h) - \overbrace{a(v - \Pi_h v, \Pi_h v - v_h)}^{=0} \\ &\leq C_{cont}\,\|v - \Pi_h v\|_{H_0^1(\Omega)}\,\|v - v_h\|_{H_0^1(\Omega)}\,, \end{aligned}$$

hence,

$$\|v - \Pi_h v\|_{H_0^1(\Omega)} \leq \frac{C_{cont}}{C_{ell}} \inf_{v_h \in V_h} \|v - v_h\|_{H_0^1(\Omega)}\,, \quad \forall v \in H_0^1(\Omega). \tag{3.7}$$

Besides, by an argument similar to the one in the proof of Lemma 3.3.4 involving the Minkowsky inequality, for all $v \in M(\lambda_k)$ such that $\|v\|_H = 1$, it yields

$$\|v - \Pi_h v\|_{H_0^1(\Omega)} \leq \left(\sum_{j=1}^{k} \|u_j - \Pi_h u_j\|_{H_0^1(\Omega)}^2 \right)^{1/2},$$

9. see Subsection 2.2.2.

so, taking into consideration Remark 3.3.2 applied to each u_j and $\Pi_h u_j$ of the above sum, and taking the supremum over all $v \in M(\lambda_k)$ such that $\|v\|_H = 1$, it holds that

$$\lim_{h\to 0} \sup_{\substack{v\in M(\lambda_k)\\ \|v\|_H=1}} \|v - \Pi_h v\|_{H_0^1(\Omega)} = 0.$$

So, by Lemma 3.3.4, for $h > 0$ small enough, $\sigma_{h,k} > 0$ so that the assumption of Lemma 3.3.3 holds. Finally, it yields

$$\lambda_{h,k} \leq \frac{\lambda_k}{\sigma_{h,k}^2} \leq \frac{\lambda_k}{1 - C_1 \sup\limits_{\substack{v\in M(\lambda_k)\\ \|v\|_H=1}} \|v - \Pi_h v\|^2_{H_0^1(\Omega)}}.$$

For $x > 0$ sufficiently small, it is clear that

$$\frac{1}{1-x} \leq 1 + 2x,$$

and applied with

$$x = C_1 \sup_{\substack{v\in M(\lambda_k)\\ \|v\|_H=1}} \|v - \Pi_h v\|^2_{H_0^1(\Omega)},$$

which is as small as desired since C_1 does not depend on h, it leads to the expected result, that is,

$$\begin{aligned} \lambda_{h,k} &\leq \left(1 + 2C_1 \sup_{\substack{v\in M(\lambda_k)\\ \|v\|_H=1}} \|v - \Pi_h v\|^2_{H_0^1(\Omega)}\right) \lambda_k \\ &\overset{(3.7)}{\leq} \left(1 + 2C_1 \frac{C_{cont}^2}{C_{ell}^2} \sup_{\substack{v\in M(\lambda_k)\\ \|v\|_H=1}} \inf_{v_h \in V_h} \|v - v_h\|^2_{H_0^1(\Omega)}\right) \lambda_k. \end{aligned}$$

■

Remark 3.3.3. This result implies in particular that if λ_k is simple, then $\lambda_{h,k}$ is also simple, for $h > 0$ small enough.

Notice that the error $|\lambda_{h,k} - \lambda_k|$ depends on the square of the distance between the k first eigenspaces and the *approximated space* V_h. Because V_h involves piecewise linear functions, for a function $v \in H^2(\Omega)$, there exists [10] a constant $C_3 > 0$ independent of h, such that

$$\|v - \Pi_h v\|^2_{H_0^1(\Omega)} \leq C_3 h^2 \|v\|^2_{H_0^2(\Omega)},$$

10. See Theorem 2.2.8.

where $\|\cdot\|_{H_0^2(\Omega)}$ is defined in Proposition A.2.17. Thus, if the eigenfunctions are in $H^2(\Omega)$, applying this inequality to $v = \sum_{j=1}^k \alpha_j u_j \in M(\lambda_k)$, $\|v\|_H = 1$, yields

$$\begin{aligned}\sup_{\substack{v\in M(\lambda_k)\\ \|v\|_H=1}} \|v - \Pi_h v\|^2_{H_0^1(\Omega)} &\leq C_3 h^2 \left\| \sum_{j=1}^k \alpha_j \Delta u_j \right\|^2_{L^2(\Omega)} \leq C_3 h^2 \left\| \sum_{j=1}^k \alpha_j \lambda_j u_j \right\|^2_{L^2(\Omega)} \\ &\leq C_3 \lambda_k^2 h^2 \|v\|^2_{L^2(\Omega)} \leq \frac{C_3}{C_-} \lambda_k^2 h^2, \end{aligned} \tag{3.8}$$

where C_- is the constant in the equivalence (3.3) of the norms $\|\cdot\|^2_L(\Omega)$ and $\|\cdot\|_H$. So, the estimation

$$|\lambda_{h,k} - \lambda_k| \leq O(h^2),$$

is obtained if the eigenfunctions are in $H^2(\Omega)$. This case arises for example if Ω is convex, see [Gri85, Theorem 3.2.1.2] and the discussion at the end of Subsection 3.1.

Remark 3.3.4. Actually, the convergence of λ_k depends only on the regularity of the eigenfunctions of the associated eigenspace and not about all the previous eigenfunctions, see [KO06] for details.

As mentioned, a more precise bound valid in a general case is now exhibited. It can be found in [BO87, Theorem 3.1]. For convenience for the rest of the present subsection only, the eigenvalues are numbered without multiplicity, that is, for $k \in \mathbb{N} \setminus \{0\}$, $\lambda_{k,1} = \cdots = \lambda_{k,q_k} =: \lambda_k$ denotes the k-th eigenvalue of multiplicity q_k, and $u_{k,i}$, $i = 1, \ldots, q_k$, denotes the eigenfunctions associated to λ_k. Moreover, we indicate by E_k the eigenspace associated to λ_k and use a similar notation, with a subscript h, for the approximated eigenvalues, eigenfunctions and eigenspaces.

Theorem 3.3.6 ([BO87, Theorem 3.1]). *There exist two positive constants C and h_0, both independent of k, such that, for $h \leq h_0$,*

$$\lambda_{h,k,i} - \lambda_{k,i} \leq C \epsilon_{k,i}(h)^2, \quad i = 1, \ldots, q_k, \quad k \in \mathbb{N} \setminus \{0\},$$

where

$$\epsilon_{k,i}(h) := \inf_{\substack{v\in E_k\\ a(v,v)=1\\ a(v,u_{h,k,j})=0,\, j=1,\ldots,i-1}} \inf_{v_h \in V_h} a(v - v_h, v - v_h)^{1/2}.$$

3.4 Estimation of the error $\|u_{h,k} - u_k\|_{H_0^1(\Omega)}$

Let us give a bound on the error $\|u_{h,k} - u_k\|_{H_0^1(\Omega)}$ by adapting slightly the work from [RT83, Chapter 6], similarly as what is performed in the previous section. The main restriction in the following development is that λ_k is supposed to be simple. However, a stronger result from [BO87], holding for a multiple eigenvalue, is mentioned without proof. The regularity of the eigenfunctions is also addressed, where the order of convergence is $O(h)$. The notations of the previous section are used.

Except for Theorem 3.4.3 at the end of the subsection, let us assume that λ_k is simple. So it makes sense to consider

$$\rho_{h,k} = \max_{\substack{1\le j\le N_h \\ j\neq k}} \frac{\lambda_k}{\lambda_{h,j} - \lambda_k}.$$

Lemma 3.4.1. *For $h > 0$ small enough and a convenient choice of $u_{h,k}$,*

$$\|u_{h,k} - u_k\|_H \le 2(1 + \rho_{h,k}) \|u_k - \Pi_h u_k\|_H ,$$

where the norm $\|\cdot\|_H$ comes from the inner product previously introduced in equation (3.2).

Proof. Set $v_{h,k} = (\Pi_h u_k | u_{h,k})_H u_{h,k}$ and let us find an upper bound for the two first terms in the right hand side of the following inequality

$$\|u_{h,k} - u_k\|_H \le \|u_{h,k} - v_{h,k}\|_H + \|v_{h,k} - \Pi_h u_k\|_H + \|\Pi_h u_k - u_k\|_H . \tag{3.9}$$

For the first one, by definition of $v_{h,k}$,

$$v_{h,k} - u_{h,k} = ((\Pi_h u_k | u_{h,k})_H - 1) u_{h,k},$$

and since the family $\{u_{h_i}\}_{i=1}^{N_h}$ is orthonormal for $(\cdot|\cdot)_H$, it yields

$$\|v_{h,k} - u_{h,k}\|_H = |\,(\Pi_h u_k | u_{h,k})_H - 1|.$$

The triangle inequality applied twice gives

$$\overbrace{\|u_k\|_H}^{=1} - \|u_k - v_{h,k}\|_H \le \overbrace{\|v_{h,k}\|_H}^{=|(\Pi_h u_k, u_{h,k})_H|} \le \overbrace{\|u_k\|_H}^{=1} + \|u_k - v_{h,k}\|_H ,$$

which can also be written as,

$$\Big|\, |(\Pi_h u_k, u_{h,k})_H| - 1 \Big| \le \|u_k - v_{h,k}\|_H .$$

Upon changing the sign of $u_{h,k}$, assume that $(\Pi_h u_k, u_{h,k})_H \ge 0$, and then

$$\|v_{h,k} - u_{h,k}\|_H \le \|u_k - v_{h,k}\|_H \le \|u_k - \Pi_h u_k\|_H + \|\Pi_h u_k - v_{h,k}\|_H .$$

Thus, an upper bound for the first term in (3.9) composed by the second and third terms has been found. It remains to show that

$$\|\Pi_h u_k - v_{h,k}\|_H \le \rho_{h,k} \|u_k - \Pi_h u_k\|_H .$$

For this purpose, let us write $\Pi_h u_k$ in the orthonormal basis $\{u_{h,j}\}_{j=1}^{N_h}$ of V_h:

$$\Pi_h u_k - v_{h,k} = \sum_{j=1}^{N_h} (\Pi_h u_k | u_{h,j})_H u_{h,j} - (\Pi_h u_k | u_{h,k})_H u_{h,k} = \sum_{\substack{j=1 \\ j\neq k}}^{N_h} (\Pi_h u_k | u_{h,j})_H u_{h,j}.$$

So,

$$\|\Pi_h u_k - v_{h,k}\|_H^2 = \sum_{\substack{j=1 \\ j\neq k}}^{N_h} (\Pi_h u_k | u_{h,j})_H^2 . \tag{3.10}$$

Besides, by definition of the solutions u_k and $u_{h,j}$, and of the operator Π_h, it holds that, for all $j = 1, \ldots, N_h$,

$$\begin{aligned} \lambda_{h,j} (\Pi_h u_k | u_{h,j})_H &= a(\Pi_h u_k, u_{h,j}) = a(\Pi_h u_k - u_k, u_{h,j}) + a(u_k, u_{h,j}) \\ &= a(u_k, u_{h,j}) = \lambda_k (u_k | u_{h,j})_H . \end{aligned}$$

Removing $\lambda_k (\Pi_h u_k | u_{h,j})_H$ both sides and then dividing by $\lambda_{h,j} - \lambda_k$ (possible for $h > 0$ small enough by convergence of $\lambda_{h,j}$ to λ_j , $j = 1, \ldots, N_h$) for all j different from k, it yields

$$(\Pi_h u_k | u_{h,j})_H = \rho_{h,k} (u_k - \Pi_h u_k | u_{h,i})_H ,$$

and finally in (3.10),

$$\begin{aligned} \|\Pi_h u_k - v_{h,k}\|_H^2 &= \rho_{h,k}^2 \sum_{\substack{j=1 \\ j\neq k}}^{N_h} (u_k - \Pi_h u_k | u_{h,j})_H^2 \leq \rho_{h,k}^2 \sum_{j=1}^{N_h} (u_k - \Pi_h u_k | u_{h,j})_H^2 \\ &= \rho_{h,k}^2 \|u_k - \Pi_h u_k\|_H^2 . \end{aligned}$$

■

The following theorem is the main result we wanted to develop.

Theorem 3.4.2. *For $h > 0$ small enough, there exists a constant $C_{vect} > 0$, such that*

$$\|u_{h,k} - u_k\|_H \leq C_{vect} \sup_{\substack{v \in M(\lambda_k) \\ \|v\|_H = 1}} \inf_{v_h \in V_h} \|v - v_h\|_H .$$

Proof. The assumptions on the metric g implies that $\|\cdot\|_H$ is equivalent to $\|\cdot\|_{L^2(\Omega)}$, which is itself equivalent to $\|\cdot\|_{H_0^1(\Omega)}$ by the Poincaré's inequality, since Ω is bounded. So, there exists a constant $C(g)$ such that,

$$\begin{aligned} \|u_k - \Pi_h u_k\|_H^2 &\leq C(g) \|u_k - \Pi_h u_k\|_{H_0^1(\Omega)}^2 \overset{(3.7)}{\leq} C(g) \frac{C_{cont}^2}{C_{ell}^2} \inf_{v_h \in V_h} \|u_k - v_h\|_{H_0^1(\Omega)}^2 \\ &\leq C(g) \frac{C_{cont}^2}{C_{ell}^2} \sup_{\substack{v \in M(\lambda_k) \\ \|v\|_H = 1}} \inf_{v_h \in V_h} \|v - v_h\|_{H_0^1(\Omega)}^2 , \end{aligned} \tag{3.11}$$

where the fact that $u_k \in M(\lambda_k)$, $\|u_k\|_H = 1$, is used for the last inequality. Moreover,

$$\begin{aligned} a(u_{h,k} - u_k, u_{h,k} - u_k) &= \lambda_{h,k} + \lambda_k - 2\lambda_k (u_k | u_{h,k})_H \\ &= \lambda_{h,k} + \lambda_k \left(1 - 2 (u_k | u_{h,k})_H\right) \\ &= \lambda_{h,k} + \lambda_k (\|u_{h,k} - u_k\|_H^2 - 1), \end{aligned}$$

hence

$$\begin{aligned}\|u_{h,k}-u_k\|^2_{H^1_0(\Omega)} &\leq \frac{1}{C_{ell}}a(u_{h,k}-u_k,u_{h,k}-u_k)\\ &\leq \frac{1}{C_{ell}}\left(\lambda_{h,k}-\lambda_k+\lambda_k\|u_{h,k}-u_k\|^2_H\right).\end{aligned}$$

On the first hand, Proposition 3.3.5 yields

$$\lambda_{h,k}-\lambda_k \leq C_2 \sup_{\substack{v\in M(\lambda_k)\\ \|v\|_H=1}} \inf_{v_h\in V_h}\|v-v_h\|^2_{H^1_0(\Omega)},$$

on the other hand, for $h>0$ small enough, Lemma 3.4.1 and inequality (3.11) imply,

$$\begin{aligned}\|u_{h,k}-u_k\|^2_H &\leq 4(1+\rho_{h,k})^2\|u_k-\Pi_h u_k\|^2_H\\ &\leq 4(1+\rho_{h,k})^2 C(g)\frac{C^2_{cont}}{C^2_{ell}}\sup_{\substack{v\in M(\lambda_k)\\ \|v\|_H=1}}\inf_{v_h\in V_h}\|v-v_h\|^2_{H^1_0(\Omega)}.\end{aligned}$$

By gathering all the constants in C_{vect} as follows,

$$C_{vect}:=\left(\frac{1}{C_{ell}}\left(C_2+\lambda_k\,4\,(1+\rho_{h,k})^2\,C(g)\,\frac{C^2_{cont}}{C^2_{ell}}\right)\right)^{1/2},$$

it finally yields,

$$\|u_{h,k}-u_k\|^2_{H^1_0(\Omega)} \leq C^2_{vect}\sup_{\substack{v\in M(\lambda_k)\\ \|v\|_H=1}}\inf_{v_h\in V_h}\|v-v_h\|^2_{H^1_0(\Omega)}.$$

■

As a consequence, if the eigenfunctions u_j belong to $H^2(\Omega)$ for all $j=1,\ldots,k$, the order of convergence for $\|u_{h,k}-u_k\|_{H^1_0(\Omega)}$ is

$$\begin{aligned}\|u_{h,k}-u_k\|_{H^1_0(\Omega)} &\leq C_{vect}\sup_{\substack{v\in M(\lambda_k)\\ \|v\|_H=1}}\inf_{v_h\in V_h}\|v-v_h\|_{H^1_0(\Omega)}\\ &\leq C_{vect}\sup_{\substack{v\in M(\lambda_k)\\ \|v\|_H=1}}\|v-\Pi_h v\|_{H^1_0(\Omega)}\\ &\leq C_{vect}\left(\frac{C_3}{C_-}\right)^{1/2}\lambda_k h,\end{aligned}$$

where the last inequality comes from (3.8). So, the order of convergence in the norm $\|\cdot\|_{H^1_0(\Omega)}$ is $O(h)$ in the case of a simple eigenvalue and for sufficiently regular eigenfunctions.

Let us finally give a more precise bound valid even if the multiplicity of λ_k equals $m\geq 1$. The result presented at the end of the last subsection is completed as follows.

Theorem 3.4.3 ([BO87, Theorem 3.1]). *The eigenfunctions $u_{k,i}$ can be chosen such that, for $h \leq h_0$,*

$$\|u_{h,k,i} - u_{k,i}\|_{H_0^1(\Omega)} \leq C\epsilon_{k,i}(h).$$

where

$$\epsilon_{k,i}(h) := \inf_{\substack{v \in E_k \\ a(v,v)=1 \\ a(v,u_{h,k,j})=0,\, j=1,\ldots,i-1}} \inf_{v_h \in V_h} a(v - v_h, v - v_h)^{1/2},$$

3.5 Numerical experiments on surfaces

The main idea is to use a chart (U, π) of the manifold (M, g) and to make the computations in the open set $\pi(U) \subset \mathbb{R}^2$ endowed with the metric induced by g. The examples of manifolds (M, g) presented in this section are $\mathbb{R}^2$, the sphere $\mathbb{S}^2$, the Poincaré disc $\mathbb{D}^2$ and a family of surfaces of revolution with various non-constant curvatures. After some numerical validations for two domains of $\mathbb{R}^2$ known theoretically, namely a ball and a square, a comparison of the first eigenvalues of a ball in $\mathbb{R}^2$, $\mathbb{S}^2$ and $\mathbb{D}^2$ is carried out. Finally, a last example is considered. It consists in removing a small ball, namely the *obstacle*, from a ball of radius 1. We focus on the behaviour of the first five eigenvalues with respect to the position of the obstacle inside the ball in $\mathbb{R}^2$, in $\mathbb{S}^2$ and in $\mathbb{D}^2$.

For each of these cases, and when there is no ambiguity about the current space, B denotes the ball centred at the origin of volume 1 (for the volume element induced by the corresponding metric g). If not stated otherwise, the discretization of B is carried out by a triangulation with triangles of type $\mathcal{P}_1$ as mentioned previously. From 500 equidistributed points on the boundary, 20225 nodes are built altogether.

3.5.1 About the use of masslumping

The numerical approximations of the eigenvalues presented in this document are frequently computed both with and without masslumping. This subsection is dedicated to a brief discussion about this notion. The previous notations are used.

The equation (3.6) points out that the eigenvalue $\lambda_{k,h}$ associated to the approximated space $V_h \subset H_0^1(\Omega)$ is above the exact one λ_k. It is always the case when the approximation is computed without masslumping. However, some approximations computed with masslumping are below the theoretical value. It is due to the fact that the use of masslumping may provide only an approximated value of $\lambda_{k,h}$ and thus does not represent a contradiction to the equation (3.6). Indeed, integrals of polynomial functions of degree 2 are involved to compute an approximated eigenvalue $\lambda_{k,h}$, while the quadrature rule with masslumping is exact up to degree 1 only as mentioned in the Remark 2.2.5. On the contrary, not using masslumping gives the exact value of $\lambda_{k,h}$. Hence, the eigenvalue given without masslumping always provides an upper bound for the exact eigenvalue.

Unfortunately, the approximated eigenvalue computed with masslumping does not furnish a lower bound for the exact eigenvalue in general. Indeed, in [AD03] the authors use masslumping to evaluate the eigenvalues associated to two meshes of a square in $\mathbb{R}^2$:

one providing an approximated eigenvalue below the exact one, the other an approximated eigenvalue above. Nevertheless, their other numerical simulations—using meshes having some *nice* properties— seem to show that the eigenvalues approximated with masslumping are below when the associated eigenfunctions belong to $H^2(\Omega)$. But no theoretical result is derived when masslumping is used.

3.5.2 Numerical validations

This subsection deals with a square and a ball in $\mathbb{R}^2$, and a hemisphere of $\mathbb{S}^2$. These domains having associated eigenvalues that are known theoretically, they have been chosen to verify that the program runs correctly. Furthermore, a ball in the Poincaré disc $\mathbb{D}^2$ is also considered in order to study and compare the asymptotic behaviour when the volume goes to zero. The canonical representation of $\mathbb{D}^2$ (and of $\mathbb{R}^2$) are chosen. The matrix $G_{\mathbb{D}^2}(u,v)$, representing the hyperbolic metric at each point (u,v) of $\mathbb{D}^2$ is given by

$$G_{\mathbb{D}^2}(u,v) = \frac{4}{\left(1-u^2-v^2\right)^2} I,$$

where I denotes the 2 by 2 identity matrix. For the sphere, the stereographic map (U, π_N) is used, where $U = \mathbb{S}^2 \setminus \{(0,0,1)\}$ and

$$\begin{array}{rcl} \pi_N : U & \to & \mathbb{R}^2 \\ (x,y,z) & \mapsto & \pi_N(x,y,z) = \dfrac{1}{1-z}(x,y). \end{array}$$

The corresponding matrix $G_{\mathbb{S}^2}$ evaluated in a point $(u,v) \in \mathbb{R}^2$ is given by

$$G_{\mathbb{S}^2}(u,v) = \frac{4}{\left(1+u^2+v^2\right)^2} I.$$

First, the knowledge of the exact value of $\lambda_k(B)$, for B in the plane $\mathbb{R}^2$ enables to check the validity of the program (see [CH53, § V.5]). The first ten eigenvalues $\lambda_k(B)$ are reported in Table 3.1, where $j_{n,k}$ denotes the k-th root of the Bessel function J_n. It also contains the corresponding values obtained numerically for comparison.

Remark 3.5.1. Notice that the present experiments *substantiate* the suggestion in [AD03], surmising that the eigenvalues obtained with masslumping stay below the exact ones.

To verify numerically that the estimation of the error $e_{h,k} := |\lambda_k - \lambda_{h,k}|$ is of order h^2 as mentioned in the previous section, we shall consider a domain Ω where the exact eigenvalues are known as well as an exact boundary approximation is possible. Moreover, the eigenfunctions must be in $H^2(\Omega)$, which is the case if Ω is convex as mentionned before. A mesh refinement is then carried out: each triangle is divided in four similar triangles in order to have nested meshes with smaller and smaller parameter h, so at each refinement, h is halved.

Table 3.1: Exact value of $\lambda_k(B)$, $k = 1, \ldots, 10$, for $B \subset \mathbb{R}^2$ and numerical approximation obtained.

Eigenvalue	Exact value for $B \subset \mathbb{R}^2$	Approximation obtained with (left) and without (right) masslumping	
λ_1	$j_{0,1}^2\pi \simeq 18.168$	18.167	18.170
λ_2	$j_{1,1}^2\pi \simeq 46.125$	46.117	46.131
λ_3	$j_{1,1}^2\pi \simeq 46.125$	46.117	46.140
λ_4	$j_{2,1}^2\pi \simeq 82.858$	82.831	82.889
λ_5	$j_{2,1}^2\pi \simeq 82.858$	82.839	82.897
λ_6	$j_{0,2}^2\pi \simeq 95.729$	95.697	95.775
λ_7	$j_{3,1}^2\pi \simeq 127.885$	127.829	127.967
λ_8	$j_{3,1}^2\pi \simeq 127.885$	127.829	127.967
λ_9	$j_{1,2}^2\pi \simeq 154.625$	154.542	154.697
λ_{10}	$j_{1,2}^2\pi \simeq 154.625$	154.546	154.796

In $\mathbb{R}^2$ we consider the square $S := [0,1] \times [0,1]$. A simple separation of variables shows that the spectrum of S is the set

$$\left\{(k^2 + l^2)\pi^2 \mid l, k \in \mathbb{N} \setminus \{0\}\right\}.$$

The experimental error $e_{h,1}$ obtained seems to verify the Theorem 3.3.6 (the slopes in Figure 3.1 are approximatively equal to 2).

For the sphere, no simple example with exact boundary approximation has been found. However, it is known that the first eigenvalue of $-\Delta_g$ on $\mathbb{S}^2$ is 2 and that the coordinate functions in $\mathbb{R}^3$ are associated eigenfunctions (see [Cha84, Section II.4, Proposition 1]). In particular, they have a hemisphere as a nodal domain, and so the first eigenvalue of a hemisphere is also 2, that is,

$$\lambda_1(B_{\pi/2}(\mathbf{S})) = 2,$$

where $B_{\pi/2}(\mathbf{S})$ is the ball centred in $\mathbf{S} = (0,0,-1)$ of radius $\pi/2$ in $\mathbb{S}^2$, that is the southern hemisphere. Notice that the order of convergence in that case is the same, despite of the approximation of the domain. For both examples, the computed error $e_{h,1}$ is represented in Table 3.2 and in Figure 3.1.

When considering the case of the Poincaré disc, the following asymptotic result is carried out: the value of $\lambda_{1,\mathbb{D}^2}(B_\epsilon^{\mathbb{D}^2}(0,0))\,\mathrm{vol}(B_\epsilon^{\mathbb{D}^2}(0,0))$ is expected to be *close* to the same quantity for the ball in $\mathbb{R}^2$ (equipped with the canonical metric), where $B_\epsilon^{\mathbb{D}^2}(0,0)$ denotes the ball of a small radius ϵ centred at $(0,0)$ in the Poincaré disc. Thanks to the

Table 3.2: Error resulting from the approximation of $\lambda_1(S) \simeq 19.739$, on nested meshes of the square $S \subset \mathbb{R}^2$ (left) and of $\lambda_1(B_{\pi/2}(\mathbf{S})) = 2$, on nested meshes of the hemisphere $B_{\pi/2}(\mathbf{S}) \subset \mathbb{S}^2$ (right).

h	$e_{h,1}(S)$ with (left) and without (right) masslumping		h	$e_{h,1}(B_{\pi/2}(\mathbf{S}))$ with (left) and without (right) masslumping	
$\frac{0.2\sqrt{2}}{2^2}$	-0.164	0.488	0.492	-0.072	0.171
$\frac{0.2\sqrt{2}}{2^3}$	-0.041	0.122	0.253	-0.020	0.046
$\frac{0.2\sqrt{2}}{2^4}$	-0.010	0.030	0.135	-0.006	0.012
$\frac{0.2\sqrt{2}}{2^5}$	-0.003	0.008	0.0706	-0.002	0.003
$\frac{0.2\sqrt{2}}{2^6}$	-0.0006	0.0019	0.0380	-0.0004	0.0007

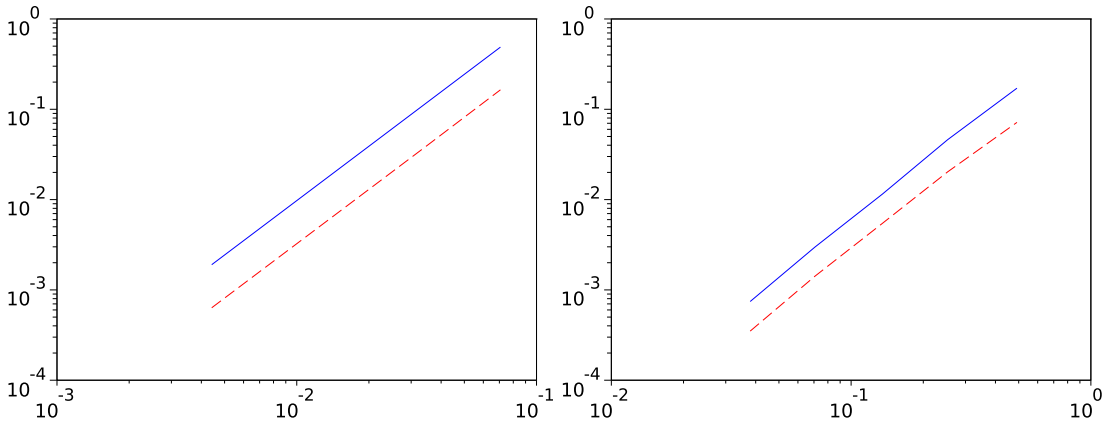

Figure 3.1: Graph of $h \mapsto e_{h,1}(S)$ (left) and of $h \mapsto e_{h,1}(B_{\pi/2}(\mathbf{S}))$ (right) in a logarithmic scale. The blue plain curves correspond to computations whithout masslumping and the red dashed ones to computations with masslumping.

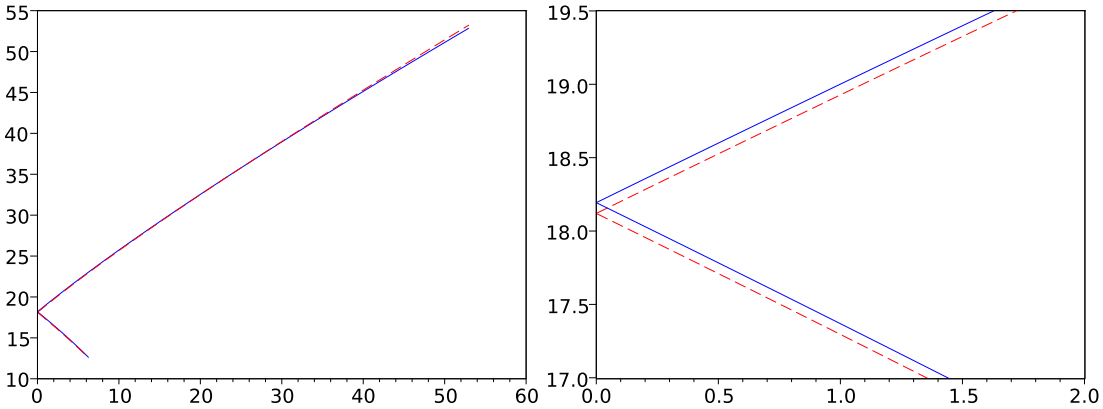

Figure 3.2: Graph of $\mathrm{vol}(B_r^M(0,0)) \mapsto \lambda_{1,\mathbb{D}^2}(B_r^M(0,0))\,\mathrm{vol}(B_r^M(0,0))$ for $M = \mathbb{S}^2$, $\mathbb{D}^2$. The blue plain curves correspond to computations without masslumping and the red dashed ones to computations with masslumping. The plot on the right is a detail for small volumes.

invariance under homothety of the functional $\Omega \mapsto \lambda_{k,\mathbb{R}^2}(\Omega)\,\mathrm{vol}(\Omega)$, $k \in \mathbb{N} \setminus \{0\}$, defined on regular bounded domains in $\mathbb{R}^2$,

$$\lambda_{1,\mathbb{R}^2}(B_\epsilon^{\mathbb{R}^2}(0,0))\,\mathrm{vol}(B_\epsilon^{\mathbb{R}^2}(0,0)) = \lambda_{1,\mathbb{R}^2}(B^{\mathbb{R}^2})\,\mathrm{vol}(B^{\mathbb{R}^2}) = j_{0,1}^2\pi \simeq 18.168.$$

The obtained value for the approximation of the smallest ball $B_{3\cdot 10^{-4}}^{\mathbb{D}^2}(0,0)$ is 18.196 without masslumping and 18.123 with masslumping. The obtained curve is increasing with respect to the volume of the ball. The same analysis holds near the point $(0,0,-1) \in \mathbb{S}^2$, for the sphere. The corresponding values obtained are 18.191, respectively 18.118, and the curve is decreasing with respect to the volume of the ball, see Figure 3.2. Asymptotically, these values are consistent with those computed for $\lambda_1(B)$, with $B \subset \mathbb{R}^2$.

3.5.3 Comparison of balls in $\mathbb{R}^2$, in $\mathbb{S}^2$ and in $\mathbb{D}^2$

Of course, some other eigenvalues can also be computed. The first forty eigenvalues of the ball B in the manifolds $\mathbb{R}^2$, $\mathbb{S}^2$ and $\mathbb{D}^2$ have been performed. It pointed out that for a fixed subscript k, sometimes $\lambda_k(B)$ is smaller in $\mathbb{R}^2$ than in $\mathbb{S}^2$ ($k = 11$, 12, 16, 17, 20, 21, 26, 27, 31, 32, 33, 34, 39 and 40), whereas it is smaller in $\mathbb{D}^2$ than in $\mathbb{R}^2$ for some other subscripts ($k = 11$, 12, 16, 20, 21, 24, 25, 31, 32, 37 and 38). See Figure 3.3 displaying these forty eigenvalues, and Table 3.3 where the first twenty eigenvalues are reported [11]. It leads to compare (theoretically) the spectrum of a ball of volume V in the sphere $\mathbb{S}^2$ and in $\mathbb{R}^2$. The spectrum of the ball B in $\mathbb{S}^2$ is not known explicitely, but the spectrum of a hemisphere, that is $V = 2\pi$, is well known, see [BB80, pp. 243 – 244]: all $k(k+1)$, $k \in \mathbb{N}^*$ is an eigenvalue with multiplicity k. Besides, the spectrum of the ball

11. A complete table with all the forty eigenvalues is given in the Appendix. See Table C.1.

of same volume in $\mathbb{R}^2$ is obtained in ranking the first zeros $j_{n,k}$ of the Bessel functions and rescaling by the corresponding factor, namely 0.5. We expect that the number of subscripts k for which $\lambda_k(B)$ is smaller in $\mathbb{R}^2$ than in $\mathbb{S}^2$ to be infinite, and that the reverse inequality holds, replacing $\mathbb{S}^2$ by $\mathbb{D}^2$.

Open question 1. *The inequalities*

$$\lambda_{k,\mathbb{R}^2}(B) \leq \lambda_{k,\mathbb{S}^2}(B) \tag{3.12}$$

and

$$\lambda_{k,\mathbb{D}^2}(B) \leq \lambda_{k,\mathbb{R}^2}(B) \tag{3.13}$$

holds for an infinity of subscripts k, where B denotes the ball of volume 1 in the corresponding space.

Of course, the other natural question arising at that point, is to know if the converse inqualities to (3.12) and (3.13) hold.

Open question 2. *Is the number of subscripts k for which*

$$\lambda_{k,\mathbb{R}^2}(B) \geq \lambda_{k,\mathbb{S}^2}(B),$$

respectively

$$\lambda_{k,\mathbb{D}^2}(B) \geq \lambda_{k,\mathbb{R}^2}(B),$$

infinite?

A way to tackle *theoretically* these problems, at least for $\mathbb{R}^2$ and the sphere, is to compare the eigenvalues of a ball of volume 2π in these three spaces as mentioned above. Indeed, the spectrum is explicitly known in that case. The difficulty is to rank the zeros of the Bessel functions in order to study the asymptotic behaviour of these functions.

Table 3.3: Computation of $\lambda_k(B)$, $k = 1, \ldots, 20$, for the ball B in $\mathbb{R}^2$, in $\mathbb{S}^2$ and in the Poincaré disc $\mathbb{D}^2$.

Eigenvalue	Approximation with (left) and without (right) masslumping in $\mathbb{R}^2$		$\mathbb{S}^2$		$\mathbb{D}^2$	
λ_1	18.167	18.170	17.343	17.346	18.974	18.977
λ_2	46.117	46.131	44.879	44.892	47.327	47.340
λ_3	46.117	46.140	44.879	44.901	47.327	47.349
λ_4	82.831	82.889	81.631	81.689	84.025	84.084
λ_5	82.839	82.897	81.640	81.697	84.034	84.092
λ_6	95.697	95.775	92.782	92.858	98.528	98.607
λ_7	127.829	127.967	127.139	127.277	128.583	128.722
λ_8	127.829	127.967	127.139	127.277	128.583	128.722
λ_9	154.542	154.697	150.382	150.532	158.583	158.741
λ_{10}	154.546	154.796	150.385	150.629	158.587	158.843
λ_{11}	180.790	181.066	181.096	181.374	180.679	180.955
λ_{12}	180.790	181.066	181.097	181.374	180.680	180.955
λ_{13}	222.383	222.803	217.423	217.835	227.224	227.653
λ_{14}	222.440	222.855	217.478	217.886	227.283	227.707
λ_{15}	235.074	235.544	228.408	228.866	240.102	240.592
λ_{16}	241.513	242.007	243.303	243.801	240.102	240.592
λ_{17}	241.514	242.007	243.303	243.801	241.550	242.033
λ_{18}	299.020	299.776	293.707	294.450	304.240	305.009
λ_{19}	299.020	299.777	293.707	294.452	304.240	305.011
λ_{20}	309.835	310.650	313.603	314.428	306.687	307.494

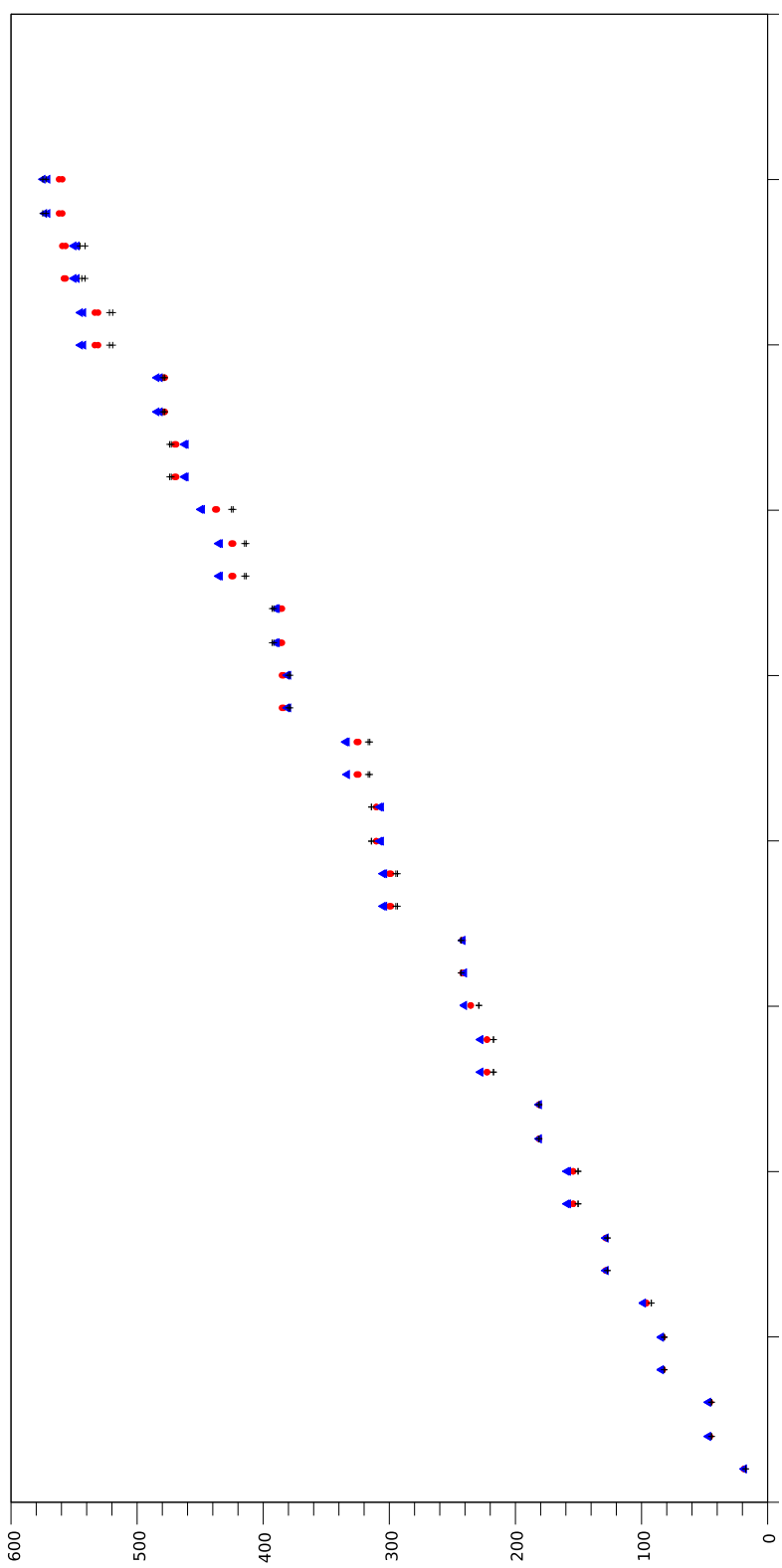

Figure 3.3: Graph of $k \mapsto \lambda_k(B)$ for the ball B in $\mathbb{R}^2$ (red points), in $\mathbb{S}^2$ (black crosses) and in the Poincaré disc $\mathbb{D}^2$ (blue triangles).

3.5.4 Numerical experiments in non-constant curvature

Investigations have also been carried out in manifolds with non-constant curvature using a family of surfaces of revolution obtained by rotating (around the y-axis) a family of curves $t \in \mathbb{R} \mapsto (0, \alpha(t), \beta(t)) \in \mathbb{R}^3$. Without loss of generality, assume $\dot{\alpha}^2 + \dot{\beta}^2 = 1$. Direct calculations show that the corresponding matrix associated to the metric in a point $(t, \theta) \in \mathbb{R} \times]-\pi, \pi[$ is

$$G(t, \theta) = \begin{pmatrix} 1 & 0 \\ 0 & \beta^2(t) \end{pmatrix},$$

and that the curvature is

$$\kappa(t) = -\frac{\beta''(t)}{\beta(t)}.$$

In particular, B is an Euclidean ball and the surface of revolution is smooth if $\alpha(0) = \beta(0) = 0$ and $\dot{\beta}(0) = 1$. Such conditions are for example satisfied by

$$\beta(t) = t + bt^3,$$

where b is a real parameter which gives a control of the curvature

$$\kappa(t) = -\frac{6b}{1 + bt^2},$$

(only negative values of b—so $\dot{\beta}^2 \leq 1$—give surfaces of revolution embedded into $\mathbb{R}^3$). Some values in a range from -1 to 1 are assigned to the parameter b in the expression of β. It results to various curved manifolds: negative curvature for b positive, zero curvature for $b = 0$, and positive curvature for b negative. Results for $\lambda_k(B)$, $k = 1, \ldots, 9$, are collected in Table 3.4 and Figure 3.4. The values corresponding to the zero curvature case $b = 0$ are consistent with those computed for $B \subset \mathbb{R}^2$. An eigenfunction associated to the first eigenvalue for the parameter $b = -0.5$ is plotted in Figure 3.5. Notice that this function is a radial function and that its amplitude (1.802) is smaller than the one (1.926) of the corresponding eigenfunction for the zero curvature space, as expected.

3.5.5 Ball with an obstacle

In this last subsection, the domain considered is a ball of radius 1 in $\mathbb{R}^2$, in $\mathbb{S}^2$ and in the Poincaré disc $\mathbb{D}^2$ in which lies an obstacle consisting in a ball of radius 0.01. This problem is addressed in a slightly different setting in [HKK01] as well as in [CGI+00] where numerical simulations are performed. In the present document, the idea is to move radially the obstacle from the centre to the boundary in order to see where $\lambda_k(B_x)$ is maximal, where B_x denotes the ball with this obstacle centred at $(x, 0)$. Thanks to symmetries of the ball, it is obviously sufficient to move the obstacle along the positive part of the x-axis.

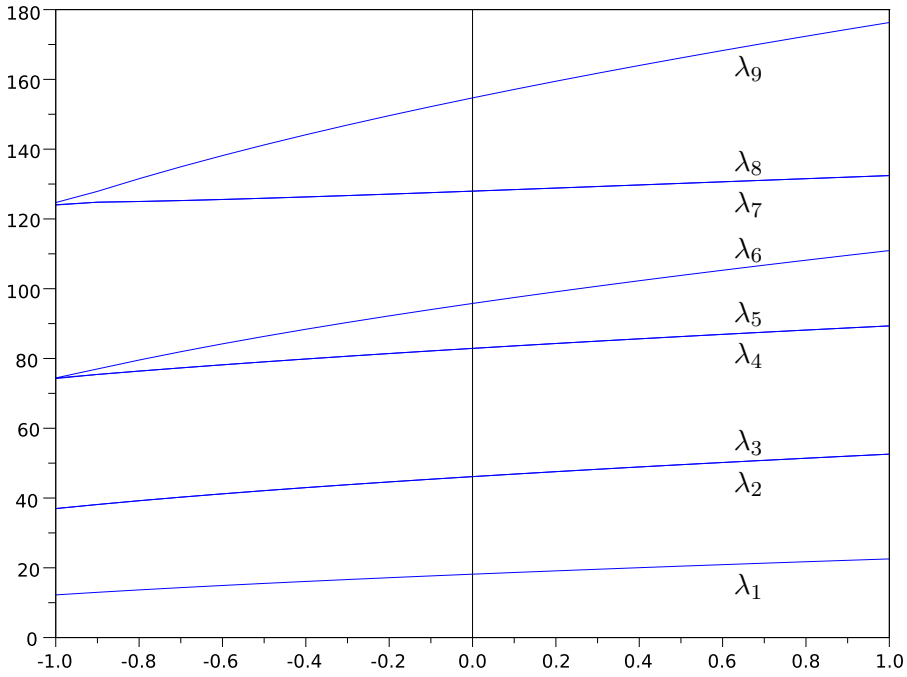

Figure 3.4: Plot of $\lambda_k(B)$, $k = 1, \ldots, 9$, with respect to the parameter b defining the family of surfaces of revolution. The line at $b = 0$ emphasizes the results for the zero curvature space.

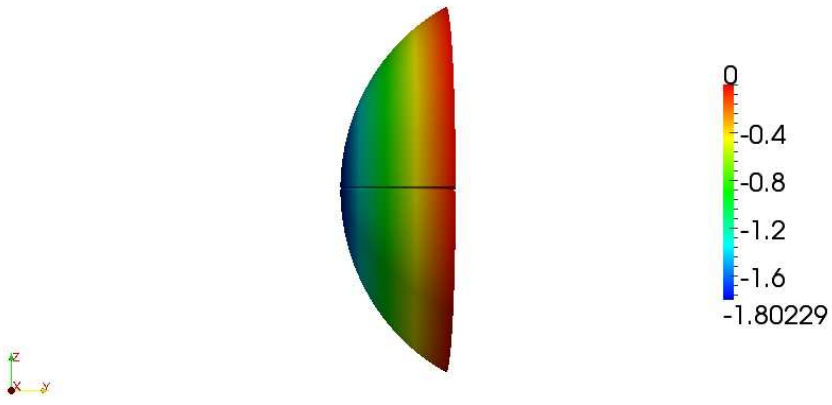

Figure 3.5: Plot of $u_1(B)$, for the parameter $b = -0.5$.

Table 3.4: Approximation of $\lambda_1(B)$, in a family of manifolds with non-constant curvature controlled by the parameter b: the first line in every cell corresponds to values with masslumping, the second one to values without masslumping).

b	-1	-0.9	-0.8	-0.7	-0.6	-0.5	-0.4
$\lambda_1(B)$	12.232	12.972	13.662	14.313	14.931	15.521	16.087
	12.235	12.974	13.664	14.315	14.933	15.524	16.090

b	-0.3	-0.2	-0.1	0	0.1	0.2	0.3
$\lambda_1(B)$	16.633	17.160	17.671	18.167	18.650	19.120	19.579
	16.636	17.163	17.674	18.170	18.653	19.123	19.582

b	0.4	0.5	0.6	0.7	0.8	0.9	1
$\lambda_1(B)$	20.028	20.468	20.898	21.320	21.735	22.142	22.542
	20.031	20.471	20.901	21.323	21.738	22.145	22.546

J. Hersch in [Her63] proved that the maximum of $\lambda_1(B_x)$ is reached by B_0 in $\mathbb{R}^2$, that is when the obstacle is at the centre of the ball. The same stands in $\mathbb{S}^2$ and in $\mathbb{D}^2$, as stated in [AA05]. A. El Soufi and R. Kiwan extended this result to the second eigenvalue in $\mathbb{R}^2$, in $\mathbb{S}^2$ and in $\mathbb{D}^2$, see [ESK08]. Numerically, these results have been recovered and some investigations have been carried out for $\lambda_k(B_x)$, k up to 5, in $\mathbb{R}^2$, in $\mathbb{S}^2$ and in $\mathbb{D}^2$. The results are collected in Tables 3.5, 3.6 and 3.7. Five different domains corresponding to five different locations for the obstacle are displayed. Notice that the choice $B_{0.98}$ to represent an obstacle *at the boundary* of the ball comes from numerical reasons. But such a location for the obstacle is not expected to realize the maximum of $\lambda_k(B_x)$ for any k, since the eigenfunctions $u_k(B_x)$ are zero on the boundary of B.

In $\mathbb{R}^2$, for $k = 3$, some more accurate computations have been made to locate with precision the centre of the obstacle. In order to do that, the radius of the obstacle ball has been reduced to 0.001. The maximum of $\lambda_{3,\mathbb{R}^2}(B_x)$ is about 16.558, and is attained for an obstacle centred near (0.447, 0). Notice that this position for the centre of the obstacle corresponds more or less to the point where $u_3(B_1)$ attains its extremum, namely $(0.481, 0)$, where $u_3(B_1)$ denotes the third eigenfunction defined on the ball of radius 1 without obstacle and normalized in $\mathbb{R}^2$. It is in accordance with the formula in Theorem 1 of [Oza81]. It claims, for all simple eigenvalue $\lambda_{k,\mathbb{R}^2}(B_1)$ of the non-perforated domain, that

$$\lambda_{k,\mathbb{R}^2}(B_x) = \lambda_{k,\mathbb{R}^2}(B_1) + \frac{2\pi}{|\log r|} u_k(B_1)(x)^2 + O(|\log r|^{-2}),$$

where $u_k(B_1)$ denotes the eigenfunction associated to $\lambda_{k,\mathbb{R}^2}(B_1)$. An analogous formula holds for multiples eigenvalues as stated in [Flu95, Theorem 9]. See also Appendix C.2 for additional numerical simulations about the placement of an obstacle.

Qualitatively in $\mathbb{S}^2$ and in $\mathbb{D}^2$, similar results are found: for $k = 1$ or 2, $\lambda_{k,\mathbb{D}^2}(B_x)$ is

maximal for $x = 0$ as expected, whereas for $k = 3, 4$ or 5, the maximum corresponds to $x \neq 0$.

Table 3.5: Approximation of $\lambda_{k,\mathbb{R}^2}(B_x)$, $k = 1, \ldots, 5$, for various obstacles centred at $x = 0$, 0.25, 0.5, 0.75 and 0.98.

Eigenvalue	Approximation obtained for the domain				
	B_0	$B_{0.25}$	$B_{0.5}$	$B_{0.75}$	$B_{0.98}$
λ_1	**7.890**	7.378	6.560	6.001	5.787
λ_2	**14.6925**	14.6924	14.688	14.685	14.684
λ_3	14.695	16.163	**17.003**	15.612	14.705
λ_4	26.382	26.394	**26.398**	26.389	26.385
λ_5	26.385	26.652	**28.743**	27.588	26.419

Table 3.6: Approximation of $\lambda_{k,\mathbb{S}^2}(B_x)$, $k = 1, \ldots, 5$, for various obstacles centred at $x = 0$, 0.25, 0.5, 0.75 and 0.98.

Eigenvalue	Approximation obtained for the domain				
	B_0	$B_{0.25}$	$B_{0.5}$	$B_{0.75}$	$B_{0.98}$
λ_1	**7.575**	7.084	6.271	5.688	5.452
λ_2	**14.716**	14.713	14.709	14.705	14.704
λ_3	14.716	16.205	**17.198**	15.735	14.729
λ_4	27.497	27.510	**27.517**	27.507	27.500
λ_5	27.500	27.725	**29.595**	28.626	27.542

Table 3.7: Approximation of $\lambda_{k,\mathbb{D}^2}(B_x)$, $k = 1, \ldots, 5$, for various obstacles centred at $x = 0$, 0.25, 0.5, 0.75 and 0.98.

Eigenvalue	Approximation obtained for the domain				
	B_0	$B_{0.25}$	$B_{0.5}$	$B_{0.75}$	$B_{0.98}$
λ_1	**7.568**	7.091	6.352	5.836	5.635
λ_2	**13.486**	13.485	13.481	13.479	13.478
λ_3	13.489	14.737	**15.521**	14.326	13.498
λ_4	23.288	23.297	**23.302**	23.294	23.290
λ_5	23.290	23.518	**25.297**	24.472	23.323

Chapter 4

Preliminaries to optimization of eigenvalues with respect to the domain

This chapter is dedicated to define notions and tools about the optimization process to reach a domain with a minimal associated k-th Dirichlet-Laplace eigenvalue among all domains of a given volume. These concepts are not new, even though they are adapted and presented in our context. It paves the way for the next chapter, where the optimization problem is stated and the numerical results are displayed.

The main reference is [MS76]. It is a prepublication of more than two hundreds pages. A lot of definitions and notions whose scope is beyond this thesis are defined to achieve [MS76, Theorem 5.2] which is the main result to derive the central formula (4.6). Another goal of this chapter, and especially its first section, is to provide the reader some selected portions of it in a judicious sequence, focusing only on its relevant parts for our goal. Indeed, the extracted notions displayed here are scattered throughout the abundant and very detailed results of this reference. Section 4.1 represents an easier and quicker way to enter this matter. In particular, certain parts of some proofs, especially about existence results are only sketched. Moreover, the scope of some of their very general assertions are restricted for the sake of clarity. However, special care is taken to describe how the results are reported in the present document.

The main consequence of the consideration of the metric in the shape optimization process, compared to the planar case, is that the volume constraint is unavoidable in a curved manifold. A Uzawa algorithm is chosen to deal with this constraint. It is introduced in the second section and applied to the considered optimization problem.

The third section deals with some technical aspects to make use numerically of the optimization formula (4.6) derived in Section 4.1. Indeed, some theoretically non-existent obstacles arise with the numerical implementation. Some of them are presented in that section.

4.1 Details of the shape optimization step

First, a theoretical framework for the shape optimization is introduced, relying on an analysis of the perturbations of a domain. A reference on this topic is the general work [MS76]. Hadamard was a precursor in the domain: the well known Hadamard variational formula from his work [Had68] represents the basis of the main tool to seek a minimizing domain *in a judicious way*. It provides a variational computation with respect to the domain for an eigenvalue of an elliptic operator. The aim of this section is to adapt this formula in our context, namely in an open set of $\mathbb{R}^2$, endowed with the metric given by G, as presented before. For that purpose and in order to ensure that this remarkable formula does not come as a complete surprise, the tools introduced in [MS76] are used, omitting sometimes the proof of some of their classical properties, for the sake of clarity. However, in such situations precise references in [MS76], [All07] and [HP05] are given. Although the development in the two last references reaches almost the same goal as ours, we consider more general deformations of the initial domain to be consistent with the context of the main result, namely Proposition 4.1.11 and especially Formula 4.6.

4.1.1 Differentiation with respect to the domain

Let $J : \mathcal{F} \to \mathbb{R}$ be a functional defined over a set of *feasible shapes* Ω. In general, this functional J is called *cost functional*, because the goal is to find a domain Ω^* such that

$$J(\Omega^*) \leq J(\Omega), \quad \forall \Omega \in \mathcal{F}.$$

In a classical framework, for example for a regular mapping $f : \mathbb{R}^n \mapsto \mathbb{R}$, a way to obtain a local minimum $f(\boldsymbol{x}^*)$ of f is to find the points where the derivative of f vanishes. If the derivative of f is known explicitly, descent methods can be then applied to find $\boldsymbol{x}^*$ numerically. By analogy, the main idea is to set a framework in which a notion of differentiation for the cost functional J makes sense. For that purpose, the set of all feasible shapes must admit a structure of normed vector space. A classical way of proceeding is to consider an initial domain[1] $\Omega_0 \in \mathcal{F}$ and to restrict the feasible shapes to some deformations of it in the following way: let consider $\theta \in W^{1,\infty}(\mathbb{R}^2, \mathbb{R}^2)$ which is bounded and has a bounded derivative[2]. The mapping θ can be interpreted as a vector field over $\mathbb{R}^2$, called in this context *deformation field*. The set of all *feasible shapes from* Ω_0 is then

$$\mathcal{F}(\Omega_0) := \left\{ \Omega_\theta = (\mathrm{id}+\theta)(\Omega_0) : \theta \in W^{1,\infty}(\mathbb{R}^2, \mathbb{R}^2) \right\}, \tag{4.1}$$

where $(\mathrm{id}+\theta)(\Omega_0) = \{\boldsymbol{x} + \theta(\boldsymbol{x}) : \boldsymbol{x} \in \Omega_0\}$, see Figure 4.1. The following lemma states that for θ small enough, $\mathrm{id}+\theta$ is a diffeomorphism, that is a differentiable bijection with a differentiable inverse, and so that a deformation is *reversible* in the sense that from Ω_θ, one can reach Ω_0 back.

1. In the sequel, Ω_0 is a polygonal set.
2. In the sense of the distributions theory. See Section A.2 in the appendix for any notion on Sobolev spaces.

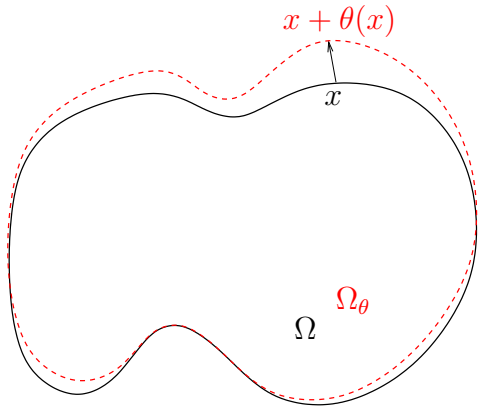

Figure 4.1: An initial domain Ω and the resulting Ω_θ under the *deformation field* θ.

Lemma 4.1.1 ([All07, Lemma 6.13]). *For all* $\theta \in W^{1,\infty}(\mathbb{R}^2,\mathbb{R}^2)$, $\|\theta\|_{W^{1,\infty}(\mathbb{R}^2,\mathbb{R}^2)} < 1$, *the mapping* $T = \mathrm{id}+\theta : \Omega_0 \mapsto \Omega_\theta$ *is a diffeomorphism such that* $T^{-1}-\mathrm{id} \in W^{1,\infty}(\mathbb{R}^2,\mathbb{R}^2)$.

Proof. First, let show that T is a bijection: denoting by $\|\cdot\|$ the Euclidean norm on $\mathbb{R}^2$, for all $\boldsymbol{x},\boldsymbol{y} \in \mathbb{R}^2$, it holds that

$$\|\theta(\boldsymbol{x}) - \theta(\boldsymbol{y})\| = \left| \int_0^1 D\theta(\boldsymbol{y} + t(\boldsymbol{x}-\boldsymbol{y}))(\boldsymbol{x}-\boldsymbol{y})\,\mathrm{d}t \right| \leq \|\theta\|_{W^{1,\infty}(\mathbb{R}^2,\mathbb{R}^2)} \|\boldsymbol{x}-\boldsymbol{y}\|,$$

so θ is a contraction mapping since $\|\theta\|_{W^{1,\infty}(\mathbb{R}^2,\mathbb{R}^2)} < 1$. Moreover, for $\boldsymbol{y} \in \mathbb{R}^2$, it is straightforward that the mapping given by $S(\boldsymbol{x}) = \boldsymbol{y}-\theta(\boldsymbol{x})$ is also a contraction mapping, and so it admits a unique fixed point $\boldsymbol{x_0}$, that is $S(\boldsymbol{x_0}) = \boldsymbol{x_0}$. Thus, $\boldsymbol{y} = T(\boldsymbol{x_0})$ and T is onto. Besides, for $\boldsymbol{x},\boldsymbol{y} \in \mathbb{R}^2$, $\boldsymbol{x} \neq \boldsymbol{y}$, one gets

$$\|T(\boldsymbol{x}) - T(\boldsymbol{y})\| \geq \|\boldsymbol{x}-\boldsymbol{y}\| - \|\theta(\boldsymbol{x}) - \theta(\boldsymbol{y})\| \geq \left(1 - \|\theta\|_{W^{1,\infty}(\mathbb{R}^2,\mathbb{R}^2)}\right) \|\boldsymbol{x}-\boldsymbol{y}\| > 0,$$

so T is one-to-one.

It remains to show that $T^{-1} - \mathrm{id}$ belongs to $W^{1,\infty}(\mathbb{R}^2,\mathbb{R}^2)$. First, since $T^{-1} - \mathrm{id} = (\mathrm{id}-T) \circ T^{-1}$, one gets $\left\|T^{-1} - \mathrm{id}\right\|_{L^\infty(\mathbb{R}^2,\mathbb{R}^2)} = \|\theta\|_{L^\infty(\mathbb{R}^2,\mathbb{R}^2)} < 1$. Besides, the condition $\|\theta\|_{W^{1,\infty}(\mathbb{R}^2,\mathbb{R}^2)} < 1$ implies $(DT)^{-1} = \sum_{j\geq 0} (-D\theta)^j < \infty$ and so T^{-1} is differentiable with $D(T^{-1}) = (DT)^{-1} \circ T^{-1}$. Finally,

$$D(T^{-1} - \mathrm{id}) = (DT)^{-1} \circ T^{-1} - I = \left((DT)^{-1} - I\right) \circ T^{-1} = \left(\sum_{j\geq 1} (-D\theta)^j\right) \circ T^{-1},$$

where I is the 2 by 2 identity matrix. Hence,

$$\left\|D(T^{-1} - \mathrm{id})\right\|_{L^\infty(\mathbb{R}^2,\mathbb{R}^2)} \leq \frac{\|D\theta\|_{L^\infty(\mathbb{R}^2,\mathbb{R}^2)}}{1 - \|D\theta\|_{L^\infty(\mathbb{R}^2,\mathbb{R}^2)}},$$

which completes the proof. ■

Remark 4.1.1. The set of all the mappings T appearing in Lemma 4.1.1 is denoted by

$$\mathcal{T} = \left\{ T : \mathbb{R}^2 \to \mathbb{R}^2 \mid T - \mathrm{id} \in W^{1,\infty}(\mathbb{R}^2, \mathbb{R}^2) \text{ and } T^{-1} - \mathrm{id} \in W^{1,\infty}(\mathbb{R}^2, \mathbb{R}^2) \right\}. \quad (4.2)$$

The space $W^{1,\infty}(\mathbb{R}^2, \mathbb{R}^2)$ is commonly used as class of regularity for the deformation θ. However, we could have worked with bounded mappings in $\mathcal{C}^2(\mathbb{R}^2, \mathbb{R}^2)$ having bounded derivative as well, or with mappings in $W^{2,\infty}(\mathbb{R}^2, \mathbb{R}^2)$. It would have been more consistent with the last result, which adapts the Hadamard Variational Formula involving an open set of class $\mathcal{C}^2$, or of class $W^{2,\infty}$.

The geometric interpretation of the next proposition is: if two *small enough* deformation fields θ_1 and θ_2 have the same normal component on $\partial\Omega_0$, then the deformated domains $(\mathrm{id}+\theta_1)(\Omega_0)$ and $(\mathrm{id}+\theta_2)(\Omega_0)$ are the same up to the second order. But to state it properly, the notions of differentiability usually used in the context of shape optimization are required. They are recalled here.

Definition 4.1.2. Let B_1 and B_2 be Banach spaces and F be a mapping from an open set $U \subset B_1$ into B_2. The mapping F is called *Fréchet differentiable* at an element $u \in U$ if there exists a bounded linear mapping $DF(u) : B_1 \to B_2$ such that

$$\|F(u+h) - F(u) - DF(u)h\|_{B_2} = o\left(\|h\|_{B_1}\right).$$

The linear mapping $DF(u)$ is called the *Fréchet derivative* of F at u.

The Fréchet derivative, verifies the usual properties of a derivative, in particular the product rule and the chain rule hold, see [Car67, Chapter 2].

Definition 4.1.3 ([All07, Definition 6.15])**.** Let Ω_0 be a bounded open set in $\mathbb{R}^2$ and J be a mapping from the set of all feasible shapes $\mathcal{F}(\Omega_0)$ given by (4.1) into $\mathbb{R}$. The mapping J is called *differentiable with respect to the domain* in Ω_0 if the mapping

$$\begin{array}{rcl} \Psi : W^{1,\infty}(\mathbb{R}^2, \mathbb{R}^2) & \longrightarrow & \mathbb{R} \\ \theta & \longmapsto & J\left((\mathrm{id}+\theta)(\Omega_0)\right), \end{array}$$

is Fréchet differentiable at 0.

The Fréchet derivative of Ψ at 0 is denoted in this case by $J'(\Omega_0)$ in order to have, using Definition 4.1.2:

$$J\left((\mathrm{id}+\theta)\left(\Omega_0\right)\right) = J\left(\Omega_0\right) + J'\left(\Omega_0\right)\theta + o\left(\|\theta\|_{W^{1,\infty}(\mathbb{R}^2,\mathbb{R}^2)}\right). \quad (4.3)$$

Remark 4.1.2. At that point, it is possible to guess that the functional which maps $\theta \in W^{1,\infty}(\mathbb{R}^2, \mathbb{R}^2)$ into $\mathrm{id}+\theta$ in $\mathcal{T}$, where $\mathcal{T}$ is the set of deformations defined by (4.2), will be often used in the sequel. So, it might be tempting to differentiate it, but $\mathcal{T}$ is not a Banach space. Actually, admitting a more general definition of the differentiability, it is possible to give a sense to the derivative of $\theta \in W^{1,\infty}(\mathbb{R}^2, \mathbb{R}^2) \mapsto (\mathrm{id}+\theta)(\Omega_0) \in \mathcal{F}(\Omega_0)$, for

an open set $\Omega_0 \subset \mathbb{R}^2$ and $\mathcal{F}(\Omega_0)$ given by (4.1). But the main issue is that a multivalued functional taking values in $W^{1,\infty}(\mathbb{R}^2,\mathbb{R}^2)$ is obtained, and that the identity id defined on $W^{1,\infty}(\mathbb{R}^2,\mathbb{R}^2)$ is one of these possible values. Howewer, this topic is beyond the scope of this thesis. See [MS76, Chapters 2 and 3] where this notion of differentiability is developed with caution.

In our context, the metric considered on $\mathbb{R}^2$ comes from a parametrisation and can be given, at each point $\boldsymbol{x} \in \mathbb{R}^2$ by a matrix $G(\boldsymbol{x})$ satisfying the assumptions recalled at the beginning of Section 5.1. Denoting by $(\cdot|\cdot)_G$ the corresponding inner product, the proposition briefly discussed above can be given as follows.

Proposition 4.1.4 ([All07, Prop. 6.17]). *Let $\Omega_0 \subset \mathbb{R}^2$ be a domain of class $\mathcal{C}^1$, $\boldsymbol{n}$ be the outward unit normal (with respect to $(\cdot|\cdot)_G$) vector field on $\partial\Omega_0$ and J be a mapping differentiable with respect to the domain in Ω_0. If θ_1, $\theta_2 \in W^{1,\infty}(\mathbb{R}^2,\mathbb{R}^2)$ satisfy $\theta_2 - \theta_1 \in \mathcal{C}^1(\mathbb{R}^2,\mathbb{R}^2)$ and $(\theta_1|\boldsymbol{n})_G = (\theta_2|\boldsymbol{n})_G$ on $\partial\Omega_0$, then the derivative $J'(\Omega_0)$ satisfies*

$$J'(\Omega_0)\theta_1 = J'(\Omega_0)\theta_2.$$

To prove this proposition, some classical results in dynamical systems are needed but not repeated here. See [HSD04, Chapter 17] and [Ma09] for a more general framework and for proves. For a vector field $\theta \in W^{1,\infty}(\mathbb{R}^2,\mathbb{R}^2) \cap \mathcal{C}^1(\mathbb{R}^2,\mathbb{R}^2)$, and $\boldsymbol{x} \in \mathbb{R}^2$, let us consider the differential equation with initial conditions:

$$(E_{\theta,\boldsymbol{x}}) \left\{ \begin{array}{rcl} \dfrac{\mathrm{d}y}{\mathrm{d}t} & = & \theta\left(y(t)\right), \\ y(0) & = & \boldsymbol{x}. \end{array} \right.$$

Since θ is of class $\mathcal{C}^1(\mathbb{R}^2,\mathbb{R}^2)$, there exists a unique solution $y : I \to \mathbb{R}^2$ defined on an open interval $I \subset \mathbb{R}$ containing 0 by the Cauchy-Lipschitz's Theorem. By the Gronwall's Lemma, it is actually defined on $I = \mathbb{R}$ because θ is bounded. Thus, the flow

$$\begin{array}{rcl} \varphi_\theta : \mathbb{R}\times\mathbb{R}^2 & \longrightarrow & \mathbb{R}^2 \\ (t,\boldsymbol{x}) & \longmapsto & \varphi_\theta(t,\boldsymbol{x}) = y(t), \end{array}$$

where y is the unique solution of $(E_{\theta,\boldsymbol{x}})$ is well defined. It follows that for all $t \in \mathbb{R}$, $\varphi_\theta(t,\cdot)$ is a bijection of inverse $\varphi_\theta(-t,\cdot)$, and of regularity $\mathcal{C}^1(\mathbb{R}^2,\mathbb{R}^2)$.

In addition, the following lemma is helpful.

Lemma 4.1.5 ([All07, Lemma 6.20]). *Let Ω_0 be a regular domain in $\mathbb{R}^2$, $\boldsymbol{n}$ be the outward unit normal (with respect to $(\cdot|\cdot)_G$) vector field on $\partial\Omega_0$ and $\theta \in W^{1,\infty}(\mathbb{R}^2,\mathbb{R}^2)$. If $(\theta|\boldsymbol{n})_G = 0$ on $\partial\Omega_0$, then, $\varphi_\theta(t,\Omega_0) = \Omega_0$, for all $t \in \mathbb{R}$.*

Proof. Set $t \in \mathbb{R}$ and $\boldsymbol{x} \in \partial\Omega_0$. By uniqueness of the solutions y to $(E_{\theta,\boldsymbol{x}})$, since $\mathrm{d}y/\mathrm{d}t = \theta(y(t))$ is tangent to $\partial\Omega_0$ (for $(\cdot|\cdot)_G$) by assumption, the fact that the integral curves are tangent to θ implies $\varphi_\theta(t,\boldsymbol{x}) \in \partial\Omega_0$. Conversely, for all $\boldsymbol{x'} \in \partial\Omega_0$, $\boldsymbol{x} := \varphi_\theta(-t,\boldsymbol{x'}) \in \partial\Omega_0$ by the same argument and is such that $\varphi_\theta(t,\boldsymbol{x}) = \boldsymbol{x'}$. So $\varphi_\theta(t,\partial\Omega_0) = \partial\Omega_0$.

By uniqueness of the solutions y to $(E_{\theta,\boldsymbol{x}})$, an initial condition $\boldsymbol{x} \in \Omega_0$ implies that the solution remains in Ω_0 by the first part above, that is $\varphi_\theta(t,\boldsymbol{x}) \in \Omega_0$. Conversely, for all $\boldsymbol{x'} \in \Omega_0$, $\boldsymbol{x} := \varphi_\theta(-t,\boldsymbol{x'}) \in \Omega_0$ is such that $\varphi_\theta(t,\boldsymbol{x}) = \boldsymbol{x'}$. So, $\varphi_\theta(t,\Omega_0) = \Omega_0$. ∎

Proof of the proposition 4.1.4. Set $\theta := \theta_2 - \theta_1 \in \mathcal{C}^1(\mathbb{R}^2, \mathbb{R}^2)$, so that $(\theta|\boldsymbol{n})_G = 0$ and by the previous lemma, $\varphi_\theta(t, \Omega_0) = \Omega_0$. For $\boldsymbol{x} \in \mathbb{R}^2$, using the same notations as before for $(E_{\theta,\boldsymbol{x}})$ and φ_θ, let us introduce the mappings

$$\begin{array}{rccl}
\Gamma_1 : & \mathcal{V}(0) & \longrightarrow & W^{1,\infty}(\mathbb{R}^2, \mathbb{R}^2) \\
& t & \longmapsto & \Gamma_1(t) = \varphi_\theta(t, \cdot) - \mathrm{id}, \\
\Gamma_2 : & W^{1,\infty}(\mathbb{R}^2, \mathbb{R}^2) & \longrightarrow & \mathbb{R} \\
& \alpha & \longmapsto & \Gamma_2(\alpha) = J\left((\mathrm{id}+\alpha)\left(\Omega_0\right)\right), \\
\Gamma : & \mathbb{R} & \longrightarrow & \mathbb{R} \\
& t & \longmapsto & \Gamma(t) = \Gamma_2 \circ \Gamma_1(t),
\end{array}$$

where $\mathcal{V}(0)$ is a small neighbourhood of 0 in $\mathbb{R}$, such that $\varphi_\theta(t, \cdot) - \mathrm{id}$ belongs to $W^{1,\infty}(\mathbb{R}^2, \mathbb{R}^2)$ for all $t \in \mathcal{V}(0)$. Actually, $\varphi_\theta(t, \cdot) \in \mathcal{C}^1(\mathbb{R}^2, \mathbb{R}^2)$ implies that $\varphi_\theta(t, \cdot)$ and $D\varphi_\theta(t, \cdot)$ exist. Moreover, $\varphi_\theta(t, \cdot) - \mathrm{id}$ is uniformly bounded since

$$\|\varphi_\theta(t, \boldsymbol{x}) - \boldsymbol{x}\| = \left\| \int_0^t \theta(y(s)) \mathrm{d}s \right\| \leq \|\theta\|_{L^\infty(\mathbb{R}^2, \mathbb{R}^2)} \varepsilon, \quad \forall \boldsymbol{x} \in \mathbb{R}^2,$$

where ε is the diameter of $\mathcal{V}(0)$, and the same computation applied to $D\varphi_\theta(t, \boldsymbol{x})$, which is the flow associated to $(E_{D\theta,\boldsymbol{x}})$ [3], proves that $\varphi_\theta(t, \cdot) - I$ is uniformly bounded [4].

Then, notice that $\Gamma(t) = J\left(\varphi_\theta(t, \Omega_0)\right) = J\left(\Omega_0\right)$ is constant, by Lemma 4.1.5. So, taking the (usual) derivative yields

$$\frac{\mathrm{d}}{\mathrm{d}t} J\left(\varphi_\theta(t, \Omega_0)\right) = 0, \quad \forall t \in \mathbb{R}.$$

Let us now compute the Fréchet derivative of Γ_1 at 0 and of Γ_2 at 0. For all $\boldsymbol{x} \in \mathbb{R}^2$, a simple limited development of the solution y to $(E_{\theta,\boldsymbol{x}})$ of order 1 at 0 yields

$$y(t) = y(0) + Dy(0)t + o\left(|t|\right),$$

which is equivalent to

$$\varphi_\theta\left(t, \boldsymbol{x}\right) = \boldsymbol{x} + \theta(\boldsymbol{x})t + o\left(|t|\right).$$

By definition, the Fréchet derivative of Γ_1 at 0 is the bounded linear mapping $D\Gamma_1(0) : \mathbb{R} \to W^{1,\infty}(\mathbb{R}^2, \mathbb{R}^2)$ defined by

$$\Gamma_1(t) = \Gamma_1(0) + D\Gamma_1(0)t + o(|t|),$$

or equivalently,

$$\varphi_\theta\left(t, \cdot\right) - \mathrm{id} = \varphi_\theta(0, \cdot) - \mathrm{id} + D\Gamma_1(0)t + o\left(|t|\right).$$

3. See for example [Ma09, Proposition 3.22].

4. See [MS76, Theorem 3.1] for a complete proof. However, their proof requires the notion of differentiability touched on in Remark 4.1.2.

So, $D\Gamma_1(0) = \theta$. Besides, since J is differentiable with respect to the domain in Ω_0, the Fréchet derivative of Γ_2 at 0 is $J'(\Omega_0)$ by definition. Finally, by the chain rule applied at $t = 0$, since $\Gamma_1(0) = 0$, it yields

$$0 = \frac{\mathrm{d}}{\mathrm{d}t}\left(J(\varphi_\theta(0,\cdot)\right) = \frac{\mathrm{d}}{\mathrm{d}t}\left(\Gamma_2 \circ \Gamma_1(0)\right) = J'(\Omega_0)\,\theta.$$

As $\theta = \theta_2 - \theta_1$, the proof is completed by linearity. ■

The following lemma, given without proof, is useful throughout the rest of this section. It is concerned with the derivative of a composition of a mapping g, depending on θ, with the deformation id+θ. Hence, with the previous notations, if g is applied over Ω_θ, then $g \circ (\mathrm{id}+\theta)$ is defined on Ω_0. And in order to integrate g over Ω_θ, it is particularly helpful to carry out this composition to differentiate the integral on the fixed domain Ω_0, instead of Ω_θ.

Lemma 4.1.6 ([HP05, Lemma 5.3.3]). *Let $g : W^{1,\infty}(\mathbb{R}^2,\mathbb{R}^2) \to L^1(\mathbb{R}^2)$ be Fréchet differentiable at 0 such that $g(0) \in W^{1,1}(\mathbb{R}^2)$ and $\Psi : W^{1,\infty}(\mathbb{R}^2,\mathbb{R}^2) \to \mathcal{T}$ be defined by $\Psi(\theta) = \mathrm{id}+\theta$. Then $\Phi : W^{1,\infty}(\mathbb{R}^2,\mathbb{R}^2) \to L^1(\mathbb{R}^2)$ given by $\theta \mapsto g(\theta) \circ \Psi(\theta)$ is Fréchet differentiable at $0 \in W^{1,\infty}(\mathbb{R}^2,\mathbb{R}^2)$ and the expression of its derivative is given by*

$$D\Phi(0)\theta = D(g \circ \Psi)(0)\theta = Dg(0)\theta + \left(\boldsymbol{\nabla g}(0)\,|\theta\right)_G.$$

Remark 4.1.3. See [HP05, Lemma 5.3.3] for a proof in case of $(\cdot|\cdot)_G$ being the usual inner product in $\mathbb{R}^2$. Looking at a sketch of the proof, starting from

$$\|g(\theta) \circ \Psi(\theta) - g(0) - Dg(0)\theta - (\boldsymbol{\nabla g}|\theta)_G\|_{L^1(\mathbb{R}^2)},$$

the term $g(0) \circ (\mathrm{id}+\theta) - g(0) - (\boldsymbol{\nabla g}(0)|\theta)_G$ appears. This last term is equal after calculations to $o(\|\theta\|_{W^{1,\infty}(\mathbb{R}^2,\mathbb{R}^2)})$. Besides, other terms arise which are bounded from above by $o(\|\theta\|_{W^{1,\infty}(\mathbb{R}^2,\mathbb{R}^2)})$.

The following result sets the assumptions to differentiate with respect to θ under the $\int$ sign in a general context.

Proposition 4.1.7. *Let $\Omega \subset \mathbb{R}^2$ be a bounded measurable set and $f : W^{1,\infty}(\mathbb{R}^2,\mathbb{R}^2) \to L^1(\mathbb{R}^2)$ be Fréchet differentiable at $0 \in W^{1,\infty}(\mathbb{R}^2,\mathbb{R}^2)$. Then, the mapping*

$$\begin{array}{rccl} \Phi: & W^{1,\infty}(\mathbb{R}^2,\mathbb{R}^2) & \longrightarrow & \mathbb{R} \\ & \theta & \longmapsto & \Phi(\theta) = \displaystyle\int_\Omega f(\theta)(\boldsymbol{x})\sqrt{\det G(\boldsymbol{x})}\,\mathrm{d}\boldsymbol{x}, \end{array}$$

is Fréchet differentiable at $0 \in W^{1,\infty}(\mathbb{R}^2,\mathbb{R}^2)$ and

$$D\Phi(0)\theta = \int_\Omega Df(0)\theta(\boldsymbol{x})\sqrt{\det G(\boldsymbol{x})}\,\mathrm{d}\boldsymbol{x}.$$

Proof. First, notice that the notions of measurability of Ω or integrability over Ω coincide for the measures $\mathrm{d}\boldsymbol{x}$ and $\sqrt{\det G(\boldsymbol{x})}\,\mathrm{d}\boldsymbol{x}$, thanks to the assumptions on G.

To show the continuity of the linear mapping $W^{1,\infty}(\mathbb{R}^2,\mathbb{R}^2) \to \mathbb{R}$ given by

$$\theta \mapsto \int_\Omega Df(0)\theta(\boldsymbol{x})\sqrt{\det G(\boldsymbol{x})}\,\mathrm{d}\boldsymbol{x},$$

notice that

$$\left|\int_\Omega Df(0)\theta(\boldsymbol{x})\sqrt{\det G(\boldsymbol{x})}\,\mathrm{d}\boldsymbol{x}\right| \leq C\,\|Df(0)\|_{L^1(\mathbb{R}^2)}\,\|\theta\|_{L^\infty(\mathbb{R}^2,\mathbb{R}^2)} \leq C'\,\|\theta\|_{W^{1,\infty}(\mathbb{R}^2,\mathbb{R}^2)},$$

where C and C' are two positive constants by assumption on f. Then, the following equality must be proven for $\theta \in W^{1,\infty}(\mathbb{R}^2,\mathbb{R}^2)$,

$$\left|\Phi(\theta) - \Phi(0) - \int_\Omega Df(0)\theta(\boldsymbol{x})\sqrt{\det G(\boldsymbol{x})}\,\mathrm{d}x\right| = o(\|\theta\|_{W^{1,\infty}(\mathbb{R}^2,\mathbb{R}^2)}),$$

or equivalently,

$$\int_\Omega (f(\theta)(\boldsymbol{x}) - f(0)(\boldsymbol{x}))\,\sqrt{\det G(\boldsymbol{x})}\,\mathrm{d}\boldsymbol{x} = \int_\Omega Df(0)\theta(\boldsymbol{x})\sqrt{\det G(\boldsymbol{x})}\,\mathrm{d}\boldsymbol{x} + o(\|\theta\|_{W^{1,\infty}(\mathbb{R}^2,\mathbb{R}^2)}).$$

Since f is Fréchet differentiable at 0,

$$f(\theta) - f(0) = Df(0)\theta + o(\|\theta\|_{W^{1,\infty}(\mathbb{R}^2,\mathbb{R}^2)}),$$

and because $Df(0)\theta$ belongs to $L^1(\mathbb{R}^2)$ for all $\theta \in W^{1,\infty}(\mathbb{R}^2,\mathbb{R}^2)$, it yields

$$\int_\Omega (f(\theta)(\boldsymbol{x}) - f(0)(\boldsymbol{x}))\,\sqrt{\det G(\boldsymbol{x})}\,\mathrm{d}\boldsymbol{x} = \int_\Omega Df(0)\theta(\boldsymbol{x})\sqrt{\det G(\boldsymbol{x})} + o(\|\theta\|_{W^{1,\infty}(\mathbb{R}^2,\mathbb{R}^2)})\,\mathrm{d}\boldsymbol{x}.$$

Finally, since Ω is bounded, then $\int_\Omega o(\|\theta\|_{W^{1,\infty}(\mathbb{R}^2,\mathbb{R}^2)}) = o(\|\theta\|_{W^{1,\infty}(\mathbb{R}^2,\mathbb{R}^2)})$, that completes the proof. ■

Assume now that the integral to be differentiated also depends on a moving domain. This is the topic of the next result.

Corollary 4.1.8. *Let $\Omega \subset \mathbb{R}^2$ be a bounded measurable set and $f : W^{1,\infty}(\mathbb{R}^2,\mathbb{R}^2) \to L^1(\mathbb{R}^2)$ be such that $f(\theta)\circ(\mathrm{id}+\theta)$ is Fréchet differentiable at $0 \in W^{1,\infty}(\mathbb{R}^2,\mathbb{R}^2)$. Then, the mapping*

$$\begin{array}{rccl} \Phi: & W^{1,\infty}(\mathbb{R}^2,\mathbb{R}^2) & \longrightarrow & \mathbb{R} \\ & \theta & \longmapsto & \Phi(\theta) = \displaystyle\int_{\Omega_\theta} f(\theta)(\boldsymbol{x})\sqrt{\det G(\boldsymbol{x})}\,\mathrm{d}\boldsymbol{x}, \end{array}$$

where $\Omega_\theta := (\mathrm{id}+\theta)\Omega$, is Fréchet differentiable at $0 \in W^{1,\infty}(\mathbb{R}^2,\mathbb{R}^2)$ and

$$D\Phi(0)\theta = \int_{\Omega} \left[Df(0)\theta(\boldsymbol{x}) + \mathrm{div}(\theta(\boldsymbol{x})f(0)(\boldsymbol{x}))\right]\sqrt{\det G(\boldsymbol{x})}\,\mathrm{d}\boldsymbol{x}.$$

Proof. As before, the measure $\sqrt{\det G(\boldsymbol{x})}\,\mathrm{d}\boldsymbol{x}$ has no particular influence compared to the usual Lebesgue measure. Using the substitution of variables in a Lipschitz's framework [5], it yields

$$\Phi(\theta) = \int_{\Omega} f(\theta)\circ(\mathrm{id}+\theta)(\boldsymbol{x})|\det D_{\boldsymbol{x}}(\mathrm{id}+\theta)(\boldsymbol{x})|\sqrt{\det G(\boldsymbol{x})}\,\mathrm{d}\boldsymbol{x},$$

where $D_{\boldsymbol{x}}(\mathrm{id}+\theta)(\boldsymbol{x}) = I + D_{\boldsymbol{x}}\theta(\boldsymbol{x})$ denotes the jacobian matrix of $\boldsymbol{x} \in \mathbb{R}^2 \mapsto (\mathrm{id}+\theta)(\boldsymbol{x}) \in \mathbb{R}^2$ at $\boldsymbol{x}$. Introduce the mappings

$$\begin{array}{rccl} \varphi_1: & W^{1,\infty}(\mathbb{R}^2,\mathbb{R}^2) & \longrightarrow & L^1(\mathbb{R}^2) \\ & \theta & \longmapsto & \varphi_1(\theta) = f(\theta)\circ(\mathrm{id}+\theta), \\ \varphi_2: & W^{1,\infty}(\mathbb{R}^2,\mathbb{R}^2) & \longrightarrow & \mathbb{R} \\ & \theta & \longmapsto & \varphi_2(\theta) = |\det(I + D_{\boldsymbol{x}}\theta)|, \end{array}$$

and set $\varphi = \varphi_1 \cdot \varphi_2$. The absolute value in the expression of φ_2 is actually not necessary for small $\theta \in W^{1,\infty}(\mathbb{R}^2,\mathbb{R}^2)$ because of the continuity of the determinant. Applying Proposition 4.1.7 to the integrand $\varphi(\theta)$ leads to

$$D\Phi(0)\theta = \int_{\Omega_0} D\varphi(0)\theta(\boldsymbol{x})\sqrt{\det G(\boldsymbol{x})}\,\mathrm{d}\boldsymbol{x}.$$

Now, we compute $D\varphi(0)\theta$. On the first hand, by Lemma 4.1.6 applied to $g = f$,

$$D\varphi_1(0)\theta = Df(0)\theta + (\boldsymbol{\nabla f}(0)|\theta)_G\,.$$

On the other hand, if $L^\infty(\mathbb{R}^2,\mathbb{R}^4)$ denotes the space of the 2 by 2 matrices whose components belong to $L^\infty(\mathbb{R}^2)$, endowed with the norm given by $\|H\|_{L^\infty(\mathbb{R}^2,\mathbb{R}^4)} := \mathrm{ess\,sup}_{x\in\mathbb{R}^2}\{\sum_{1\le i,j\le 2}|H_{i,j}(x)|\}$, the Fréchet derivative at 0 of

$$\begin{array}{rccl} \alpha_1: & W^{1,\infty}(\mathbb{R}^2,\mathbb{R}^2) & \longrightarrow & L^\infty(\mathbb{R}^2,\mathbb{R}^4) \\ & \theta & \longmapsto & \alpha_1(\theta) = I + D_{\boldsymbol{x}}\theta, \end{array}$$

5. See for example [MS76, Lemma 4.1].

is given by $\theta \mapsto D_{\boldsymbol{x}}\theta$ since $\|D_{\boldsymbol{x}}\theta\|_{L^\infty(\mathbb{R}^2,\mathbb{R}^4)} \leq \|\theta\|_{W^{1,\infty}(\mathbb{R}^2,\mathbb{R}^2)}$ and since $\alpha_1(\theta) - \alpha_1(0) = D_{\boldsymbol{x}}\theta$, whereas the Fréchet derivative at I of

$$\begin{array}{rccl} \alpha_2 : & L^\infty(\mathbb{R}^2,\mathbb{R}^4) & \longrightarrow & \mathbb{R} \\ & H & \longmapsto & \alpha_2(H) = \det(I+H), \end{array}$$

is given by $H \mapsto \operatorname{trace}(H)$ by a classical result [6]. Hence, by the chain rule,

$$D\varphi_2(0)\theta = D\alpha_2(I)\left(D\alpha_1(0)\theta\right) = \operatorname{trace}(D_{\boldsymbol{x}}\theta) = \operatorname{div}(\theta),$$

where the last equality comes from the definition of the divergence in $\left(\mathbb{R}^2,(\cdot|\cdot)_G\right)$, see Definition 2.1.26. Finally, applying the product rule yields

$$\begin{aligned} D\varphi(0)\theta =& D\varphi_1(0)\theta\ \varphi_2(0) + \varphi_1(0)D\varphi_2(0)\theta \\ =& Df(0)\theta + (\boldsymbol{\nabla} \boldsymbol{f}(0)|\theta)_G + f(0)\operatorname{div}(\theta) = Df(0)\theta + \operatorname{div}(\theta f(0)), \end{aligned}$$

the last equality being stated in Proposition 2.1.27. ■

The next proposition is an adaptation of the previous results to the framework of the differentiation with respect to the domain.

Proposition 4.1.9. *Let $\Omega_0 \subset \mathbb{R}^2$ be a bounded measurable set and $f \in W^{1,1}(\mathbb{R}^2)$. Consider the functional*

$$\begin{array}{rccl} J : & \mathcal{F}(\Omega_0) & \longrightarrow & \mathbb{R} \\ & \Omega & \longmapsto & J(\Omega) = \displaystyle\int_\Omega f(\boldsymbol{x})\sqrt{\det G(\boldsymbol{x})}\,\mathrm{d}\boldsymbol{x}. \end{array}$$

Then, J is differentiable with respect to the domain at Ω_0, and for $\theta \in W^{1,\infty}(\mathbb{R}^2,\mathbb{R}^2)$,

$$J'(\Omega_0)\theta = \int_{\Omega_0} \operatorname{div}(\theta(\boldsymbol{x})f(\boldsymbol{x}))\sqrt{\det G(\boldsymbol{x})}\,\mathrm{d}\boldsymbol{x},$$

where div *is the divergence operator defined on $\left(\mathbb{R}^2,(\cdot|\cdot)\right)_{G}$.*

Proof. By definition of the derivative with respect to the domain, we have to compute the Fréchet derivative of $\theta \in W^{1,\infty}(\mathbb{R}^2,\mathbb{R}^2) \mapsto J((\mathrm{id}+\theta)(\Omega_0)) \in \mathbb{R}$ at $\theta = 0$. By Corollary 4.1.8, since the integrand does not depend on θ, it yields

$$J'(\Omega_0)\theta = \int_{\Omega_0} \operatorname{div}(\theta(\boldsymbol{x})f(\boldsymbol{x}))\sqrt{\det G(\boldsymbol{x})}\,\mathrm{d}\boldsymbol{x}.$$

■

6. For a more general statement, see for example [MS76, Lemma 4.2].

An example of application of this last result consists in the derivative with respect to the domain of the functional given by vol. The expression obtained is helpful for taking into consideration the volume constraint in the optimization process. For that matter, it is sufficient to assume that Ω_0 is polygonal.

Corollary 4.1.10. *Let $\Omega_0 \subset \mathbb{R}^2$ be a polygonal set. The functional*

$$\begin{array}{rccl} \mathrm{vol}: & \mathcal{F}(\Omega_0) & \longrightarrow & \mathbb{R} \\ & \Omega & \longmapsto & \mathrm{vol}(\Omega) = \displaystyle\int_\Omega \sqrt{\det G(\boldsymbol{x})}\,\mathrm{d}\boldsymbol{x}, \end{array}$$

is differentiable with respect to the domain at Ω_0 and its derivative is given, for $\theta \in W^{1,\infty}(\mathbb{R}^2,\mathbb{R}^2)$, by

$$\mathrm{vol}'(\Omega_0)\theta = \int_{\partial\Omega_0} (\theta(\boldsymbol{x})\,|\boldsymbol{n}(\boldsymbol{x}))_G \sqrt{\det G(\boldsymbol{x})}\,\mathrm{d}\sigma, \tag{4.4}$$

where $\boldsymbol{n}(\boldsymbol{x})$ is the outward unit normal (with respect to $(\cdot|\cdot)_G$) vector on the boundary $\partial\Omega_0$ at the point x and $\mathrm{d}\sigma$ is the corresponding curve element on $\partial\Omega_0$.

Proof. With $f \in W^{1,1}(\mathbb{R}^2)$ such that $f \equiv 1$ in a neighbourhood of Ω_0, Proposition 4.1.9 gives

$$\mathrm{vol}'(\Omega_0)\theta = \int_{\Omega_0} \mathrm{div}(\theta(\boldsymbol{x}))\sqrt{\det G(\boldsymbol{x})}\,\mathrm{d}\boldsymbol{x} = \int_{\partial\Omega_0} (\theta(\boldsymbol{x})\,|\boldsymbol{n}(\boldsymbol{x}))_G \sqrt{\det G(\boldsymbol{x})}\,\mathrm{d}\sigma,$$

the last equality being obtained by applying the Divergence Theorem, see Theorem 2.1.31, thanks to the regularity of $\partial\Omega_0$.[7] ■

4.1.2 Application to $J(\Omega) = \lambda_k(\Omega)$

Let Ω_0 be an initial domain. The purpose of this subsection is to apply the differentiation results to the cost functional given by

$$\begin{array}{rccl} J: & \mathcal{F}(\Omega_0) & \to & \mathbb{R} \\ & \Omega & \mapsto & J(\Omega) = \lambda_k(\Omega) := \lambda_{k,\Omega}, \end{array} \tag{4.5}$$

where $\mathcal{F}(\Omega_0)$ still denotes the set of all feasible shapes defined by (4.1). To show that J is differentiable with respect to the domain, the results from [HP05] must be slightly adapted. On the one hand, the metric g is taken into account in the computations, in the other hand, a deformation field θ of class $W^{1,\infty}(\mathbb{R}^2,\mathbb{R}^2)$ is considered in the Hadamard Variational Formula. The methodology in [HP05, § 5.6 and 5.7], consisting in deriving informally the formula in a first step and proving it rigorously afterwards provides a good explanation of where does this variational formula comes from. However, the way

7. See [MS76, Thorem 4.2] for a statement with less regularity.

to obtain the expression $\lambda_k'(\Omega_0)\theta$ relies on a regularity assumption of the associated eigenfunction $u_k(\Omega_0)$ that is not justified here. A rigorous proof of this assumption may be found in [HP05, Section 5.7, pp. 210–211].

Proposition 4.1.11. *Let $\Omega_0 \subset \mathbb{R}^2$ be a bounded open set of class $\mathcal{C}^2$ and $\lambda_k(\Omega_0)$ be the eigenvalue appearing in $(\mathcal{P}_{opt})$ which is supposed to be simple, with associated eigenfunction denoted by $u_k(\Omega_0)$. Then, the functional*

$$\begin{array}{rccc} \lambda_k : & \mathcal{F}(\Omega_0) & \longrightarrow & \mathbb{R} \\ & \Omega & \longmapsto & \lambda_k(\Omega) \end{array}$$

is differentiable with respect to the domain at Ω_0 and its derivative is given, for $\theta \in W^{1,\infty}(\mathbb{R}^2,\mathbb{R}^2)$, by

$$\lambda_k'(\Omega_0)\theta = -\int_{\partial\Omega_0} \left(\frac{\partial u_k(\Omega_0)(\boldsymbol{x})}{\partial \boldsymbol{n}(\boldsymbol{x})}\right)^2 (\theta(x)\,|\boldsymbol{n}(\boldsymbol{x})\,)_G \sqrt{\det G(\boldsymbol{x})}\,\mathrm{d}\sigma. \tag{4.6}$$

where $\boldsymbol{n}(\boldsymbol{x})$ is the outward unit normal (with respect to $(\cdot|\cdot)_G$) vector on the boundary $\partial\Omega_0$ at the point x and $\mathrm{d}\sigma$ is the curve element on $\partial\Omega_0$.

Remark 4.1.4. The regularity assumption on the boundary of Ω_0 can be weakened. Indeed, assuming Ω_0 of class $W^{2,\infty}(\mathbb{R}^2)$ is sufficient. See [MS76, Theorem 5.2] applied to the operator defined by $u \mapsto -\Delta_g u - \lambda_k u$.[8] In this theorem of Murat-Simon, another result holds for Ω_0 of class $W^{1,\infty}(\mathbb{R}^2)$—for instance a polygonal set—. However it does not provide an explicit formula which could be used numerically.

Proof. For convenience, set $u_k(\theta) : (\mathrm{id}+\theta)(\Omega_0) \to \mathbb{R}$ and let $\lambda_k(\theta) \in \mathbb{R}$ be the solution of $(\mathcal{WP})$ on $\Omega_\theta := (\mathrm{id}+\theta)(\Omega_0)$. With these notations we have to compute the Fréchet derivative of λ_k at $0 \in W^{1,\infty}(\mathbb{R}^2,\mathbb{R}^2)$. Since Ω_0 is of class $\mathcal{C}^2$, the weak eigenfunction $u_k(0)$ of $(\mathcal{WP})$ over Ω_0 satisfies $u_k(0) \in H^2(\Omega_0)$, and so, is also an eigenfunction of $(\mathcal{P})$, see [GT01, Theorem 8.12]. Assume for the moment that λ_k, u_k, $\boldsymbol{\nabla u_k}$ and $\Delta_g u_k$ are Fréchet differentiable at $0 \in W^{1,\infty}(\mathbb{R}^2,\mathbb{R}^2)$. Thus, differentiating at $0 \in W^{1,\infty}(\mathbb{R}^2,\mathbb{R}^2)$ the equality

$$-\Delta_g u_k(\theta)(\boldsymbol{x}) = \lambda_k u_k(\theta)(\boldsymbol{x}), \quad \forall \boldsymbol{x} \in \Omega_0,$$

yields

$$-\Delta_g\left(Du_k(0)(\boldsymbol{x})\right) = \left(D\lambda_k(0)\right) u_k(0)(\boldsymbol{x}) + \lambda_k(0) Du_k(0)(\boldsymbol{x}), \quad \forall \boldsymbol{x} \in \Omega_0.$$

Then multiply by $u_k(0)$ the last equality and integrate over Ω_0

$$\begin{aligned} &-\int_{\Omega_0} u_k(0)(\boldsymbol{x})\Delta_g\left(Du_k(0)(\boldsymbol{x})\right)\sqrt{\det G(\boldsymbol{x})}\,\mathrm{d}\boldsymbol{x} = \\ &= \int_{\Omega_0} \left[\left(D\lambda_k(0)\right) u_k^2(0)(\boldsymbol{x}) + \lambda_k(0) u_k(0)(\boldsymbol{x}) Du_k(0)(\boldsymbol{x})\right]\sqrt{\det G(\boldsymbol{x})}\,\mathrm{d}\boldsymbol{x}. \end{aligned} \tag{4.7}$$

8. Their result can be applied to this operator since the solution of $-\Delta_g u - \lambda_k u = 0$ is unique.

Since the eigenfunctions are normalized for the norm $\|\cdot\|_H$, Corollary 4.1.8 applied to

$$\theta \mapsto \int\limits_{(\mathrm{id}+\theta)(\Omega_0)} u_k^2(\theta) \circ (id+\theta)(\boldsymbol{x}) \sqrt{\det G(\boldsymbol{x})}\, \mathrm{d}\boldsymbol{x},$$

whose integrand $\theta \in W^{1,\infty}(\mathbb{R}^2,\mathbb{R}^2) \mapsto u_k^2(\theta) \circ (\mathrm{id}+\theta)$ is Fréchet differentiable at 0 by Lemma 4.1.6, implies

$$\int\limits_{\Omega_0} \left[2u_k(0)Du_k(0)\theta + \mathrm{div}(\theta\ u_k^2(0))\right](\boldsymbol{x}) \sqrt{\det G(\boldsymbol{x})}\, \mathrm{d}\boldsymbol{x} = 0. \tag{4.8}$$

The Divergence Theorem 2.1.31 provides the equality

$$\int\limits_{\Omega_0} \mathrm{div}(\theta\ u_k^2(0))(\boldsymbol{x}) \sqrt{\det G(\boldsymbol{x})}\, \mathrm{d}\boldsymbol{x} = \int\limits_{\partial\Omega_0} u_k^2(0)(\boldsymbol{x})\, (\theta(\boldsymbol{x})|\boldsymbol{n}(\boldsymbol{x}))_G \sqrt{\det G(\boldsymbol{x})}\, \mathrm{d}\boldsymbol{x}$$

and since $u_k(0)$ vanishes on $\partial\Omega_0$, (4.8) becomes

$$\int\limits_{\Omega_0} u_k(0)(\boldsymbol{x}) Du_k(0)\theta(\boldsymbol{x}) \sqrt{\det G(\boldsymbol{x})}\, \mathrm{d}\boldsymbol{x} = 0. \tag{4.9}$$

Thus, equality (4.7) may be rewritten as

$$-\int\limits_{\Omega_0} u_k(0)(\boldsymbol{x}) \Delta_g \left(Du_k(0)(\boldsymbol{x})\right) \sqrt{\det G(\boldsymbol{x})}\, \mathrm{d}\boldsymbol{x} = D\lambda_k(0).$$

By applying the Green Formula twice to the left hand side and after noticing that two terms are vanishing because $u_k(0) \equiv 0$ on $\partial\Omega_0$ and because of equality (4.9), it follows

$$D\lambda_k(0) = \int\limits_{\partial\Omega_0} \frac{\partial u_k(0)}{\partial \boldsymbol{n}} Du_k(0) \sqrt{\det G}\, \mathrm{d}\sigma. \tag{4.10}$$

Now, we compute $Du_k(0)$ on $\partial\Omega_0$. From Lemma 4.1.6, it holds that

$$D\left(u_k(\theta) \circ (\mathrm{id}+\theta)\right)(0)\theta = Du_k(0)\theta + \left(\boldsymbol{\nabla u_k}(0)|\theta\right)_G. \tag{4.11}$$

Moreover, $u_k(\theta) \circ (\mathrm{id}+\theta) : \Omega_0 \to \mathbb{R}$ is constant equal to zero on $\partial\Omega_0$, hence for $\boldsymbol{x} \in \partial\Omega_0$, it yields

$$\boldsymbol{\nabla u_k}(0)(\boldsymbol{x}) = \boldsymbol{n}(\boldsymbol{x})\, (\boldsymbol{\nabla u_k(0)}(\boldsymbol{x})|\boldsymbol{n}(\boldsymbol{x}))_G = \boldsymbol{n}(\boldsymbol{x}) \frac{\partial u_k(0)(\boldsymbol{x})}{\partial \boldsymbol{n}},$$

and combining with (4.11) restricted to $\partial\Omega_0$ it follows

$$Du_{k\,|\partial\Omega_0}(0)\theta = -\frac{\partial u_k(0)}{\partial \boldsymbol{n}}\, (\boldsymbol{n}|\theta)_G.$$

This last equality plugged in (4.10) gives the expecting formula for $D\lambda_k(0)$.

The assumptions asserting that λ_k, u_k, $\boldsymbol{\nabla u_k}$ and $\Delta_g u_k$ are Fréchet differentiable at $0 \in W^{1,\infty}(\mathbb{R}^2,\mathbb{R}^2)$ still should be justified to complete the proof. In the sequel, only a sketch of the proof is outlined following [HP05]. The idea is to show that $\theta \in W^{1,\infty}(\mathbb{R}^2,\mathbb{R}^2) \mapsto (\lambda_k(\theta), u_k(\theta)) \in \mathbb{R} \times H^1(\mathbb{R}^2)$ is equal to another mapping which is of class $\mathcal{C}^\infty$. For that purpose, we introduce the operator $\Psi : W^{1,\infty}(\mathbb{R}^2,\mathbb{R}^2) \times H^1_0(\Omega_0) \times \mathbb{R} \to H^{-1}(\Omega_0) \times \mathbb{R}$ defined by

$$\Psi(\theta, v, \lambda) = (-\operatorname{div}(A(\theta)\boldsymbol{\nabla v} \det(I + D_{\boldsymbol{x}}\theta)) - \lambda v \det(I + D_{\boldsymbol{x}}\theta), \int_{\Omega_0} v^2 \det(I + D_{\boldsymbol{x}}\theta) - 1).$$

where $A(\theta) = (I + D_{\boldsymbol{x}}\theta)^{-1}(I + D_{\boldsymbol{x}}\theta)^{-T}$. Notice that the problem displaced over Ω_0 using the substitution of variables $y = (\mathrm{id}+\theta)x$ can be expressed by the equality

$$\Psi(\theta, u_k(\theta) \circ (\mathrm{id}+\theta), \lambda_k(\theta)) = (0, 0).$$

Proving that Ψ belongs to the $\mathcal{C}^\infty$ class is not the most difficult part but is technical. Then, the Open Mapping Theorem implies that the Fréchet derivative of Ψ with respect to (v, λ) is an isomorphism. To complete the proof, a version of the Implicit Function Theorem is used to show that there exists a mapping $\theta \in W^{1,\infty}(\mathbb{R}^2,\mathbb{R}^2) \mapsto (v(\theta), \lambda(\theta)) \in H^1_0(\Omega_0) \times \mathbb{R}$ of class $\mathcal{C}^\infty$ defined on a neighbourhood $\mathcal{V}$ of 0 in $W^{1,\infty}(\mathbb{R}^2,\mathbb{R}^2)$, and that there exists a neighbourhood $\mathcal{O}$ of $(0, u_k(0), \lambda_k(0))$ in $W^{1,\infty}(\mathbb{R}^2,\mathbb{R}^2) \times H^1_0(\Omega_0) \times \mathbb{R}$ such that, $v(0) = u_k(0)$, $\lambda(0) = \lambda_k(0)$ and

$$\Psi^{-1}(\{(0, 0)\}) \cap \mathcal{O} = \{(\theta, v(\theta), \lambda(\theta)) : \theta \in \mathcal{V}\}.$$

Thus, $\theta \in W^{1,\infty}(\mathbb{R}^2,\mathbb{R}^2) \mapsto (v(\theta), \lambda(\theta)) \in H^1_0(\Omega_0) \times \mathbb{R}$ coincides with the function $\theta \in W^{1,\infty}(\mathbb{R}^2,\mathbb{R}^2) \mapsto (u(\theta) \circ (\mathrm{id}+\theta), \lambda_k(\theta)) \in H^1_0(\Omega_0) \times \mathbb{R}$, which *shows* the Fréchet differentiability of the eigenvalue and eigenfunction with respect to θ, as well as it justifies the computations involving the Fréchet derivatives of $\boldsymbol{\nabla u_k}(\theta)$ and $\Delta_g u_k(\theta)$. ■

Remark 4.1.5. Another proof in a regular context with an approach coming from the Riemannian geometry can be found in [ESI07], where the Corollary 2.1 corresponds to the statement of the adapted Hadamard Variational Formula given above. However, it provides abstract formulas, whereas its translation in the open set of a chart is required for the numerical applications.

4.1.3 Taking the multiplicity into consideration

The fact that a multiple eigenvalue is not Fréchet-differentiable is well known, see for instance [Hen06, Subsection 2.5.1]. So, general deformations as defined in (4.1) are not possible anymore, but given a fixed $\theta \in W^{1,\infty}(\mathbb{R}^2,\mathbb{R}^2)$, feasible shapes must be restricted to shapes of the form $\Omega_{t\theta} = (\mathrm{id}+t\theta)(\Omega_0)$, for $t > 0$ small enough. Thus, in order to deal with a similar formula as (4.6) when multiplicity occurs, directional derivatives are used. This is a classical approach in such a context. The following result is proved in a general context, see [Mun00, Theorem 4.3.1], and stated in [Hen06] for the eigenvalue problem of the Laplace operator in the Euclidean case.

Proposition 4.1.12 (Adapted from [Hen06, Theorem 2.5.8]). *Let $\Omega_0 \subset \mathbb{R}^2$ be a bounded open set of class $\mathcal{C}^2$ and $\lambda_k(\Omega_0)$ be the eigenvalue appearing in $(\mathcal{P}_{opt})$ of multiplicity $m \geq 1$, with associated eigenfunctions denoted by $u_{k1}(\Omega_0), \ldots, u_{km}(\Omega_0)$. Then, for a small $\varepsilon > 0$, the functional*

$$\begin{array}{rccc} \lambda_k : & (-\varepsilon, \varepsilon) & \to & \mathbb{R} \\ & t & \mapsto & \lambda_k(\Omega_{t\theta}) \end{array}$$

has a derivative at $t = 0$, that is for all $\theta \in W^{1,\infty}(\mathbb{R}^2, \mathbb{R}^2)$, the limit

$$\lim_{t \to 0} \frac{\lambda_k(\Omega_{t\theta}) - \lambda_k(\Omega_0)}{t}$$

exists and is one of the eigenvalues of the m by m matrix D, whose components are defined by

$$D_{i,j} = -\int_{\partial\Omega_0} \left(\frac{\partial u_{ki}(\Omega_0)(\boldsymbol{x})}{\partial \boldsymbol{n}(\boldsymbol{x})} \frac{\partial u_{kj}(\Omega_0)(\boldsymbol{x})}{\partial \boldsymbol{n}(\boldsymbol{x})} \right) (\theta(\boldsymbol{x}) \,|\boldsymbol{n}(\boldsymbol{x})\,)_G \sqrt{\det G(\boldsymbol{x})}\, \mathrm{d}\sigma. \tag{4.12}$$

for $i, j = 1, \ldots, m$, where $\boldsymbol{n}(x)$ is the outward unit normal (with respect to $(\cdot|\cdot)_G$) vector on the boundary $\partial\Omega_0$ at the point x and $\mathrm{d}\sigma$ is the curve element on $\partial\Omega_0$.

Remark 4.1.6. When the eigenvalue $\lambda_k(\Omega_0)$ is simple, that is $m = 1$, this result corresponds to Proposition 4.1.11.

In our context, looking at the multiplicity for an eigenvalue makes sense, since for $k \geq 2$, the k-th eigenvalue $\lambda_k(\Omega^*)$ associated to the domain Ω_k^* minimizing $\lambda_k(\Omega)$ among all domain Ω of fixed volume, is expected to have multiplicity $m > 1$, at least for the Euclidean case, see [Hen06, Open problem 1]. When multiplicity occurs, another approach is to consider the sub-differential of $\lambda_k(\Omega)$, see for instance [Cox95] about this topic.

4.2 Dealing with the volume constraint: the Uzawa algorithm

Having the formula (4.6) at our disposal, the optimization problem $(\mathcal{P}_{opt})$ can be now addressed. Formally, because the functional $\Omega \mapsto \mathrm{vol}(\Omega)\lambda_k(\Omega)$, is in general not invariant under homothety in $(\mathbb{R}^2, (\cdot|\cdot)_G)$, the volume of the shape Ω has to be controlled during the optimization process. For this purpose, introduce the Lagrangian $\mathcal{L}$ of the problem $(\mathcal{P}_{opt})$, given by

$$\begin{array}{rccc} \mathcal{L} : \mathcal{F}(\Omega_0) \times \mathbb{R} & \to & \mathbb{R} \\ (\Omega, \mu) & \mapsto & \mathcal{L}(\Omega, \mu) = J(\Omega) + \mu(\mathrm{vol}(\Omega) - V_0), \end{array}$$

where the functional J is given by (4.5) and $\mathcal{F}(\Omega_0)$ still denotes the set of all feasible shapes from an initial domain Ω_0 of class $\mathcal{C}^2$ and of volume V_0 satisfying $0 < V_0 < \mathrm{vol}(\pi(U)) =: V$, where (U, π) denotes the chart of M such that $\Omega_0 \subset \pi(U)$. The positive parameter μ is called the *Lagrange multiplier* for the problem $(\mathcal{P}_{opt})$. Instead of dealing with the optimization problem and its volume constraint, we have to find a saddle point of $\mathcal{L}$ without constraint, that is to find $(\Omega', \mu') \in \mathcal{F}(\Omega_0) \times \mathbb{R}$, such that

$$\mathcal{L}(\Omega', \mu) \leq \mathcal{L}(\Omega', \mu') \leq \mathcal{L}(\Omega, \mu'), \quad \forall (\Omega, \mu) \in \mathcal{F}(\Omega_0) \times \mathbb{R}. \tag{4.13}$$

This fact is more precisely stated in the next lemma. A general study of the Lagrangian can be found in [FG82] and in [IK08] with applications to optimization problems of various types, or in [Cia82, Chapter 9], [All07, Chapter 3] and [IK08, Section 4.6], with an application to the Uzawa algorithm—the method that will be implemented numerically—to find a saddle point of the Lagrangian.

Lemma 4.2.1. [9] *With the previous notations, if $(\Omega^*, \mu^*) \in \mathcal{F}(\Omega_0) \times \mathbb{R}$ is a saddle point of the Lagrangian, then the set Ω^* is a solution to problem $(\mathcal{P}_{opt})$.*

Proof. The inequality

$$\mathcal{L}(\Omega^*, \mu) \leq \mathcal{L}(\Omega^*, \mu^*), \quad \forall \mu \in \mathbb{R},$$

in the definition of a saddle point (4.13), can be rewritten as

$$(\mu - \mu^*)(\mathrm{vol}(\Omega^*) - V_0) \leq 0, \quad \forall \mu \in \mathbb{R},$$

and so, $\mathrm{vol}(\Omega^*) = V_0$. Moreover, the other inequality in (4.13) yields

$$J(\Omega^*) \leq J(\Omega) + \mu^*(\mathrm{vol}(\Omega) - V_0), \quad \forall \Omega \in \mathcal{F}(\Omega_0),$$

and, restricting to $\Omega \in \mathcal{F}(\Omega_0)$ of volume V_0, it gives $J(\Omega^*) \leq J(\Omega)$. Thus, Ω^* is solution of $(\mathcal{P}_{opt})$. ■

The idea behind the Uzawa algorithm is the following: assume that the second component $\mu^* \in \mathbb{R}$ of a saddle point of $\mathcal{L}$ is at our disposal. Finding a minimizer Ω^* of the problem (with constraint) $(\mathcal{P}_{opt})$ is equivalent to find the first component Ω^* of the saddle point, *ie* a solution to the so called *primal* problem (without constraint):

$$(\mathcal{P}_{\mu^*}) \begin{cases} \text{Find a set } \Omega^* \in \mathcal{F}(\Omega_0), \text{ such that} \\ \mathcal{L}(\Omega^*, \mu^*) \leq \mathcal{L}(\Omega, \mu^*), \quad \forall \Omega \in \mathcal{F}(\Omega_0). \end{cases}$$

The point is first to be able to find μ^*. It comes readily [10] that μ^* satisfies

$$\inf_{\Omega \in \mathcal{F}(\Omega_0)} \mathcal{L}(\Omega, \mu^*) = \sup_{\mu \in \mathbb{R}} \inf_{\Omega \in \mathcal{F}(\Omega_0)} \mathcal{L}(\Omega, \mu).$$

9. Lemma 4.2.1 is a version adapted to the context of differentiation with respect to the domain of [Cia82, Theorem 9.3-2].

10. The aim is to show that inf and sup commute when the definition of μ^* is used. See for example [Cia82, Theorem 9.3-1].

So, the following *dual* problem has to be solved:

$$(\mathcal{Q})\ \Big\{\ \text{Find } \mu^* \in \mathbb{R},\ \text{such that } L(\mu^*) = \sup_{\mu\in\mathbb{R}} L(\mu),$$

where $L : \mathbb{R} \to \mathbb{R}$, is given by

$$\mu \mapsto L(\mu) = \inf_{\Omega\in\mathcal{F}(\Omega_0)} \mathcal{L}(\Omega, \mu).$$

Thus, to find numerically the solution Ω^*, two sequences $\left(\Omega^{(n)}\right)_{n\in\mathbb{N}}$ and $\left(\mu^{(n)}\right)_{n\in\mathbb{N}}$ are built simultaneously using a *descent* (or *gradient*) *method*. For this purpose, the expressions of the derivative (with respect to the domain) of the Lagrangian with respect to Ω and the (classical) derivative of the Lagrangian with respect to μ are required. Their computation comes readily thanks to the equations (4.4) and (4.6) derived in the last subsections: for $\Omega \in \mathcal{F}(\Omega_0)$, $\theta \in W^{1,\infty}(\mathbb{R}^2, \mathbb{R}^2)$ and $\mu \in \mathbb{R}$, it holds that

$$\frac{\partial\mathcal{L}}{\partial\Omega}(\Omega,\mu)\theta = \int_{\partial\Omega}\left(\mu - \left(\frac{\partial u_k(\Omega)(\boldsymbol{x})}{\partial\boldsymbol{n}(\boldsymbol{x})}\right)^2\right)(\theta(\boldsymbol{x})|\boldsymbol{n}(\boldsymbol{x}))_G\sqrt{\det G(\boldsymbol{x})}\mathrm{d}\sigma, \quad (4.14)$$

$$\frac{\partial\mathcal{L}}{\partial\mu}(\Omega,\mu) = \mathrm{vol}(\Omega) - V_0. \quad (4.15)$$

The initialization of the algorithm consists in an arbitrary Lagrange multiplier $\mu^{(0)} > 0$ and in an arbitrary polygonal domain $\Omega^{(0)}$ of volume V_0. Formula (4.14) is useful to find a minimizer $\Omega^{(n+1)}$ of $(\mathcal{P}_{\mu^{(n)}})$ (without volume constraint anymore), whereas Formula (4.15) is useful to find a maximizer of $(\mathcal{Q})$. More precisely, these two steps are performed as follows:

(i) compute $\Omega^{(n+1)}$;
To find the infimum of $\Omega \mapsto \mathcal{L}(\Omega, \mu^{(n)})$, one wants equation (4.14) to vanish, for all deformation fields θ. Numerically, the domains Ω used are polygonal sets, so the only points controlled are their vertices $P_i^{(n)}$, $i = 1, \ldots, N_{\partial\Omega^{(n)}}$. Following the idea of a descent algorithm, the new position $P_i^{(n+1)}$ of $P_i^{(n)}$ is the point on the line passing through $P_i^{(n)}$ in the direction [11] of $\boldsymbol{n}(P_i^{(n)})$ at a distance d_i, given by

$$d_i = \int_{\partial\Omega^{(n)}}\left(\mu^{(n)} - \left(\frac{\partial u_k(\Omega^{(n)})(\boldsymbol{x})}{\partial\boldsymbol{n}(\boldsymbol{x})}\right)^2\right)(\theta(\boldsymbol{x})|\boldsymbol{n}(\boldsymbol{x}))_G\sqrt{\det G(\boldsymbol{x})}\mathrm{d}\sigma, \quad (4.16)$$

where $\theta \in W^{1,\infty}(\mathbb{R}^2, \mathbb{R}^2)$ is such that:
- $\theta(P_i) = \boldsymbol{n}(P_i)$;
- $\theta(P_j) = 0$, for $j \neq i$.

In the Euclidean case, this can be simply [12] written as $P_i^{(n+1)} = P_i^{(n)} - d_i\boldsymbol{n}(P_i^{(n)})$.

11. See Remark 4.2.1 below for the numerical implementation of $\boldsymbol{n}(P_i)$.
12. For a general manifold of dimension 2, it is more complicated. This aspect is the aim of Section 4.3.

(ii) compute $\mu^{(n+1)}$;
In the same spirit, the next Lagrange multiplier in the Uzawa algorithm is given by

$$\mu^{(n+1)} = \mu^{(n)} + c(\mathrm{vol}(\Omega^{(n)}) - V_0),$$

where $c > 0$ is a fixed parameter.

(iii) if a given stopping criterion is not reached [13], back to step (i).

This optimization process is summarized in the following algorithm.

Uzawa Algorithm (in our shape optimization context)

Given $\mu^{(0)} > 0$, $\Omega^{(0)}$ a domain of volume V_0 and tol a thresold.
$n \leftarrow 0$; $crit \leftarrow 2\,tol$;
while $crit > tol$
    Compute $\Omega^{(n+1)}$ using a descent method given by (4.16);
    Compute $\mu^{(n+1)} \leftarrow \mu^{(n)} + c(vol(\Omega^{(n)}) - V_0)$;
    update $crit$;
end

Algorithm 3.

Remark 4.2.1. Let us clarify some relevant points for numerical implementation. First, the value for the parameter c at step (ii) has been fixed at 1000 after some calibration experiments. Furthermore, the stopping criterion chosen is to ask the ratios

$$\frac{\mathcal{L}(\Omega^{(n+k)}, \mu^{(n+k)}) - \mathcal{L}(\Omega^{(n)}, \mu^{(n)})}{\mathcal{L}(\Omega^{(n)}, \mu^{(n)})}, k = 1, \ldots, 10,$$

to be all smaller than a certain small tolerance $\varepsilon > 0$. This equates to ask the last ten computed values of the Lagrangian to vary little compared to the tolerance ε. This latter has been adjusted at $\varepsilon = 10^{-6}$. Although the volume is note preserved all along the algorithm, notice that the volume of the final domain is very close to V_0 as stated by Lemma 4.2.1 and illustrated in an example in Appendix B.

Finally, the outward unit *normal* (with respect to $(\cdot|\cdot)_G$) vector $\boldsymbol{n}$ on the boundary $\partial\Omega$ at a vertex P_i of Ω is implemented numerically from a generalization to surfaces of the idea in [ESG82]: $\boldsymbol{n}$ is defined at a vertex P of a polygonal set in $(\mathbb{R}^2, (\cdot|\cdot)_G)$ by [14]

$$\boldsymbol{n}(P) = \frac{\displaystyle\sum_{K \in E(P)} \mathrm{vol}(K) \boldsymbol{\nabla\varphi_{K,P}}}{\left\| \displaystyle\sum_{K \in E(P)} \mathrm{vol}(K) \boldsymbol{\nabla\varphi_{K,P}} \right\|},$$

where:

- $E(P)$ denotes the set of elements K whose P is a vertex;

13. See Remark 4.2.1.
14. This vector depends on the metric through the gradient terms $\boldsymbol{\nabla\varphi_{K,P}}$.

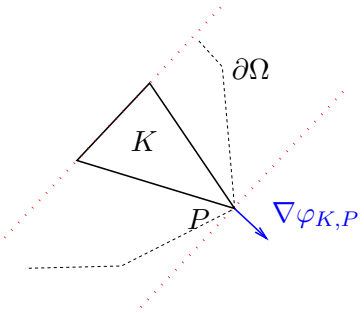

Figure 4.2: The blue arrow represents the contribution of the element K to the normal vector at point P lying on the boundary $\partial\Omega$. The red dotted lines are parallel to the side opposite P, and orthogonal to $\boldsymbol{n}$ in the Euclidean plane.

- $\varphi_{K,P}$ is the element shape function over K, taking value 1 at P.

It means that the contribution of an element to the normal vector at one of its vertices lying on the boundary consists in the gradient of the element shape function associated to the mentioned vertex, weighted by the volume of the element. In [ESG82], this definition of a normal vector is stated in the Euclidean plane, namely where $G = I$ the 2 by 2 identity matrix. Geometrically, this gradient points in the orthogonal direction of the side opposite the vertex in question, see Figure 4.2.

4.3 Technical aspect about the way to move the boundary of a domain in a surface

The last section shows that the consideration of the metric modifies deeply the processing of the optimization problem, compared to the Euclidean case in $\mathbb{R}^2$. The main illustration is the introduction of a Lagrange multiplier to solve the issue of lack of invariance under homothety of the functional $\Omega \to \lambda_k(\Omega)$. However, another technical consequence, is the displacement of a node $P_i^{(n)}$ lying on the boundary of $\partial\Omega^{(n)}$ given by the equation (4.16) which is repeated here: for all $i = 1, \dots, N_{\partial\Omega^{(n)}}$, the point $P_i^{(n)}$ becomes, in the next step of the optimization, the point $P_i^{(n+1)}$ lying on the line passing through $P_i^{(n)}$ in the direction of $\boldsymbol{n}(P_i^{(n)})$ at a distance $d_i^{(n)}$ given by

$$d_i^{(n)} = \int_{\partial\Omega^{(n)}} \left(\mu^{(n)} - \left(\frac{\partial u_k(\Omega^{(n)})(\boldsymbol{x})}{\partial \boldsymbol{n}(\boldsymbol{x})} \right)^2 \right) (\theta(\boldsymbol{x})|\boldsymbol{n}(\boldsymbol{x}))_G \sqrt{\det G(\boldsymbol{x})} \mathrm{d}\sigma,$$

where $\theta \in W^{1,\infty}(\mathbb{R}^2, \mathbb{R}^2)$ is such that:

- $\theta(P_i^{(n)}) = \boldsymbol{n}(P_i^{(n)})$;
- $\theta(P_j^{(n)}) = 0$, for $j \neq i$.

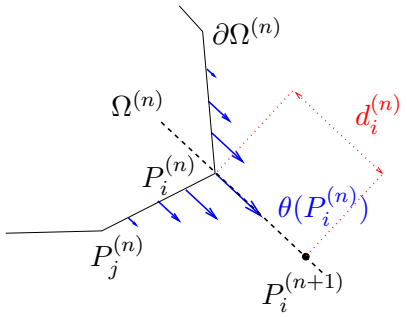

Figure 4.3: The blue arrows represent the deformation field θ which transport the point $P_i^{(n)}$ onto the point $P_i^{(n+1)}$ for the next step of the optimization process.

Because of the discretization, the deformation field θ is supposed to be linear between two adjacent vertices, so the above integral reduces to

$$d_i^{(n)} = \int_{e_{i,-}^{(n)} \cup e_{i,+}^{(n)}} \left(\mu^{(n)} - \left(\frac{\partial u_k(\Omega^{(n)})(\boldsymbol{x})}{\partial \boldsymbol{n}(\boldsymbol{x})} \right)^2 \right) (\theta(\boldsymbol{x}) | \boldsymbol{n}(\boldsymbol{x}))_G \sqrt{\det G(\boldsymbol{x})} \mathrm{d}\sigma,$$

where $e_{i,-}^{(n)}$ and $e_{i,+}^{(n)}$ denote the two different edges of $\partial\Omega^{(n)}$ containing $P_i^{(n)}$. See Figure 4.3. This integral is approximated numerically using the trapezoidal rule on each edge $e_{i,-}^{(n)}$ and $e_{i,+}^{(n)}$. Once the computation of the *amplitude of the displacements* d_i completed for all $i = 1, \ldots, N_{\partial\Omega^{(n)}}$, the locus of $P_i^{(n+1)}$ still has to be determined. Indeed, contrary to the Euclidean case where the new position is simply defined by $P_i^{(n+1)} = P_i^{(n)} - d_i \boldsymbol{n}(P_i^{(n)})$, it is less straightforward for a general metric represented by G. In this latter, the *Euclidean distance* $\delta_i^{(n)} > 0$ corresponding to the amplitude $d_i^{(n)}$ has to be determined, that is, if $\gamma : [0,1] \to [P_i^{(n)}, P_i^{(n+1)}]$, $t \mapsto P_i^{(n)} + t(P_i^{(n+1)} - P_i^{(n)})$, denotes the parametrization of the *Euclidean* segment $[P_i^{(n)}, P_i^{(n+1)}]$ whose extremities are $P_i^{(n)}$ and $P_i^{(n+1)}$, where $P_i^{(n+1)} = P_i^{(n)} - \delta_i^{(n)} \boldsymbol{n}(P_i^{(n)})$, then $\delta_i^{(n)}$ has to be chosen such that

$$\begin{aligned} d_i^{(n)} &= \int_0^1 \|\dot{\gamma}(t)\|_G \, \mathrm{d}t := \int_0^1 \left[\left(P_i^{(n+1)} - P_i^{(n)} \right)^T G(\gamma(t)) \left(P_i^{(n+1)} - P_i^{(n)} \right) \right]^{1/2} \mathrm{d}t \\ &= \delta_i^{(n)} \int_0^1 \left[\boldsymbol{n}(P_i^{(n)})^T \, G(\gamma(t)) \, \boldsymbol{n}(P_i^{(n)}) \right]^{1/2} \mathrm{d}t. \end{aligned}$$

Approximating the right hand side using the trapezoidal rule leads to

$$d_i^{(n)} \simeq \frac{\delta_i^{(n)}}{2} \left(1 + \left[\boldsymbol{n}(P_i^{(n)})^T \, G(P_i^{(n+1)}) \, \boldsymbol{n}(P_i^{(n)}) \right]^{1/2} \right), \tag{4.17}$$

where we used the fact that $\boldsymbol{n}(P_i^{(n)})$ is unitary. The required quantity $\delta_i^{(n)}$ also appears in $G(P_i^{(n+1)})$, which cannot be determined explicitly in general. So, thanks to the regularity assumption on the metric g, the components $G_{i,j} : \mathbb{R}^2 \to \mathbb{R}$ of G are smooth, and it holds that

$$G_{i,j}(P_i^{(n+1)}) = G_{i,j}(P_i^{(n)}) + DG_{i,j}(\xi_{i,j})(P_i^{(n+1)} - P_i^{(n)}), \quad i,j = 1,2,$$

for some $\xi_{i,j}$ between $P_i^{(n)}$ and $P_i^{(n+1)}$. The approximations $\xi_{i,j} \simeq P_i^{(n)}$ and a few computations yield

$$d_i^{(n)} \simeq \frac{\delta_i^{(n)}}{2}\left(1 + \left[1 + \delta_i^{(n)}\ (\boldsymbol{n}DG\boldsymbol{n})(P_i^{(n)})\ \boldsymbol{n}(P_i^{(n)})\right]^{1/2}\right),$$

where $(\boldsymbol{n}DG\boldsymbol{n})(P_i^{(n)})$ is just a compressed notation for

$$(\boldsymbol{n}DG\boldsymbol{n})(P_i^{(n)}) = \boldsymbol{n}(P_i^{(n)})^T \begin{pmatrix} DG_{1,1}(P_i^{(n)})\boldsymbol{n}(P_i^{(n)}) & DG_{1,2}(P_i^{(n)})(P_i^{(n)}) \\ DG_{2,1}(P_i^{(n)})\boldsymbol{n}(P_i^{(n)}) & DG_{2,2}(P_i^{(n)})(P_i^{(n)}) \end{pmatrix} \boldsymbol{n}(P_i^{(n)}).$$

Hence, it finally reduces to find the zero of the function defines from $\mathbb{R}_{>0}$ into itself by

$$\delta_i^{(n)} \mapsto \frac{\delta_i^{(n)}}{2}\left(1 + \left[1 + \delta_i^{(n)}\ (\boldsymbol{n}DG\boldsymbol{n})(P_i^{(n)})\ \boldsymbol{n}(P_i^{(n)})\right]^{1/2}\right) - d_i^{(n)},$$

which is carried out using a Newton-Raphson's method.

Remark 4.3.1. Other alternatives to determine the locus of $P_i^{(n+1)}$ have been studied, the most *natural*[15] being the displacement along the geodesic passing through $P_i^{(n)}$ and tangent to $\boldsymbol{n}(P_i^{(n)})$. The drawback is that a different routine providing the geodesics of the current surface must be given for each different surface. This is considerably more onerous than computing the derivatives of the components $G_{i,j}$, $i,j = 1,2$, of the matrix G. However, it has been implemented for the sphere $\mathbb{S}^2$ where it is easy and reasonably efficient to determine exactly the new position $P_i^{(n+1)}$ of $P_i^{(n)}$ using a *geodesic displacement*, but experimental computations provide results of *similar* quality as when the points are displaced as explained in the present section.

The arguments that the user has to provide to the program is

- an initial domain consisting of two lists: one for the coordinates of each vertex on the boundary of the initial domain in the open set of the chart, and one for the edges, each of them being represented by couples of positive integers corresponding to the number of the nodes at its extremities;
- the expression of the metric in the open set of the chart, that is a function taking in argument a point $\boldsymbol{x}$ in the open set of the chart and returning the matrix $G(\boldsymbol{x})$ representing the metric at the corresponding point on the surface;
- a function returning the derivatives of the components $G_{i,j}$ of G at a point x in the open set of the chart.

15. Because geodesics generalize the notion of lines used for the shape optimization in the Euclidean case.

Chapter 5

Optimization of eigenvalues of the Dirichlet-Laplacian with respect to the domain

This chapter is based on the prepublication [Str12b], that involves possible redundancies with previous chapters. His goal is to answer, using numerical methods, the following classical question [1]: what is the domain Ω_k^* of the manifold (M, g) which minimizes $\lambda_k(\Omega)$ among all domains of a given area, and what is the value of the corresponding $\lambda_k(\Omega_k^*)$?

Existence of optimal shapes in the class of quasi-open sets of $\mathbb{R}^d$, $d \in \mathbb{N}$, has been recently proved, see [Buc12] and [MP13]. Moreover, it has been shown that they are bounded and have finite perimeter. However, results giving explicit domains for this optimization problem exist only for the subscripts $k = 1$ or 2. In $\mathbb{R}^2$, the Faber-Krahn inequality [2] states that the domain minimizing λ_1 among all domain of fixed volume is a disc. The same result still holds in the sphere $\mathbb{S}^2$ and in the Poincaré disc $\mathbb{D}^2$. For $k = 2$ in $\mathbb{R}^2$, the analogous result, due to Krahn and Szegő [3] asserts that the optimal domain Ω_2^* is the union of two identical discs. For higher order eigenvalues and other manifolds, almost no explicit results exist. This is a good motivation to investigate this problem.

The difficulty to find optimal shapes is the main reason to deal with it numerically. E. Oudet is a precursor in this field with his work [Oud04]. It is concerned with domains in $\mathbb{R}^2$ and Dirichlet boundary conditions, and it uses the Finite Element Method and a descent algorithm to find optimal shapes. Other approaches can be found in the literature, as one based on the Method of Fundamental Solutions [4], used by P. R. S. Antunes and P. Freitas [AF12]. Their work improves Oudet's results and extends it to other boundary conditions as well as higher order eigenvalues optimization. The algorithm used is based on the method explained in Chapter 3 for the computation of the eigen-

1. The notations of the previous chapter are used again. Moreover, the concepts appearing in that article are given more accurately in the sequel.
2. Theorem 1.1.1.
3. Theorem 1.1.2.
4. [BT05] and [FHM67] are classical references on this issue.

values and eigenfunctions, and consists in *shape optimization* to find a candidate to the optimal domain. This step, including a Uzawa algorithm to take into consideration the volume constraint to work in manifolds different from $\mathbb{R}^2$, was detailed in Chapter 4. Actually, optimization on surfaces different from the plane does not seem to have been studied numerically.

In the first section, the optimization problem is stated, while some numerical results are presented in the second section, which come from [Str12b]. To check the validity of the program, a comparison is carried out with the results in [AF12] of the shapes obtained for the optimizers in $\mathbb{R}^2$ of the first fifteen eigenvalues. Furthermore, a validation is made for small domains in the sphere $\mathbb{S}^2$ and in the Poincaré disc $\mathbb{D}^2$, where a *similar* behaviour is expected. To illustrate various types of curvature, other examples in the sphere $\mathbb{S}^2$, in the Poincaré disc $\mathbb{D}^2$ and in a hyperboloid are also carried out.

5.1 Theoretical statement of the optimization problem

In spite of redundancies with the previous chapter, let us recall the main tools and notations about the underlying problem.

Let (M, g) be a smooth, complete Riemannian manifold of dimension 2 and of volume $V_M \in (0, \infty]$, let $\Omega_M \subset M$ be a domain in M, let Δ_g denote the Laplace operator given by (2.9) and (U, π) denote a chart where $\Omega_M \subset U \subset M$ and $\pi : U \to \mathbb{R}^2$ is a diffeomorphism onto its range. As before, the metric g is represented at each point $x \in M$ by the matrix $G(\pi(x))$ using the chart (U, π). In order to use the results of Chapter 3, assume that there exists a compact set K such that $\Omega_M \subset K \subset U$. So, the assumptions (H_1) and (H_2) on the metric g hold, that is the components $G_{i,j}$, $i, j = 1, 2$, of the matrix G satisfy:

(H_1) $G_{i,j}$ is bounded on Ω_M for $i, j = 1, 2$;

(H_2) there exists $C > 0$ such that $\det G \geq C$ on Ω_M.

Besides, with regard to the regularity of $\partial\Omega$, the assumption asserting that $\Omega := \pi(\Omega_M)$ has a polygonal boundary is sufficient to derive the weak formulation $(\mathcal{WP})$ of the underlying problem $(\mathcal{P})$, defined in Section 3.1, and is effective in the numerical computations. As before, the notation H stands for the space $L^2(\Omega)$ endowed with the scalar product defined by (3.2) in Section 3.1. The Spectral Theorem implies henceforth that there exist a sequence $(u_k)_{k\in\mathbb{N}\setminus\{0\}}$ of weak eigenfunctions defining a Hilbert basis of H and a sequence $(\lambda_k)_{k\in\mathbb{N}\setminus\{0\}}$ of associated weak eigenvalues such that

$$0 < \lambda_1 \leq \lambda_2 \leq \cdots \nearrow \infty.$$

The framework for the optimization problem is now set up: For $k \in \mathbb{N} \setminus \{0\}$ and a

certain fixed volume $0 < V < V_M$:

$$(\mathcal{P}_{opt}) \begin{cases} \text{Find a set } \Omega_k^* \subset M \text{ of volume } V, \text{ such that the } k\text{-th eigenvalue } \lambda_k \\ \text{appearing in problem } (\mathcal{WP}) \text{ satisfies} \\ \qquad\qquad \lambda_k(\Omega_k^*) \leq \lambda_k(\Omega), \\ \text{for all sets } \Omega \subset M \text{ of volume } V. \end{cases}$$

Remark 5.1.1. The main aspect of the discussion about the relation between the solutions and the weak solutions of the eigenvalue problem made at Section 3.1 lies in the regularity of $\partial\Omega$ or in the convexity of Ω. During the opimization process, the convexity of the polygonal domains are not guaranteed, so it might happen that over a solution Ω^* of the optimization problem, the problem $(\mathcal{P})$ does not make sense. This is the main reason why the *underlying problem* consists in $(\mathcal{WP})$ instead of $(\mathcal{P})$, also with the fact that this formulation is used numerically. Nevertheless, from now on, the scalar $\lambda(\Omega^*)$ resulting from the optimization process is abusively called an *eigenvalue* instead of a weak eigenvalue.

A natural question which arises now is the existence of a solution to the optimization problem. To answer it, the studies in [Buc12] and [MP13] expand the scope of the optimization problem to the class of quasi-open sets of $\mathbb{R}^2$. Indeed, in that framework his result [5] ensures the existence of a bounded solution Ω_k^* for each $k \in \mathbb{N} \setminus \{0\}$. So, it makes sense to study $(\mathcal{P}_{opt})$ numerically.

With regard to the approximated problem, the discretization using the Finite Element Method is described in Section 3.2, in particular it leads to solve the approximated problem $(\mathcal{WP}_h)$ defined in that section.

The main steps of an iteration of the optimization algorithm take place as follows:

I. Establishing a mesh given by the discretization of a boundary;

II. Solving the finite dimensional eigenproblem given in $(\mathcal{WP}_h)$;

III. Moving the boundary nodes of the mesh and hence get a new domain.

The first step consists in meshing a domain enclosed by a polygonal curve into triangles, to be compatible with the type of elements used. At the very beginning of the algorithm, an arbitrary—or guessed—closed curve is given. At the second step, the eigenvalue problem is solved numerically using a Lanczos process, as explained in Chapter 3 and recalled in Section 2.3. Finally, the third main step deals with the shape optimization itself. The domain is modified through a displacement of the nodes lying on its boundary. Hence, a new discretization of the boundary is obtained and if a stopping criterion is not reached, the algorithm goes back to step I. The point of this third step is to deform the domain in a *clever* way, in order to get a sequence of domains with increasingly lower associated eigenvalue. It is explained in Chapter 4.

5. His result extends to $\mathbb{R}^N$, $N \geq 1$.

5.2 Numerical computations

The aim of this subsection is to present the numerical computations obtained using the algorithm described above, to compare them with results from the literature and to investigate new examples on surfaces. It corresponds to Section 4 of the prepublication [Str12b].

5.2.1 Surfaces studied numerically

As mentioned in the previous section, the main idea is to use a chart (U, π) of the manifold (M, g) and to make the computations in the open set $\pi(U) \subset \mathbb{R}^2$ endowed with the corresponding metric. The manifolds (M, g) considered in this section are $\mathbb{R}^2$, the sphere $\mathbb{S}^2$, the Poincaré disc $\mathbb{D}^2$ and the upper sheet $H \subset \mathbb{R}^3$ of a hyperboloid.

The canonical representation of $\mathbb{R}^2$ and $\mathbb{D}^2$ are chosen. Recall that the metric tensor $G_{\mathbb{D}^2}$ evaluated in a point $(u, v) \in \mathbb{D}^2$ is given by

$$G_{\mathbb{D}^2}(u, v) = \frac{4}{\left(1 - u^2 - v^2\right)^2} I,$$

where I denotes the 2 by 2 identity matrix. For the sphere, the stereographic map (U, π_N) is used, where $U = \mathbb{S}^2 \setminus \{(0, 0, 1)\}$ and

$$\begin{array}{rcl} \pi_N : U & \to & \mathbb{R}^2 \\ (x, y, z) & \mapsto & \pi_N(x, y, z) = \dfrac{1}{1 - z}(x, y). \end{array}$$

The corresponding metric tensor $G_{\mathbb{S}^2}$ evaluated in a point $(u, v) \in \mathbb{R}^2$ is given by

$$G_{\mathbb{S}^2}(u, v) = \frac{4}{\left(1 + u^2 + v^2\right)^2} I.$$

The upper sheet of the hyperboloid defined by the equation $x^2 + y^2 - z^2 = -1$ is parametrized by $(\mathbb{R}_{>0} \times]0, 2\pi[, \alpha)$, where α is given by

$$\begin{array}{rcl} \alpha^{-1} : \mathbb{R}_{>0} \times]0, 2\pi[& \to & \mathbb{R}^3 \\ (r, \theta) & \mapsto & \left(r\cos(\theta), r\sin(\theta), \sqrt{1 + r^2}\right). \end{array}$$

The corresponding metric tensor G_H induced by the Euclidean metric of $\mathbb{R}^3$ on H and evaluated in a point $(r, \theta) \in \mathbb{R}_{>0} \times]0, 2\pi[$ is given by

$$G_H(r, \theta) = \begin{pmatrix} \dfrac{1 + 2r^2}{1 + r^2} & 0 \\ 0 & r^2 \end{pmatrix}.$$

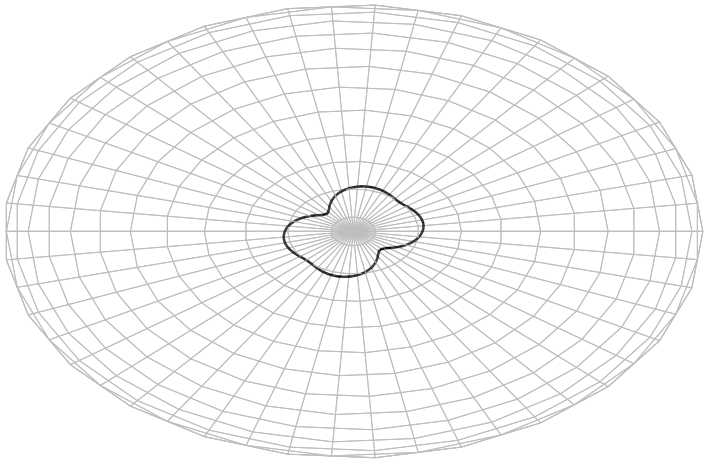

Figure 5.1: Plot of the optimizer for $\lambda_5(\Omega^*_{5,\mathbb{S}^2})$ among all domain of volume 0.1 in the sphere $\mathbb{S}^2$.

5.2.2 Numerical investigations

First, the program has been used to find the optimizer $\Omega^*_{k,\mathbb{R}^2}$, $k = 1, \dots, 15$, for the first fifteen eigenvalues in $\mathbb{R}^2$. Even if the volume constraint is not necessary in this case, no modifications have been done to compare the results with those in the article [AF12, p. 13]. Beginning with various initial discretized boundaries, the *best* shapes obtained match the ones in [AF12]. They are presented in Table 5.1, each eigenvalue being computed with and without masslumping. A discussion about the use of masslumping is done in Subsection 3.5.1. See also [AD03].

Another numerical experiment consists in computing the optimizers for *small* domains in the sphere and in the Poincaré disc. The optimizer for the k-th eigenvalue is denoted in the sphere by $\Omega^*_{k,\mathbb{S}^2}$, and in the Poincaré disc by $\Omega^*_{k,\mathbb{D}^2}$. Similar optimizers as in $\mathbb{R}^2$ are expected. Such computations have been made, with a fixed volume $V_0 = 0.1$, see Table 5.2. The domains in the Poincaré disc are also exhibited in this table. However the visualization of domains in the sphere being not always practical, only one is shown here, see Figure 5.1. All these results confirm the above expectation.

Then the value of the volume V_0 has been increased up to 2 for domains in the sphere and in the Poincaré disc. The relation between $\mathrm{vol}(\Omega^*_{k,\mathbb{S}^2})$ and $\lambda_k(\Omega^*_{k,\mathbb{S}^2})$ is exhibited in Figure 5.2.

Several remarks can be added to the results of these tables. A first observation is about the domains obtained having two connected components, namely the candidates for

Table 5.1: Numerical approximation of $\lambda_k(\Omega^*_{k,\mathbb{R}^2})$, $k = 1, \dots, 15$, for $\Omega^*_{k,\mathbb{R}^2} \subset \mathbb{R}^2$ the optimizer of volume 1 for the k-th eigenvalue and corresponding shapes. The last column contains the eigenvalues $\lambda_k(\tilde{\Omega})$ from [AF12].

k	$\lambda_k(\Omega^*_{k,\mathbb{R}^2})$ with (up) and without (down) masslumping	$\Omega^*_{k,\mathbb{R}^2}$	$\lambda_k(\tilde{\Omega})$ in [AF12]
1	18.16 18.17		-
2	36.32 36.39		-
3	46.27 46.30		-
4	64.56 64.78		-
5	78.46 78.53		78.2
6	88.89 89.05		88.52
7	106.40 106.51		106.14
8	119.84 120.01		118.9
9	133.71 134.06		132.68
10	144.39 144.82		142.72
11	160.32 160.55		159.39
12	173.97 174.37		172.85
13	188.47 188.84		186.97
14	201.64 202.22		198.96
15	210.65 211.16		209.63

Table 5.2: Numerical approximation of $\lambda_k(\Omega^*_{k,M})$, for $\Omega^*_{k,M}$ the optimizer of volume 0.1 in $M = \mathbb{S}^2$ and $\mathbb{D}^2$ for the k-th eigenvalue, $k = 1, \ldots, 15$.

k	$\lambda_k(\Omega^*_{k,\mathbb{S}^2}) \subset \mathbb{S}^2$ with (up) and without (down) masslumping	$\lambda_k(\Omega^*_{k,\mathbb{D}^2}) \subset \mathbb{D}^2$ with (up) and without (down) masslumping	$\Omega^*_{k,\mathbb{D}^2}$
1	180.746 180.855	182.591 182.639	
2	363.523 364.356	363.266 364.827	
3	460.671 460.927	463.821 464.068	
4	635.875 639.377	645.270 653.612	
5	782.932 784.251	788.515 789.829	
6	887.979 888.975	892.784 894.214	
7	1062.208 1063.127	1085.715 1089.251	
8	1197.243 1199.235	1199.010 1207.212	
9	1328.802 1330.355	1338.065 1341.360	
10	1437.185 1439.525	1441.793 1445.205	
11	1580.123 1583.765	1622.091 1632.550	
12	1736.980 1738.957	1752.412 1757.700	
13	1886.076 1890.493	1884.925 1887.360	
14	1996.383 1999.437	2019.539 2026.394	
15	2120.629 2125.772	2138.361 2148.878	

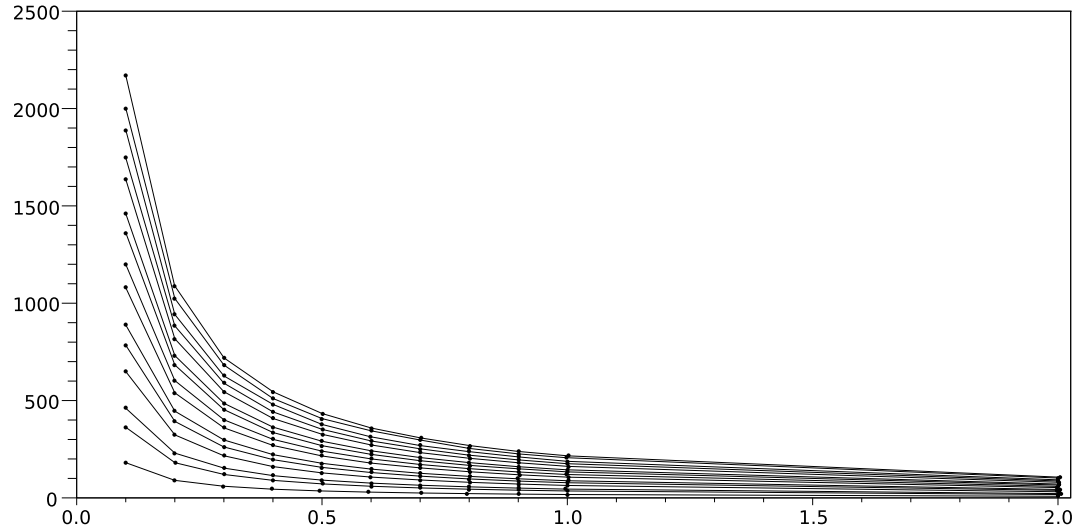

Figure 5.2: Plot of $\lambda_k(\Omega^*_{k,\mathbb{S}^2})$ with respect to $\mathrm{vol}(\Omega^*_{k,\mathbb{S}^2})$ for $k = 1, \dots, 15$.

the optimizer of the second and the fourth eigenvalue. The ratio between the volume of their connected components has been performed in $\mathbb{R}^2$, in the sphere and in the Poincaré disc. First for the plane: theoretically, the ratio for the second eigenvalue is 1 by the Krahn-Szegő Theorem. Moreover, if the optimizer for the fourth eigenvalue is the union of two discs, in accordance with the numerical results, this ratio is

$$\frac{j^2_{0,1}}{j^2_{1,1}} \simeq 0.394,$$

by a result from B. Colbois and A. El Soufi [CES12]. Numerically, we found 0.390. Although no such results exist in $\mathbb{S}^2$ and in the Poincaré disc, due to the non-invariance by homothety of $\Omega \mapsto \mathrm{vol}(\Omega)\lambda_k(\Omega)$ in these manifolds, the corresponding ratios have been computed for comparison. In $\mathbb{S}^2$, they are about 0.997 and 0.392 respectively, whereas for the Poincaré disc, they are about 0.999 and 0.387.

Besides, another remark is related to the evolution of $\lambda_k(\Omega^*_{k,E})$, $k = 1, \dots, 15$, with respect to the volume of $\Omega^*_{k,M}$ for the three models $M = \mathbb{R}^2, \mathbb{S}^2, \mathbb{D}^2$. In the plane, this relation is of the form $\lambda_k(\Omega^*_{k,\mathbb{R}^2}) = cst_k/\mathrm{vol}(\Omega^*_{k,\mathbb{R}^2})$, $k = 1, \dots, 15$, where cst_k is a positive constant, explicitly known for $k = 1$ and 2 by the Faber-Krahn and the Krahn-Szegő Theorems. The corresponding plots for $\mathbb{S}^2$ are given in Figure 5.2. In each case, the shape of the optimizer does not change considerably for close volume, as illustrated in Figure 5.4, for $\lambda_{10}(\Omega^*_{10,\mathbb{S}^2})$. To compare the three models, see Figure 5.3 which shows the evolution for the first two eigenvalues. Notice that these eigenvalues decrease less in the Poincaré disc than in $\mathbb{R}^2$ and in the sphere, where the slope is the deepest.

Finally, some computations in the upper sheet H of the hyperboloid have been per-

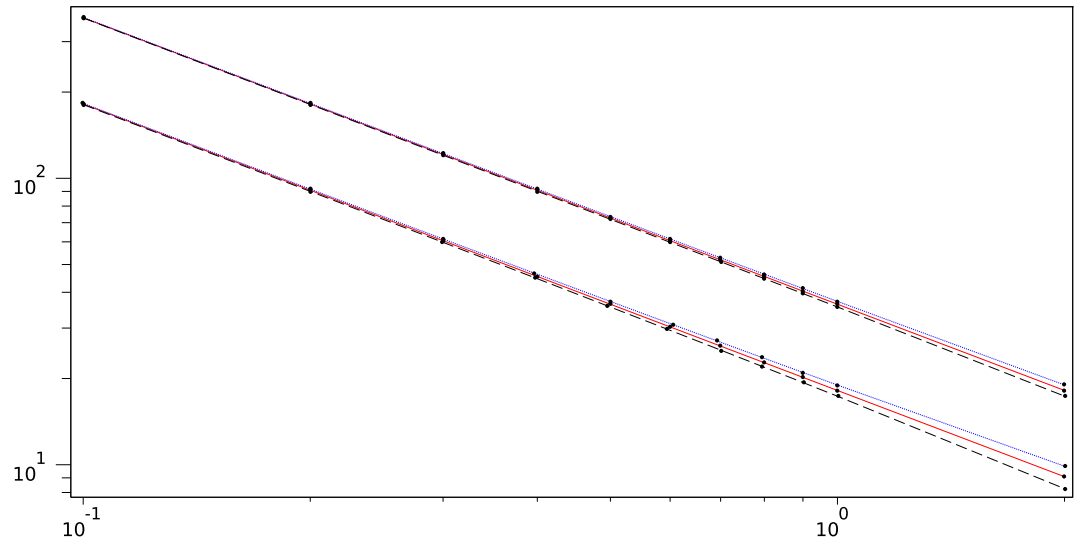

Figure 5.3: Plot of $\lambda_k(\Omega^*_{k,M})$ with respect to $\mathrm{vol}(\Omega^*_{k,M})$ for $k = 1, 2$ and $M = \mathbb{R}^2, \mathbb{S}^2, \mathbb{D}^2$, in a logarithmic scale. The blue dotted curve, the red plain curve and the dashed black curve concern the Poincaré disc, $\mathbb{R}^2$ and the sphere respectively. The modulus of the slope for the Poincaré disc is less than 1, whereas it is equal to 1 for $\mathbb{R}^2$ and it is larger than 1 for the sphere.

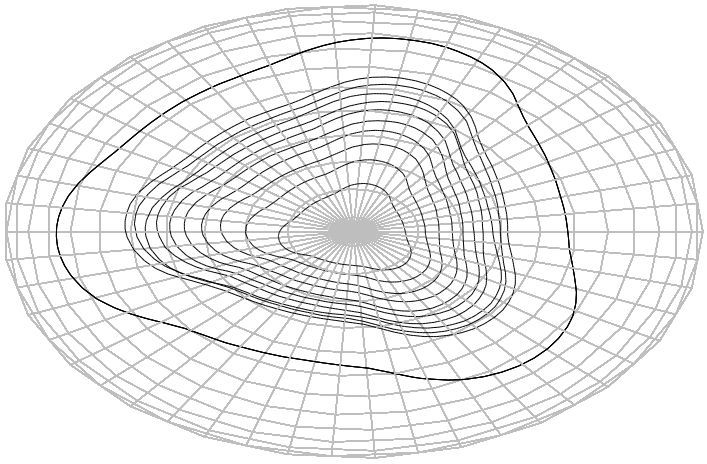

Figure 5.4: Plot of the optimizers for $\lambda_{10}(\Omega^*_{10,\mathbb{S}^2})$ and $\mathrm{vol}(\Omega^*_{10,\mathbb{S}^2}) = 0.1, 0.2, \ldots, 0.9, 1$ and 2.

formed. The Gaussian curvature of this model is given by

$$\kappa(r,\theta) = \frac{1}{(1+2r^2)^2}.$$

In particular, the Gaussian curvature is non-constant, strictly positive and attains its maximum at the point $(0,0)$ with $\kappa(0,0) = 1$. Not surprisingly, numerical experiments show that the optimizer $\Omega^*_{1,H}$ for λ_1 is a disc centred at $(0,0,1)$. But, although the curvature lies between 0 and 1 in the hyperboloid, this eigenvalue is larger than the first eigenvalue of a ball of same volume in the plane (curvature 0), which is larger than the first eigenvalue of a ball of same volume in the sphere (curvature 1). For instance, denoting by $B_{M,0.01}$ the ball of volume 0.01 in M, it yields numerically

$$\begin{aligned}
\lambda_1(B_{\mathbb{S}^2,0.01}) &\simeq 1816.57 < \\
\lambda_1(B_{\mathbb{R}^2,0.01}) &\simeq 1816.80 < \\
\lambda_1(B_{\mathbb{D}^2,0.01}) &\simeq 1817.67 < \\
\lambda_1(B_{H,0.01}) &\simeq 1819.10.
\end{aligned}$$

For the second eigenvalue, the obtained candidate $\Omega^*_{2,H}$ for the optimizer is two discs of same volume, tangent at the point $(0,0,1)$. The eigenvalue computed is about 3643.50. So, as for the first eigenvalue, the same ranking with respect to the space occurs for the second eigenvalue.

Since the Gaussian curvature is radial and maximum at $(0,0)$, an optimizer $\Omega^*_{k,H}$ having its centre of mass at the origin is expected. The results found for the first two eigenvalues confirm this property. We focused also on the cases $k = 4$ and $k = 13$ since the corresponding optimizer found in the spaces previously studied are not symmetric. Numerically, for a volume equals 0.1, the candidates for the optimizer are those expected (*same shape* as the corresponding domains found before) and their centre of mass are at $(0,0,1)$ (actually at a distance of about 10^{-9} of this point). See Figure 5.5. Looking at the eigenvalues obtained, both $\lambda_4(\Omega^*_{4,H}) \simeq 658.329$ and $\lambda_{13}(\Omega^*_{13,H}) \simeq 1905.911$ are above the corresponding eigenvalues in $\mathbb{R}^2$, in $\mathbb{S}^2$ and in $\mathbb{D}^2$.

In conclusion, the algorithm presented in this chapter gives the same optimizers in $\mathbb{R}^2$ as those found previously by the community, and permits to extend the study to other surfaces, even if they do not embed into $\mathbb{R}^3$. It can thereby give a intuition in some cases not yet well known theoretically. Thus, some particularities arise quickly because few results exist, as the fact that the eigenvalues of the optimizers for domains in the hyperboloid lie above those in $\mathbb{R}^2$ and in $\mathbb{S}^2$.

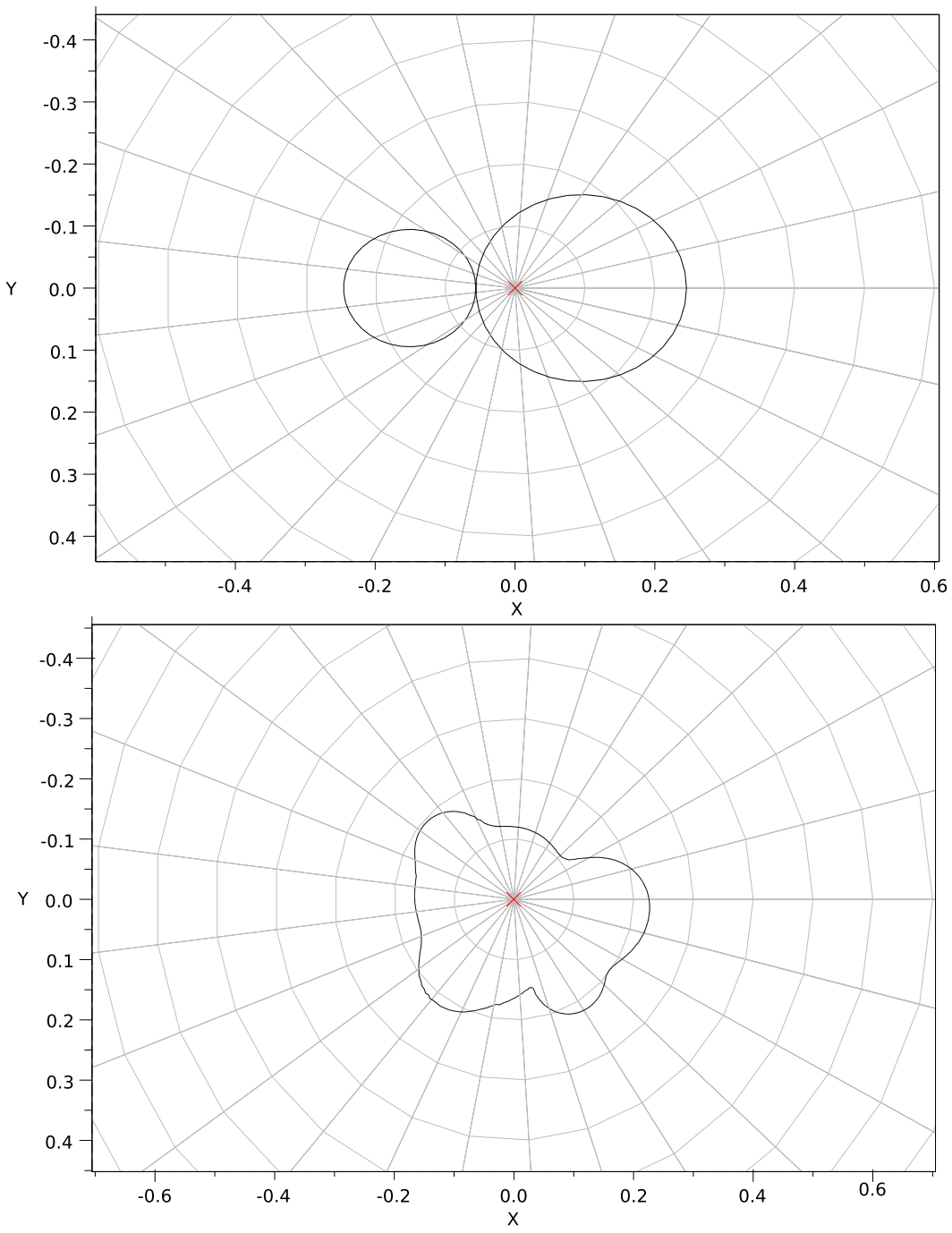

Figure 5.5: Plot of the optimizers $\Omega^*_{4,H}$ for the fourth eigenvalue (above), and $\Omega^*_{13,H}$ for the thirteenth eigenvalue (below), among all domain of volume 0.1. Their center of mass, indicated by a red cross, lie at the origin.

Appendix A

Some notions on functional analysis, distributions theory and Sobolev spaces

The present appendix is intended to serve as a referral for fundamental notions employed in this document. It takes place aside from the other chapters, for sake of clarity for most of the readers who are familiar with these notions and who might have seen this reminder more as a way of losing track than as a gain of comprehension if it was inside the main content. It is concerned with functional analysis, especially distributions theory and Sobolev spaces. It is from various books, namely [Bre11], [Kre78], [Hör83], [Rud73] and [Sch66], which could be considered as references on these topics. Refer to them for the proof of the results reported here. The notations of this appendix come from [Sch66].

A.1 General notions and results about Hilbert spaces

In this section, $(H, (\cdot\,|\,\cdot))$ denotes a Hilbert space over $\mathbb{R}$, H^* the topological dual space of H, and V and W two Banach spaces. Moreover, let $\mathcal{B}(V;W)$ be the set of all bounded linear operators defined on V and taking values in W, and $\mathcal{B}(V)$, instead of $\mathcal{B}(V;V)$, be the set of all bounded linear operators defined from V to itself.

Definition - Proposition A.1.1 ([Rud73, Theorem 4.10]). If $T \in \mathcal{B}(H)$, then there exists a unique bounded linear operator $T^* \in \mathcal{B}(H)$, called *adjoint operator* of T, satisfying

$$(Tx|y) = (x|T^*y), \quad \forall x, y \in H.$$

T is called *self-adjoint* if $T = T^*$.

Definition A.1.2 ([Rud73, Definition 4.16]). A bounded linear operator $T \in \mathcal{B}(V;W)$ is called *compact* if for all bounded subsets $A \subset V$, $T(A) \subset W$ has a compact closure.

Remark A.1.1. An equivalent definition of a compact operator can be readily deduced: A bounded linear operator $T \in \mathcal{B}(V;W)$ is called *compact* if every bounded sequence

$\{x_n\}_n$ in V contains a subsequence $\{x_{n_i}\}_{n_i}$ such that $\{T(x_{n_i})\}_{n_i}$ converges to a point of W.

Theorem A.1.3 (Riesz Representation Theorem, [Kre78, Theorem 3.8-1]). *The topological dual space H^* of H is canonically isomorph to H, that is, for every bounded linear functional $l \in H^*$, there exists a unique $t_l \in H$ such that*

$$l(v) = (v|t_l), \quad \forall v \in H,$$

and $\|l\|_{H^*} = \|t_l\|_H$.

Definition A.1.4 ([Bre11, Definition in Section 5.3]). A bilinear form $a : H \times H \to \mathbb{R}$ is said to be

(i) *continuous*, if there is a constant $C > 0$ such that $|a(u,v)| \leq C \|u\|_H \|v\|_H$, for all $u, v \in H$;

(ii) *coercive* or *H-elliptic*, if there is a constant $\alpha > 0$ such that $a(v,v) \geq \alpha \|v\|_H^2$, for all $v \in H$.

Theorem A.1.5 (Lax-Milgram Theorem, [Bre11, Corollary 5.8]). *Let $a : H \times H \to \mathbb{R}$ be a continuous, coercive, bilinear form and $l \in H^*$ be a bounded linear form. Then, there exists a unique element $u \in H$ such that*

$$a(u,v) = l(v), \quad \forall v \in H.$$

Moreover, denoting by $J : H \to \mathbb{R}$ the functional given by $J(v) = \frac{1}{2}a(v,v) - l(v)$, if a is symmetric, then $u \in H$ is characterized by the property

$$J(u) = \min_{v \in H} J(v).$$

A.2 Distributions theory and Sobolev spaces

Throughout this section, $N \in \mathbb{N}$ denotes the dimension of the ambient space $\mathbb{R}^N$, $N \geq 2$.

Definition A.2.1. A *domain* is a bounded open set of $\mathbb{R}^N$.

Henceforth, Ω denotes a domain of $\mathbb{R}^N$ and K a compact set of $\mathbb{R}^N$, although some definitions or results may be extended to a more general context, for instance for unbounded open sets. However, the framework within Sobolev spaces are used in the main part of the document takes place in a domain $\Omega \subset \mathbb{R}^N$.

Notation A.2.2 ([Sch66, Chapter I]). In the sequel, the following notations are used:

$$\begin{aligned}
\mathcal{C}_c &= \left\{\phi \in \mathcal{C}(\mathbb{R}^N) \mid \operatorname{supp}\phi \text{ is a compact set of } \mathbb{R}^N\right\}, \\
\mathcal{C}_{c,\Omega} &= \{\phi \in \mathcal{C}_c \mid \operatorname{supp}\phi \subset \Omega\}, \\
\mathcal{C}_c^\infty &= \left\{\phi \in \mathcal{C}^\infty(\mathbb{R}^N) \mid \operatorname{supp}\phi \text{ is a compact set of } \mathbb{R}^N\right\}, \\
\mathcal{C}_c^\infty(K) &= \{\phi \in \mathcal{C}_c^\infty \mid \operatorname{supp}\phi \subset K\}, \\
\mathcal{C}_c^\infty(\Omega) &= \{\phi \in \mathcal{C}^\infty(\Omega) \mid \operatorname{supp}\phi \text{ is a compact set in } \Omega\}.
\end{aligned}$$

Definition A.2.3. The space $\mathcal{C}_c^\infty$, respectively $\mathcal{C}_c^\infty(\Omega)$, is called *space of test functions*, respectively *space of test functions* on Ω.

Following the approach in [Sch66, p. 24], the space $\mathcal{C}_c^\infty(K)$ is endowed with the following topology: a sequence $(\phi_j)_j$ of functions in $\mathcal{C}_c^\infty(K)$ *converges* to 0 in $\mathcal{C}_c^\infty(K)$ if the sequences $(\phi_j)_j$ and $(\partial^\alpha \phi_j)_j$, converge uniformly to 0 in $\mathbb{R}^N$, for all multi-indices $\alpha = (\alpha_1, \ldots, \alpha_N) \in \mathbb{N}^N$ where

$$\partial^\alpha = \frac{\partial^{\alpha_1 + \cdots + \alpha_N}}{\partial x_1^{\alpha_1} \cdots \partial x_N^{\alpha_N}}.$$

This defines a notion of *sequential continuity* on $\mathcal{C}_c^\infty(K)$. This topology is defined by the family of semi-norms:

$$N_\alpha(\phi) = \sup_{\boldsymbol{x} \in \mathbb{R}^N} \|\partial^\alpha \phi(\boldsymbol{x})\|_{\mathbb{R}^N}, \quad \alpha \in \mathbb{N}^N.$$

If $\mathcal{C}_{c,K}$ is endowed with the topology of the uniform convergence, then the topology induced by $\mathcal{C}_{c,K}$ on $\mathcal{C}_c^\infty(K)$ is coarser than this new one on $\mathcal{C}_c^\infty(K)$. Indeed, if $(\phi_j)_j$, $\phi_j \in \mathcal{C}_c^\infty$ for all j, converges to 0 for this new topology, it converges also uniformly to 0.

Definition A.2.4 ([Sch66, Section I.2]). A *distribution* T is a linear form on $\mathcal{C}_c^\infty$, which is sequentially continuous, that is, if $(\phi_j)_j$ is a sequence of functions in $\mathcal{C}_c^\infty$, with $\operatorname{supp} \phi_j$ in a compact subset K for all j, which converges to 0 in $\mathcal{C}_c^\infty(K)$, then $(T(\phi_j))_j$ converges to 0 in $\mathbb{R}$.

Notation A.2.5. A distribution is said to be a *continuous* linear form on $\mathcal{C}_c^\infty$, and for a test-function $\phi \in \mathcal{C}_c^\infty$, the notation $\langle T, \phi \rangle$ is frequently used instead of $T(\phi)$. Moreover, it follows readily that the set of all distributions forms a vector space, denoted by $\mathcal{C}_c^{\infty\prime}$— analogously $\mathcal{C}_c^{\infty\prime}(\Omega)$, obtained by substituting $\mathbb{R}^N$ by Ω, denotes the set of all distributions on Ω—.

Theorem A.2.6 ([Hör83, Theorem 2.1.4]). *A linear form T on $\mathcal{C}_c^\infty$ is a distribution if and only if for every compact set $K \subset \mathbb{R}^N$, there exist a constant $C > 0$ and a positive integer $d \in \mathbb{N}$ such that*

$$|\langle T, \phi \rangle| \leq C \sum_{\substack{\alpha \in \mathbb{N}^N, \\ |\alpha| \leq d}} \sup_{\boldsymbol{x} \in K} |\partial^\alpha \phi(\boldsymbol{x})|, \quad \forall \phi \in \mathcal{C}_c^\infty(K).$$

where $|\alpha| = \sum_{j=1}^N \alpha_j$.

The *weak topology* in $\mathcal{C}_c^{\infty\prime}$ shall be used: a sequence $(T_j)_j$, $T_j \in \mathcal{C}_c^{\infty\prime}$ for all j, converges to T if $(\langle T_j, \phi \rangle)_j$ converges to $\langle T, \phi \rangle$, for every $\phi \in \mathcal{C}_c^\infty$.

Theorem A.2.7 ([Hör83, Theorem 2.1.8]). [1] *Let $(T_j)_j$ be a sequence, $T_j \in \mathcal{C}_c^{\infty\prime}$. If the limit*

$$\langle T, \phi \rangle := \lim_{j \to \infty} \langle T_j, \phi \rangle$$

1. The analogous result holds in $\mathcal{C}_c^{\infty\prime}(\Omega)$.

exists for every $\phi \in \mathcal{C}_c^\infty$, *then* $T \in \mathcal{C}_c^{\infty\prime}$. *Thus,* $(T_j)_j$ *converges to* T *in* $\mathcal{C}_c^{\infty\prime}$. *So,* $\mathcal{C}_c^{\infty\prime}$ *is a complete vector space.*

Definition - Proposition A.2.8 ([Hör83, Definition 3.1.1]). Let $T \in \mathcal{C}_c^{\infty\prime}$ be a distribution. For every multi-index $\alpha = (\alpha_1, ..., \alpha_N) \in \mathbb{N}^N$, the *derivative in the sense of the distributions theory* of T, or simply *derivative* of T, denoted by $\partial^\alpha T$, is the distribution defined by

$$\langle \partial^\alpha T, \phi \rangle = (-1)^{|\alpha|} \langle T, \partial^\alpha \phi \rangle, \quad \forall \phi \in \mathcal{C}_c^\infty,$$

where $|\alpha| = \sum_{j=1}^N \alpha_j$.

Remark A.2.1 (Distributions defined on a differentiable manifold [Sch66, Section I.5]). The notion of distribution can be generalized to the context of a N-dimensional differentiable manifold M of class $\mathcal{C}^\infty$. Similarly, the following

$$\mathcal{C}_c^\infty(M) = \{\phi \in \mathcal{C}^\infty(M) \mid \operatorname{supp} \phi \text{ is a compact set}\}$$

is defined and the associated space of distributions on M is denoted by $\mathcal{C}_c^{\infty\prime}(M)$. This latter space has properties analogous to $\mathcal{C}_c^{\infty\prime}$, except for certain aspects:

- A smooth vector field is needed to define derivative of distributions on M;
- A function $f : M \to \mathbb{R}$ can generally not be regarded as a distribution on M: a volume element [2] $\mathrm{d}\Phi$ must be chosen beforehand.

The book [Heb96] provides more details about distributions and Sobolev spaces on a Riemannian manifold.

Definition A.2.9 (Sobolev spaces $W^{m,p}(\Omega)$ [Heb96, Definition 2.1], [AF03, Definition 3.2]). Let $m \in \mathbb{N}$ and $p \in [1, \infty]$. The function space $W^{m,p}(\Omega)$ defined by

$$W^{m,p}(\Omega) = \left\{u \in L^p(\Omega) \mid \partial^\alpha u \in L^p(\Omega),\, \alpha \in \mathbb{N}^N,\, |\alpha| \leq m\right\},$$

and endowed with the norm

$$\|u\|_{W^{m,p}(\Omega)} = \left(\sum_{\alpha \in \mathbb{N}^N, |\alpha| \leq m} \|\partial^\alpha u\|_{L^p(\Omega)}^p \right)^{1/p},$$

if $p \neq \infty$, or

$$\|u\|_{W^{m,\infty}(\Omega)} = \max_{\alpha \in \mathbb{N}^N, |\alpha| \leq m} \|\partial^\alpha u\|_{L^\infty(\Omega)},$$

if $p = \infty$, is called *Sobolev space of order* m. [3]

If $p = 2$, $W^{m,2}(\Omega)$ is denoted by $H^m(\Omega)$.

Remark A.2.2. For $m \in \mathbb{N}$, we define $W^{m,\infty}(\mathbb{R}^N, \mathbb{R}^{N'})$ as the space of all mappings $\psi : \mathbb{R}^N \to \mathbb{R}^{N'}$, $(x_1, \ldots, x_N) \mapsto \psi(x_1, \ldots, x_N) = (\psi_1(x_1, \ldots, x_N), \ldots, \psi_{N'}(x_1, \ldots, x_N))$, such that $\psi_i \in W^{m,\infty}(\mathbb{R}^N)$, for all $1 \leq i \leq N'$.

2. See Subsection 2.1.1.

3. For an unbounded open set Ω, the spaces $W^{m,p}(\Omega)$ can also be defined from $L^p(\Omega)$, in particular, $W^{m,p}(\mathbb{R}^N)$ also makes sense.

Theorem A.2.10 ([AF03, Theorems 3.3 and 3.6]). *For all $m \in \mathbb{N}$ and $p \in [1, \infty]$, the Sobolev spaces $(W^{m,p}(\Omega), \|\cdot\|_{W^{m,p}(\Omega)})$ are Banach spaces. Moreover, for all $m \in \mathbb{N}$ and $p \in [1, \infty[$, $(W^{m,p}(\Omega), \|\cdot\|_{W^{m,p}(\Omega)})$ are separable. In particular, for all $m \in \mathbb{N}$, $H^m(\Omega)$ are separable Hilbert spaces endowed with the inner product given by*

$$(u|v)_{H^m(\Omega)} = \sum_{\alpha \in \mathbb{N}^N, |\alpha| \leq k} (\partial^\alpha u | \partial^\alpha v)_{L^2(\Omega)} .$$

Definition - Proposition A.2.11 ([Heb96, Definition 2.6], [AF03, Definition 3.2]). For a positive integer $m \in \mathbb{N}$, set the following notations:

- $H_0^m(\Omega)$ denotes the closure of $\mathcal{C}_c^\infty(\Omega)$ in $H^m(\Omega)$;
  Endowed with the inner product induced by $H^m(\Omega)$, $H_0^m(\Omega)$ is a Hilbert space.
- $H^{-m}(\Omega)$ denotes the topological dual space of $H_0^m(\Omega)$.

By the Riesz Representation Theorem A.1.3, $H^{-m}(\Omega)$ can be identified to $H_0^m(\Omega)$. Moreover, the following result characterizes a distribution T on Ω belonging to $H^{-m}(\Omega)$.

Proposition A.2.12 ([AF03, Theorem 3.9]). *A distribution T on Ω belongs to $H^{-m}(\Omega)$ if and only if there exist functions $f_\alpha \in L^2(\Omega)$ such that T can be written as*

$$T = \sum_{\alpha \in \mathbb{N}^N, |\alpha| \leq m} \partial^\alpha f_\alpha, \quad f_\alpha \in L^2(\Omega).$$

Analogously, the space $H_0^m(\mathbb{R}^N)$ can be defined by taking the closure of $\mathcal{C}_c^\infty$ in $H^m(\mathbb{R}^N)$, for $m \in \mathbb{N}$. It leads that $H_0^m(\mathbb{R}^N) = H^m(\mathbb{R}^N)$. In the same way, $H^{-m}(\mathbb{R}^N)$ represents the topological dual space of $H_0^m(\mathbb{R})$ and a characterization using the Fourier transform holds.

Sobolev spaces are also defined for fractional order $s \in \mathbb{R}$. Several ways exist to introduce them leading to equivalent definitions. For instance [Ada75, Chapter 7] uses complex interpolations to define $W^{s,p}(\mathbb{R}^N)$ over the whole space as a first step, then over a sufficiently smooth domain $\Omega \subset \mathbb{R}^N$ thanks to continuation operators. Following [DNPV12, Section 2], we present in this appendix an approach starting from *a kind of* generalization of the Hölder condition for $L^p(\Omega)$. Sobolev spaces of fractional order between 0 and 1 are defined first, then extended to any positive real number.

Definition A.2.13. Let $\Omega \subset \mathbb{R}^N$ be an open set. For $\sigma \in (0,1)$ and $p \in [1, \infty)$, the *Sobolev space of order σ* denoted by $W^{\sigma,p}(\Omega)$ is the functional space defined by

$$W^{\sigma,p}(\Omega) = \left\{ u \in L^p(\Omega) \mid (x,y) \mapsto \frac{|u(x) - u(y)|}{|x-y|^{\frac{N}{p}+\sigma}} \in L^p(\Omega \times \Omega) \right\},$$

and endowed with the norm

$$\|u\|_{W^{\sigma,p}(\Omega)} = \left(\|u\|_{L^p(\Omega)}^p + \int_\Omega \int_\Omega \frac{|u(x) - u(y)|^p}{|x-y|^{n+\sigma p}} \mathrm{d}x\mathrm{d}y \right)^{1/p}.$$

As expected, the following proposition derived from [DNPV12, Proposition 2.1 & Corollary 2.3] holds.

Proposition A.2.14 (derived from [DNPV12]). *For an open subset $\Omega \subset \mathbb{R}^N$, and two scalars $\sigma \in (0,1)$ and $p \in [1,\infty)$, Sobolev spaces $(W^{\sigma,p}(\Omega), \|\cdot\|_{W^{\sigma,p}(\Omega)})$ are Banach spaces. Moreover, for $\sigma \leq \sigma' < 1$, there exists a positive constant $C := C(n,s,p)$ such that for every measurable function $u : \Omega \to \mathbb{R}$,*

$$\|u\|_{W^{\sigma,p}(\Omega)} \leq C\|u\|_{W^{\sigma',p}(\Omega)}, \tag{A.1}$$

meaning that

$$W^{\sigma',p}(\Omega) \subseteq W^{\sigma,p}(\Omega). \tag{A.2}$$

Furthermore, if $\partial\Omega$ is a polygon, the equation (A.1) *and the inclusion* (A.2) *can be extended to $\sigma' = 1$.*

The definition of Sobolev spaces for $s \in \mathbb{R} \cap (1,\infty)$ can be given.

Definition A.2.15. Let $\Omega \subset \mathbb{R}^N$ be an open set, $s \in (0,\infty)$ and $p \in [1,\infty)$. Setting $s = m + \sigma$, with $m \in \mathbb{N}$ and $\sigma \in [0,1)$ the *Sobolev space of order s* denoted by $W^{s,p}(\Omega)$ is the functional space defined by

$$W^{s,p}(\Omega) = \left\{ u \in W^{m,p}(\Omega) \mid \partial^\alpha u \in W^{\sigma,p}(\Omega),\, \alpha \in \mathbb{N}^N,\, |\alpha| = m \right\},$$

and endowed with the norm

$$\|u\|_{W^{s,p}(\Omega)} = \left(\|u\|^p_{W^{m,p}(\Omega)} + \sum_{|\alpha|=m} \|\partial^\alpha u\|_{W^{\sigma,p}(\Omega)} \right)^{1/p}.$$

Remark A.2.3. From the previous results, it comes readily that Sobolev spaces $W^{s,p}(\Omega)$ are also Banach spaces for $s \in \mathbb{R}_+$, and for $s = m \in \mathbb{N}$, that Definition A.2.15 coincides with Definition A.2.9.

Let us go back to $H^m_0(\Omega)$ for a positive integer $m \in \mathbb{N}$ and a domain Ω, and define another norm, equivalent to the norm induced by $H^m(\Omega)$, on this function space.

Proposition A.2.16 (Poincaré's Inequality [AF03, Theorem 6.30]). *There exists a positive constant $C := C(\Omega) > 0$, such that for all $\phi \in \mathcal{C}^\infty_c(\Omega)$,*

$$\|\phi\|_{L^2(\Omega)} \leq C \left(\sum_{\alpha \in \mathbb{N}^N, |\alpha|=1} \|\partial^\alpha \phi\|^2_{L^2(\Omega)} \right)^{1/2}.$$

It extends[4]*, using a density argument, to every $u \in H^1_0(\Omega)$, that is*

$$\|u\|^2_{L^2(\Omega)} \leq C \left(\sum_{\alpha \in \mathbb{N}^N, |\alpha|=1} \|\partial^\alpha u\|^2_{L^2(\Omega)} \right)^{1/2}.$$

4. For this result, it is necessary that Ω has *finite width*, that is Ω is bounded in one direction. Moreover, this assertion still holds for $1 \leq p < \infty$ instead of $p = 2$.

Proposition A.2.17 ([AF03, Corollary 6.31]). *The semi-norm on $H^m(\Omega)$ given by*

$$\|u\|_{H_0^m(\Omega)} = \left(\sum_{\alpha \in \mathbb{N}^N, |\alpha|=m} \|\partial^\alpha u\|^2_{L^2(\Omega)} \right)^{1/2}, \quad u \in H^m(\Omega),$$

is a norm on $H_0^m(\Omega)$, equivalent to the standard norm $\|\cdot\|_{H^m(\Omega)}$.

Finally, let us recall some results about Sobolev spaces, which shall be very helpful in the main part of the document.

Theorem A.2.18 (Particular case [5] of the Rellich-Kondrachov Theorem [AF03, Theorem 6.3]). *Let Ω be a domain of $\mathbb{R}^2$. The injection $H_0^1(\Omega) \hookrightarrow L^2(\Omega)$ is compact. Moreover, if Ω has a Lipschitz boundary, then the injection $H^1(\Omega) \hookrightarrow L^2(\Omega)$ is compact.*

Let us assume henceforth that Ω is regular, for example, $\partial\Omega$ is of class $\mathcal{C}^1$. Consider the mapping $u \mapsto u_{|\partial\Omega}$ defined on $\mathcal{C}_c^1(\overline{\Omega})$, namely the functional space $\mathcal{C}^1(\overline{\Omega})$ with compact support in Ω, taking values in $L^2(\partial\Omega)$. Using a density argument, it can be extended to $H^1(\Omega)$ in a bounded linear operator called the *trace operator*, or simply *trace*, on $\partial\Omega$, and also denoted by $u \mapsto u_{|\partial\Omega}$. The following properties [6] of the trace operator are worthwhile:

1. If u belongs to $H^1(\Omega)$, then $u_{|\partial\Omega}$ is in $H^{1/2}(\partial\Omega)$ and there exists a constant $C > 0$ such that
$$\left\| u_{|\partial\Omega} \right\|_{H^{1/2}(\partial\Omega)} \leq C \|u\|_{H^1(\Omega)}, \quad \forall u \in H^1(\Omega);$$
2. The trace operator defined from $H^1(\Omega)$ surjects onto $H^{1/2}(\partial\Omega)$;
3. The kernel of the trace operator is $H_0^1(\Omega)$;
4. In that framework, the *Green Formula* holds:
$$\int_\Omega \frac{\partial u}{\partial x_i} v = -\int_\Omega u \frac{\partial v}{\partial x_i} + \int_{\partial\Omega} uv \, (\boldsymbol{n}|\boldsymbol{e_i}) \, \mathrm{d}\sigma, \quad \forall u, v \in H^1(\Omega),$$
where $\boldsymbol{n}$ denotes the ouward unit vector field normal to $\partial\Omega$. By extension:
$$-\int_\Omega \Delta u v = \int_\Omega (\boldsymbol{\nabla u}|\boldsymbol{\nabla v}) - \int_{\partial\Omega} \frac{\partial u}{\partial n} v \, \mathrm{d}\sigma, \quad \forall u, v \in H^2(\Omega),$$
where $\dfrac{\partial u}{\partial n} := (\boldsymbol{\nabla u}|\boldsymbol{n})$ is the normal derivative of u.

5. The statement in [AF03] is more general.
6. See [AF03, Chapters 5 and 7].

Appendix B

A complete example: the optimization of λ_7 in the Poincaré disc

The motivation to present an example in the Poincaré disc $\mathbb{D}^2$ comes from the need to take the metric into consideration to deal with it. Moreover, displaying the resulting domains is convenient in this manifold. On the other hand, the choice of λ_7 depends on various reasons, including the fact that it is the first non symmetric optimizer among other local minima we can reach starting from various initial domain.

B.1 Starting from various initial domains

The method of optimization described in the main part of the document is based on a descent algorithm, which provides *local* minima. Starting from various initial domains is necessary to enhance the effectiveness of the method to find *global* minima. In this example, four different initial domains of volume 0.1 are considered: a square Ω_s, a disc Ω_d, two squares of same volume Ω_{2s} and tow discs of same volume Ω_{2d}. The square and the disc are centred at the origin, whereas the connected components in the two other examples are (arbitrarily) centred at $(0, \pm 0.2)$. Each domain's boundary is discretized uniformly using 100 points, except for Ω_{2s}, whose boundary contains 104 points, that is each edge is subdivided into 13 pieces. Then, a mesh is built. See figure B.1.

Remark B.1.1. The mesh created for these domains does not take the metric into consideration.

Each of these initial domains leads to a different candidate for the optimal domain. To be consistent with the notations in the main part of the document, let Ω^*_{dom} denote the domain returned by the algorithm starting from Ω_{dom}, for dom being s, d, $2s$ and $2d$. See Figure B.2.

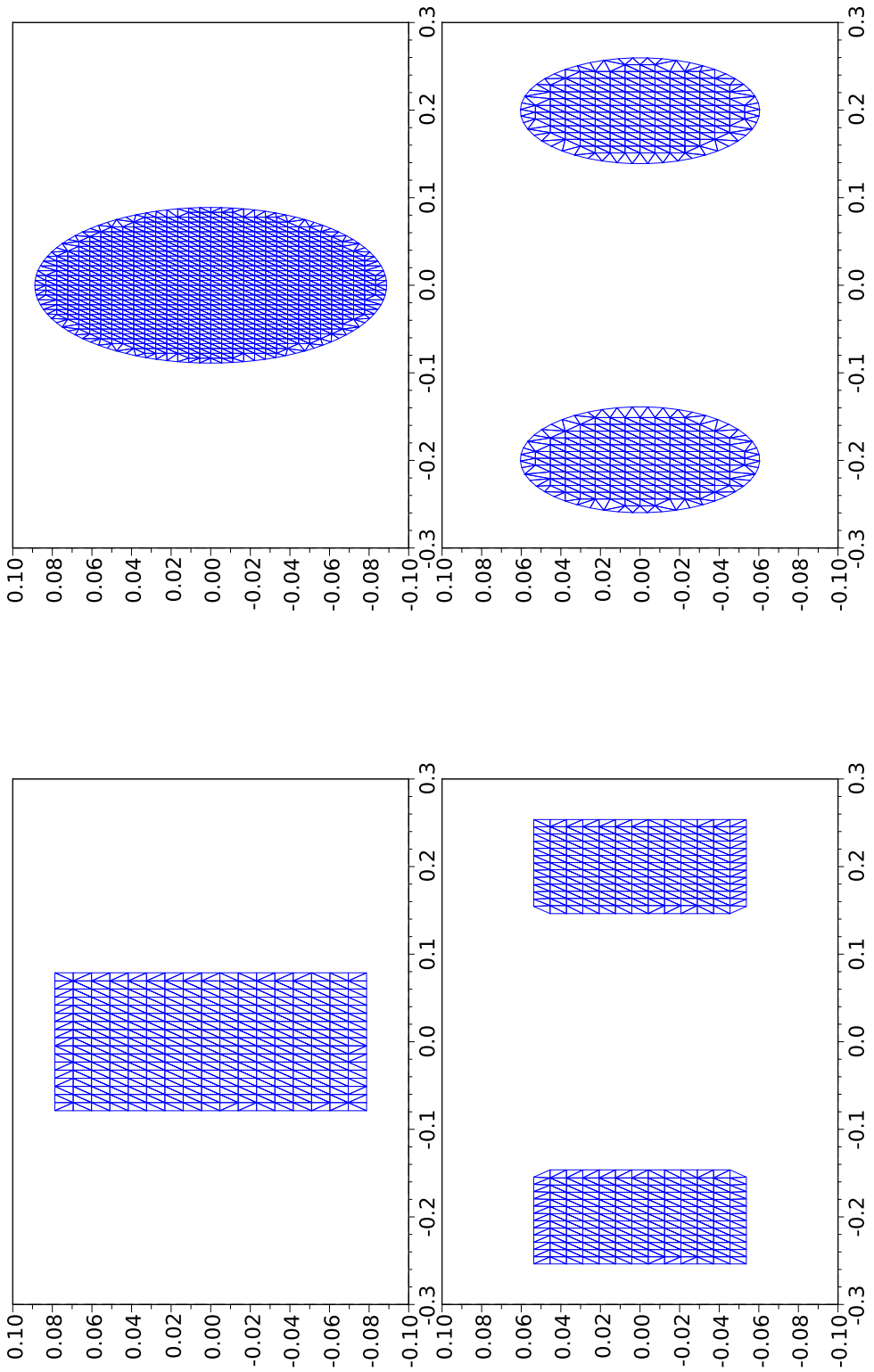

Figure B.1: Plot of the four different initial domains Ω_s, Ω_d, Ω_{2s} and Ω_{2d}, for the optimization of λ_7 in $\mathbb{D}^2$.

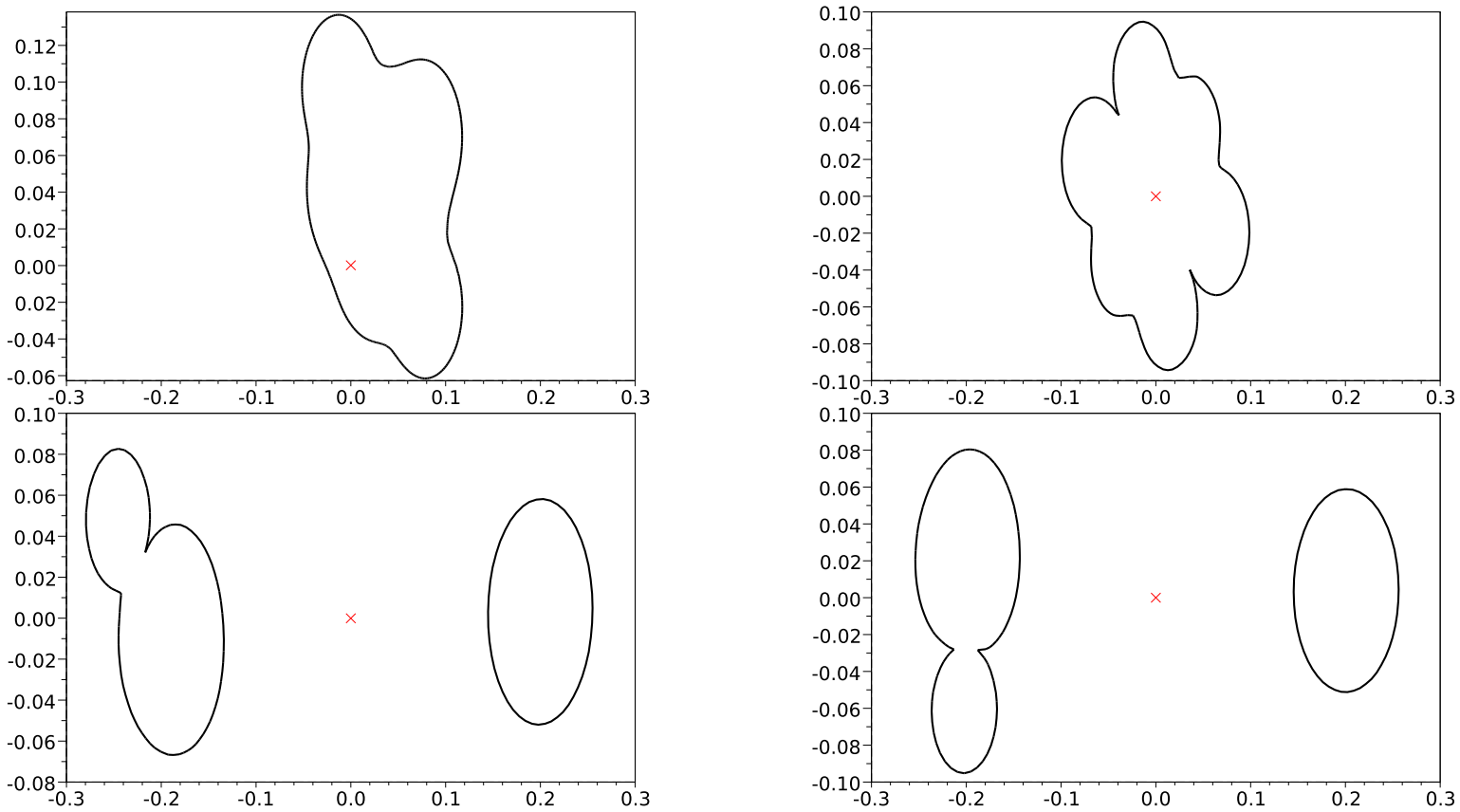

Figure B.2: Plot of the four candidates for the optimal domain of λ_7 with volume 0.1 in $\mathbb{D}^2$, starting respectively from Ω_s (top left), Ω_d (top right), Ω_{2s} (bottom left) and Ω_{2d} (bottom right).

Let us discuss the shape of the domains obtained. On the first hand, we recognize the candidate for the optimal shape obtained in Subsection 5.2.2, namely Ω_s^*. On the other hand, both examples starting from the disconnected domains Ω_{2s} and Ω_{2d} seem to lead to the same candidate. An interesting result is the theorem from Wolf and Keller recalled below. According to its authors, it is about how to find the minimizing planar domain if it is disconnected, and the minimum value of λ_k in this case. Let us introduce their notations. Let D_k^* be a domain in $\mathbb{R}^2$ which minimizes λ_k among all domains of unit area, and let $\lambda_k^* = \lambda(D_k^*)$ be the minimum value of λ_k. Let rD be the domain obtained from the domain D by multiplying all its lengths by the positive real number r.

Theorem B.1.1 ([WK94, Theorem 8.1]). *Assume that $D_k^* \subset \mathbb{R}^2$ is the union of two disjoint domains, each of positive area. Then*

$$\lambda_k^* = \lambda_i^* + \lambda_{k-i}^* = \min_{1 \leq j \leq (k-1)/2} (\lambda_j^* + \lambda_{k-j}^*).$$

Here i is a value of $j \leq (k-1)/2$ which minimizes $\lambda_j^* + \lambda_{k-j}^*$. Furthermore

$$D_k^* = \left(\left(\frac{\lambda_i^*}{\lambda_k^*} \right)^{1/2} D_i^* \right) \bigcup \left(\left(\frac{\lambda_{k-i}^*}{\lambda_k^*} \right)^{1/2} D_{k-i}^* \right).$$

It means that, in the plane, if a candidate to be an optimal domain for λ_k has two connected components, then each of its connected components is an optimal domain for λ_i and λ_{k-i}, for $1 \leq i \leq (k-1)/2$, up to the suitable rescaling. Drawing a parallel in the hyperbolic case is undoubtedly *very precarious*, but Ω_{2s}^* and Ω_{2d}^* can be compared to the candidates to be the optimizer of λ_3 and λ_4, which seem to be a disc and two discs respectively. Moreover, looking at the volume of the approximated balls appearing in Figure B.2, we observe that the two larger balls have almost the same volume, and the ratio with the smallest ball (about 0.390 for Ω_{2d}^* and 0.401 for Ω_{2s}^*) fits quite well the comparison made in Section 5.2.2 for λ_4 (the ratio was 0.387). Qualitatively, it seems that the algorithm starting from a disconnected domain may reach a domain consisting of connected components obtained for eigenvalues of smaller order, illustrating *somehow* this result in the Poincaré disc.

Once the candidate to be an optimal domain is obtained, two successive refinements of the mesh are performed: during a refinement, every triangle is divided into four similar triangles by connecting the middle of each of its edges, as illustrated in Figure B.3. Thus, the diameter of the mesh, as defined in Subsection 2.2.2, is halved [1] at each refinement, so one may expect the error to be divided by 16 at the end. The values for λ_7 associated to each domain Ω_s^*, Ω_d^*, Ω_{2s}^* and Ω_{2d}^*, are collected in Table B.1.

The domain Ω_s^* has the smallest seventh eigenvalue among the four domains obtained. Henceforth, only this example is considered. Its value is not exactly the same as the corresponding value in Table 5.2 because the discretizations are not the same. As mentioned in Section 4.2, the Lagrange multiplier should converge. It is the case as shown in Figures B.4 and B.5, where the evolution of the Lagrange multiplier during the optimization

1. The same refinement is used consecutively for the numerical checkings in Subsection 3.5.2.

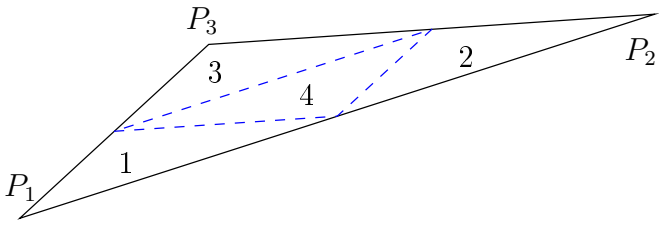

Figure B.3: The triangle with vertices P_1, P_2 and P_3 is split into four similar triangles numbered from 1 to 4 by connecting the middle of each of its edges (respresented here using the blue dashed line segments).

Ω^*	Ω_s^*	Ω_d^*	Ω_{2s}^*	Ω_{2d}^*	
$\lambda_7(\Omega^*)$	1065.435	1262.799	1126.055	1121.961	with masslumping
	1066.916	1266.005	1130.169	1124.818	without masslumping

Table B.1: Value of $\lambda_7(\Omega^*)$, for the candidate Ω_s^*, Ω_d^*, Ω_{2s}^* and Ω_{2d}^* of volume 0.1.

process is represented, together with the evolution of the volume, the eigenvalue and the value of the cost functional. Besides, observe that the volume converges to the initial volume as requested by the constraint imposed in the optimization problem. Moreover, the value obtained after the refinements is not plotted, which explains the gap between the optimal value and the last value represented at the extremity of the curve.

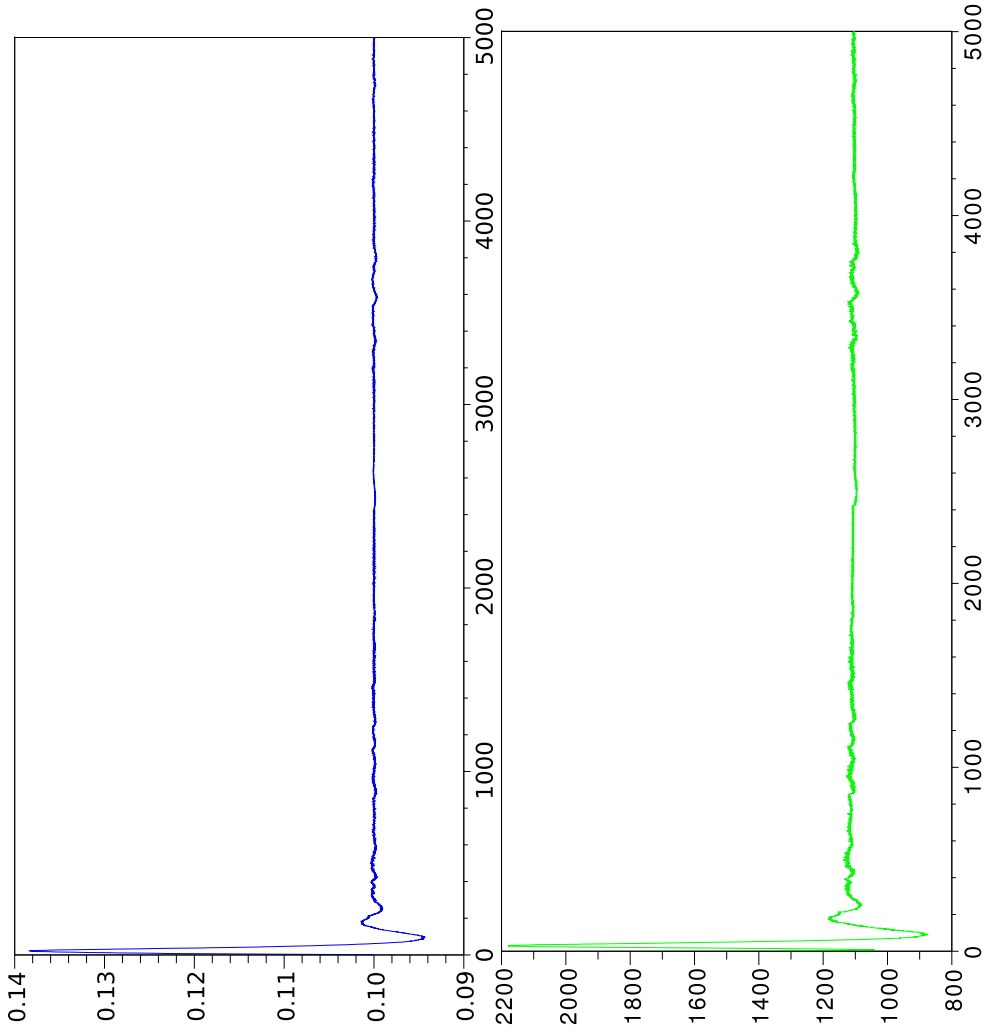

Figure B.4: Evolution of the volume of the domain (top) and of the cost functional $\mathcal{L}$ (bottom) with respect to the iteration of the optimization process starting from Ω_s.

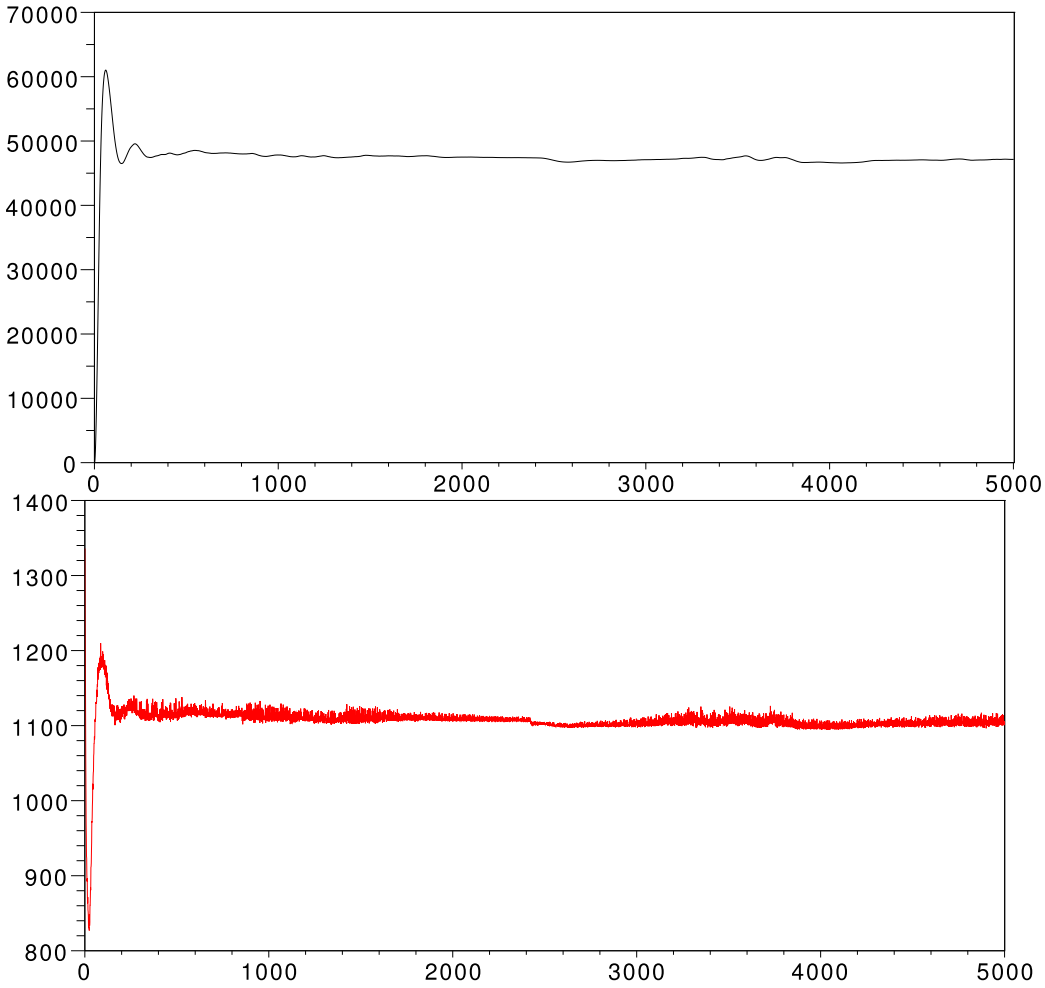

Figure B.5: Evolution of the eigenvalue of the domain (top) and of the Lagrange multiplier (bottom) with respect to the iteration of the optimization process starting from Ω_s. The eigenvalue is computed without masslumping.

k	$\lambda_k(\Omega_s^*)$
1	213.121
2	462.824
3	566.903
4	738.546
5	1059.066
6	1063.027
7	1066.916
8	1497.089

Table B.2: Value of the first eight eigenvalues of Ω_s^* computed without masslumping.

B.2 Taking the multiplicity into consideration

As recommended in [LSY98, Section A.1.4], to perform an approximation of the k-th eigenvalue, a few additional eigenvalues to the first k ones are computed to avoid splitting a *cluster* of eigenvalues. Computing the first eight eigenvalues is sufficient to notice that $\lambda_7(\Omega_s^*)$ and $\lambda_8(\Omega_s^*)$ are distant enough from each other. The first eight eigenvalues associated to Ω_s^* are reported in Table B.2. The multiplicity of the seventh eigenvalue appears: $\lambda_5(\Omega_s^*)$, $\lambda_6(\Omega_s^*)$ and $\lambda_7(\Omega_s^*)$ are within a range of about 0.74%. So, instead of using Formula (4.6) which holds only for a simple eigenvalue, Formula (4.12) is this time performed to take into consideration the multiplicity of $\lambda_7(\Omega_s^*)$ during the shape optimization step. However, note this latter formula does not give a clue about which directional derivative choosing among the three—in this case—eigenvalues of the matrix D appearing in (4.12).

Thus, after detecting that multiplicity occurs by checking that the eigenvalue to be optimized and the previous one are in a range of 1% [2], the optimization process is split into three processes: one using the smallest eigenvalue of the matrix D for defining the direction of the deformation in the shape optimization, a second one using the largest, and a last one using Formula (4.6) valid for a simple eigenvalue. Nevertheless, no significant improvement can be noticed by taking into account the multiplicity of the eigenvalue to be optimized, compared to the optimization process using Formula 4.6. Indeed, neither the value, namely 1068.794 (1065.521 and 1066.916 using respectively the smallest eigenvalue of D, the largest eigenvalue D and using Formula 4.6), nor the shape of the optimal domains resulting seem really different from each other. Moreover, an additional cost is induced by such a modification. Indeed, the normal derivative of an eigenfunction u_j, $j = 1, \ldots, k$,—such a quantity appears in both Formulas 4.6 and 4.12—is determined by solving the system resulting from

$$\int_{\partial\Omega^{(n)}} \frac{\partial u_j}{\partial \boldsymbol{n}} v \, \mathrm{d}\sigma = \int_{\Omega^{(n)}} g(\boldsymbol{\nabla u_j}, \boldsymbol{\nabla v}) \, \mathrm{d}V_g - \lambda \int_{\Omega^{(n)}} u_j v \, \mathrm{d}V_g, \quad \forall v \in H^1(\Omega^{(n)}),$$

2. This threshold is arbitrary and may be reached even when no multiplicity occurs.

where $\Omega^{(n)}$ denotes the current domain and the other notations are the same as in the main part of the document. In the algorithm, the computation of the normal derivative of the eigenfunction takes place after the computation of the eigenfunction itself and of the eigenvalue. So numerically, finding $\partial u_j/\partial \boldsymbol{n}$ consists in solving a linear problem [3] of size N_n by $N_{\partial\Omega^{(n)}}$, where N_n is the number of nodes of the current domain $\Omega^{(n)}$ and $N_{\partial\Omega^{(n)}}$ is the number of nodes on the boundary of $\Omega^{(n)}$. Thus, for an eigenvalue of multiplicity m, m systems have to be solved to find the partial derivative of the associated eigenfunctions.

Besides, as explained in Section 2.3 about the Lanczos method, the approximation of the associated eigenfunctions are also performed by the algorithm. They are displayed in Figure B.6.

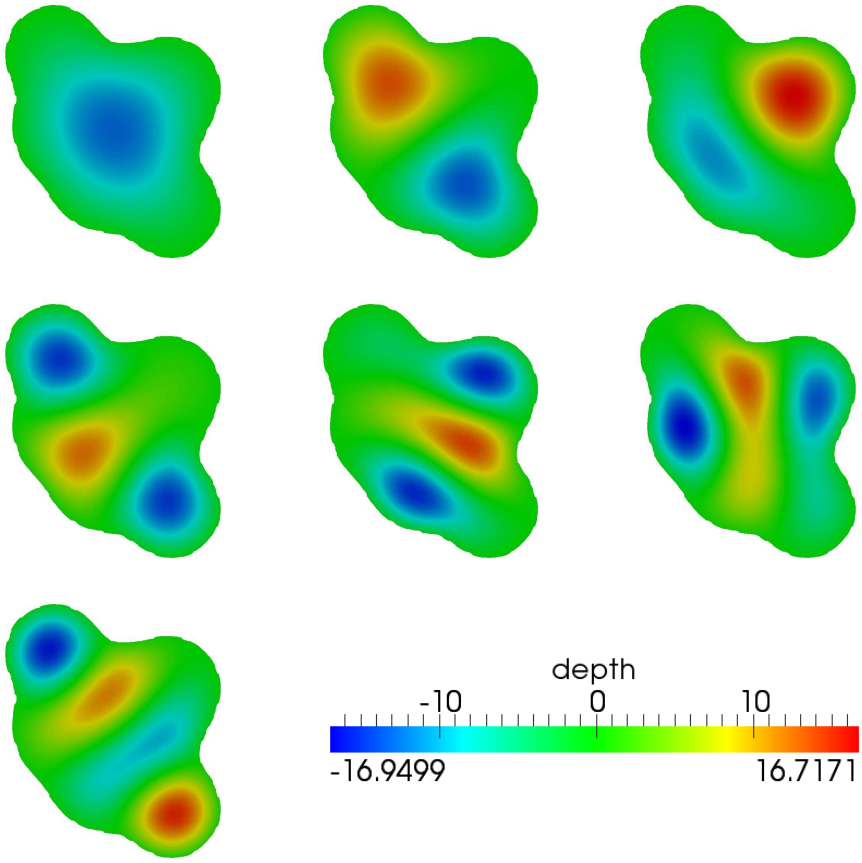

Figure B.6: First seven eigenfunctions of Ω_s^*.

3. After processing the Galerkin method as explained in Section 2.2.2.

Appendix C

Some additional numerical values

This appendix is devoted to collect additional values resulting from numerical experiments. For the sake of clarity, they are aside from the main part of the document. The knowledge of these values is not essential for the general comprehension, but can be useful for a future accurate study or comparison.

C.1 Computation of the first forty eigenvalues of a ball of volume 1 in $\mathbb{R}^2$, in the sphere $\mathbb{S}^2$ and in the Poincaré disc $\mathbb{D}^2$

Figure 3.3 represents the values of $\lambda_{k,\mathbb{R}^2}(B)$, $\lambda_{k,\mathbb{S}^2}(B)$ and $\lambda_{k,\mathbb{D}^2}(B)$ for $k = 1, \dots, 40$, where B denotes the ball of volume 1 in the manifold indicated in subscript. The corresponding values are presented in Table C.1 below.

Table C.1: Computation of $\lambda_k(B)$, $k = 1, \ldots, 40$, for the ball B in $\mathbb{R}^2$, in $\mathbb{S}^2$ and in the Poincaré disc $\mathbb{D}^2$.

Eigenvalue	Approximation with (left) and without (right) masslumping in $\mathbb{R}^2$		$\mathbb{S}^2$		$\mathbb{D}^2$	
λ_1	18.167	18.170	17.343	17.346	18.974	18.977
λ_2	46.117	46.131	44.879	44.892	47.327	47.340
λ_3	46.117	46.140	44.879	44.901	47.327	47.349
λ_4	82.831	82.889	81.631	81.689	84.025	84.084
λ_5	82.839	82.897	81.640	81.697	84.034	84.092
λ_6	95.697	95.775	92.782	92.858	98.528	98.607
λ_7	127.829	127.967	127.139	127.277	128.583	128.722
λ_8	127.829	127.967	127.139	127.277	128.583	128.722
λ_9	154.542	154.697	150.382	150.532	158.583	158.741
λ_{10}	154.546	154.796	150.385	150.629	158.587	158.843
λ_{11}	180.790	181.066	181.096	181.374	180.679	180.955
λ_{12}	180.790	181.066	181.097	181.374	180.680	180.955
λ_{13}	222.383	222.803	217.423	217.835	227.224	227.653
λ_{14}	222.440	222.855	217.478	217.886	227.283	227.707
λ_{15}	235.074	235.544	228.408	228.866	240.102	240.592
λ_{16}	241.513	242.007	243.303	243.801	240.102	240.592
λ_{17}	241.514	242.007	243.303	243.801	241.550	242.033
λ_{18}	299.020	299.776	293.707	294.450	304.240	305.009
λ_{19}	299.020	299.777	293.707	294.452	304.240	305.011
λ_{20}	309.835	310.650	313.603	314.428	306.687	307.494

Eigenvalue	Approximation with (left) and without (right) masslumping in $\mathbb{R}^2$		$\mathbb{S}^2$		$\mathbb{D}^2$	
λ_{21}	309.839	310.650	313.607	314.429	306.691	307.494
λ_{22}	324.787	325.470	316.046	316.711	333.280	333.983
λ_{23}	324.803	325.911	316.059	317.141	333.298	334.435
λ_{24}	384.120	385.371	378.916	380.150	380.312	381.556
λ_{25}	384.125	385.372	378.920	380.152	380.312	381.558
λ_{26}	385.633	386.892	391.878	393.159	389.297	390.566
λ_{27}	385.634	386.893	391.879	393.159	389.302	390.568
λ_{28}	423.475	425.004	413.099	414.591	433.568	435.138
λ_{29}	423.677	425.173	413.295	414.754	433.778	435.313
λ_{30}	436.168	437.804	424.086	425.682	447.897	449.579
λ_{31}	468.795	470.659	472.890	474.803	460.862	462.698
λ_{32}	468.800	470.659	472.891	474.803	460.867	462.698
λ_{33}	477.519	479.450	478.020	479.921	482.228	484.183
λ_{34}	477.520	479.450	478.024	479.921	482.229	484.183
λ_{35}	531.227	533.605	519.654	521.981	542.510	544.946
λ_{36}	531.227	533.619	519.654	521.996	542.510	544.959
λ_{37}	556.639	558.653	541.658	543.616	548.257	550.861
λ_{38}	556.684	559.959	541.695	544.891	548.258	550.861
λ_{39}	559.239	561.890	571.948	574.659	571.185	573.260
λ_{40}	559.240	561.891	571.949	574.659	571.238	574.601

C.2 Placement of a circular obstacle inside a ball in $\mathbb{R}^2$, in $\mathbb{S}^2$ and in $\mathbb{D}^2$

This section is a complement to Subsection 3.5.5. It is concerned with some additional numerical results about the placement of a circular obstacle inside a ball in $\mathbb{R}^2$, in $\mathbb{S}^2$ and in $\mathbb{D}^2$. In each of these surfaces, the domain is a ball of radius 1 from which a smaller ball—called the obstacle—has been removed. In this appendix, obstacles of radius $r = 0.1$, 0.01 and 0.001 are considered for the computation of the eigenvalues 3, 4 and 5. Thanks to symmetry of the domain, it is sufficient to consider obstacles centred at a point $(x, 0) \in M$. Hence, let denote by $B^r_{x,M}$ the ball of radius r, centred in $(x, 0) \in M$. Furthermore, let $\lambda^{r,*}_{k,M}$ be the maximum—with respect to the location of the obstacle—of the k-th eigenvalue and let $(x^{r,*}_{k,M}, 0)$ be the centre of the obstacle of radius r where this maximum is attained.

Tables C.2, C.3 and C.4 present the value of $\lambda^{r,*}_{k,M}$ together with the position of the centre $x^{r,*}_{k,M}$, for $k = 3, 4, 5$, for $r = 0.1, 0.01, 0.001$ and for $M = R^2, \mathbb{S}^2, \mathbb{D}^2$.

Moreover, Figures C.1 to C.9 show the evolution of $\lambda_{k,M}(B^r_{x,M})$ with respect to the location x of the centre of the obstacle, for k, M and r as above. In each of these figures, three couples of graphs are plotted corresponding to the three different values 0.1, 0.01 and 0.001 of the radius r of the obstacle. The blue plain curves correspond to computations without masslumping and the red dashed ones to computations with masslumping. Eigenvalues computed for the radius 0.1 are larger than those for the radius 0.01, which are larger than those for the radius 0.001 as expected by domain monotonicity. Moreover, the maximum of each graph is emphasized with a small vertical blue dashed segment, whereas the long vertical black dashed segment indicates the abscissa of the point where $u_{k,M}(B_1)$ attains its maximum, where $u_{k,M}(B_1)$ denotes the k-th eigenfunction defined on the ball of radius 1 without obstacle in M.

Observe that for $k = 3$ and 5, as r becomes smaller and smaller, the maximum of $\lambda^{r,*}_{k,M}$ is achieved by a point closer and closer to a point maximizing $u_k(B_1)$. On the contrary for the fourth eigenvalue, the position of the obstacle has less influence on $\lambda^{r,*}_{4,M}$. Indeed, $u_4(B_1)$ has nodal lines passing through the centre of the ball. Hence, adding a small obstacle near a nodal line with Dirichlet condition on its boundary does not affect *too much* the eigenfunction and *a fortiori* the eigenvalue. Because of the orthogonality of the eigenfunctions, the same argument does not apply for the fifth eigenfunction. In that case, the obstacle is not near a nodal line. See Figure C.13 representing the first fifteen eigenfunctions $u_{k,\mathbb{R}^2}(B_1)$.

Finally, Figures C.10 to C.12 display a comparison in $M = \mathbb{R}^2, \mathbb{S}^2, \mathbb{D}^2$ of the evolution of the k-th eigenvalue $\lambda_{k,M}(B^{0.001}_{x,M})$ with respect to the location x of the centre of the obstacle, $k = 3, 4, 5$. The *small variations* of the curves plotted seem to be caused by sudden modifications of the mesh near the obstacle.

Table C.2: Maximal value $\lambda^{r,*}_{k,\mathbb{R}^2}$ of the k-th eigenvalue of the ball in $\mathbb{R}^2$ with an obstacle centred at $(x^{r,*}_{k,\mathbb{R}^2}, 0)$, $k = 3, \dots, 5$.

Eigenvalue	centre of the optimal obstacle	Approximations obtained for the optimal domain with an obstacle of radius 0.1		0.01		0.001	
$\lambda^{r,*}_{3,\mathbb{R}^2}$	$(x^{r,*}_{3,\mathbb{R}^2})$	20.206	(0.38)	17.139	(0.43)	16.558	(0.447)
$\lambda^{r,*}_{4,\mathbb{R}^2}$	$(x^{r,*}_{4,\mathbb{R}^2})$	27.400	(0.43)	26.403	(0.44)	26.389	(0.444)
$\lambda^{r,*}_{5,\mathbb{R}^2}$	$(x^{r,*}_{5,\mathbb{R}^2})$	31.838	(0.41)	28.765	(0.5)	28.204	(0.52)

Table C.3: Maximal value $\lambda^{r,*}_{k,\mathbb{S}^2}$ of the k-th eigenvalue of the ball in $\mathbb{S}^2$ with an obstacle centred at $(x^{r,*}_{k,\mathbb{S}^2}, 0)$, $k = 3, \dots, 5$.

Eigenvalue	centre of the optimal obstacle	Approximations obtained for the optimal domain with an obstacle of radius 0.1		0.01		0.001	
$\lambda^{r,*}_{3,\mathbb{S}^2}$	$(x^{r,*}_{3,\mathbb{S}^2})$	20.596	(0.4)	17.288	(0.44)	16.681	(0.452)
$\lambda^{r,*}_{4,\mathbb{S}^2}$	$(x^{r,*}_{4,\mathbb{S}^2})$	28.622	(0.45)	27.517	(0.46)	27.501	(0.463)
$\lambda^{r,*}_{5,\mathbb{S}^2}$	$(x^{r,*}_{5,\mathbb{S}^2})$	31.706	(0.39)	29.746	(0.46)	29.257	(0.487)

Table C.4: Maximal value $\lambda^{r,*}_{k,\mathbb{D}^2}$ of the k-th eigenvalue of the ball in $\mathbb{D}^2$ with an obstacle centred at $(x^{r,*}_{k,\mathbb{D}^2}, 0)$, $k = 3, \dots, 5$.

Eigenvalue	centre of the optimal obstacle	Approximations obtained for the optimal domain with an obstacle of radius 0.1		0.01		0.001	
$\lambda^{r,*}_{3,\mathbb{D}^2}$	$(x^{r,*}_{3,\mathbb{D}^2})$	18.161	(0.39)	15.600	(0.44)	15.101	(0.453)
$\lambda^{r,*}_{4,\mathbb{D}^2}$	$(x^{r,*}_{4,\mathbb{D}^2})$	24.102	(0.43)	23.302	(0.46)	23.291	(0.455)
$\lambda^{r,*}_{5,\mathbb{D}^2}$	$(x^{r,*}_{5,\mathbb{D}^2})$	28.654	(0.45)	25.436	(0.53)	24.911	(0.548)

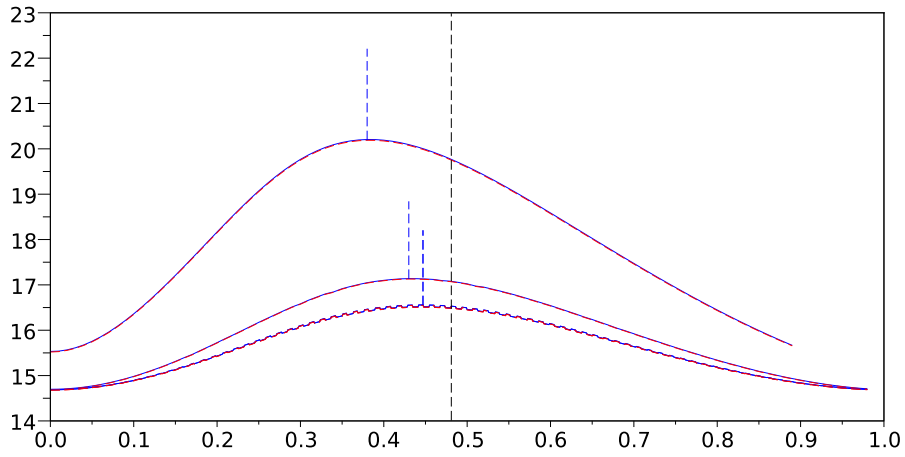

Figure C.1: Evolution of the third eigenvalue $\lambda_{3,\mathbb{R}^2}(B^r_{x,\mathbb{R}^2})$ with respect to the abscissa x of the location $(x,0)$ of the centre of the obstacle.

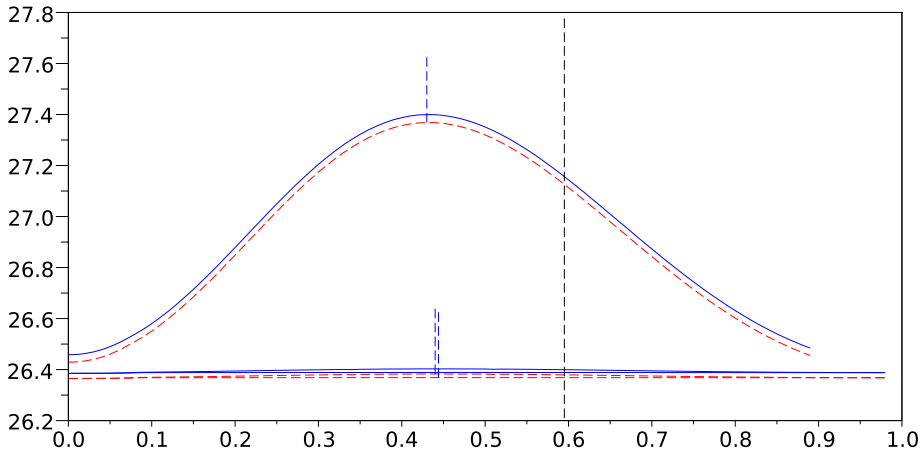

Figure C.2: Evolution of the fourth eigenvalue $\lambda_{4,\mathbb{R}^2}(B^r_{x,\mathbb{R}^2})$ with respect to the abscissa x of the location $(x,0)$ of the centre of the obstacle.

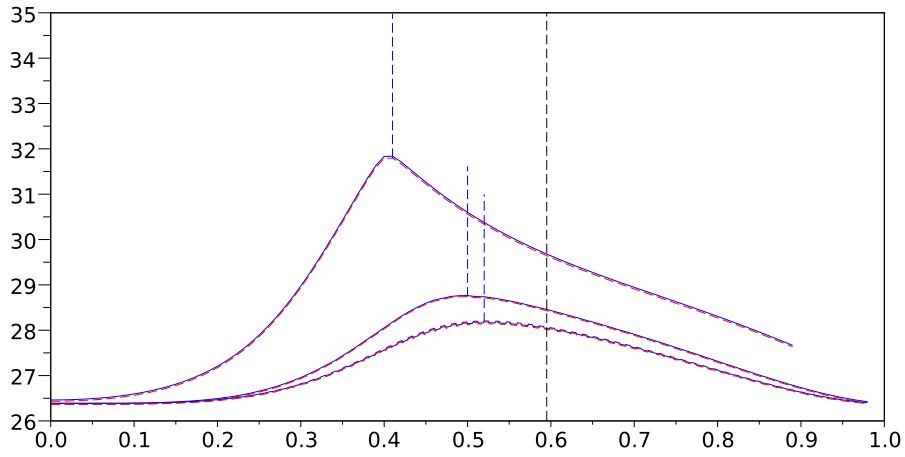

Figure C.3: Evolution of the fifth eigenvalue $\lambda_{5,\mathbb{R}^2}(B^r_{x,\mathbb{R}^2})$ with respect to the abscissa x of the location $(x,0)$ of the centre of the obstacle.

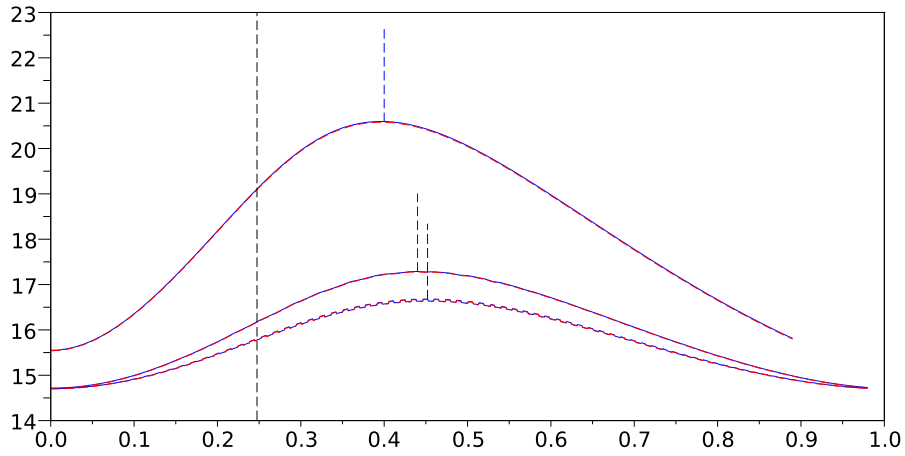

Figure C.4: Evolution of the third eigenvalue $\lambda_{3,\mathbb{S}^2}(B^r_{x,\mathbb{S}^2})$ with respect to the abscissa x of the location $(x,0)$ of the centre of the obstacle.

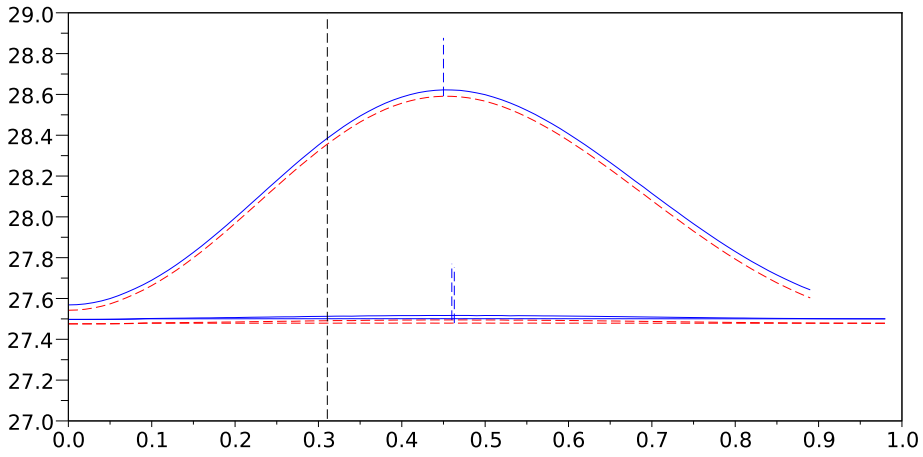

Figure C.5: Evolution of the fourth eigenvalue $\lambda_{4,\mathbb{S}^2}(B^r_{x,\mathbb{S}^2})$ with respect to the abscissa x of the location $(x, 0)$ of the centre of the obstacle.

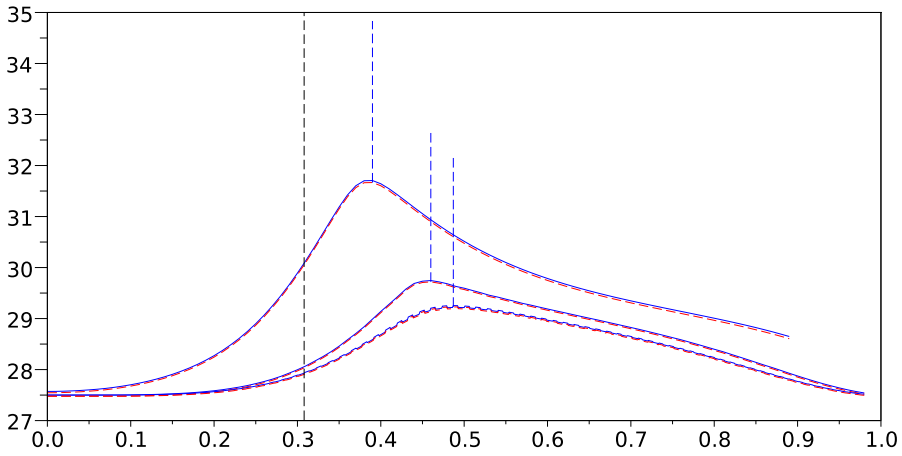

Figure C.6: Evolution of the fifth eigenvalue $\lambda_{5,\mathbb{S}^2}(B^r_{x,\mathbb{S}^2})$ with respect to the abscissa x of the location $(x, 0)$ of the centre of the obstacle.

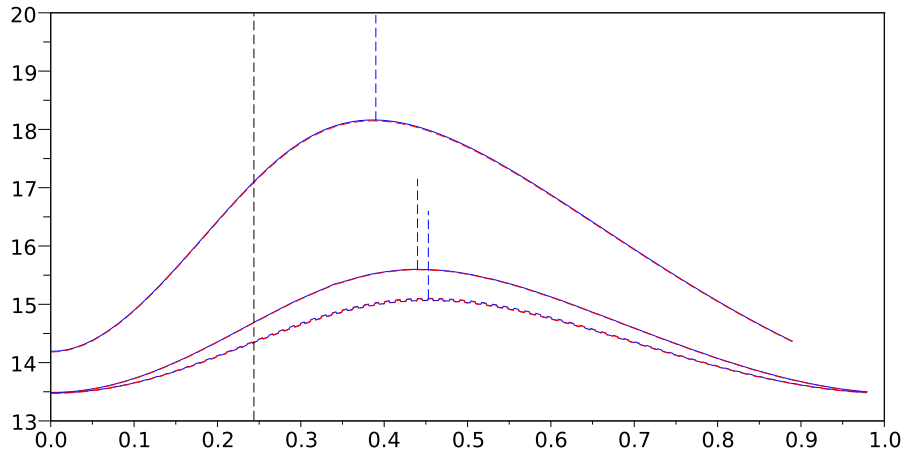

Figure C.7: Evolution of the third eigenvalue $\lambda_{3,\mathbb{D}^2}(B^r_{x,\mathbb{D}^2})$ with respect to the abscissa x of the location $(x,0)$ of the centre of the obstacle.

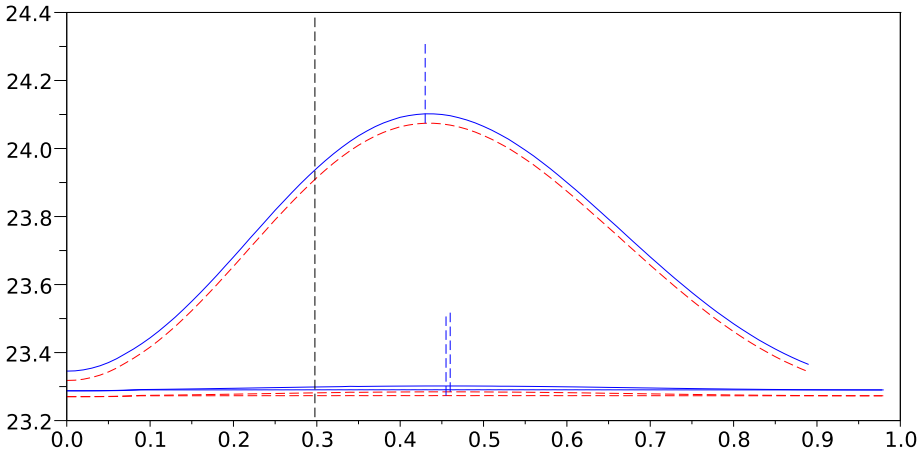

Figure C.8: Evolution of the fourth eigenvalue $\lambda_{4,\mathbb{D}^2}(B^r_{x,\mathbb{D}^2})$ with respect to the abscissa x of the location $(x,0)$ of the centre of the obstacle.

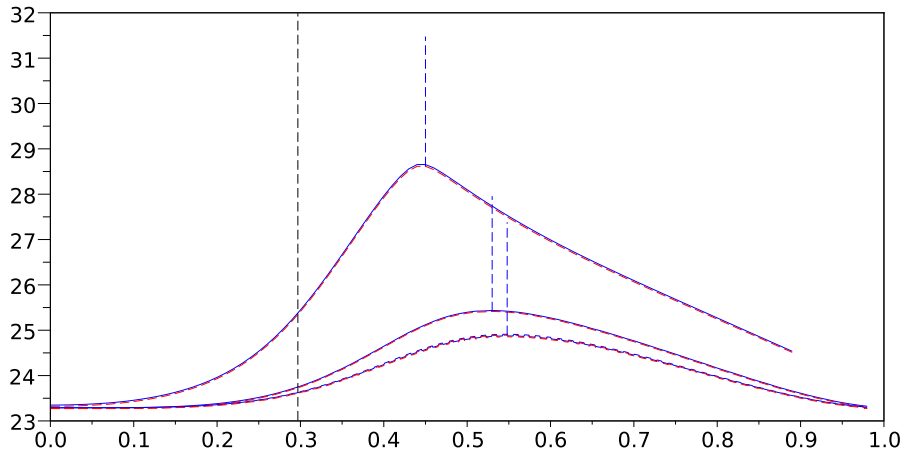

Figure C.9: Evolution of the fifth eigenvalue $\lambda_{5,\mathbb{D}^2}(B^r_{x,\mathbb{D}^2})$ with respect to the abscissa x of the location $(x,0)$ of the centre of the obstacle.

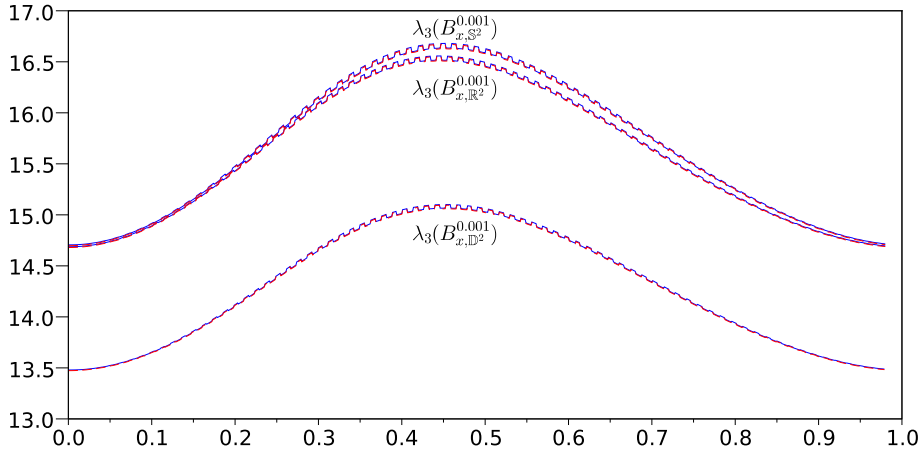

Figure C.10: Comparison of the evolution of the third eigenvalue $\lambda_{3,M}(B^{0.001}_{x,M})$ with respect to the abscissa x of the location $(x,0)$ of the centre of the obstacle in $M = \mathbb{R}^2, \mathbb{S}^2, \mathbb{D}^2$.

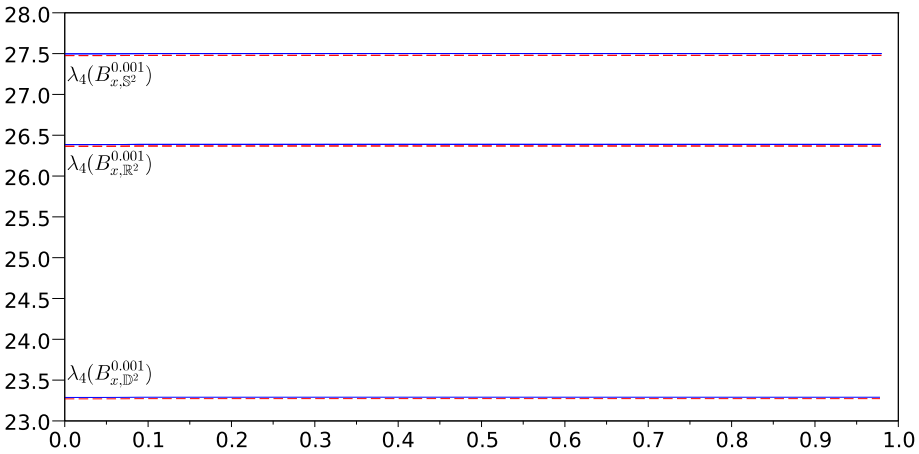

Figure C.11: Comparison of the evolution of the fourth eigenvalue $\lambda_{4,M}(B^{0.001}_{x,M})$ with respect to the abscissa x of the location $(x,0)$ of the centre of the obstacle in $M = \mathbb{R}^2, \mathbb{S}^2, \mathbb{D}^2$.

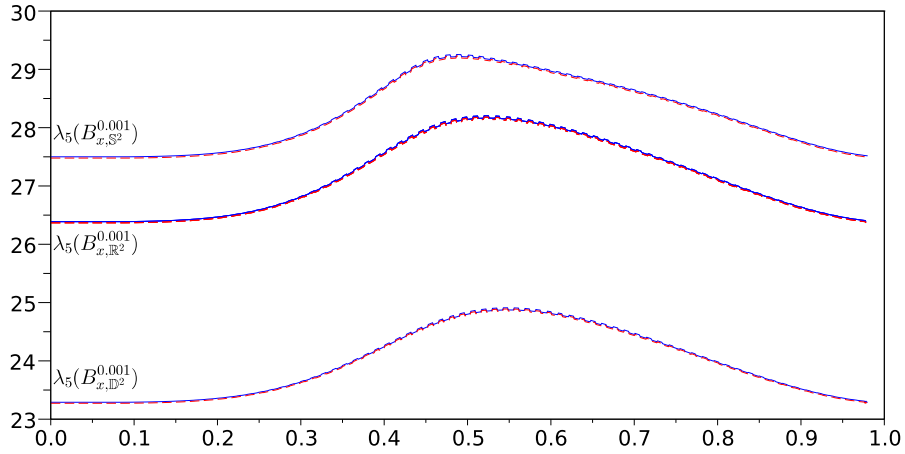

Figure C.12: Comparison of the evolution of the fifth eigenvalue $\lambda_{5,M}(B^{0.001}_{x,M})$ with respect to the abscissa x of the location $(x,0)$ of the centre of the obstacle in $M = \mathbb{R}^2, \mathbb{S}^2, \mathbb{D}^2$.

C.3 Representation of the first fifteen eigenfunctions on a ball in $\mathbb{R}^2$.

The first fifteen eigenfunctions on a ball in $\mathbb{R}^2$ are displayed in this section. As predicted by the separation of variables providing the analytic solutions, the eigenfunctions associated to a simple eigenvalue are radial functions, whereas they are periodic functions for multiple eigenvalues. In the latter case, the nodal lines—namely the curves where an eigenfunction vanishes—are lines passing through the centre.

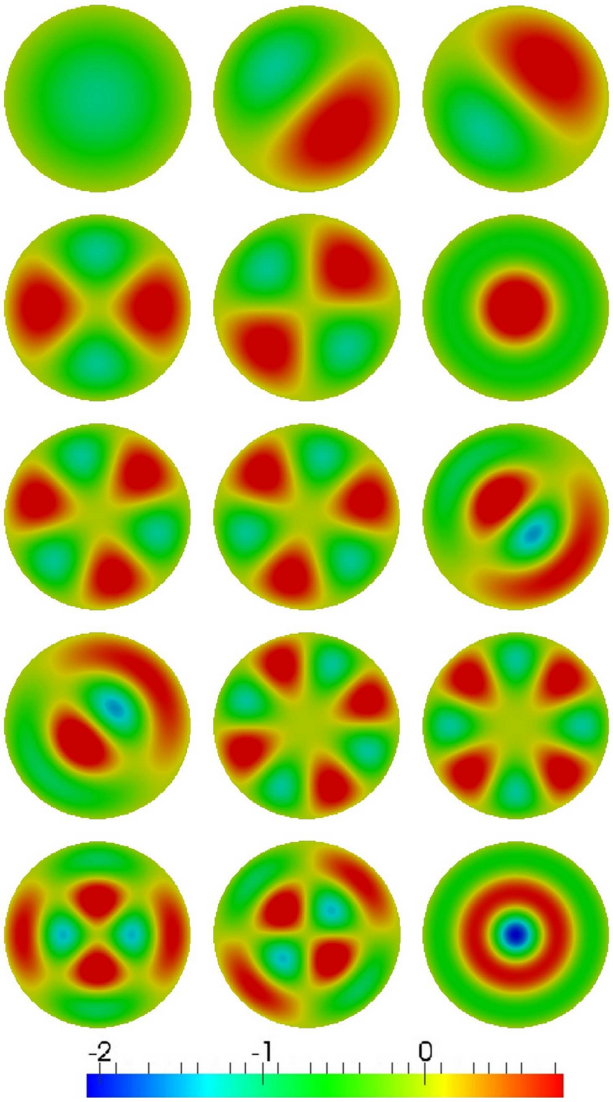

Figure C.13: First fifteen eigenfunctions on a ball in $\mathbb{R}^2$.

Bibliography

[AA05] M. H. C. Anisa and A. R. Aithal. On two functionals connected to the Laplacian in a class of doubly connected domains in space-forms. *Proc. Indian Acad. Sci. Math. Sci.*, 115(1):93–102, 2005.

[AB01] M. S. Ashbaugh and R. D. Benguria. A sharp bound for the ratio of the first two Dirichlet eigenvalues of a domain in a hemisphere of S^n. *Trans. Amer. Math. Soc.*, 353(3):1055–1087, 2001.

[AD03] M. G. Armentano and R. G. Durán. Mass-lumping or not mass-lumping for eigenvalue problems. *Numer. Methods Partial Differential Equations*, 19(5):653–664, 2003.

[Ada75] R. A. Adams. *Sobolev spaces.* Academic Press [A subsidiary of Harcourt Brace Jovanovich, Publishers], New York-London, 1975. Pure and Applied Mathematics, Vol. 65.

[AF03] R. A. Adams and J. J. F. Fournier. *Sobolev spaces*, volume 140 of *Pure and Applied Mathematics (Amsterdam).* Elsevier/Academic Press, Amsterdam, second edition, 2003.

[AF12] P. R. S. Antunes and P. Freitas. Numerical optimization of low eigenvalues of the Dirichlet and Neumann Laplacians. *J. Opt. Theory Appl.*, 154(1), 2012.

[AFK13] P. R. S. Antunes, P. Freitas, and J. B. Kennedy. Asymptotic behaviour and numerical approximation of optimal eigenvalues of the Robin Laplacian. *ESAIM: Control, Optimisation and Calculus of Variations*, 19:438–459, 2013.

[All07] G. Allaire. *Conception optimale de structures*, volume 58 of *Mathématiques & Applications (Berlin) [Mathematics & Applications].* Springer-Verlag, Berlin, 2007. With the collaboration of Marc Schoenauer (INRIA) in the writing of Chapter 8.

[BB80] P. Bérard and G. Besson. Spectres et groupes cristallographiques. II. Domaines sphériques. *Ann. Inst. Fourier (Grenoble)*, 30(3):237–248, 1980.

[BCDS94] P. Buser, J. Conway, P. Doyle, and K.-D. Semmler. Some planar isospectral domains. *Internat. Math. Res. Notices*, (9):391ff., approx. 9 pp. (electronic), 1994.

[Bér86] P. H. Bérard. *Spectral geometry: direct and inverse problems*, volume 1207 of *Lecture Notes in Mathematics.* Springer-Verlag, Berlin, 1986. With appendixes by Gérard Besson, and by Bérard and Marcel Berger.

[BGM71] M. Berger, P. Gauduchon, and E. Mazet. *Le spectre d'une variété riemannienne*. Lecture Notes in Mathematics, Vol. 194. Springer-Verlag, Berlin, 1971.

[BO87] I. Babuška and J. E. Osborn. Estimates for the errors in eigenvalue and eigenvector approximation by Galerkin methods, with particular attention to the case of multiple eigenvalues. *SIAM J. Numer. Anal.*, 24(6):1249–1276, 1987.

[Bof10] D. Boffi. Finite element approximation of eigenvalue problems. *Acta Numer.*, 19:1–120, 2010.

[Boo75] W. M. Boothby. *An introduction to differentiable manifolds and Riemannian geometry*. Academic Press [A subsidiary of Harcourt Brace Jovanovich, Publishers], New York-London, 1975. Pure and Applied Mathematics, No. 63.

[Bre11] H. Brezis. *Functional analysis, Sobolev spaces and partial differential equations*. Universitext. Springer, New York, 2011.

[BT05] T. Betcke and L. N. Trefethen. Reviving the method of particular solutions. *SIAM Rev.*, 47(3):469–491 (electronic), 2005.

[Buc12] D. Bucur. Minimization of the k-th eigenvalue of the Dirichlet Laplacian. *Arch. Ration. Mech. Anal.*, 206(3):1073–1083, 2012.

[Car67] H. Cartan. *Calcul différentiel*. Hermann, Paris, 1967.

[CES12] B. Colbois and A. El Soufi. Extremal eigenvalues of the Laplacian on Euclidean domains and closed surfaces. Preprint, 2012.

[CGI+00] S. Chanillo, D. Grieser, M. Imai, K. Kurata, and I. Ohnishi. Symmetry breaking and other phenomena in the optimization of eigenvalues for composite membranes. *Comm. Math. Phys.*, 214(2):315–337, 2000.

[CH53] R. Courant and D. Hilbert. *Methods of mathematical physics. Vol. I*. Interscience Publishers, Inc., New York, N.Y., 1953.

[Cha84] I. Chavel. *Eigenvalues in Riemannian geometry*, volume 115 of *Pure and Applied Mathematics*. Academic Press Inc., Orlando, FL, 1984. Including a chapter by Burton Randol, With an appendix by Jozef Dodziuk.

[Cia78] P. G. Ciarlet. *The finite element method for elliptic problems*. North-Holland Publishing Co., Amsterdam, 1978. Studies in Mathematics and its Applications, Vol. 4.

[Cia82] P. G. Ciarlet. *Introduction à l'analyse numérique matricielle et à l'optimisation*. Collection Mathématiques Appliquées pour la Maîtrise. [Collection of Applied Mathematics for the Master's Degree]. Masson, Paris, 1982.

[Cox95] S. J. Cox. The generalized gradient at a multiple eigenvalue. *J. Funct. Anal.*, 133(1):30–40, 1995.

[CW02] J. K. Cullum and R. A. Willoughby. *Lanczos algorithms for large symmetric eigenvalue computations. Vol. 1*, volume 41 of *Classics in Applied Mathematics*. Society for Industrial and Applied Mathematics (SIAM), Philadelphia, PA, 2002. Theory, Reprint of the 1985 original [Birkhäuser Boston, Boston, MA; MR0808962 (87h:65064a)].

[dC76] M. P. do Carmo. *Differential geometry of curves and surfaces*. Prentice-Hall Inc., Englewood Cliffs, N.J., 1976. Translated from the Portuguese.

[dC94] M. P. do Carmo. *Differential forms and applications*. Universitext. Springer-Verlag, Berlin, 1994. Translated from the 1971 Portuguese original.

[DNPV12] E. Di Nezza, G. Palatucci, and E. Valdinoci. Hitchhiker's guide to the fractional Sobolev spaces. *Bull. Sci. Math.*, 136(5):521–573, 2012.

[EG02] A. Ern and J.-L. Guermond. *Éléments finis: théorie, applications, mise en œuvre*, volume 36 of *Mathématiques & Applications (Berlin) [Mathematics & Applications]*. Springer-Verlag, Berlin, 2002.

[ESG82] M. S. Engelman, R. L. Sani, and P. M. Gresho. The implementation of normal and/or tangential boundary conditions in finite element codes for incompressible fluid flow. *Internat. J. Numer. Methods Fluids*, 2(3):225–238, 1982.

[ESI07] A. El Soufi and S. Ilias. Domain deformations and eigenvalues of the Dirichlet Laplacian in a Riemannian manifold. *Illinois J. Math.*, 51(2):645–666 (electronic), 2007.

[ESK08] A. El Soufi and R. Kiwan. Where to place a spherical obstacle so as to maximize the second Dirichlet eigenvalue. *Commun. Pure Appl. Anal.*, 7(5):1193–1201, 2008.

[Fab23] G. Faber. Beweis, dass unter allen homogenen membranen von gleicher fläche und gleicher spannung die kreisförmige den tiefsten grundton gibt. *Sitzungsber. Bayer. Akad. Wiss. München, Math.-Phys. Kl.*, pages 169 – 172, 1923.

[FG82] M. Fortin and R. Glowinski. *Méthodes de lagrangien augmenté*, volume 9 of *Méthodes Mathématiques de l'Informatique [Mathematical Methods of Information Science]*. Gauthier-Villars, Paris, 1982. Applications à la résolution numérique de problèmes aux limites. [Applications to the numerical solution of boundary value problems].

[FHM67] L. Fox, P. Henrici, and C. Moler. Approximations and bounds for eigenvalues of elliptic operators. *SIAM J. Numer. Anal.*, 4:89–102, 1967.

[Flu95] M. Flucher. Approximation of Dirichlet eigenvalues on domains with small holes. *J. Math. Anal. Appl.*, 193(1):169–199, 1995.

[GHL04] S. Gallot, D. Hulin, and J. Lafontaine. *Riemannian geometry*. Universitext. Springer-Verlag, Berlin, third edition, 2004.

[GMS92] J. R. Gilbert, C. Moler, and R. Schreiber. Sparse matrices in MATLAB: design and implementation. *SIAM J. Matrix Anal. Appl.*, 13(1):333–356, 1992.

[GNP09] A. Girouard, N. Nadirashvili, and I. Polterovich. Maximization of the second positive Neumann eigenvalue for planar domains. *J. Differential Geom.*, 83(3):637–661, 2009.

[Gri85] P. Grisvard. *Elliptic problems in nonsmooth domains*, volume 24 of *Monographs and Studies in Mathematics*. Pitman (Advanced Publishing Program), Boston, MA, 1985.

[Gri92] P. Grisvard. *Singularities in boundary value problems*, volume 22 of *Recherches en Mathématiques Appliquées [Research in Applied Mathematics]*. Masson, Paris, 1992.

[GT01] D. Gilbarg and N. S. Trudinger. *Elliptic partial differential equations of second order*. Classics in Mathematics. Springer-Verlag, Berlin, 2001. Reprint of the 1998 edition.

[GVL96] G. H. Golub and C. F. Van Loan. *Matrix computations*. Johns Hopkins Studies in the Mathematical Sciences. Johns Hopkins University Press, Baltimore, MD, third edition, 1996.

[GWW92] C. Gordon, D. L. Webb, and S. Wolpert. One cannot hear the shape of a drum. *Bull. Amer. Math. Soc. (N.S.)*, 27(1):134–138, 1992.

[Had68] J. Hadamard. Mémoire sur le problème d'analyse relatif à l'équilibre des plaques élastiques encastrées, (1907). In *Œuvres de J. Hadamard*, volume 2, pages 515–642. CNRS, Paris, 1968.

[Heb96] E. Hebey. *Sobolev spaces on Riemannian manifolds*, volume 1635 of *Lecture Notes in Mathematics*. Springer-Verlag, Berlin, 1996.

[Hen06] A. Henrot. *Extremum problems for eigenvalues of elliptic operators*. Frontiers in Mathematics. Birkhäuser Verlag, Basel, 2006.

[Her63] J. Hersch. The method of interior parallels applied to polygonal or multiply connected membranes. *Pacific J. Math.*, 13:1229–1238, 1963.

[HKK01] E. M. Harrell, II, P. Kröger, and K. Kurata. On the placement of an obstacle or a well so as to optimize the fundamental eigenvalue. *SIAM J. Math. Anal.*, 33(1):240–259 (electronic), 2001.

[Hon54] I. Hong. On an inequality concerning the eigenvalue problem of membrane. *Kōdai Math. Sem. Rep.*, 6:113–114, 1954. {Volume numbers not printed on issues until Vol. **7** (1955).}.

[Hör83] L. Hörmander. *The analysis of linear partial differential operators. I*, volume 256 of *Grundlehren der Mathematischen Wissenschaften [Fundamental Principles of Mathematical Sciences]*. Springer-Verlag, Berlin, 1983. Distribution theory and Fourier analysis.

[HP05] A. Henrot and M. Pierre. *Variation et optimisation de formes*, volume 48 of *Mathématiques & Applications (Berlin) [Mathematics & Applications]*. Springer, Berlin, 2005. Une analyse géométrique. [A geometric analysis].

[HSD04] M. W. Hirsch, S. Smale, and R. L. Devaney. *Differential equations, dynamical systems, and an introduction to chaos*, volume 60 of *Pure and Applied Mathematics (Amsterdam)*. Elsevier/Academic Press, Amsterdam, second edition, 2004.

[IK08] K. Ito and K. Kunisch. *Lagrange multiplier approach to variational problems and applications*, volume 15 of *Advances in Design and Control*. Society for Industrial and Applied Mathematics (SIAM), Philadelphia, PA, 2008.

[JU08] M. Jumonji and H. Urakawa. The eigenvalue problems for the Laplacian on compact embedded surfaces and three dimensional bounded domains. *Interdiscip. Inform. Sci.*, 14(2):191–223, 2008.

[Kac66] M. Kac. Can one hear the shape of a drum? *Amer. Math. Monthly*, 73(4, part II):1–23, 1966.

[Kes06] S. Kesavan. *Symmetrization & applications*, volume 3 of *Series in Analysis*. World Scientific Publishing Co. Pte. Ltd., Hackensack, NJ, 2006.

[KO06] A. V. Knyazev and J. E. Osborn. New a priori FEM error estimates for eigenvalues. *SIAM J. Numer. Anal.*, 43(6):2647–2667 (electronic), 2006.

[Kra25] E. Krahn. Über eine von Rayleigh formulierte Minimaleigenschaft des Kreises. *Math. Ann.*, 94(1):97–100, 1925.

[Kra26] E. Krahn. Über Minimaleigenschaften der Kugel in drei und mehr Dimensionen. *Acta Univ. Dorpat A*, 9:1–44, 1926.

[Kre78] E. Kreyszig. *Introductory functional analysis with applications*. John Wiley & Sons, New York-London-Sydney, 1978.

[LSY98] R. B. Lehoucq, D. C. Sorensen, and C. Yang. *ARPACK users' guide*, volume 6 of *Software, Environments, and Tools*. Society for Industrial and Applied Mathematics (SIAM), Philadelphia, PA, 1998. Solution of large-scale eigenvalue problems with implicitly restarted Arnoldi methods.

[Ma09] J.-P. Marco and al. *Mathématiques L3 - Analyse*. Pearson Education, New Jersey, 2009.

[Mil64] J. Milnor. Eigenvalues of the Laplace operator on certain manifolds. *Proc. Nat. Acad. Sci. U.S.A.*, 51:542, 1964.

[MP13] D. Mazzoleni and A. Pratelli. Existence of minimizers for spectral problems. *J. Math. Pures Appl.*, 2013. to appear.

[MS67] H. P. McKean, Jr. and I. M. Singer. Curvature and the eigenvalues of the Laplacian. *J. Differential Geometry*, 1(1):43–69, 1967.

[MS76] F. Murat and J. Simon. Sur le contrôle par un domaine géométrique. Prépublication du Laboratoire d'Analyse Numérique, no 76015, Université de Paris 6, 222 pages, 1976.

[Mun00] A. Munnier. *Stabilité de liquides en apesanteur, régularité maximale de valeurs propres pour certaines classes d'opérateurs*. PhD thesis, Université de Franche-Comté, 2000.

[Oud04] É. Oudet. Numerical minimization of eigenmodes of a membrane with respect to the domain. *ESAIM Control Optim. Calc. Var.*, 10(3):315–330 (electronic), 2004.

[Oza81] S. Ozawa. Singular Hadamard's variation of domains and eigenvalues of the Laplacian. II. *Proc. Japan Acad. Ser. A Math. Sci.*, 57(5):242–246, 1981.

[Pai71] C. C. Paige. *The computation of eigenvalues and eigenvectors of very large sparse matrices.* PhD thesis, University of London, 1971.

[Par80] B. N. Parlett. *The symmetric eigenvalue problem.* Prentice-Hall Inc., Englewood Cliffs, N.J., 1980. Prentice-Hall Series in Computational Mathematics.

[Pól55] G. Pólya. On the characteristic frequencies of a symmetric membrane. *Math. Z.*, 63:331–337, 1955.

[PS09] F. Pacard and P. Sicbaldi. Extremal domains for the first eigenvalue of the Laplace-Beltrami operator. *Ann. Inst. Fourier (Grenoble)*, 59(2):515–542, 2009.

[QSS07] A. Quarteroni, R. Sacco, and F. Saleri. *Numerical mathematics*, volume 37 of *Texts in Applied Mathematics.* Springer-Verlag, Berlin, second edition, 2007.

[Ray45] J. W. S. Rayleigh, Baron. *The Theory of Sound.* Dover Publications, New York, N. Y., 1945. 2d ed.

[Reu06] M. Reuter. *Laplace Spectra for Shape Recognition.* Books on Demand GmbH, 2006.

[RT83] P.-A. Raviart and J.-M. Thomas. *Introduction à l'analyse numérique des équations aux dérivées partielles.* Collection Mathématiques Appliquées pour la Maîtrise. [Collection of Applied Mathematics for the Master's Degree]. Masson, Paris, 1983.

[Rud73] W. Rudin. *Functional analysis.* McGraw-Hill Book Co., New York, 1973. McGraw-Hill Series in Higher Mathematics.

[Saa80] Y. Saad. On the rates of convergence of the Lanczos and the block-Lanczos methods. *SIAM J. Numer. Anal.*, 17(5):687–706, 1980.

[Saa03] Y. Saad. *Iterative methods for sparse linear systems.* Society for Industrial and Applied Mathematics, Philadelphia, PA, second edition, 2003.

[Sch66] L. Schwartz. *Théorie des distributions.* Publications de l'Institut de Mathématique de l'Université de Strasbourg, No. IX-X. Nouvelle édition, entiérement corrigée, refondue et augmentée. Hermann, Paris, 1966.

[Str12a] R. Straubhaar. Numerical computation of eigenvalues of the Dirichlet-Laplace operator on domains in surfaces. Submitted, 2012.

[Str12b] R. Straubhaar. Numerical optimization of eigenvalues of the Dirichlet-Laplace operator on domains in surfaces. Submitted, 2012.

[Wei56] H. F. Weinberger. An isoperimetric inequality for the N-dimensional free membrane problem. *J. Rational Mech. Anal.*, 5:633–636, 1956.

[WK94] S. A. Wolf and J. B. Keller. Range of the first two eigenvalues of the Laplacian. *Proc. Roy. Soc. London Ser. A*, 447(1930):397–412, 1994.